Order Number 9003204

Magnetite and ilmenite as provenance indicators

Grigsby, Jeffry Dale, Ph.D.

University of Cincinnati, 1989

U·M·I
300 N. Zeeb Rd.
Ann Arbor, MI 48106

MAGNETITE AND ILMENITE AS PROVENANCE INDICATORS

A Dissertation submitted to the

Division of Graduate Studies and Research
of the University of Cincinnati

in partial fulfillment of the
requirements for the degree of

DOCTOR OF PHILOSOPHY

in the Department of Geology
of the College of Arts and Sciences

1989

by

Jeffry D. Grigsby

B.S., University of Akron, 1983

M.S., New Mexico State University, 1984

UNIVERSITY OF CINCINNATI

November 23 19 88

I hereby recommend that the thesis prepared under my supervision by Jeffry D. Grigsby

entitled Magnetite and Ilmenite as Provenance Indicators

be accepted as fulfilling this part of the requirements for the degree of Doctor of Philosophy

Approved by:

ABSTRACT

The petrographic and compositional characteristics of detrital magnetite and ilmenite separated from 31 modern sand samples derived from 8 known igneous and metamorphic parent rocks indicates that magnetite is a useful provenance indicator. In contrast, detrital ilmenite shows no trends with variations in parent rock and its use in provenance research is suspect.

Petrographically detrital magnetite can be classified into 3 groups: 1) homogeneous grains, 2) grains with trellis- or composite-type magnetite-ilmenite intergrowths, and 3) grains with pleonaste or ulvospinel exsolution textures. A ternary plot with these three groups as corners shows that: 1) detrital magnetite grains derived from felsic plutonic, intermediate volcanic and sedimentary banded-iron formation sources are dominated by homogeneous grains, 2) grains derived from felsic volcanic sources are dominated by composite-type magnetite-ilmenite intergrowths (composite-type/trellis-type ratio > 1), 3) grains derived from mafic plutonic sources (including serpentinized ultramafics and meta-anorthosites) are dominated by ulvospinel or pleonaste exsolution, and 4) grains derived from mafic volcanic sources are dominated by trellis-type magnetite-ilmenite intergrowths (a composite-type/trellis-type ratio < 1). In addition, the presence of heating

martite or pseudobrookite replacement textures is a strong indication of a volcanic source.

Electron probe microanalysis of the homogeneous magnetite grains, treated by discriminant function analysis, indicates that Ti, Mg, V, and Al can best discriminate between felsic plutonic/volcanic, intermediate volcanic, and mafic plutonic parent rocks. A plot of the weight percent Mg/(Mg+Al) vs. Ti+V indicates that the detrital magnetite grains from these three rock groups can be correctly classified 96% of the time. However, detrital magnetite grains derived from basaltic and metamorphic parent rocks extend into the felsic volcanic/plutonic field and may lead to error in provenance interpretation.

Nevertheless, the petrographic and chemical analyses of detrital magnetite separated from a beach sand collected near Rosarito, Mexico found basalt to be the dominant source. This compared well to the point count analysis of the light sand fraction which gave 54% plagioclase, 28% volcanic rock fragments, 19% quartz, 8% K-feldspar, and 7% quartzofeldspathic rock fragments. Thus indicating that detrital magnetite is a viable alternative in provenance research, especially in mature, quartz rich sands.

ACKNOWLEDGEMENTS

I would like to express my gratitude to Dr. J. Barry Maynard for his advice and guidance during my residence at the University of Cincinnati. In addition, special thanks go to Dr's. David Meyer and Kees Dejong for their help in the preparation of this manuscript, Dr. Atila Kilinc and Dr. Mike Garcia who instilled in me respect for the complexity of basaltic volcanism, and Dr. Abijit Basu for our long discussions concerning the much maligned opaque Fe-Ti oxides in provenance studies.

I would also like to thank the following people who aided in the collection of samples used in this research: fellow graduate students Mike Armstrong, Ned Baker, and Tom Hudson; Dr's. Holly Huyck, J. B. Maynard, Paul Potter, and Kees Dejong (Univ. of Cincinnati); Dr's. H. S. Yu (Taiwan Institute of Oceanography) and N. O. Oskarsson (Nordic Volcanological Institute); Dr. Sally Sutton (Univ. of Texas, Austin); Dale Kramer (Peace Corp volunteer, Fiji); and Margo Emory-Moore (graduate student, Newfoundland).

Last, but most important of all, I would like to thank my wife Mellanie and parents, James H. and Velma J. Grigsby, to whom I dedicate this work. Their love and support has been essential to my success, and has carried me through the many peaks and valleys of graduate school.

TABLE OF CONTENTS

Appendices

LIST OF TABLES

LIST OF FIGURES

CHAPTER I

INTRODUCTION

The term provenance is defined as the place of origin. In sedimentary petrology provenance refers to the nature of the source rocks in a particular area and the identification of these source rocks through the study of sedimentary detritus derived from them. Tectonic events produce highlands and provide source rocks that shed sediments into surrounding basins. Although these highlands serve as the primary control on the eventual sandstone composition (Dickinson et al., 1983) relief, climate, transport mechanisms, depositional environment, and diagenesis can all be important secondary factors. Because it is the goal of all provenance studies to determine the source of clastic sediments, and to decipher earth history through paleogeograghic reconstructions of the earth's crust, it is important not only to understand the above processes and their effects but also to understand the influence of source rocks on the detrital grains themselves.

Provenance studies have undergone a renaissance since the acceptance of plate tectonics. For over 200 years geologists supported many different theories of mountain building, volcanism, and other major phenomena of the earth. Today, through the unifying theory of plate

tectonics, scientists have a single concept with which to interpret the classification and distribution of rocks, the history of sedimentary rock sequences, the position and characteristics of volcanoes, earthquake belts, mountain systems, deep-sea trenches, and ocean basins. The acceptance of this theory was brought about through the work of many scientists including the important studies of Hess (1962) who advocated sea-floor spreading; Vine and Matthews (1963) who recognized the relationship between ocean floor magnetic anomalies and sea-floor spreading; Wilson (1965) who proposed transform faults, a new class of faults; and Dewey and Bird (1970) who suggested a relationship between mountain belts and convergent plate boundaries. Although the relationship between tectonics and sandstone mineralogy has long been of interest to sandstone petrologists, the theory being that sandstone composition will reflect the tectonic history of both the source area and the site of deposition (Krynine, 1943), the acceptance of plate tectonics has brought renewed vigor in provenance research.

Most recent work concerning tectonics and sandstone mineralogy concentrates on thin-section petrology of the light minerals. Ternary diagrams are produced using Quartz, Feldspar, and Rock Fragments, or subsets of these grains, as corners. Detrital percentages, calculated from

point counts, are plotted in these diagrams to indicate specific tectonic settings (Dickinson and Suczek, 1979; Dickinson, 1985; Zuffa, 1985). Although these studies have led to a greater understanding of the relationship between provenance and sandstone composition they have failed to consider the importance of heavy minerals.

Heavy minerals, the minor, high-density, accessory minerals of sands, have traditionally been used for provenance determination (Milner, 1926; Boswell, 1933; Krumbein and Pettijohn, 1938; Stow, 1939), and as stated by Stategger (1987) "the study of these minerals allows for an adequate interpretation of plate tectonic setting where analysis of light mineral based petrology has failed (Mack, 1984)." However, because heavy minerals are sensitive to the processes of weathering, transportation, deposition, and diagenesis (intrastratal solution) the heavy mineral suite found in a sandstone does not necessarily reflect the source area mineralogy. Although the effects of weathering in the source area and during transport may be minimal (Morton, 1985a), hydraulic sorting and intrastratal solution can severely restrict their usefulness (Pettijohn, 1941; Rittenhouse, 1943; Morton, 1985a).

The most effective method to counteract the problems of intrastratal solution and hydraulic sorting is to examine the relative abundance of the physical and chemical

varieties of one mineral (termed a varietal study). Classical methods of varietal studies have involved optical differentiation based on color, shape, or other physical properties of grains. Minerals especially scrutinized in this manner have included tourmaline (Krynine, 1946) and zircon (Poldervaart, 1956; Vintanage, 1957). With the advent of the electron microprobe it is now possible to make further advances in these studies by determining quickly and accurately the compositional variation of a particular mineral species. This method has been particularly successful in the study of garnets (Morton, 1985b), although this approach may also be applied to a variety of other detrital minerals including pyroxenes, amphiboles, epidotes, tourmalines, and detrital opaque minerals such as magnetite and ilmenite.

In order to use composition of a mineral as a provenance indicator the mineral should satisfy the following requirements: 1) be common in a variety of parent rocks, 2) be variable in composition, 3) reflect with its composition the type of source rock (though compositional variation should be limited), and 4) be relatively stable. Of the minerals listed above, pyroxene, amphibole, and epidote are moderately to extremely susceptible to intrastratal solution (Morton, 1984). Therefore, the study of these minerals is likely to be

limited to modern sands or sands that have been sealed or protected from intrastratal solution. In addition, amphiboles show such a high degree of compositional variation (Leake, 1978) that an accurate determination of their compositional range requires analysis of a large number of grains. However, electron probe microanalyses of pyroxenes and amphiboles have met with some success (Nisbet and Pearce, 1977; Mange-Rajetsky, 1981; Cawood, 1983; Morton, 1984). Tourmalines, because of their ultrastability, should offer the best opportunity in provenance determination, but because of the presence of boron in the structure, which is not detectable with an energy-dispersive system, accurate compositional analysis is difficult to achieve (Morton, 1985a).

Magnetite and ilmenite appear to be the ideal minerals for the type of varietal study discussed above. This is because 1) both occur in a wide variety of igneous rocks, both extrusive and intrusive, as well as pegmatites, other vein rocks, and metamorphic rocks (Ramdohr, 1980), 2) both show compositional variations based on source rock paragenesis (Hutton, 1950; Buddington and Lindsley, 1964), 3) both are relatively abundant in sands and sandstones, 4) both are relatively stable (Pettijohn, 1941), 5) both are easily separated using magnetic techniques (Rosenblum, 1958; Force, 1976; Lumpkin and Zaikowski, 1980), and 6)

previous studies of detrital ilmenite (Darby, 1984; Darby and Tsang, 1987) and magnetite (Luepke, 1980) have suggested that variation in their composition is sufficient to provide an unmistakable signature to determine sediment source.

The purpose of this investigation is to test the utility of detrital magnetite and ilmenite as provenance indicators. The modeling of source rocks using petrographic and chemical analysis of magnetite and ilmenite will offer an extension in provenance studies of sand and sandstone that past investigations have lacked.

CHAPTER II

HISTORY OF PROVENANCE STUDIES

Two types of studies have been undertaken in the past to predict provenance through the analysis of mineral grains: 1) the study of mineral-suites/associations and 2) the study of a single mineral or mineral group. The following section will discuss these two types of studies as well as the processes that affect provenance interpretation other than source rock, namely hydraulic conditions and mineral stability. In addition, the history of magnetite and ilmenite in provenance studies will be discussed.

Mineral Suites/Associations

The earliest studies of mineral suites/associations to predict provenance emphasized heavy minerals (Milner, 1926; Boswell, 1933). As Boswell stated, " the detrital constituents which showed the greatest mineralogical variety were found to be present in only small proportions. Most of them possessed a higher specific gravity than that of the dominant constituent.... Such accessory minerals are usually the guide minerals when problems of source and correlation are under discussion." Milner (1926) presented one of the earliest classifications of heavy minerals in which he grouped certain mineral associations with specific parent rock types. Similar classification systems by

Krumbein and Pettijohn (1938), Feo-Codecido (1956), and Baker (1962) followed. These systems gradually lost favor in the scientific community as it was learned that additional processes, other than source rock, affected these associations.

Heavy minerals were gradually replaced by the study of the light mineral fraction in provenance research. With the acceptance of plate tectonics came more interest in what the light fractions of sandstones could reveal. Dickinson (1970) established operational definitions for various grain types in the light fraction of sands. These grain types included quartz, feldspar, and rock fragments and subsets of these grains. These definitions have been generally accepted though the method of counting rock fragments has been debated (Zuffa, 1980; Ingersoll et al., 1984). In general, these detrital modes are calculated from point counts of thin sections and plotted within triangular diagrams of the ternary system QFL where Q is total quartzose grains (both monocrystalline and polycrystalline quartz), F is total feldspar grains (all are monocrystalline), and L is total unstable lithic fragments (all are polycrystalline). Subsets of this system such as QmFLt (Qm = monocrystalline quartz, F = total feldspar, and Lt = total polycrystalline lithic fragments including polycrystalline quartz) are also used. These triangles are

then divided into different fields indicating specific plate tectonic settings and source rock types (Dickinson and Suczek, 1979; Dickinson et al., 1983; Dickinson, 1985; Zuffa, 1985). Although exceptions do exist (Mack, 1984) these studies have been very important to the understanding of past tectonic events.

Varietal Studies

A varietal study is defined as the study of the types of one mineral or mineral group in a light or heavy mineral suite. The most frequently employed method of varietal study has been to distinguish grains optically on the basis of color, form, habit, or inclusions. Other properties presently receiving attention include cathodoluminescence and compositions as determined by electron microprobe.

Quartz, because of its persistence through geologic time, has received considerable attention in varietal studies. Among the earliest investigations were those of Sorby (1880), Mackie (1899), and Dake (1921). Krynine (1940, 1946) did a comprehensive study based on grain shape, inclusions, and extinction. Other studies in grain shape include Ehrlich and Weinberg (1970), Brown et al. (1980) and Hudson and Ehrlich (1980). Basu et al. (1975) studied quartz from known source rocks and measured the undulosity of monocrystalline quartz, and coupled that with the quantity of polycrystalline quartz and number of

crystal units per grain. This led to the discrimination between plutonic, low rank, and high rank metamorphic rocks. Young (1976) continued this work through the study of the origin of polycrystalline quartz. Currently the cathodoluminescence of quartz is receiving much attention (Matter and Ramseyer, 1985; Owen and Carozzi, 1986; Baker, 1988).

Feldspar has also been commonly used in varietal studies. Gorai (1951) made careful studies of twinning in plagioclase and its abundance in igneous and metamorphic rocks. Oscillatory zoning, progressive zoning and lack of zoning have also been shown to be important indicators of provenance (Pittman, 1963). Rimsaite (1967) studied the varietal properties of feldspar in potential source rocks and defined nine classes based on zoning, intergrowth habits, twinning, and fracturing. X-ray analysis has been employed by Suttner and Basu (1977) to study disorder in single crystals of alkali feldspars. They found sanadine to be highly disordered indicating rapid cooling (volcanic origin) whereas disorder in microcline and orthoclase was less, which they correlated with the slower cooling history of a batholith or metamorphic belt. Travena and Nash (1981) plotted the microprobe composition of over 2000 feldspars from igneous and metamorphic rocks and compared them with sandstone of known volcanic provenance. Plots on

a triangular diagram of the system Ca-Na-K showed high-K plagioclase from volcanic sources but low-K plagioclase from plutonic and metamorphic sources. Maynard (1984) investigated the composition of plagioclase in modern deep sea fans and found a correlation between the Ca content of plagioclase and tectonic setting, but he could not relate K content to known volcanic sources.

Heavy minerals have been analyzed in similar fashion. Minerals especially scrutinized, where variations in color or grain shape with source rock have been emphasized, include tourmaline and zircon (Mackie, 1923; Krynine, 1946; Poldervaart, 1956; Vintanage, 1957; Callender and Folk, 1958), garnet (Dreimanis et al., 1957; Connally, 1964) and hornblende (Van Andel and Poole, 1960). As stated by McDonald (1968) "although this is clearly a successful method for distinguishing sand bodies of differing provenance it remains a highly subjective approach."

Compositional analysis of a mineral or mineral group through the use of the electron microprobe is presently receiving much attention. Studies to date have concentrated on amphiboles (Mange-Rajetsky, 1981), pyroxenes (Nisbet and Pearce, 1977; Cawood, 1983) and garnets (Morton, 1985b), and currently interest in the opaque Fe-Ti oxides is beginning to rise (Luepke, 1980; Darby, 1984; Basu and Hood, 1985; Basu and Molinaroli,

1986; Darby and Tsang, 1987; Basu and Molinaroli, in press).

Processes that affect Provenance Interpretation other than Source Rock

Hydraulic Conditions

Changes in hydraulic conditions during deposition of a sand unit, as reflected by variations in grain size, sorting, etc., can cause fluctuations in mineral proportions between samples. In other words, changes in mineral proportions in a sand do not necessarily reflect changes in sediment source. This is particularly true when dealing with heavy minerals in provenance studies.

Studies of grain size distribution in modern sands (Rubey, 1933; Pettijohn and Ridge, 1933; Russell, 1936; Rittenhouse, 1943) have shown that the mean grain size of any given heavy mineral species tends to be smaller than the mean size of the whole sample. Therefore, heavy mineral grains are hydraulically equivalent to larger quartz grains. Hydraulic equivalence can be defined as "the difference in size between a given heavy mineral species and the size of a quartz sphere with the same settling velocity in water" (Rubey, 1933), but because hydraulic equivalence affects light minerals as well, a better way to state this definition is that "two different mineral grains are said to be hydraulically equivalent if they have the same settling velocity in water"

(Rittenhouse, 1943). In light minerals, size and shape are the principal factors controlling settling velocity (Pettijohn et al., 1987), whereas in heavy minerals density is the determining factor (Rittenhouse, 1943) although shape, grain size availability of a mineral species, entrainment potential of a mineral, and nature of the depositing medium can cause hydraulic sizes to differ markedly from those predicted (Briggs et al., 1962; Briggs, 1965; Lowright et al., 1972; Slingerland, 1977; Morton, 1985a).

Several procedures have been developed to overcome hydraulic effects on the mineral proportions in a sand. Grain size variations can be countered through the determination of hydraulic ratios (Rittenhouse, 1943). A hydraulic ratio is defined as the weight of a given heavy mineral in a known size range divided by the weight of light minerals of equivalent hydraulic size multiplied by 100. This method must be applied to fine or very fine sands in order to overcome the availability problem of some minerals which do not occur in the coarser size fractions. If so, regional variations in hydraulic ratios of a mineral can be ascribed to source area availability (Morton, 1985a).

The effects of hydraulic sorting can also be eliminated by only using those minerals that show

variations that are independent of grain size. This is achieved by scatter plots of mean grain size verses mineral proportions (Galehouse, 1967). In this case proportions of heavy minerals that can be shown to be independent of grain size can be used to map petrological provinces. However, Morton (1985b) in a study of garnets from the Middle Jurassic Etive Formation from a well in the North Sea found that sorting may affect the results of these scatter plots and demonstrates the importance of plotting other grain size parameters as well as mean size when adapting this method.

Other methods include: 1) the study of gross variations that are determined by averaging a large number of samples of variable grain size over a study area (Hubert, 1971), although this method may be suspect if regional grain size trends occur, 2) the study of minerals showing regional patterns of presence/absence. Hydraulic sorting is unlikely to eliminate entire heavy mineral species from a suite, so these regional patterns may be utilized in provenance studies provided the patterns were not caused by intrastratal solution (Morton, 1985a), 3) statistical analysis of heavy mineral associations by extended Q-mode factor analysis. This method has been shown to be rather reliable in predicting source rock though the effect of hydraulic sorting is not clear

(Stattegger, 1987), and 4) the study of varieties of one or more individual mineral species either physically or chemically (Morton, 1985a&b, Darby, 1984, Darby and Tsang, 1987). This last type of study is density independent and the most reliable technique in over coming the effects of hydraulic sorting.

Mineral Stability

As early as 1891 (Derby, 1891) questions were being raised about mineral stability. Thoulet (1913) published one of the earliest stability diagrams and was followed by further studies into mineral stability by Boswell (1923, 1933), Russell (1937), Goldich (1938), Stow (1938), Pettijohn (1941), and Milner (1962) and interest in this area has continued to the present (Luepke, 1984). Mineral stability can be divided into two types: 1) mechanical stability (ability of a mineral to withstand abrasion) and 2) chemical stability (ability of a mineral to resist solution or alteration in a particular chemical environment).

Mechanical stability. Mechanical stability has been studied both experimentally and empirically. Thiel (1940) determined the relative resistance of various minerals in abrasion mills and more recently Dietz (1973) compared experimental results with those found under natural conditions and concluded that "a mineral's ability to

withstand abrasion does not depend solely on hardness but on other factors such as cleavage, crystal structure, and brittleness." Studies that have dealt with abrasion in natural settings have yielded contradictory results. Russell (1937) whose work on Mississippi River sands indicated little or no change in sand composition owing to abrasion is not in agreement with the conclusions of Cameron and Blatt (1971) who found some selective losses in high-gradient streams. Suttner et al. (1981) also recognized that abrasion is more intense in high- rather than low-energy environments. Though it appears that mechanical stability may have an influence on the eventual sand composition, it is difficult to estimate its importance when reconst· cting the provenance history of a sandstone.

Chemical stability. Chemical stability has been found to exert a large influence on sandstone composition. The chemical stability of a particular mineral is dependent on the nature of the mineral (chemical composition and crystallographic properties), which is controlled internally by the source rock, and on the chemical conditions of the surrounding medium (pH, Eh, etc.), which are controlled by external forces such as climate, relief, depositional environment, and diagenetic environment. Which of these produces the largest influence on the

chemical stability of a mineral is uncertain. Goldich (1938), in a classic paper, studied soil profiles and showed that the common rock forming minerals could be arranged in an order dependent on the degree of weathering. This order was the reverse of Bowen's Reaction Series so that minerals formed at high temperatures and pressures were the least stable under surface conditions. Therefore, the chemical stability of a mineral is dependent on the temperature and pressure of formation that in turn will determine the minerals response to weathering. Weathering, of course, is influenced by climate and relief. Basu (1976) and Suttner et al. (1981), in studies of modern fluvial sands, showed a marked contrast in the proportions of quartz, feldspar, and rock fragments under differing climatic conditions. This shows that sands from similar source rocks can be markedly different in humid and arid climates. On the other hand, Krynine (1935) noted that the effects of climate may be obscured by relief. Arkose, for example, may be produced even in humid climates if relief is high enough. Suttner et al. (1981) also noted that depositional environment may play a role in the chemical stability of minerals. They suggest that climatic influence is strongest in first-cycle fluvial sand near the source and is probably minimal in first-cycle marine sands.

Diagenesis also plays an important role in the

eventual sandstone composition. It has long been noted that there is a corresponding increase in the complexity of heavy mineral suites with decrease in age. Boswell (1923), Russel (1937), and Pettijohn (1941) all noted this disappearance in older sandstones and inferred that it was caused by dissolution and this process has been termed intrastratal solution. Support for the idea of diagenetic solution comes from Bramlette's (1941) study that showed a much larger suite of heavy-minerals in impermeable concretions in a sandstone than in the matrix of permeable sand. Nickel (1973), in an experimental dissolution study of light and heavy minerals, reproduced natural dissolution effects corresponding to weathering and intrastratal solution. Diagenesis affects both the light and heavy minerals of a sand. Intrastratal solution has a major impact, but replacement (by calcite, zeolites, kaolinite (and other clays), albite and dolomite), oxidation, and recrystallization are also common diagenetic processes that affect detrital grain types (McBride, 1985). All of these processes have a large influence on one's ability to predict provenance.

Magnetite and Ilmenite in Provenance Studies

Magnetite and ilmenite had received little attention in provenance studies until the work of Balsley and Buddington (1958) who showed a direct relationship between

these opaque Fe-Ti oxides and their intergrowths, and the parent rock type from which they were derived. On the basis of this study Rao and Rao (1965), in an ore-textural study of ilmenite grains in beach sands, concluded that different source rocks had contributed to these sands, although they did not suggest types of source rocks. Boctor (1966) continued work in this area with an ore-microscopic study of detrital magnetite and ilmenite in the Rosetta-Damietta black sands near the mouth of the Nile River, Egypt. He attempted to define textures and relate these textures to specific parent rocks in the drainage basin. Riezebos (1979) also discussed the relationship between intergrowth textures in magnetite and ilmenite and parent rocks and suggested intrusive and extrusive sources for modern sands of the Rio Magdalena (Columbia).

Compositional analysis of magnetite and ilmenite have also become important in predicting provenance. Buddington and Lindsley (1964), in a landmark study of these opaque Fe-Ti oxides in igneous and metamorphic rocks, recognized the relationship between source rock and magnetite-ilmenite composition. This led to much of the recent interest in the compositional analysis of detrital magnetite and ilmenite and their relationship to source rock.

Luepke (1980) in a compositional study of detrital magnetite grains in southwestern Oregon beach sands found

each beach to be characterized by a fairly distinct Ti/Cr range. She suggested that the high amounts of chromium found in the magnetite from two of the beaches studied were related to drainage from ultramafic bodies.

Freeman (1986) studied the composition of detrital magnetite found in pelagic limestone and suggested that grains that were high in iron with only traces of other elements (low Ti content) were derived from felsic intrusive sources and those that contained significant amounts of Ti likely originated in mafic sources.

Thomas et al. (1988), in a geochemical study of magnetite and large ion lithophile element containing minerals collected from sediments in the San Luis Valley in south-central Colorado, found that all the mineral separates established strong LREE enrichments. They concluded that sediments derived from the San Juan Mountains and the Sangre de Crista Mountains could be separated by variations in the La/Sm ratios and Sm/Eu ratios and that sediments derived from hydrothermally active areas were characterized by higher Fe/Ti ratios and Br contents. They also found that igneous rock types from the study area could be characterized by variable Th/U ratios.

Darby (1984) and Darby and Tsang (1987) have studied the variations in ilmenite composition within and among

drainage basins in Virginia and North Carolina. They demonstrated, through the use of ilmenite composition and discriminant analysis, the ability to distinguish adjacent drainage basins and to relate the chemical variations in the ilmenite grains to source rocks that the tributaries to these basins drain. They were able to show that ilmenite grains from tributaries draining similar rock types in well-separated drainage basins often resulted in the grouping of ilmenite grains into fields based on compositional variations. Conversely, samples from tributaries that drained dissimilar rock types did not group together despite their close geographic proximity. They concluded that ilmenite composition is a viable approach to determine provenance for sands in a depocenter, and although their data are insufficient to establish criteria for recognition of source rock types outside of the tributary groupings in their study area, they suggest that a more comprehensive analysis of ilmenite grains from specific source rocks would allow one to match rock types with individual ilmenite grains.

Basu and Molinaroli (in press) have investigated the petrogenic characteristics of detrital Fe-Ti oxides (magnetite, ilmenite, and hematite) collected from Holocene streams draining granitic igneous and metamorphic source rocks in the Rocky Mountain region and the Appalachian

Mountains; these sample areas representing dissected arc and recycled orogen provenances respectively. They studied both textural and compositional variations and reached the following conclusions 1) between 25% and 50% of the detrital opaque Fe-Ti oxides showed oxidation exsolution textures or other lamellar intergrowth textures, 2) the exsolution textures were present in twice an many grains derived from granitic igneous source rocks than from metamorphic source rocks, 3) exsolution lamellae along the (111) plane of magnetite characterized the dissected arc and exsolution lamellae along the (0001) planes of the ilmenite characterized the recycled orogen provenance, 4) exsolution lamellae thinner than 10um were predominant in grains derived from dissected arc provenance, whereas lamellae thicker than 10um were predominant from grains derived from a recycled orogen provenance, 5) detrital ilmenite grains derived from granitic igneous source rocks showed a wide range of TiO_2 content (average 47%), whereas those from metamorphic source rocks were closely clustered around 52%, 6) detrital opaque Fe-Ti oxides derived from metamorphic source rocks contained less than 0.5% MgO, whereas those from granitic igneous rocks contained up to 1.2% MgO, and 7) both MgO and MnO were low, 0.3% and 2.5% respectively, in detrital opaque Fe-Ti oxide minerals derived from dissected arc provenance, and relatively high,

1.2% to 8.0% respectively, in grains derived from recycled orogen provenance. They also concluded that, because of the small proportion of detrital grains showing oxidation exsolution that remain unaltered during weathering, the generalizations from geothermometric and geobarometric determinations were not always reliable. This is in contrast to earlier studies by Basu and Hood (1985) and Basu and Molinaroli (1986).

In addition, compositional analyses of skeletal spinel (composition ranging from pure magnetite (Fe_3O_4) to magnesioferrite ($MgFe_2O_4$)) found in spheroidal grains in Cretaceous/Tertiary sediments have been studied in relationship to the Cretaceous/Tertiary extinction. Kyte and Smit (1986) concluded that the high concentrations of Mg, Al, and Ni, the relatively low Ti and Cr, and the high Fe_2O_3/FeO ratios of these grains were "highly unusual" and may represent materials resulting from comet or asteroid impact suggested for Cretaceous/Tertiary time. They believe that the regional variations seen in these compositions may reflect multiple sources of impact, and a world map of the spinel compositions would be useful in localizing impact sites.

These investigations indicate the importance of further research into the relationship between the opaque Fe-Ti oxides (magnetite and ilmenite) and provenance. The

opaque minerals have not received the attention they deserve and as Blatt (1967) has stated "the potential of opaque minerals for provenance studies may be large."

CHAPTER III

MAGNETITE AND ILMENITE IN IGNEOUS AND SEDIMENTARY ROCKS

Introduction

Much of the information concerning the physical and chemical properties of magnetite and ilmenite have been learned through the study of igneous and sedimentary rocks. These studies have addressed the role of magnetite and ilmenite in 1) the crystallization history of igneous rocks, 2) the development of economically important iron, titanium, and vanadium deposits, 3) the role of authigenic magnetite in sedimentary rocks, 4) the alteration of magnetite and ilmenite in sedimentary rocks, and 5) the role of magnetite in rock magnetism and paleomagnetism in both sedimentary and igneous rocks. The following sections will review these studies and present the background necessary to understand why magnetite and ilmenite have been important minerals in past and present geologic investigations and how these investigations have led to the use of magnetite and ilmenite in provenance research.

Magnetite and Ilmenite in Igneous Rocks

Introduction

Magnetite and ilmenite form a small but ubiquitous constituent of all common igneous rocks. The importance of these minerals in the study of igneous rocks and the suggestion that these minerals may be important provenance

indicators is based on the landmark studies of Balsley and Buddington (1958) and Buddington and Lindsley (1964). The study of Balsley and Buddington (1958) found a direct relationship between the physical properties of magnetite and ilmenite and the parent rock from which they were derived. This was followed in 1964 by Buddington and Lindsley who discovered that the chemical properties of magnetite and ilmenite could also be related to the parent rock from which they were derived. The importance of the latter study is epitomized by Lindsley (1976) who states "the oxide minerals in a rock can, in many cases, be considered as a 'subsystem' of the rock, more or less independent of the silicates or other minerals present. The advantage of this approach is that the oxide 'subsystem' tends to be chemically simpler than the whole rock and thus easier to handle in both experiments and theoretical analysis." The realization of this "subsystem" has led to a better understanding of the crystallization history of igneous rocks, of rock magnetism, and of the development of economically important iron and titanium deposits. It has also paved the way for the use of magnetite and ilmenite in provenance research. The following sections will discuss studies in crystallization history (plus the role rock magnetism played in these studies), the study of magnetite and ilmenite iron-

titanium deposits, and there influence on provenance research.

Magnetite and Ilmenite and Crystallization History

Since the study of Buddington and Lindsley (1964), which involved the calculation of the temperature and oxygen fugacity of formation of igneous rocks based on the Fe-Ti oxides (magnetite and ilmenite), these calculations have become a part of most studies involving igneous rocks (for example: Carmicheal, 1967; Anderson, 1968; Puffer, 1972; Mathison, 1975; Luhr and Carmicheal, 1980). Recent studies of the Fe-Ti oxides in igneous rocks have concentrated on 1) the understanding of the physical and chemical properties of the Fe-Ti oxides (particularly the titanomagnetite series) in order to determine the subsolidus phase relations of the titanomagnetite solid solution series (Price, 1981; Lindsley, 1981) and 2) the effects of recalculation on the estimates of temperature and oxygen fugacities from the analyses of multi-component Fe-Ti oxides (Carmicheal, 1967; Anderson, 1968; Stormer, 1983). The latter study has particular relevance in the understanding of the crystallization history of igneous rocks and the relationship between magnetite-ilmenite composition and its use in provenance determination, because it shows the importance of minor elements in their composition. This importance was first recognized in the

study of magnetite in basalts in relationship to rock magnetism (Akimoto, 1954; Nêel, 1955; Chevallier, et al., 1955; Verhoogen, 1956, 1962). These early studies were interested in determining the effects of chemical (minor element composition and distribution) and physical (high-temperature oxidation) variations on the magnetic properties of magnetite. Studies concerned with variations in chemical composition and rock magnetism have been continued by Stephenson (1969), Creer and Ibbetson (1970), Creer and Stephenson (1972), Stacey and Banerjee (1974), and Nishitani (1981). The effects of physical variations (high-temperature oxidation) have been studied by Strangway, et al. (1968), Grommè et al. (1969), Ozima and Larson (1970), Stacey and Banerjee (1974), Ade-Hall (1976), and Tucker and O'Reilly (1980). These studies have shown that the addition and distribution of minor elements in magnetite, and the effects of high-temperature alteration can greatly influence the magnetic properties of basalt.

Buddington and Lindsley (1964) developed their calculations based on the assumption that the magnetite and ilmenite solid solutions were pure binary Fe-Ti oxides and no minor constituents (Ti, Mg, Mn, Al, V, Cr, Si) were considered. However, Speidel (1970) has shown that the addition of minor elements to magnetite and ilmenite has indeed a bearing on the accuracy of the temperature and

oxygen fugacity calculations. Stormer (1983), based on a solution model for coexisting Fe-Ti oxides developed by Spencer and Lindsley (1981), recalculated the estimates of temperature and oxygen fugacity from analyses of multicomponent Fe-Ti oxides. The values of Stormer (1983) were generally intermediate with respect to those of the Carmicheal (1967) and Anderson (1968) recalculation methods. Unfortunately, there is insufficient experimental data to determine adequately the effects of the minor components and to account for them in recalculation for geothermometry. As Stormer (1983) concluded "simply ignoring, or not analyzing for, minor components can lead to errors in excess of 150°C and 4 units of log fo^2."

Other studies of Fe-Ti oxides and their relationship to the crystallization history of igneous rocks have been based on petrographic as well as compositional analysis. Sanderson (1974) developed a quantitative technique in which the spatial distribution of magnetite to the constituent minerals in an igneous rock is noted petrographically, and the presence or absence of a preferred association is used to gain insight into the crystallization history of the rock.

Osborn and Boctor (1981), in a study of magnetite derived from andesites and basalts, found that the younger, higher-silica flows, contain magnetite with lower Cr_2O_3

content. This can then be related to changes in temperature and composition of the liquid phase during crystallization. The higher Cr_2O_3 content of magnetite from earlier flows reflects a higher temperature of formation, therefore a series of flows in which the Cr_2O_3 content of magnetite changes would indicate changes in the crystallization temperature of the rock. Butcher and Merkle (1987) in a similar study looked at the textural and compositional changes in magnetite in the Bushveld Complex. They were able to relate minor changes in the magnetite texture and composition to late-stage compositional modifications in the layered intrusion.

Economic Occurrence of Magnetite and Ilmenite in Igneous Rocks

The expanded use of titanium in recent years and the continued need for iron has encouraged the study of the magnetite and ilmenite concentrated in some igneous rocks. These deposits have been classified as magmatic segregation deposits, which are ore deposits, exclusive of pegmatites, that are direct crystallization products of the magma. They typically form in deep-seated intrusive bodies but have also been found in sills and volcanic flows. A magmatic segregation deposit may constitute an entire rock mass, a compositional layer, or may be defined by the presence of valuable accessory minerals in an otherwise normal igneous rock. Although the majority of Fe-Ti oxide

deposits found in igneous rocks are thought to related to magmatic segregation processes, Gillison (1956) has argued that some of these deposits are the result of pneumatolytic replacement of the host rock. Table 1 summarizes the proposed processes of formation of Fe-Ti oxide deposits in igneous rocks.

Fe-Ti oxide deposits that are the result of magmatic segregation processes have been divided into two types 1) Kiruna type, defined as massive magnetite deposits that appear to be intrusions into granitoid and syenite rocks; are characterized by a high magnetite content and appreciable apatite; form massive tabular to irregular dike-like bodies, complex stockworks, or vein-like masses (Gross, 1970a), and 2) Taberg type, defined as massive and disseminated deposits of titaniferous magnetite and ilmenite syngenetic or epigenetic in gabbro, anorthosite, and basic igneous and metamorphic rocks; have titanium present in the magnetite crystal lattice, as exsolved blades in magnetite, and in ilmenite; form irregular massive magnetite and ilmenite bodies that appear to be intrusions or injections in gabbroic host rocks or disseminated masses of magnetite and ilmenite that appear to be syngenetic in gabbro and pyroxenite rocks (Gross, 1970a). Examples of Kiruna type and Taberg type Fe-Ti oxide deposits are given in Table 2.

Table 1

Hypotheses for the Formation of Fe-Ti Oxide Deposits Related to Igneous Rocks (after Lister, 1966)

Processes of Magmatic Segregation	
1) Deposition from a residual liquid accumulation.	
a) Residual liquid injection	Stephenson (1948), Bateman (1951)
b) Filter pressing	Park and MacDiarmid (1975), Stephenson (1948), Osborn (1928)
c) Log-jam filtering and and self-filtering	Stephenson (1948), Balk (1930)
2) Injection of an immiscible Liquid	Kolker (1982), Badham and Morton (1976), Philpotts (1967), Buddington et al. (1955), Fischer (1950)
3) Crystal settling	Emslie (1975), Broderick (1917)
4) Magmatic intrusives	Frietsch (1978), Giejer (1967)
Other Processes	
1) Pneumatolytic or hydrothermal alteration	Gillison (1956), Ross (1941)

Table 2: Examples of Kiruna and Taberg type Fe-Ti oxide deposits.

Location	Principal Mineral	Chemistry of Reserves (Wt%) Fe	Si	S	P	Ti	V	Reserves (million Mt)	References
KIRUNA TYPE									
Kiruna, Sweden	Magnetite	60	-	-	0.05	-	-	2460	Marelle, 1970
Grangesberg, Sweden	Magnetite Hematite	57	-	-	1	-	-	165	Marelle, 1970
El Algarrobo, Chile	Magnetite Hematite	61	5.5	0.02	0.18	-	-	100	Alvarado, 1970
Cerro de Mercado, Mexico	Hematite Magnetite Goethite	62	-	0.25	0.14	-	-	70	Klemic, 1970
Benson, New York	Magnetite Hematite	22-25	33	0.86	0.19	-	-	10	Klemic, 1970
TABERG TYPE									
Allard Lake, Quebec	Ilmenite Magnetite	36	4.3	0.3	0.02	32	-	350	Gross, 1970b
Tellnes, Norway	Ilmenite Magnetite	64-65	-	36	-	44.8	-	300	Korneliussen, et al., 1985
Bushveld Complex, S. Africa	Magnetite	42-60	-	-	-	14-20	2.5	200	Marelle and Abdulla, 1970
Taberg, Sweden	Magnetite	32	-	-	0.1	6-7	0.16	-	Gross, 1970a
Lake Sanford, New York	Magnetite	34	-	-	-	18-20	-	-	Klemic, 1970

Magnetite and ilmenite in carbonatites and kimberlite pipes. Important economic discoveries in carbonatites (rich in niobium, rare earth elements, and thorium) and kimberlite pipes (diamonds) has led to the study of magnetite and ilmenite derived from these sources in order to determine their usefulness in economic exploration. Because magnetite and ilmenite from a wide spectrum of rocks may occur together in gravels sampled during prospecting operations, studies have been undertaken to determine which properties of these Fe-Ti oxides are most likely to establish a carbonatitic or kimberlitic origin. This research was begun by Fleischer (1965) who found that also found that "electron-probe studies of carbonatite magnetite grains show that they are invariably zoned with a general decrease in Ti, Mn, Mg, and Ca towards their grain boundaries."

Studies involving ilmenite derived from kimberlite pipes have been undertaken by Lovering and Widdowson (1968), Mitchell et al. (1973), and Nixon and Kreston (1973). They found that ilmenite derived from kimberlites were higher in MgO and enriched in the trace elements Nb, Ta, Hf, Cr, and Co relative to basic igneous rocks. Gaspar and Wyllie (1983) continued this work by comparing the composition of ilmenite derived from carbonatites with those derived from kimberlites. They concluded that the

ilmenite from carbonatites can be distinguished from ilmenite in kimberlites by high MnO, very low Cr_2O_3, and high (Nb_2O_5 + Ta_2O_5). These studies present a means of using magnetite and ilmenite as prospecting tools in mining exploration.

All of these studies have provided the background that is essential to the understanding of the physical and chemical variations associated with magnetite and ilmenite from different igneous parent rocks and forms the basis for the use of these variations in provenance research. The latter studies with kimberlites and carbonatites also presents a viable example of using magnetite and ilmenite as provenance indicators.

Magnetite and Ilmenite in Sedimentary Rocks

Introduction

Magnetite and ilmenite often constitute a major portion of the heavy minerals found in sedimentary rocks, yet they have received little attention. This may be, as stated by Leupke (1980), because they are difficult to identify by mineral species in ordinary grain mounts and thin sections, or because they are so ubiquitous they are commonly thought to reveal little about source. Whatever the reason, investigations that have included these opaque Fe-Ti oxides have shown that they may yield significant information in several aspects of geology. The following

sections will discuss 1) the development of authigenic magnetite, its importance in sediments, and its effects on provenance determination, and 2) the alteration of detrital magnetite and ilmenite in sedimentary rocks and its influence on provenance interpretation.

Authigenic Magnetite in Sedimentary Rocks

The occurrence of authigenic magnetite in sediments and sedimentary rocks has been debated since the 1930's with Spiroff (1938) suggesting that it formed at low temperatures from meteoric water. Berner (1964), in a thermodynamic study of iron minerals in marine sediments showed that authigenic magnetite was thermodynamically possible in anaerobic marine environments. He suggested that at low H_2S concentrations and a slightly reducing environment magnetite should be expected to form in marine sediments. Even so, authigenic magnetite is not as common as the other authigenic iron minerals (hematite, siderite, and pyrite). This may be because of kinetic problems when dealing with Fe^{2+} and Fe^{3+} in the same structure. Whatever the reason, studies over the past few years have emphasized two main theories to explain its formation: 1) hydrocarbon seepage, in which the seepage of hydrocarbons or associated compounds through reservoir rocks causes a chemically reducing environment, which would lead to the reduction of hydrated ferric oxides and hematite to

magnetite (Donovan, et al., 1979; Elmore, et al., 1986; Benthian, et al., 1986), and 2) magnetotactic bacteria, in which magnetite is precipitated by bacteria under microaerobic conditions (Blakemore, 1975). Since the second theory has received much study over the past decade, and because it may also explain the relationship between authigenic magnetite and hydrocarbons, it will be discussed in more detail.

Magnetotactic bacteria were first recognized by Blakemore (1975) in a study of marine marsh muds. In a microscopic study he observed micro-organisms which rapidly migrated toward one side of the mud covered slide. His first thought was that it was a phototactic response, but later found that the bacteria responded to small magnets. This suggested that geomagnetism was the stimulus for the behavior of the cells. Further study by Frankel, et al. (1981) revealed that the bacteria formed magnetosomes consisting of enveloped, single-domain magnetite particles. They found that these magnetosomes are arranged in chains with a magnetic dipole moment parallel to the axis of motility. This magnetic dipole moment is sufficiently large that the cell is oriented along the geomagnetic field line and, therefore, cells with a north seeking pole swim north along the magnetic field lines and cells with a south seeking pole swim south. Because of the inclination of the

geomagnetic field, the north seeking cells migrate downward in the northern hemisphere and the south seeking cells migrate downward in the southern hemisphere. This is thought to be advantageous because this bacteria can only survive in microaerobic conditions (Blakemore, et al., 1985), and this polarity causes them to be directed toward, and kept in, the sediment away from the sediment-water interface.

Magnetotactic bacteria are ubiquitous in both marine and fresh water sediments (Blakemore, 1981), and have been found in deep-sea sediments (Kirshvink and Chang, 1984). McCabe (1986) has suggested, based on the presence of magnetic spherules within hydrocarbon solids, that bacterial degradation of oil may also result in the formation of bacterial magnetite. This would explain the association of authigenic magnetite with hydrocarbon seepage in reservoir rocks and support the belief of Lowenstam (1981) that "magnetite precipitation in the biosphere by organisms is the only known way in which authigenic magnetite forms at low temperatures and pressures."

Bacterial magnetite has a composition of pure Fe_3O_4. The cells are approximately 3um long with an average of 20 intracellular enveloped magnetite particles of diameter 30-200nm, which are organized in a single chain that traverses

the cell longitudinally (Mann, et al., 1984; Vali, et al., 1987). The magnetite particles are single domain grains with an octahedral morphology (this is dependent on the maturity of the grain, less mature particles are irregular to spheroidal), show a typical inverse spinel structure, and are preferentially aligned with the (111) axis parallel to the chain axis (Mann et al., 1984). The magnetite is created from soluble iron in the environment or by reducing ferric iron from a hydrated iron-oxide precursor (Blakemore, 1981; Mann, et al., 1984).

The presence of bacterially produced magnetite in modern sediments suggests that the very fine-grained (<1um) octahedrally shaped magnetite found in ancient carbonates may be of similar origin. Lowenstam (1981) hypothesized that the biomineralization process described above may have originated in the Precambrian. This hypothesis can be tested by looking for the unique crystal habits and pure iron composition of fine-grained magnetite in the sedimentary rock record. Magnetite having similar morphology and composition have already been described in Mississippian limestone (Friedman, 1954), as well as Jurassic, Silurian, Devonian, and Cambrian carbonates (McCabe, et al., 1983; Elmore,et al., 1986; Vali, et al., 1987). Further research may lead to significant information in rock magnetism and the classification of

microaerobic sediments. This will not interfere with magnetite as provenance indicators. This is because the grain size is limited to less than 10um and fall far beyond the lower limits of sand-sized grains.

Alteration of Magnetite and Ilmenite in Sedimentary Rocks

Geologists are interested in the alteration of detrital magnetite and ilmenite for several reasons: 1) the alteration of ilmenite is a primary source of Ti in soils (Anand and Gilkes, 1984), 2) the alteration of ilmenite increases the economic feasibility of placer deposits (Bailey, et al., 1956; Temple, 1966), 3) the alteration of magnetite is important in the formation of a chemical remanent magnetization in sedimentary rocks (Turner, 1979; Walker, et al., 1981; Reynolds, 1982), and 4) the alteration of both ilmenite and magnetite in sedimentary rocks records important information about the chemical environment after deposition, which is useful in the exploration for sedimentary copper and uranium deposits, as well as oil and gas reservoirs (Yurkova, 1970; Adams, et al., 1974). These studies are important to the understanding of the durability of magnetite and ilmenite in sedimentary rocks if they are to be used in provenance research. The following sections will discuss the probability of magnetite and ilmenite being preserved in

the rock record and the types of alteration associated with these grains.

Detrital magnetite and ilmenite have been found to be relatively stable in the rock record (Pettijohn, 1941; Pettijohn, et al., 1987). In general, it is believed that these Fe-Ti oxides are delivered in a relatively fresh state to sites of deposition and that the alteration of these detrital grains occurs after deposition and burial at some depth in the sediments (Austin, 1960; Van Houten, 1968; Darby, 1984). Although soil development also leads to the alteration of these grains (Anand and Gilkes, 1984), Van Houten (1968) concluded that "many of the grains delivered by tropical rivers are relatively unaltered minerals derived directly from bedrock rather than from soils in the source area." It can be inferred that this would also apply to arid climates where soil development is at its minimum.

The diagenesis of magnetite and ilmenite can be placed into two diagenetic environments: 1) an oxidizing environment, and 2) a reducing environment. The type of environment in which the grains are exposed controls the type of alteration products developed and the rate of alteration.

Oxidizing diagenesis. Oxidizing environments, such as those in which red beds are developed, are the most

stable environments for both magnetite and ilmenite. This is because these Fe-Ti oxides alter through the leaching of Fe^{2+} out of their structures. In an oxidizing environment this leaching results in the precipitation of an iron-oxide coating on to the surface of the grains (Gallagher, et al., 1968; Adams, et al., 1974). This coating has been described in sedimentary rocks by many authors (for example: Walker, 1967; Van Houten, 1968; Huguenin, 1973) and may explain the stability of magnetite and ilmenite in the rock record. The formation of this iron-oxide coating would act as a protective layer controlling further dissolution by requiring diffusion of cations and oxygen through a surface barrier. Siever and Woodford (1979) in experimental analysis of the weathering of mafic silicate minerals described a similar iron-oxide coating and suggested that "dissolution in the presence of oxygen is slowed by the armoring effect of a $Fe(OH)_3$ precipitate." Walker (1967) has suggested that the original precipitate on magnetite and ilmenite occurs as $Fe(OH)_3$, which is later converted to hematite. It may be inferred that this iron-oxide coating has the same retarding affect on alteration in Fe-Ti oxides as it does in mafic silicates. This iron-oxide coating creates the greatest protection in the absence of water in arid climates or rocks of low permeability. In humid climates or permeable rocks the

iron-oxide layer may be disrupted through the absorption of water (Huguenin, 1973), resulting in the exposure of fresh surfaces and an increase in the rate of alteration. Because water is a common accessory in sedimentary rocks, the gradual alteration of these Fe-Ti oxides is observed. Magnetite is commonly completely replaced by hematite (martite), which is responsible for the acquired chemical remanent magnetism (CRM) in red beds (Reynolds, 1982), and ilmenite shows various stages of alteration as described by Bailey, et al. (1956) and Temple (1966). These stages include 1) a patchy intergrowth of altered and fresh ilmenite, 2) an amorphous Fe-Ti phase or pseudorutile ($Fe_2Ti_3O_9$), and 3) leucoxene (a term used to describe the alteration products of ilmenite. It may consist of rutile (TiO_2) or its polymorphs anatase and brookite). In any case, the alteration of ilmenite leads to the leaching of iron until the residue consists of nearly 99 percent TiO_2. This shows the importance of alteration in the development of economic placer deposits.

Reducing diagenesis. Magnetite and ilmenite are least stable under reducing conditions, and alteration is at its maximum. It may be inferred that the absence of an oxidized iron-rich rind contributes to this rapid rate. In a reducing environment ilmenite has been found to be slightly more stable than magnetite (Adams, et al., 1974)

This is demonstrated in figure 1. According to this Eh-pH diagram magnetite and ilmenite would undergo significant leaching under acid conditions within the ferrous iron field. Adams, et al. (1974) believe that the "degradation and dissolution" of organic material would promote "the development of a more acid-reducing ground water in which iron would have been more soluble." Austin (1960) also postulated an acid-reducing environment "in which alteration is accomplished by fluids containing possible combinations of humic and sulfuric acid, H_2S, and the compounds and complexes of sulfur." These conditions have been supported by the presence of pyrite replacing magnetite and ilmenite in sedimentary rocks (Adams, et al., 1974; Dimanche and Bartholome, 1976; Reynolds, 1982; Morad and Aldahan, 1986). According to Dimanche and Bartholome (1976), in mildly reducing environments, ilmenite grains decompose into rutile which liberates Fe^{2+} as follows:

$$FeTiO_3 + 2H^+ = TiO_2 + Fe^{2+} + H_2O$$

The pyrite could then be formed by a reaction of Fe^{2+} with dissolved sulfide giving the net chemical reaction

$$FeTiO_3 + 2HS^- = TiO_2 + FeS_2 + H_2O + 2e^-.$$

It can be inferred that magnetite would follow a similar

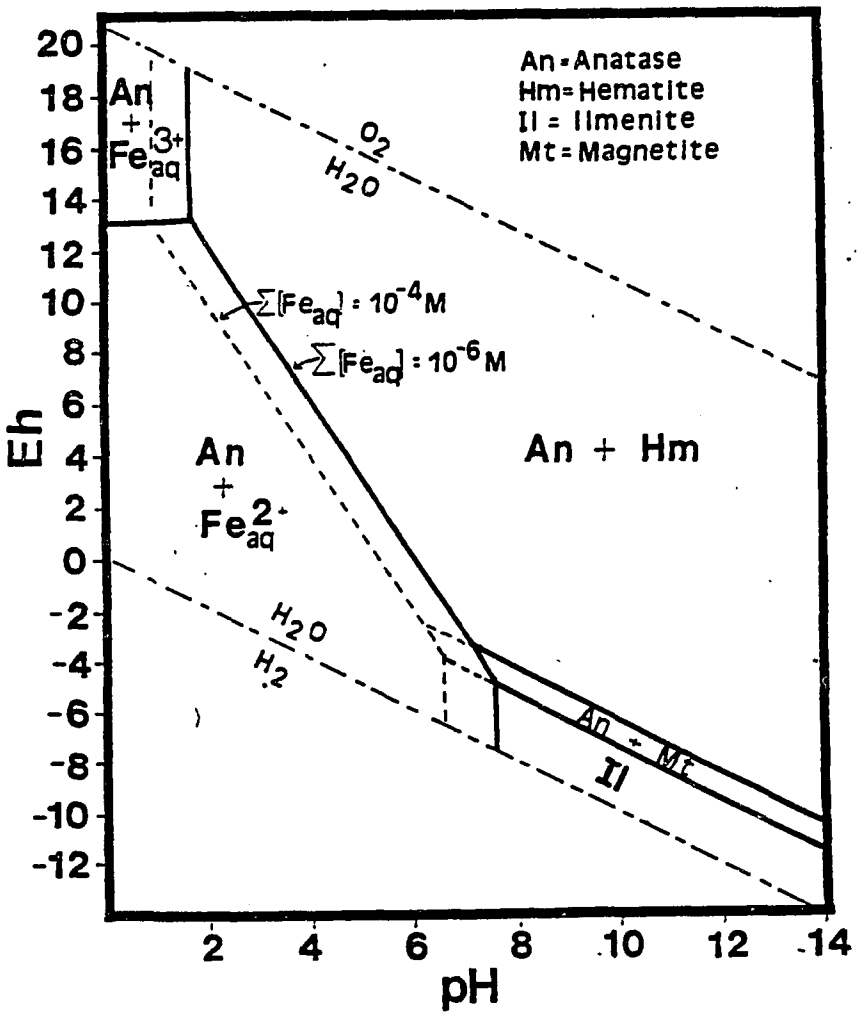

Figure 1: Eh-pH diagram illustrating the stability relations in the system Fe-Ti-O-H at 25°C and 1 atm, $[S_{aq}]=10^{-3}$, An=anatase, Mt=magnetite, Hm=hematite, Il=ilmenite, Py=pyrite (after Adams et al., 1974).

reaction, first forming hematite and releasing Fe^{2+} as follows

$$Fe_3O_4 + 2H^+ = Fe_2O_3 + Fe^{2+} + H_2O.$$

Pyrite would then form through the reaction

$$Fe_3O_4 + 2HS^- = Fe_2O_3 + FeS_2 + H_2O + 2e^-.$$

Adams, et al. (1974) suggest that the study of Fe-Ti-oxide alteration "can 1) aid recognition of originally organic-rich sediments from which the organic material has been removed or redistributed, and 2) define permeable channels along which organic rich solutions have migrated." This is important in the exploration for uranium and copper, as well as petroleum (Yurkova, 1970; Adams, et al., 1974).

In addition to the mobilization of iron in reducing environments other elements, such as Mn and Mg, are mobilized and lost into solution (Anand and Gilkes, 1974; Morad and Aldahan, 1986). Al, Si, Cr, and V show less mobilization and are usually retained with the alteration product, although the Si and Al found with the altered grains may be due to the crystallization of clays in the dissolution pits and cracks of the grains (Anand and Gilkes, 1984). Morad and Aldahan (1986) have also found that Ti may be mobilized on a "microenvironmental scale." They believe that this mobilization occurs during dissolution of the Fe-Ti grains and by their replacement by calcite, clay minerals, and quartz. The released Ti is

then precipitated as leucoxene in the interstitial space and on detrital quartz and feldspar. Reynolds (1982) suggested that the release of Ti takes place during replacement by pyrite, the Ti being reprecipitated as anatase.

In summary, the alteration of detrital magnetite and ilmenite grains in sediments occurs, in most cases, after deposition and burial. The alteration style and rate is then dependent on the chemical conditions within the sediments. Alteration occurs through dissolution or replacement, mainly by leucoxene and hematite (in oxidizing environments) and by pyrite (in reducing environments). Fe-Ti oxides may also be replaced by clays (usually illite or chlorite depending on chemical conditions), calcite (at pH>8) and quartz (at pH<8) (Morad and Aldahan, 1986). Dissolution, which is most pervasive under reducing conditions, results in the formation of microvoids, needle-like terminations, grain surface etching, and cracking (Morad and Aldahan, 1986). These cracks may be filled by clays giving an anomalous increase in the Si and Al content of the grains. Mn and Mg are mobilized during alteration whereas Si, Al, Cr, and V appear to be retained. Ti also shows mobilization in reducing conditions resulting in the formation of interstitial leucoxene.

Economic Deposits of Magnetite and Ilmenite in Sediments and Sedimentary Rocks

Opaque Fe-Ti oxides have been studied in placer deposits for economic reasons. Both magnetite and ilmenite have been mined in placer deposits for iron, titanium, and in some cases vanadium. One of the largest of these placer deposits is the Eneabba rutile-zircon-ilmenite sand deposit of western Australia. It is believed to contain between 25 and 30 million tons of recoverable heavy minerals (Lissiman and Oxenford, 1975). Other areas of important ilmenite placer deposits have included the Cabel area of western Australia (Welch, et al., 1975), the Roseland District of Virginia (Herz, et al., 1970), and the east coast of Florida (Martens, 1928). Magnetite deposits include beach deposits of southeast Papua, New Guinea, which consists of 21 million tons of sand with an average grade of 13 percent magnetite (Berkman, 1975) and ironsands from the North Island of New Zealand (Wright and Lowering, 1965). A possible future site for ilmenite exploration may be found in southeastern Brazil in the Rio Grande du Sol State. Concentrations of heavy minerals near Chui Village make up 47 percent of the sand of which opaques make up to 72 percent (ilmenite 58.4%) (DaSilva, 1979).

Besides placer deposits, magnetite has also been studied extensively in two other sedimentary ore deposits 1) banded-iron formations and 2) hydrothermal iron

deposits. Many theories have been proposed for the origin of banded-iron formations (see Maynard, 1983; Guilbert and Park, 1986), whereas the hydrothermal iron deposits have been found to be directly associated with calc-alkaline plutonism (Guilbert and Park, 1986) in which iron-rich hydrothermal fluids released from the pluton replace sedimentary rock (commonly carbonates). Examples of the banded-iron formations include the Lake Superior region Gunflint Formation and the Clinton Formation of the Eastern United States. El Romeral, Chile and Iron Springs, Utah are examples of hydrothermal iron deposits.

Discussion

The study of magnetite and ilmenite in igneous and sedimentary rocks has paved the way for future study of these opaque minerals in provenance research. Studies in igneous rocks have emphasized the presence of physical and chemical variations in magnetite and ilmenite in relationship to parent rocks and have provided the knowledge necessary for the determination of provenance. As seen in the study of kimberlites and carbonatites these minerals, based on these studies, have been successfully used in provenance research. Studies in sedimentary rocks have determined that magnetite and ilmenite are relatively stable in the rock record and have found that the effects of authigenic magnetite on provenance interpretation is

limited because of its small grain size. These findings are important if magnetite and ilmenite are to be used in ancient as well as modern sediments. The sedimentary banded-iron formations and hydrothermal iron deposits provide an additional sedimentary source of magnetite and continued work is necessary to determine the influence of these deposits on provenance research.

CHAPTER IV

PROCEDURES

Sample Collection

Thirty-one modern sand samples from eight crystalline parent rock types were collected for petrographic and chemical analysis. These sands were derived from stream and beach deposits draining known rock types from various parts of the world (Fig. 21). This sampling strategy allows one to group the sands according to their parent rock type as well as test for differences between like rock types from different parts of the world. In addition, a single sand sample of unknown source will be analyzed in order to test the techniques developed during this study.

Sample Preparation

The sand samples were washed to remove the clay size fraction and air dried. The sands were then sieved to separate the fine-sand fraction (150um to 250um) that was used for analysis. The fine-sand fraction was then weighed. The detrital Fe-Ti oxides were separated from the fine-sand fraction magnetically; magnetite manually by use of a large bar magnet and ilmenite with a Frantz Model LB-1 Barrier magnetic separator with the following operating conditions 1) a forward inclination of 30 degrees, 2) a side inclination of 50 degrees, and 3) an extraction range of 0.1 to 0.4 amps. Both the separated magnetite and

Figure 2: Location map showing world wide distribution of sample locations.

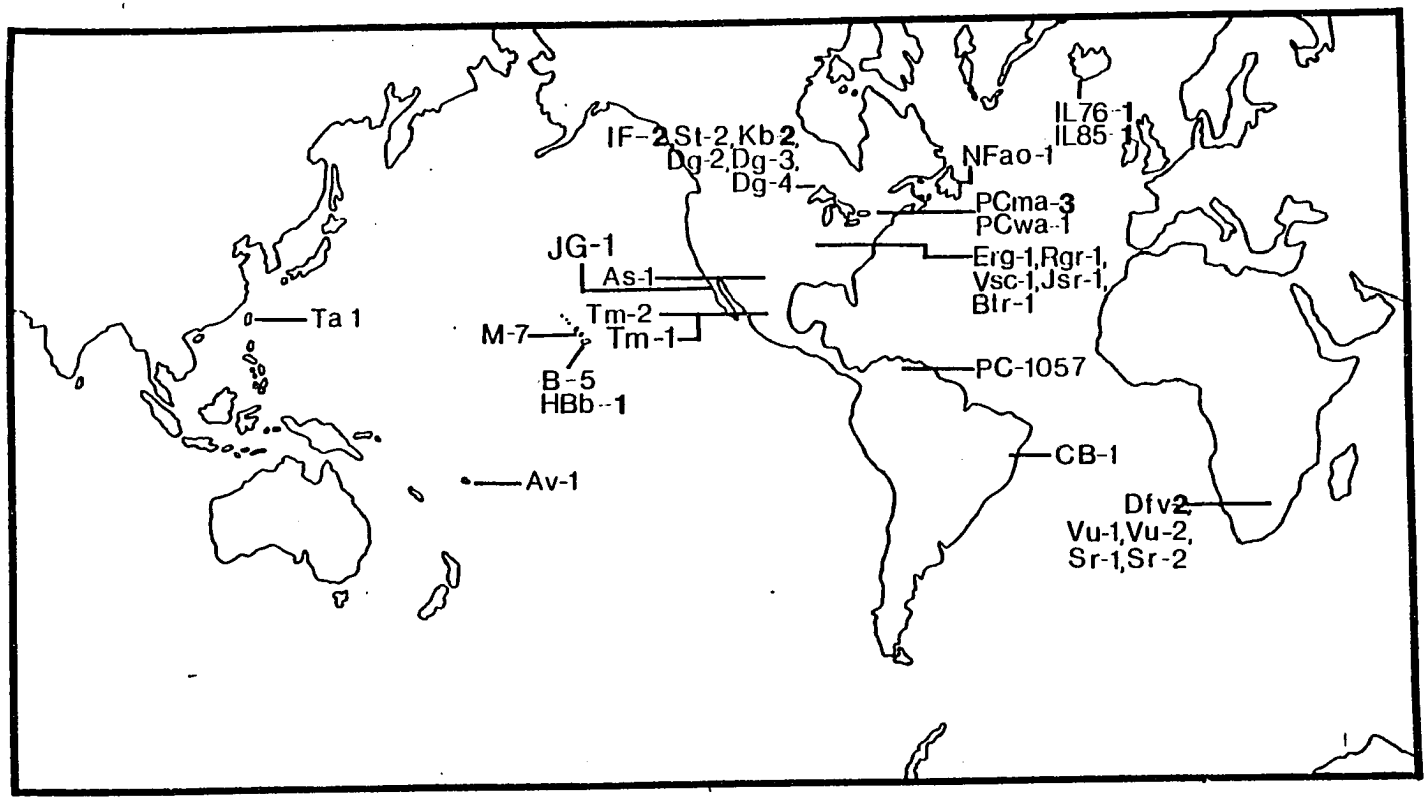

ilmenite fractions were weighed separately in order to approximate the percent in the fine sands. Polished grain mounts were prepared separately for magnetite and ilmenite, as well as the fine sand fraction from each sample in order to compare the light fractions to the opaque Fe-Ti oxides.

Terminology

In this paper the term "ilmenite" is used to include all anisotropic ilmenite-hematite solid solution phases that show tan/pink tint in reflected light, and contain greater than 30 percent TiO_2. The term "magnetite" is used to refer to all isotropic phases in the magnetite-ulvospinel solid solution series that show a pale gray to light pink tint in reflected light, and contain less than 30 percent TiO_2. The term "exsolution" will be used in the broadest sense for morphological descriptive purposes and will include both true solid-solution exsolution textures such as hematite lamellae in ilmenite and ulvospinel and pleonaste in magnetite, and oxidation "exsolution," which is the result of high-temperature oxidation and the formation of ilmenite, rutile, and hematite lamellae in magnetite (see Haggerty, 1976b for details).

Modal Analysis

Modal analysis of the polished sections were based on textural differences between grains. Magnetite was divided into six different grain types based on exsolution

textures. These grains are defined as 1) magnetite + ulvospinel, 2) magnetite + pleonaste, 3) magnetite + ilmenite [trellis- and composite-types (sandwich-types were counted with the composite-types)], 4) magnetite + hematite, 5) magnetite + pseudobrookite, and 6) homogeneous magnetite grains ± silicate and sulfide inclusions. In cases where two or more of these textural types occurred together the following procedure was taken 1) the presence of ulvospinel was counted over all other textures, 2) the presence of pleonaste + ilmenite was counted as a pleonaste texture, 3) ilmenite in magnetite, which occurs as two types, lamellae parallel to the (111) magnetite plane (trellis-type), and composite-type magnetite-ilmenite intergrowths, were counted with the composite-type getting priority over the trellis-type. Hematite and pseudobrookite were counted on a presence-absence basis only.

Ilmenite was divided into three grain types 1) homogeneous grains, 2) grains that contain hematite lamellae, and 3) twinned grains.

Electron Probe Microanalysis

Electron probe microanalysis was carried out for eight elements (Ti, Al, Mg, Mn, Si, Cr, V, Fe) with an ARL-EMX 3 channel autoprobe at the University of Cincinnati and a Cameca Camebax SX-50 at the University of Chicago. All

analyses were performed with a 15 kv electron beam regulated at 0.1200 microamps on brass. Standards used at the University of Cincinnati include 1) ilmenite for Fe, Ti, and Mn, 2) diopside for Si, 3) chromite for Al, Cr, and Mg, and 4) V_2O_5 for V. Standards used at the University of Chicago include 1) ilmenite for Ti, 2) V_2O_3 for V, 3) magnetite for Fe, 4) diopside for Si and Mg, 5) anorthite for Al, 6) Mn-metal for Mn, and 7) Cr_2O_3 for Cr. Bence-Albee (1968) correction methods were used to convert raw count data to weight-percent oxide. All Fe was calculated as FeO for analysis and recalculated to weight-percent Fe_2O_3 and FeO following the procedure of Carmicheal (1967). Approximately twenty homogeneous grains were chosen from each slide for the analysis of magnetite and about ten homogeneous ilmenite grains were chosen from each slide. Two points per grain were analyzed in order to assess the variability of the chemical compositions of individual grains. These points were then averaged giving the results found throughout this paper.

CHAPTER V

GEOLOGY OF SELECTED PROVENANCE AREAS

Introduction

In choosing the following sample areas an emphasis was placed on selecting rocks in which primary magnetite and ilmenite occurs i.e., sandstones, meta-sandstones, etc. are excluded. Some parent rock types contain both primary and secondary magnetite, such as serpentinized ultramafics, and some of these were included in the sample suite in order to determine the effects of these secondary minerals on the sand-sandstone composition. The following section is a general description of the geology of the parent rock types sampled separated into felsic, intermediate, mafic, ultramafic, and sedimentary genetic types. General locations, rock types, and sample numbers are given in Table 3.

Felsic Samples

Geology of Surgarloaf Peak, New Mexico

Surgarloaf Peak, a quartz monzonite to granite porphyry, forms most of the northern part of the Organ Batholith and is well exposed in Surgarloaf Dome at Aquirre Springs, at Agustin Pass, and throughout the Organ Mining District, and is located approximately 24Km east of Las Cruces, New Mexico in the Organ Mountains (Fig. 3). The Surgarloaf Peak quartz monzonite is roughly oval in shape

Table 3: General locations, rock types, and sample numbers of the sands collected for the current study.

ROCK TYPE		LOCATION	SAMPLE NUMBER
Felsic Plutonic	Granite	Graniteville granite, Missouri	Erg-1
		Favela granite, Rio de Janiero, Brazil	Cb-1
	Tonalite	Saganaga tonalite, Minnesota	St-2
	Qtz. Monzonite	Surgarloaf Peak qtz. monzonite, New Mexico	As-1
Felsic Volcanic	Rhyolite/ Ashflow tuff	Stouts Creek rhyolite, Missouri	Vsc-1 Jsr-1* Btr-1*
		Royal Gorge rhyolite, Missouri	Rgr-1
		Rooiberg Fesite, South Africa	Dfv-2
Intermediate Volcanic	Andesite	Nevado de Toluca, Mexico	Tm-1, Tm-2
		Ovalau, Fiji	Av-1
		Kuanyinshan Volcano, Taiwan	Ta-1
Mafic Plutonic	Gabbro/. Norite.	Duluth Gabbro, Minnesota	Dg-2, Dg-3, Dg-4
		Bushveld Complex, South Africa	Sr-1, Sr-2 Vu-1, Vu-2
Mafic Volcanic	Basalt	Puu Mahana, Hawaii Island, Hawaii	HBb-1
		Near Waiki'i, Hawaii Island, Hawaii	B-5
		Pa'ia, Maui	M-7
		Haimaey Island, Iceland	IL76-1
		Reykjanes Peninsula, Iceland	IL85-1
		North Shore Volcanic Group, Minnesota	Kb-2
Metamorphosed Intrusives	Meta-anorthosite	Marcy-type, Adirondacks, New York	pCma-3
		Whiteface-type, Adirondacks, New York	pCwa-1
	Serpentinized Ultramafics	Loma de Hierro, Venezuela	PC-1057
		Lewis Hills ophiolite, Newfoundland	NFao-1
Sedimentary	Banded-Iron Formation	Gunflint Banded-Iron Formation, Minnesota	IF-2

* undifferentiated rhyolite/ashflow tuff from Johnsons Shut-ins State Park, Missouri (stream sands from Black River draining Stouts Creek or Royal Gorge Rhyolite + others).

Figure 3: Location map of Organ, San Agustin, and southernmost San Andres Mountains, New Mexico (after Seager, 1981).

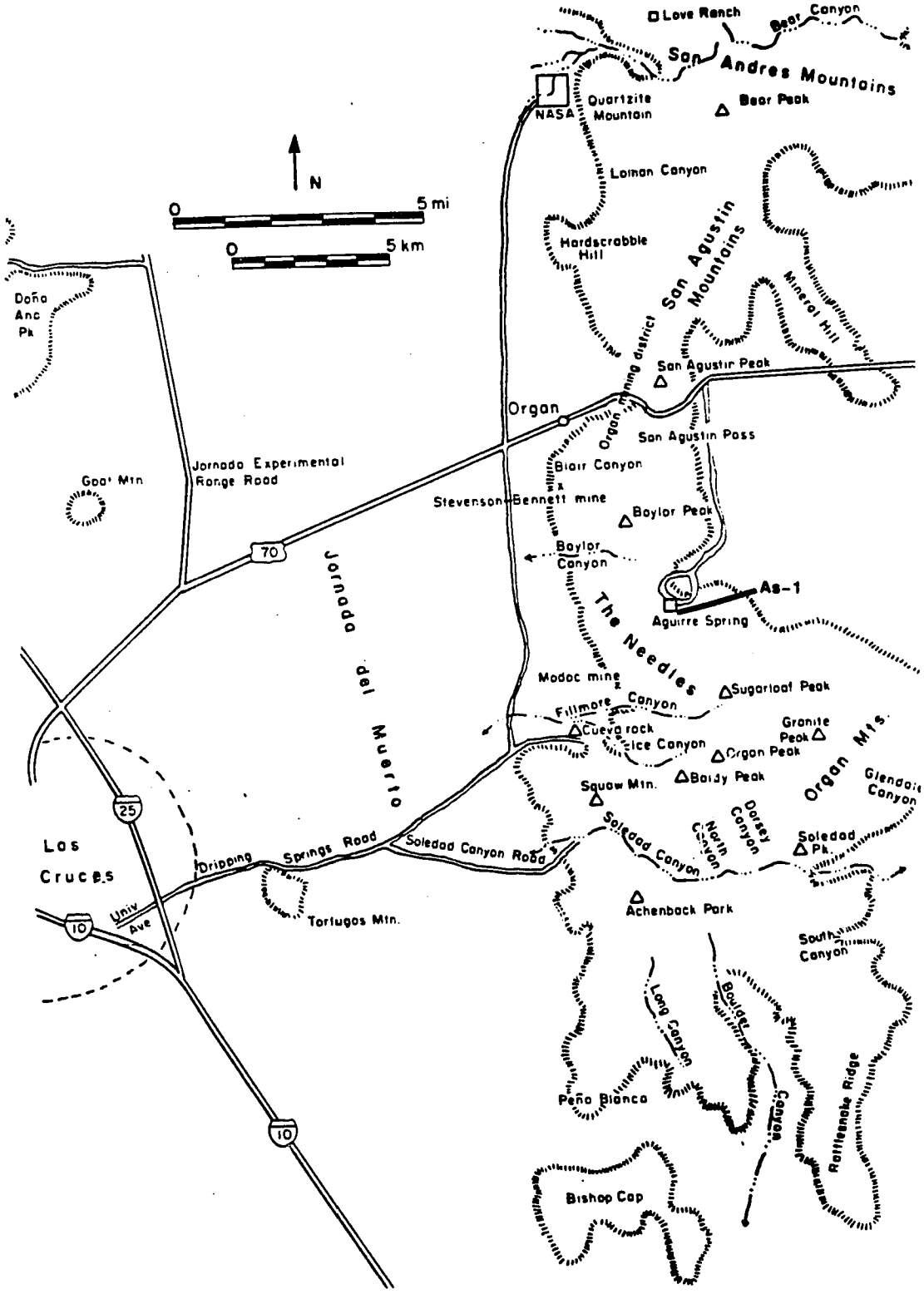

and approximately 13Km long. Biotite from San Agustin Pass has indicated an age of about 32.8 m.y. (Loring and Loring, 1980). Modal analysis has indicated that the rock is composed of orthoclase perthite (33%), plagioclase (oligocene, 38%), quartz (ranging from 10 to >20%), biotite and hornblende (10-12%), and opaques (magnetite and ilmenite, 2%) (Seager, 1981).

Geology of the Saganaga Batholith

The Saganaga Batholith is located about 48Km northwest of Grand Marais, Minnesota along the Minnesota-Ontario border (Fig. 4). The batholith occupies about 322 square kilometers and has maximum dimensions of about 32Km east-west and 23Km north-south. It is a composite intrusion containing several rock types, the dominant being gray tonalite (Hanson, 1972).

The batholith intrudes greenstone and the Northern Light Gneiss and is overlain along the western margin by metaconglomerate and associated metasedimentary rocks of the Knife Lake Group (Fig. 5; Hanson, 1972). Whole rock isochron Rb-Sr ages, and the U-Pb analyses of zircon and sphene are in close agreement and indicate an age of 2,700-2750 m.y. (Goldich et al., 1972).

The principal minerals of the tonalite are oligoclase (An_{28}, 64%), quartz (21%), hornblende (7%), biotite (4%), and microcline (2%). The accessory minerals include

Figure 4: Generalized geologic map of Saganaga Lake - Northern Light Lake area, Minnesota (after Hanson, 1972).

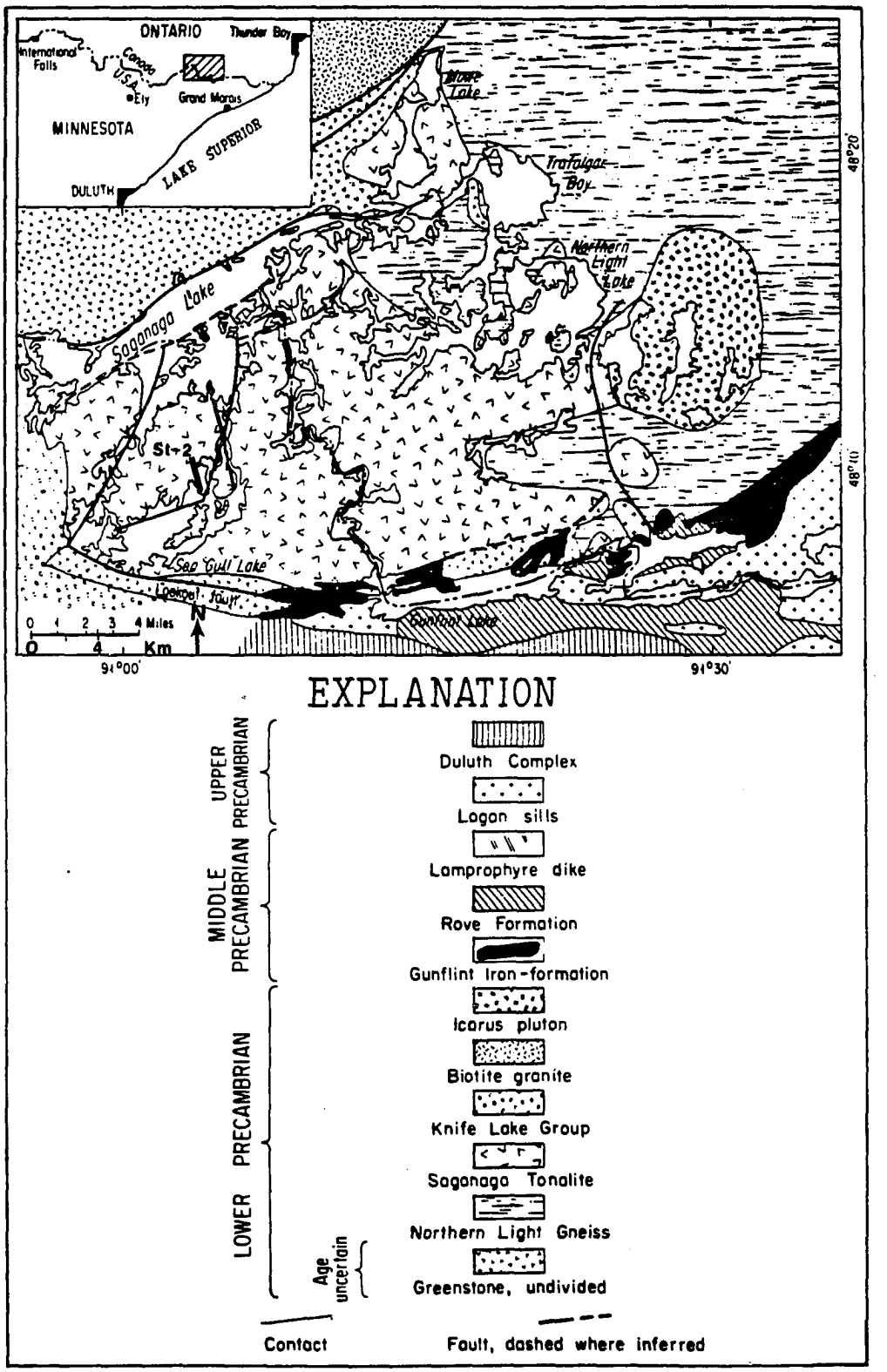

augite, sphene, magnetite, ilmenite, apatite, and zircon (Hanson, 1972).

Geology of the Favela Granite, Brazil

The Favela Granite, located in Rio de Janeiro, Brazil (Fig. 5), consists of a fine-to-medium grained light gray undeformed granite, which generally forms blankets, sheets, and mushroom-or tongue-shaped plutons (Leonardos, Jr., 1973; Pires et al., 1982). These granitic rocks are the youngest Precambrian rocks in the area with an age of approximately 450 m.y. (Leonardos, Jr., 1973).

Petrographic analyses of the Favela granite shows that feldspar (orthoclase+albite+anorthite, 59%) and quartz (28%) are the principal minerals with minor amounts of hypersthene (5%), corundum (3%), and opaques (magnetite+ilmenite, 2%) (Leonardos, Jr., 1973).

Geology of the St. Francois Mountains, Missouri

The St. Francois Mountains are located in southeastern Missouri (Fig. 6) and are thought to represent a zone of continental accretion (Berry and Bickford, 1972). The granitic intrusives and felsic volcanics exposed at the St. Francois Mountains, which structurally form the central part of the Ozark uplift, cover an area of nearly 8000 square kilometers and in actual outcrop cover about 900 square kilometers (Sides et al., 1981). Radiometric age dates (zircon U-Pb ages) indicate that these rocks are

Figure 5: Geologic map of the Rio de Janeiro area, Brazil (after Savage, 1986).

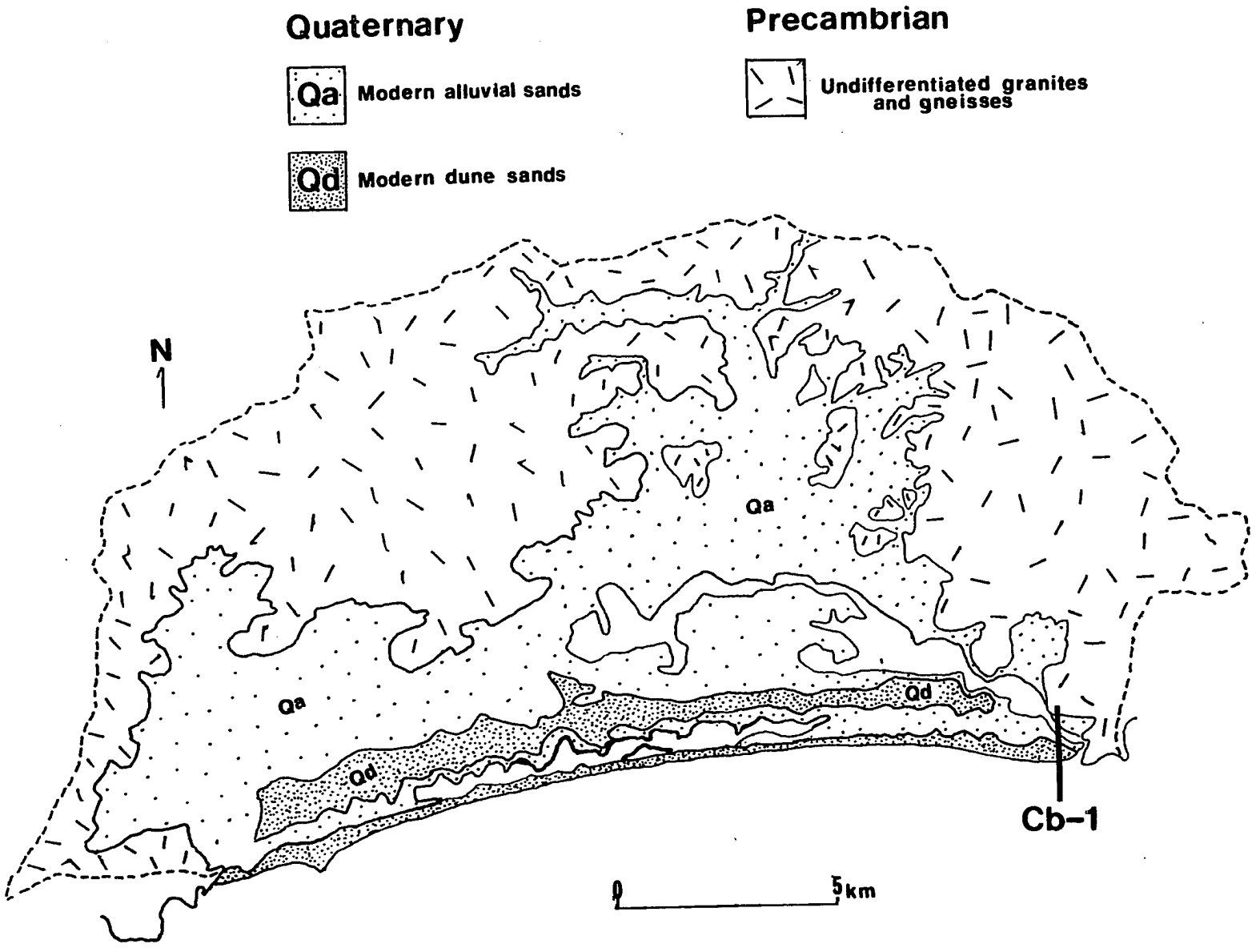

Figure 6: Location map of the St. Francois Mountains, southeast Missouri.

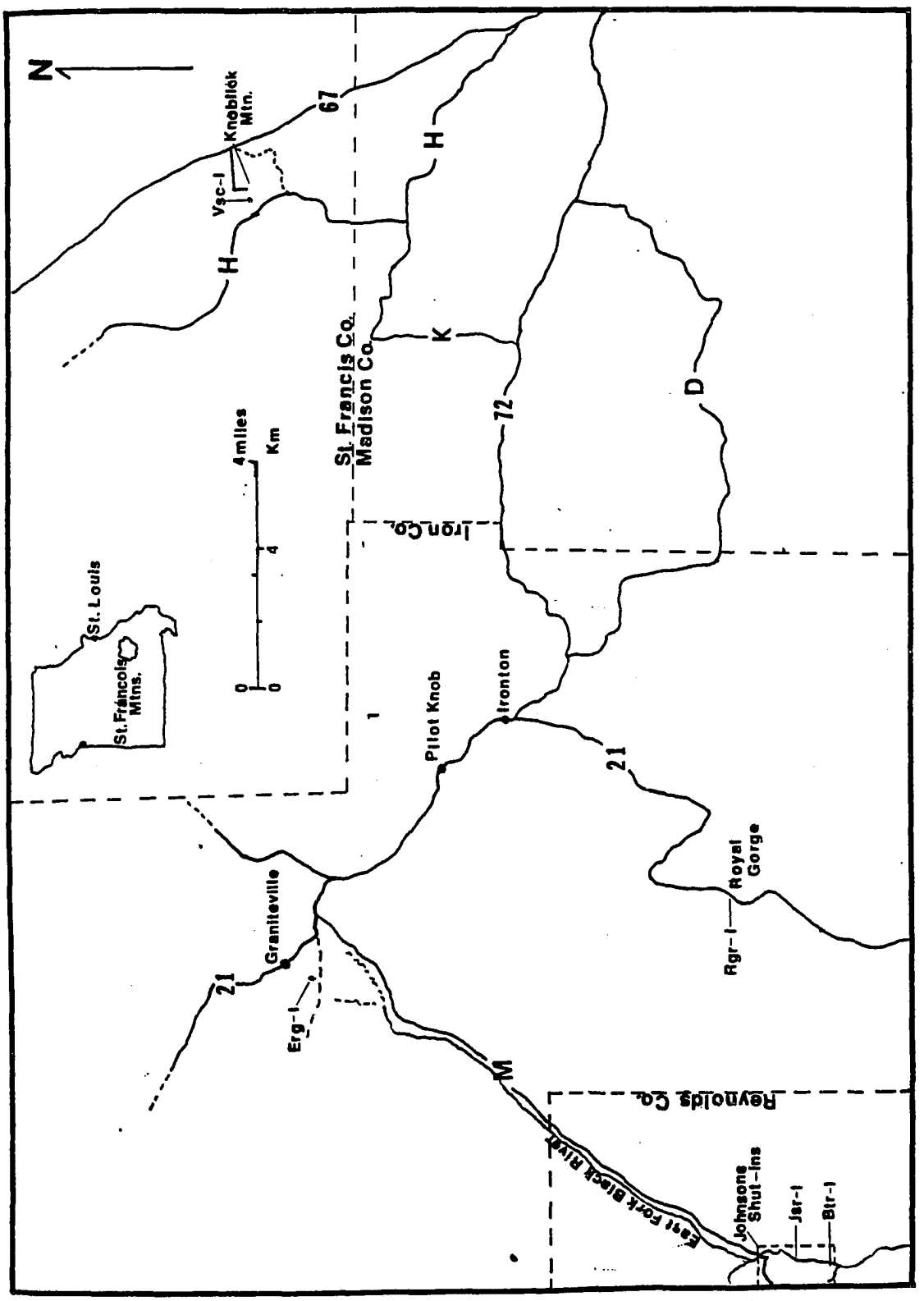

probably comagmatic and formed approximately 1.4 b.y.a. to 1.5 b.y.a. (Bickford and Mose, 1975).

The oldest rocks exposed in the St. Francois Mountains comprise a thick series of rhyolite flows and ashfall tuffs which are several thousand feet thick. These rocks make up almost two-thirds of the igneous exposures in the St. Francois mountains and are dominant in the western part of the area, whereas granite dominates in the east (Tolman and Robertson, 1969). This distribution of rock types and the recognition by Anderson (1962) that most of the volcanic rocks were of ash-flow origin led to the recognition of a large subsidence structure in the western part of the mountains, which has been interpreted to be of volcanic origin and called the Taum Sauk Caldera (Anderson, Jr. et al., 1969).

Three samples were collected from the St. Francois Mountains and the following is a discussion of the geology of these rock types.

Geology of the Graniteville Granite. The Graniteville granite is part of the composite Precambrian batholith located in Southeastern Missouri. The Graniteville granite is well exposed at Elephant Rock State Park near Graniteville, Missouri and is described by Tolman and Robertson (1969) as a medium-to coarse grained, red granite composed predominantly of quartz, feldspar

(orthoclase and microcline perthite), and biotite with the dominant accessories being magnetite and fluorite with minor zircon, epidote, rutile, garnet, ilmenite, galena, molybdenite, and chalcopyrite.

Geology of the Royal Gorge Rhyolite. Tolman and Robertson (1969) divided the pre-batholithic rocks of the St. Francois Mountains into two groups based on stratigraphic position and chemical composition. According to this classification all rock units stratigraphically below the Ketcherside tuff are placed in the Middlebrook Group and all those stratigraphically above the Ketcherside tuff belong to the Van East Group. The Royal Gorge Rhyolite, whose type locality is located at the Royal Gorge Shut-ins along Missouri Highway 21, belongs to the Middlebrook Group occurring stratigraphically below the Ketcherside tuff. As described by Tolman and Robertson (1969) the Royal Gorge rhyolite is typically light brown to purple and contains perthitic feldspar (5-20% of the rock), quartz, magnetite, and chlorite phenocrysts in an aphanitic groundmass. Because of megascopic similarities with facies of the Stouts Creek rhyolite and the absence of the Ketcherside tuff in some areas the thickness and areal extent of the Royal Gorge rhyolite is uncertain.

Geology of the Stouts Creek Rhyolite. The Stouts Creek rhyolite, a member of the Van East Group of Tolman

and Robertson (1969) and consisting of the Grassy Mountain ignimbrite and Lake Killarney unit of Sides (1976), is the most extensive unit mapped in the St. Francois Mountains covering an area of approximately 1,046 square kilometers. Tolman and Robertson (1969) have divided the Stouts Creek rhyolite, whose type locality is at Stouts Creek Shut-ins, Missouri, into three units. The lower unit is described as a "brownish-purple to gray chocolate brown" coarse aphanite with quartz and feldspar phenocrysts. Its average thickness is approximately 30m.

The middle unit is a purple aphanitic rhyolite with phenocrysts making up 10% to 20% of the rock. Quartz and feldspar phenocrysts predominate with accessories of magnetite, chlorite, fluorite, zircon, and apatite. This unit is approximately 120m thick.

The upper unit is predominantly a flow breccia whose thickness ranges from < 30m to > 60m. Total thickness of the Stouts Creek rhyolite may reach more than 200m.

Geology of the Rooiberg Felsite, South Africa

The Rooiberg Felsite is located entirely within the limits of the Bushveld Complex of South Africa (Fig. 7). It roofs and is intruded by the mafic layered rocks and granites of the Bushveld Complex and has been found to be approximately 2.1 b.y. old (Twist and French, 1983). The Rooiberg episode terminated volcanic activity in the

Figure 7: Generalized geologic map of the Bushveld Complex, South Africa (after Tankard et al., 1982).

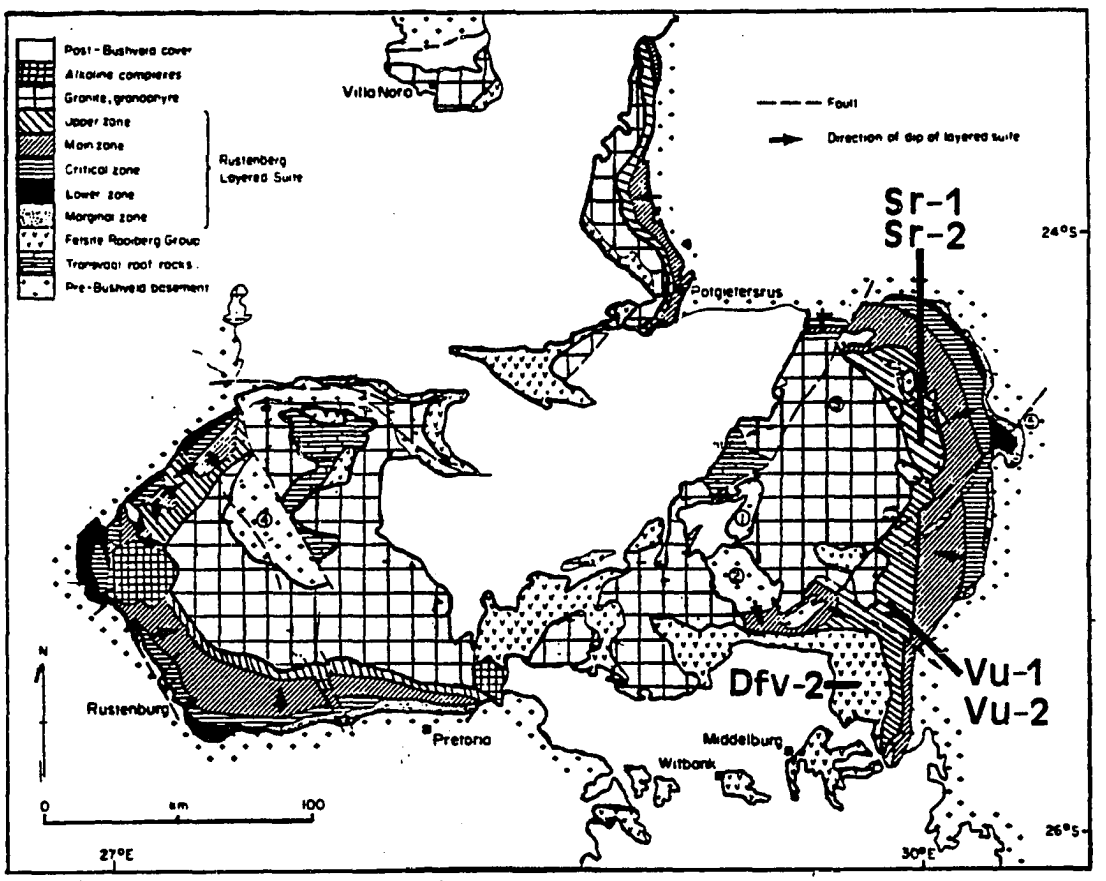

Transvaal basin and heralded the emplacement of the Bushveld Complex, but despite the close spatial and temporal relationship between these two events the nature of their relationship is not clear.

A review of the Rooiberg Felsite by Twist and French (1983) indicates that the felsite unit, which may exceed 5Km in thickness and cover an area greater than 50,000 square kilometers, is dominated by rhyolitic to dacitic lavas with minor pyroclastic and sedimentary rocks. Significant metamorphism occurs at the contact of the felsite with the intruded granites and layered mafic rocks of the Bushveld Complex, and although primary features such as flow banding and porphyritic textures are preserved, the groundmass is often recrystallized to a microgranular hornfels. Petrographically the felsite is microporphyritic with phenocrysts generally constituting less than 5 percent of the rock. Feldspar (K-feldspar and albite) is the most common phenocryst with minor quartz, amphibole, clinopyroxene, and fayalite olivine. The groundmass frequently contains laths of 0.2 to 2mm in length of polycrystalline quartz with minor clinopyroxene and magnetite.

Intermediate Samples

Geology of the Kuanyinshan Volcanic Rocks, Northern Taiwan

Kuanyinshan volcano, located in northern Taiwan (Fig. 8), is a single, central-vent composite volcano of Plio-Pleistocene to early or middle Pleistocene age (Yen, 1958). Three stages of volcanic activity have been recognized with the types of eruptions changing from Strombolian in the first stage to sub-Plinian or Plinian in the late stage. The present structure of the volcano is controlled by the Plinian eruption which resulted in the partial destruction of the early formed cone and development of an amphitheater shape on its eastern side (Hwang and Lo, 1986).

The lava flow sequence can be divided into three layers from the bottom to top 1) an augite basaltic andesite flow, 2) a two-pyroxene andesite flow, and 3) a Hypersthene andesite and Hypersthene-hornblende andesite flow. Hwang and Lo (1986) believe that these layers, or stages, of volcanic activity are related to "bulk chemical variations...formed by processes of differentiation, compositional stratification, and mixing in the magma chamber...," and that the "chemical variations of the volcanic rocks formed in each stage of activity are attributed to the different degree of fractionation." They concluded that the fractionated minerals from the first to the third stage of activity were augite-hornblende-

Figure 8: Location map of Kuanyinshan andesites, Taiwan.

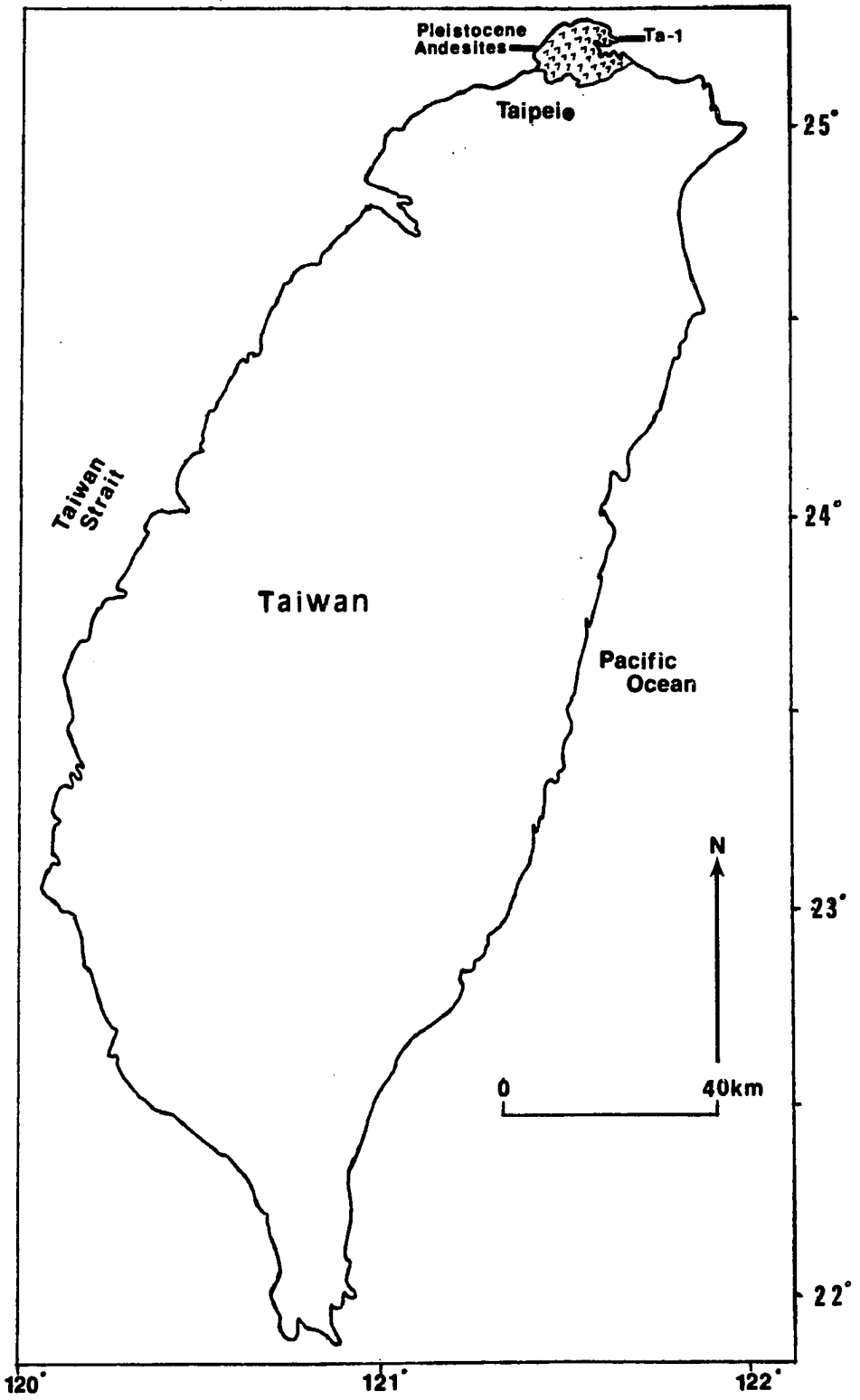

magnetite, hornblende-plagioclase-magnetite, and plagioclase-magnetite, respectively.

Geology of Ovalau, Fiji

The island of Ovalau, Fiji is located off the eastern coast of Viti Levu in longitude 178°50'E and between latitude 17°30'S and 17°50'S (Fig. 9). According to Ibbotson (1961) the island was formed by an andesitic volcano (augite-hornblende andesite) that led to the circular nature of the island, and its even, steep slopes that rise to a central vent. The caldera wall, which is breached on the southeastern and eastern sides, rises about 610 meters above sea level. The crater area is approximately 6 kilometers long and 4 kilometers wide. Augite and hornblende are the most abundant minerals with magnetite the most abundant accessory mineral, forming placer iron-sand deposits along the coast. The age of volcanic activity is believed to be from early to late Pliocene. Whole rock chemical data is not available.

Geology of Nevado de Toluca Volcano, Mexico

Nevado de Toluca volcano is located within the Mexican Volcanic Belt approximately 80Km west-southwest of Mexico City (Mooser, 1969) (Fig. 10). It is the fourth highest of the major volcanoes of central Mexico ($\approx$ 4,565m) with an elliptical crater at its summit, about 0.5Km by

Figure 9: Generalized geologic map of Ovalau, Fiji (after Ibbotson, 1960).

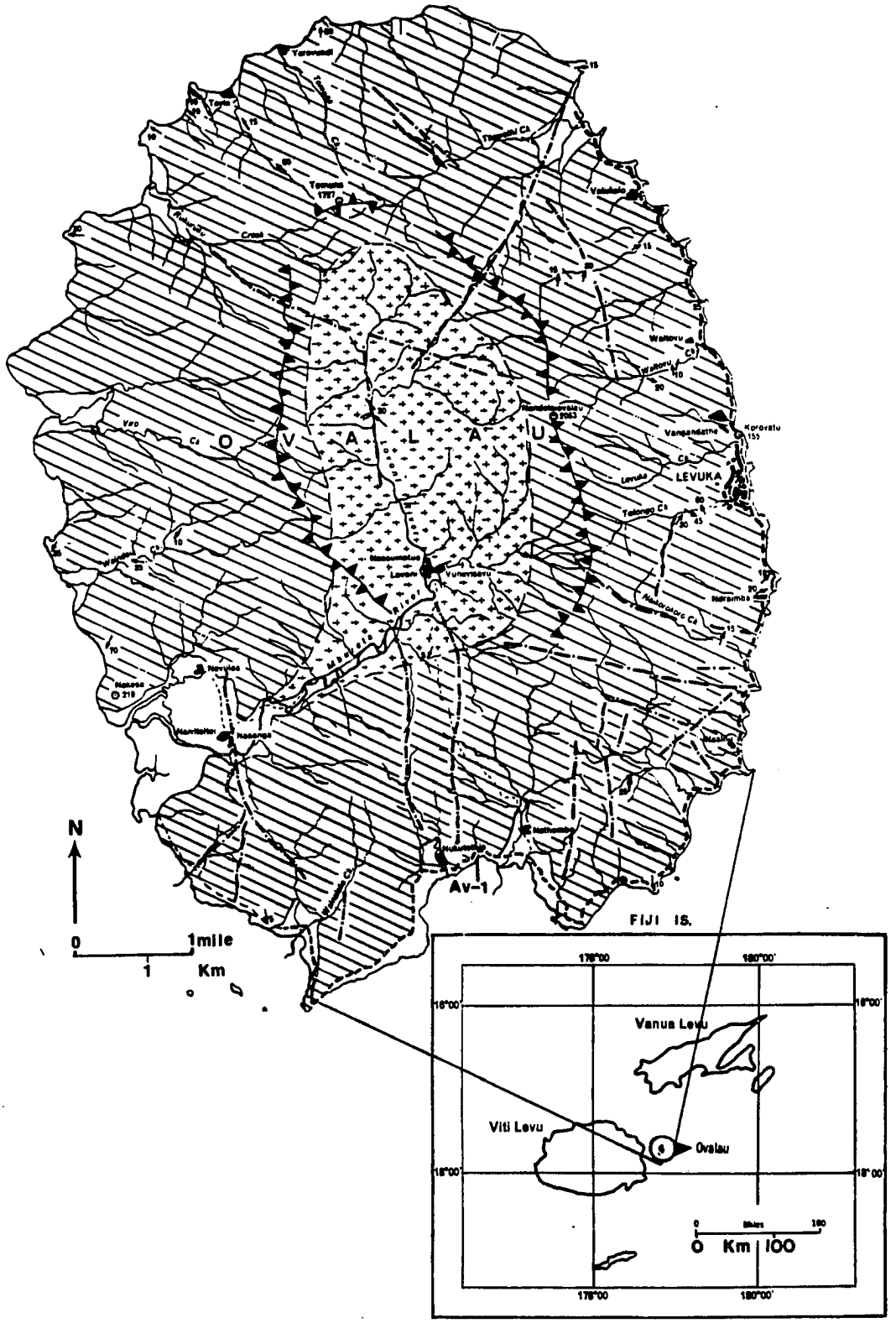

Figure 10: Generalized geologic map of Nevado de Toluca, Mexico (after Bloomfield and Valestro, 1974).

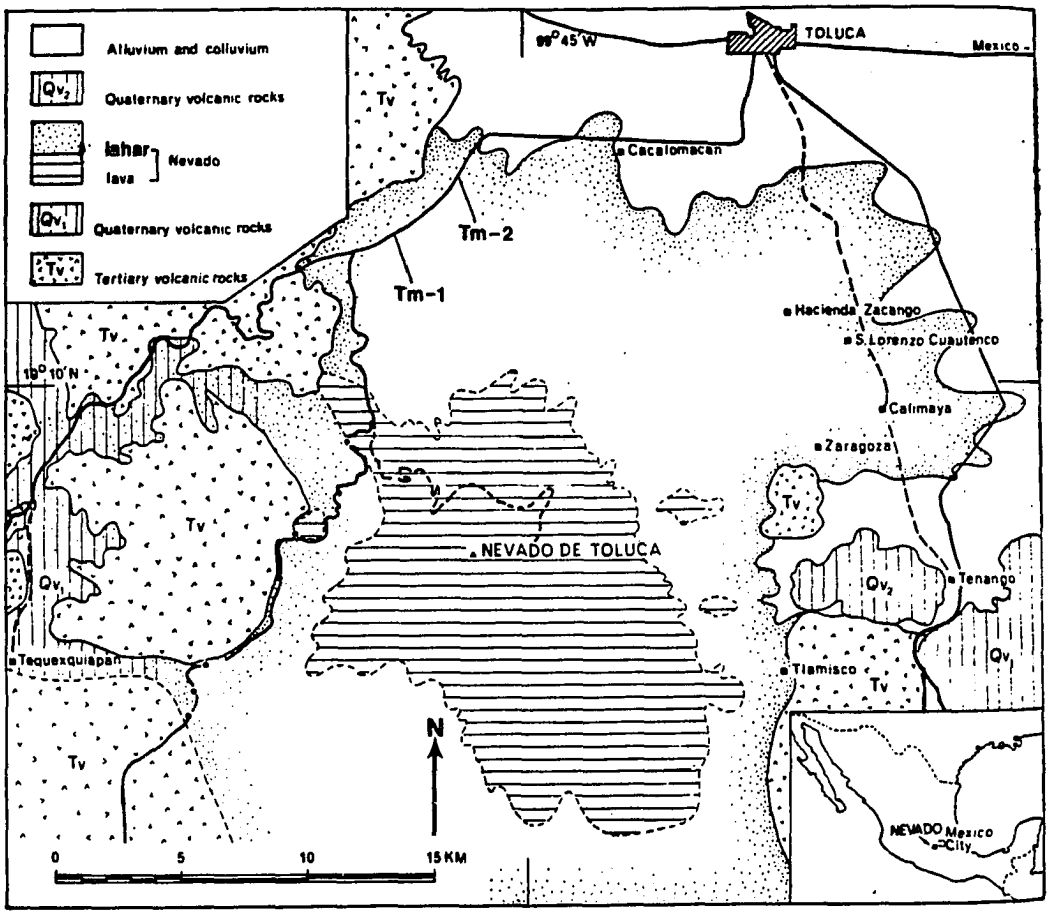

1.5Km in size, and a small dome which rises about 100m from the center of the crater (Bloomfield and Valestro, 1974).

According to Bloomfield and Valestro (1974) Nevado de Toluca is an eroded, polygenetic, strata volcano made up largely of dacitic and andesitic flows. Its piedmont slopes are mantled by thick lahar and fluvial deposits which are capped by pumice beds. The central dome is a dacitic plug that has blocked a central vent. Younger flows of andesitic basalt, Pleistocene to Holocene in age, flank the mountain to the east. The age of formation of the original lava stratavolcano is not known. Attempts at dating the mafic minerals of the andesite by the conventional K-Ar method have not been successful (Fitch and Miller, 1971; Fitch, 1972). In general, Nevado de Toluca is thought to be of late Pleistocene to Quaternary in age (Mooser, 1969; Bloomfield and Valestro, 1974).

Mafic Samples

Geology of the Bushveld Complex, South Africa

The Bushveld Complex, located in the Transvaal Basin of South Africa (Fig. 7), is a layered intrusion of ultramafic and mafic rocks that underlies an area of approximately 65,000 square kilometers. A review of the geology of the Bushveld Complex by Tankard et al. (1982) indicates that the Complex is approximately 2,095 $\pm$ 24 m.y. old. Regional gravity surveys of South Africa show that

the Bushveld Complex has a clover-shaped outline consisting of four lobes with the layered series (Rustenburg Layered Sequence) dipping toward the center of the Complex at approximately 10° to 25°. Of these lobes the eastern lobe has the best exposure of the layered sequence.

Tankard et al. (1982) has formally proposed five zones to be identified within the Eastern lobe 1) the marginal zone: a fine-grained noritic rock, characterized by the presence of metasedimentary inclusions, found between the various rock units of the layered sequence and the country rock, 2) the lower zone: made up of approximately 500m of feldspathic bronzite, harzburgite, and norite, 3) the critical zone: consisting of approximately 1500m of alternating layers of chromitite, pyroxenite, norite, anorthosite, and dunite, 4) the main zone: characterized by the appearance of abundant cumulus clinopyroxene and an absence of chromite. It consists of 3500m of gabbro and norite with minor anorthosite, and 5) the upper zone: marked by the appearance of magnetite, this zone is approximately 2000m thick and has been divided into three subzones (from bottom to top) on the basis of the appearance of 1) cumulus magnetite (Magnet Heights gabbronorite subzone), 2) cumulus iron-rich olivine (Ironstone magnetite gabbro subzone), and 3) cumulus olivine + cumulus apatite (Luipershoek olivine diorite

subzone). The Magnet Heights gabbronorite contains the main magnetite layer, which is about 1.5m thick, and nine other magnetite layers none of which exceed 30cm in thickness. Magnetite layers are also common within the other subzones of the upper zone with the top most magnetite layer of the Ironstone magnetite gabbro subzone reaching a thickness of up to 10m.

Geology of the Duluth Gabbro Complex, Minnesota

The Duluth Gabbro Complex, which covers an area of about 4,023 square kilometers extends from Duluth, Minnesota, in a crescent shape, approximately 241Km to a point near Howland, Minnesota (Fig. 11). Studies by Taylor (1964) and Phinney (1969) describes the complex as consisting of a series of multiple intrusions with the oldest unit, a coarse grained anorthositic gabbro, comprising the upper part of the complex. The next younger unit comprises the lower two-thirds of the complex, and is a layered series of troctolite and gabbro. Both these units are cut by intrusive ferrogranodiorite and granophrye, as well as by late stage basalt and aplite dikes, granophyre being most common. Radiometric dating of zircons from several rhyolitic flows of the adjacent North Shore Volcanic Group and from granitic to intermediate fractions of the Duluth Complex indicates that the

Figure 11: Generalized geologic map showing the Keweenawan rocks of northeastern Minnesota and the western Lake Superior Basin. Check pattern = Duluth Gabbro, vertical rule = Lower Keweenawan rocks, stipple = Middle Keweenawan lavas (after Green, 1972).

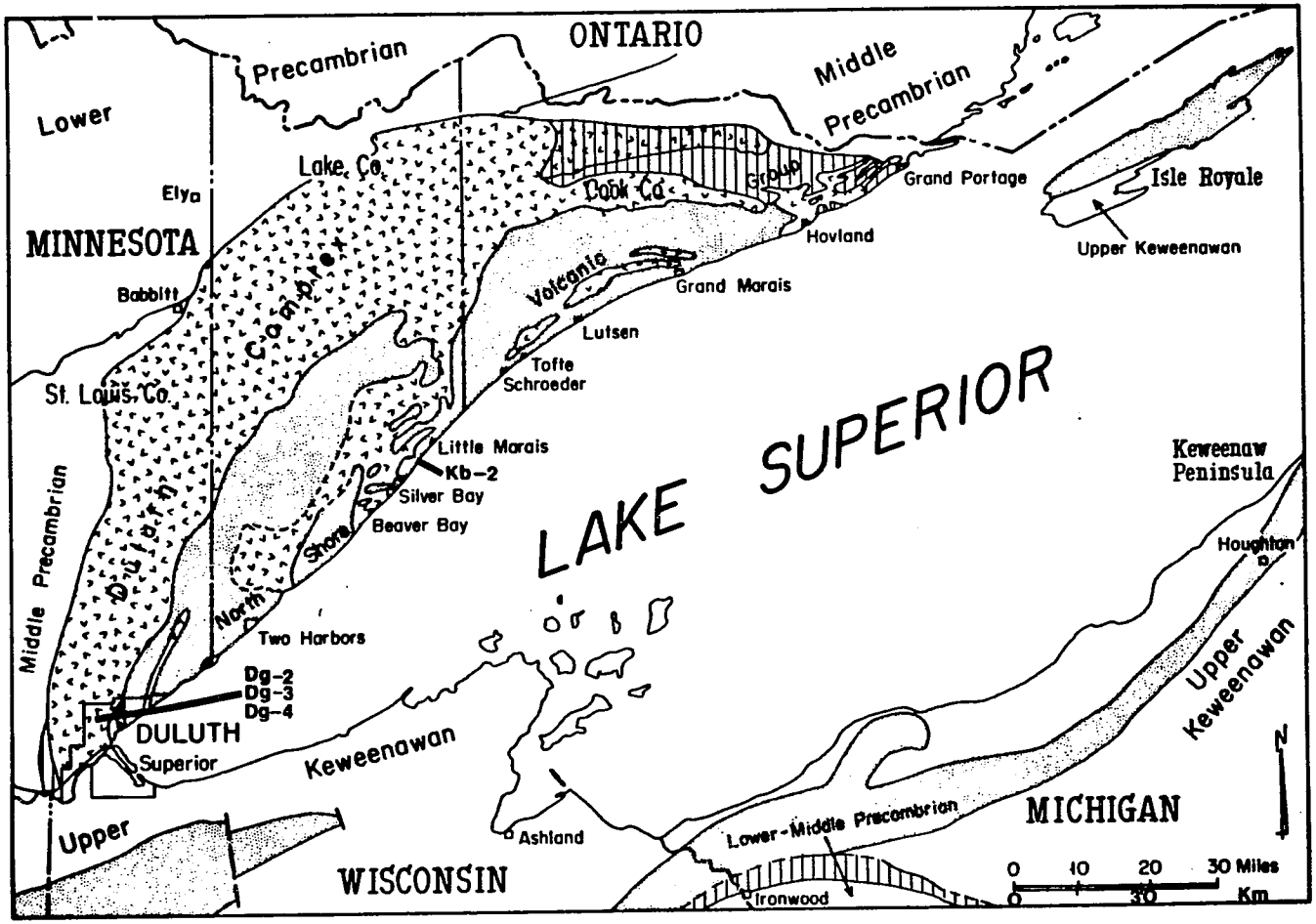

intrusive rocks and flows are nearly contemporaneous and are 1,120 ± 15 m.y. old (Phinney, 1972).

Petrographic analyses of the Duluth Gabbro rocks by Taylor (1964) indicate that the principal minerals of the anorthositic gabbro include plagioclase (69%), olivine (12%), augite (9%), and magnetite+ilmenite (9%). Those of the gabbroic rocks from the layered series include plagioclase (17-81%), pyroxene (0-49%), olivine (0-40%), and magnetite (1-24%). The average composition of the major dike rock, granophyre, consists of feldspar (68%), quartz (23%), chlorite (4%), and magnetite (2%).

Geology of the Adirondack Massif, New York

The Adirondack massif, located in the Adirondack Mountains of New York (Fig. 12), has the form of a biconvex slab ranging in thickness from 3Km on the west to 4.5Km on the east (Simmons, 1954). Two facies of anorthositic rocks have been recognized 1) anorthositic gabbro, which is largely restricted to the borders of the massif and named the Whiteface anorthosite, and 2) gabbroic anorthosite, which forms the core of the massif and is called the Marcy anorthosite (Buddington, 1953; Crosby, 1969). In contrast to anorthosite bodies elsewhere in the world the anorthositic rocks of the Adirondacks have undergone regional, granulite facies metamorphism subsequent to their emplacement (Isachsen and Moxham, 1969). The age of the

Figure 12: Generalized geologic map showing the distribution of anorthosite in the Adirondack Mountains, New York. Stippled area represents border facies of anorthosite (after Crosby, 1969).

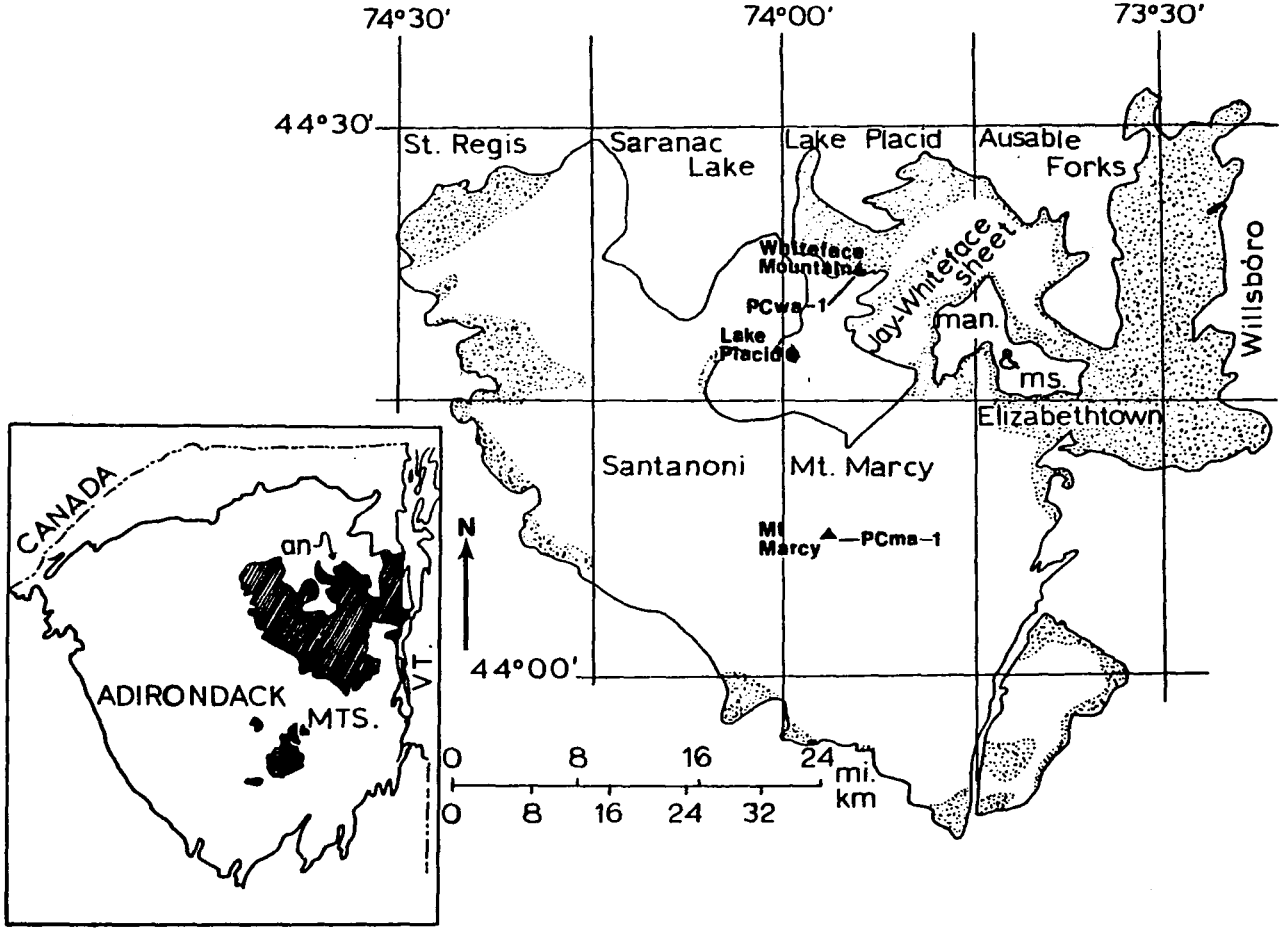

Massif has been approximated at 1,130 m.y. based on U-Th-Pb isotope systems in zircons (Silver, 1969).

Average composition of the Marcy anorthosite includes anorthite (44%), albite (40%), orthoclase (6%), hypersthene (4%), diopside (2%), quartz (2%), magnetite (1%), and ilmenite (1%). The Whiteface anorthosite consists of albite (41%), anorthite (36%), orthoclase (11%), hypersthene (5%), quartz (2%), magnetite (1%), ilmenite (1%), and diopside (Tr) (After Buddington, 1953).

Geology of the North Shore Volcanic Group, Minnesota

The North Shore Volcanic Group, located in northeastern Minnesota (Fig. 11), is of middle Keweenawan age (1,000-1,200 m.y.) and consists mainly of plateau basalts formed by fissure eruptions (Craddock, 1972). The thickness of these flows in Minnesota is uncertain, but Sandberg (1938) has approximated it at about 6,357m along the Lake Superior shore between Duluth and Two Harbors. According to Green (1972) the flows are generally tabular with individual flows or flow groups being traced for distances of up to 32Km. Evidence for subaqueous extrusion is rare.

Sandberg (1938) found that the most abundant type of lava in the Duluth-Two Harbors area was olivine basalt (71.4%) followed by rhyolite (18.2%) and porphyritic andesite (10.4%). The olivine basalt being characterized

by the presence of abundant, small (1-3mm) bytownite phenocrysts, as well as phenocrysts of augite and serpentinized olivine (2-3mm) (Green, 1972). The opaque minerals present include magnetite and ilmenite with grain size ranging from 0.01mm to 5mm (Cornwall, 1951). A typical flow contains 60% calcic plagioclase (An_{50-70}), 25% augite plus olivine, 9% chlorite plus epidote, and 6% opaque minerals (Green, 1972).

Geology of the Basaltic Eruption, Haimaey, Iceland

On January 23, 1973 a basaltic eruption occurred on the east side of the island of Haimaey, located off the south coast of Iceland (Fig. 13). Haimaey sits along the tip of a propagating rift in S.E. Iceland (N. Oskarsson, personal comm.), and as described by Thorarinsson et al. (1973), the eruption occurred along a fissure that ran N-NE to S-SW and extended a distance of approximately 3Km. The flow covered a area greater than 1.35 square kilometers and the rock type is intermediate between hawaiite and mugearite, belonging to the alkali-basalt-trachyte suite. Petrographic analyses by Thorarinsson et al. (1973) show an average composition of glassy groundmass (52.7%), plagioclase (35.5%), opaques (5.8%), and olivine (5.6%). Sand samples were collected along the new coastline formed by this eruption after three years of erosion.

Figure 13: Generalized view of the extent of the 1973 basaltic eruption on Haimaey Island, Iceland. Dashed area represents building of new beach by lava flows (after Thorarinsson et al., 1973).

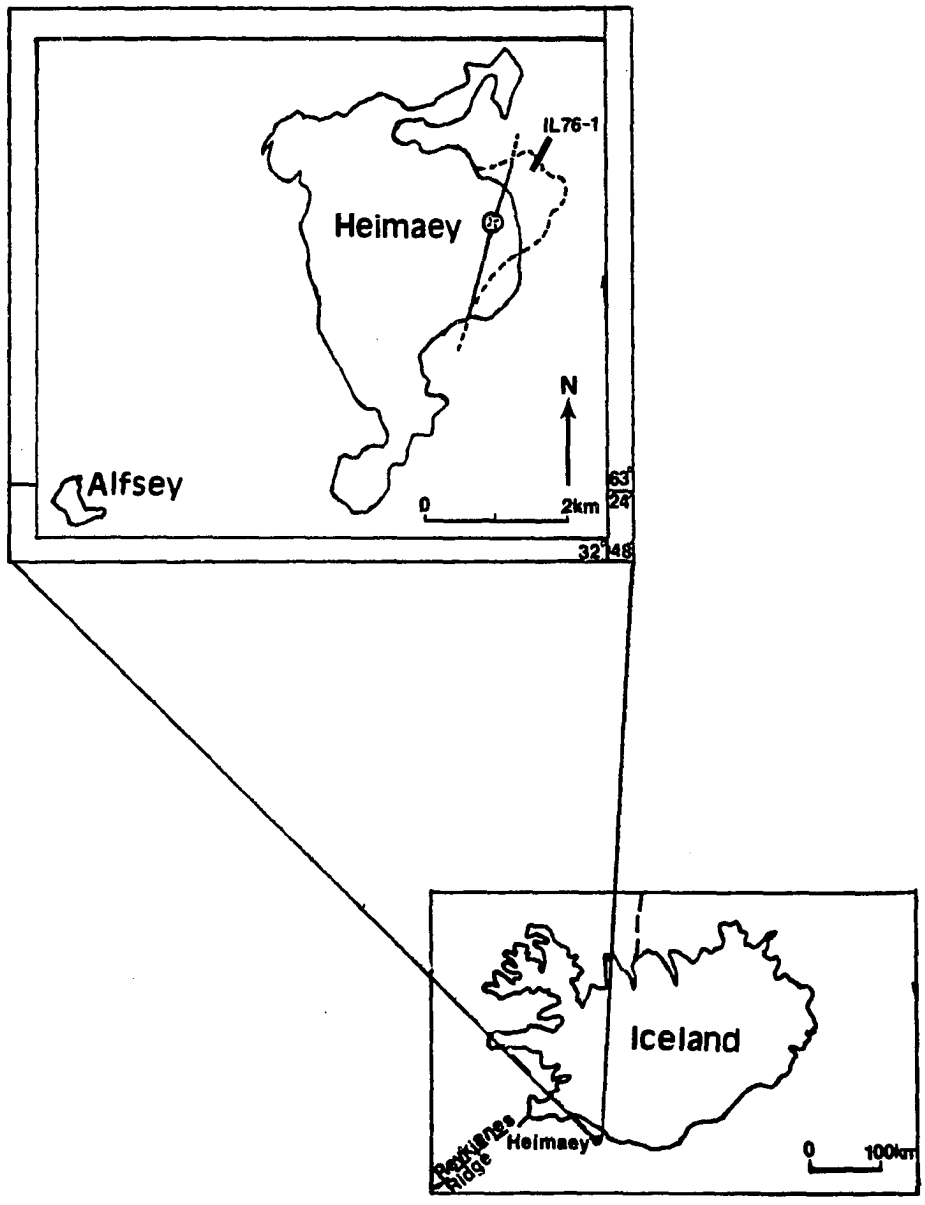

Geology of the Western Reykjanes Peninsula, Iceland

The Reykjanes Peninsula, located in southwest Iceland at the intersection of Iceland and the Reykjanes Ridge (Fig. 14), is covered by basaltic flows of Holocene age (Jakobsson et al., 1978). According to Jakobsson et al. (1978) the Holocene eruption sites on the peninsula form five distinct fissure swarms that are arranged approximately perpendicular to the assumed direction of spreading in the region, and are part of a chain of swarms arranged en echelon on the plate boundary of the northern Reykjanes Ridge (Fig. 14). Jakobsson et al. (1978) concluded that the extrusives of these swarms "...group morphologically and petrographically into small picrite basalt lava shields, large olivine tholeiite lava shields, and tholeiite fissure lavas; formed in that chronological succession." The average thickness of the fissure lavas were found to be 13m and that of the compound lava shields to be about 40m. Not a single occurrence of intermediate or acidic rocks is known to occur on the Reykjanes Peninsula west of 21°20'W (Jakobsson et al., 1978).

Petrographic analyses (Jakobsson et al., 1978) of these basalt types indicate that the picrite basalts (oceanite) exhibit a primitive mineralogy with chromite, olivine (Fo_{88}), and plagioclase (An_{90}) as the primary phenocrysts. Labradorite laths, clinopyroxene, olivine and

Figure 14: General geologic map showing the volcanic fissure swarms of southwest Iceland and northernmost Reykjanes Ridge (after Jakobsson et al., 1978).

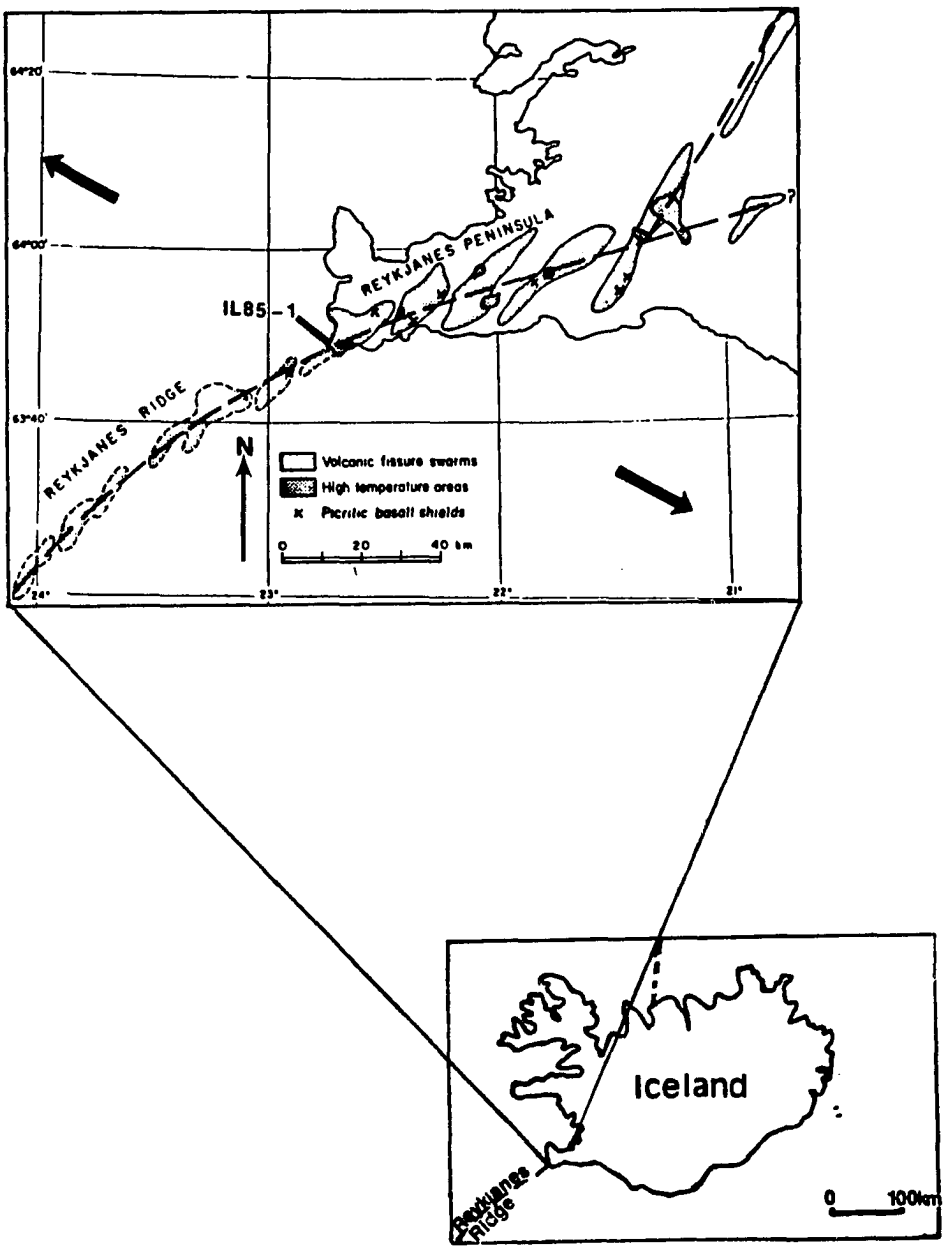

interstitial magnetite occur in the groundmass. The rock has a ophitic to poikilitic texture and it is thought to represent a primary liquid from the mantle.

The olivine tholeiite lava shields are coarse grained with olivine and plagioclase, common phenocrysts in the picrite shield lavas, rare. The groundmass consists of labradorite laths, clinopyroxene, olivine, and interstitial magnetite and ilmenite. The texture is ophitic.

The tholeiite fissure lavas are fine-grained with microphenocrysts of plagioclase and small amounts of olivine and augite. The texture is intergranular to pilotaxitic with the groundmass consisting of glass, labradorite-andesine, clinopyroxene, rare olivine, and commonly euhedral magnetite and ilmenite.

Geology of Hawaii

Geologic mapping of the Hawaiian Islands, located in the Hawaiian Archipelago (Fig. 15), has led to the recognition of a series of stages in the growth of the individual volcanoes above sea level. These stages, first described by Stearns (1940, 1946), include 1) a shield-building stage (youthful stage) in which frequent eruptions of very fluid basaltic lava build a shield volcano composed of thin extensive lava flows, 2) a caldera filling stage (mature stage) in which a caldera formed by repeated collapsing of the summit of the shield volcano accumulates

Figure 15: Map of the Hawaiian Archipelago. The small inset shows the location of the islands in the Pacific Ocean (After Macdonald et al., 1983).

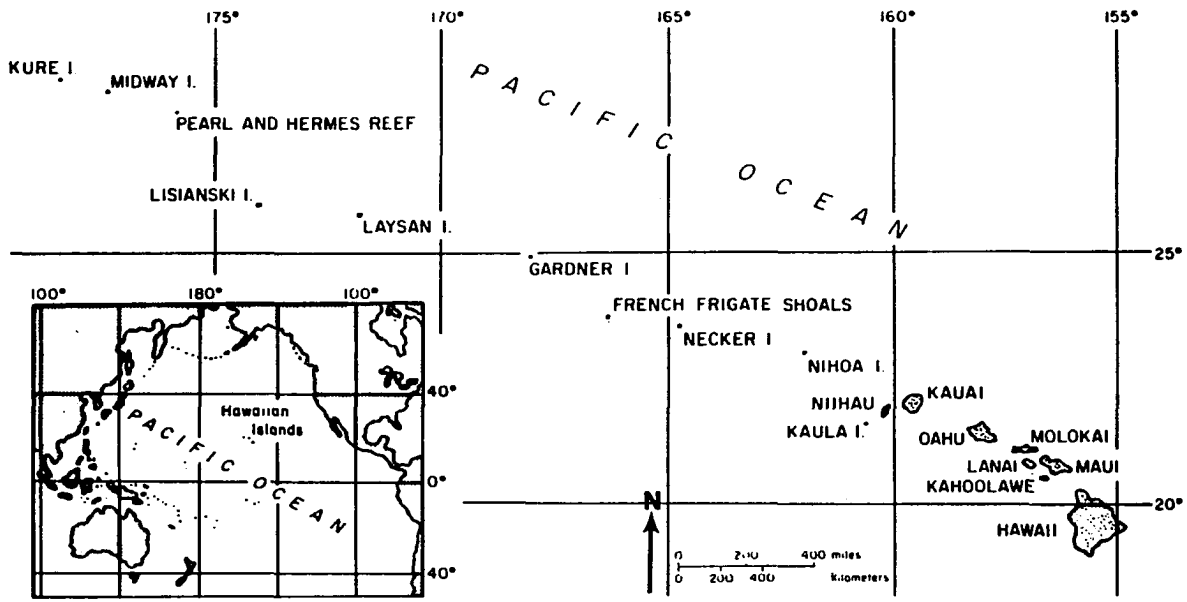

thick ponded lava flows that gradually refills it. The lavas of stages 1 and 2 are tholeiitic lavas and pyroclastic rocks form less than one percent of the total, 3) a post-caldera stage (old age stage) in which a cap is built over the top of the shield. Eruptions are more explosive and less frequent than the earlier stages, pyroclastic rocks become more abundant, and successive lava flows are separated by local erosional unconformities, soil beds, and stream deposited gravel. The rocks consist of alkalic lavas, and 4) a post-erosional stage (rejuvenated stage) in which, following a long period of volcanic quiescence and deep erosion, renewed volcanism pours flows of nepheline basalts and related alkalic and undersaturated olivine basalts over the deeply eroded surfaces. Eruptions are moderately explosive.

The rocks of the tholeiitic series in Hawaii include tholeiite, olivine tholeiite, picrite-basalt of oceanite type, and a small body of rhyodacite (Macdonald and Katsura, 1964). Those of the alkalic suite include alkalic olivine basalt, hawaiite, mugearite, trachyte, and picrite-basalt of the ankaramite type, as well as rocks transitional from mugearite to trachyte termed benmoreite (Macdonald, 1968). A review of these rock types is in Macdonald et al. (1983).

Geology of Maui. The island of Maui consists of two major volcanoes (Fig. 16). The older one is West Maui and the younger one is East Maui (Haleakala). The volcanic rocks of West Maui have been divided into three series by Stearns and Macdonald (1942) and these divisions have been summarized by Macdonald et al. (1983). The oldest series has been named the Wailuku Series and consists predominantly of the major shield building volcanics of tholeiite, olivine tholeiite, and oceanite which grade into hawaiite and alkalic basalt. These rocks 1.27 to 1.63 m.y. old and were followed by a short period of weathering.

The Honolua Series followed this period of weathering and lies unconformably on the Wailuku Series. The Honolua Series consists of trachyte and benmoreite with minor hawaiite. It has been dated between 1.15 and 1.5 m.y. old, and has an average thickness of about 20m. This was followed by a long period of erosion.

The third division, the Lahaina Volcanic Series, is the youngest series and represents the rejuvenated stage within West Maui. It consists of picrite-basalt and has been dated at approximately 1.3 m.y. old.

Two volcanic series have been recognized in East Maui (Macdonald et al., 1983). The Honomanu Series contains the oldest volcanic rocks and consists of the shield volcanics tholeiite, tholeiitic basalt, and oceanite. The average

Figure 16: Generalized geologic map of the island of Maui, Hawaii (after Macdonald et al., 1983).

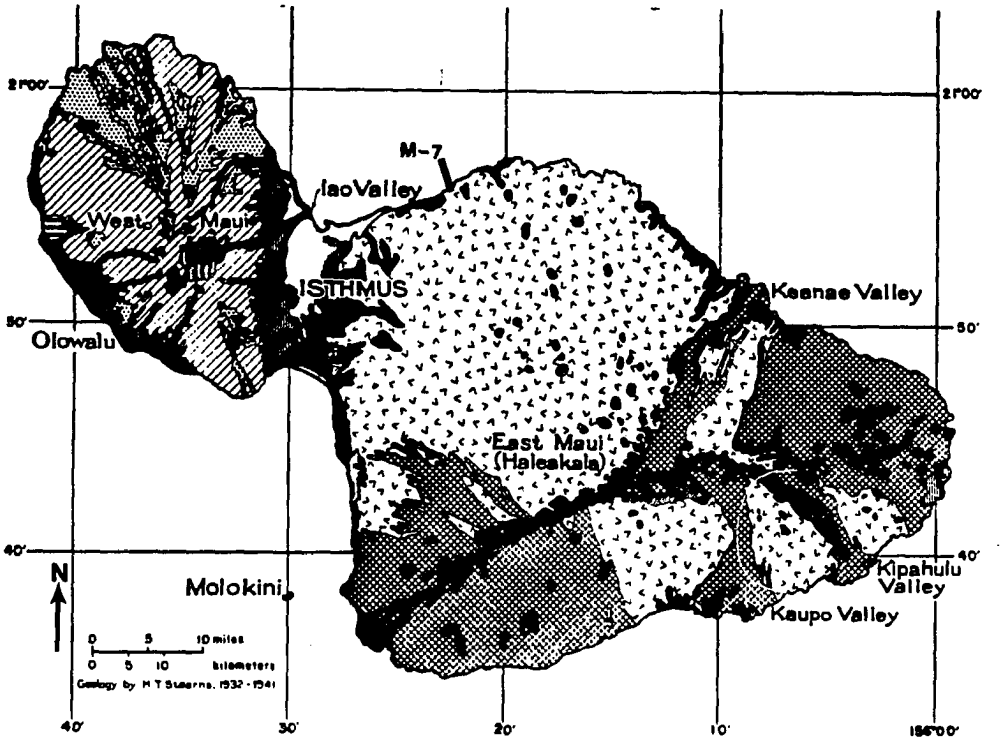

EXPLANATION

SEDIMENTARY ROCKS

RECENT — PLEISTOCENE

- Younger alluvium
- Dunes, chiefly lithified
- Older alluvium
- Mud flow

VOLCANIC ROCKS

EAST MAUI — WEST MAUI

HISTORIC

- Lava flow of 1750 (?)

RECENT

- Cone — Kipahulu member — Hana volcanic series
- Cone — Lahaina volcanic series

EROSIONAL UNCONFORMITY

PLEISTOCENE

- Cone — Kula volcanic series
- Cone — Honolua volcanic series

TERTIARY

- Honomanu volcanic series
- Caldera complex — Stock — Wailuku volcanic series

thickness of these rocks is approximately 5m and have been dated between 0.69 and 0.83 m.y. old. The Kula Volcanic Series overlies the Honomanu Series and has been dated between 0.44 and 0.86 m.y. old. It is composed predominantly of hawaiite with lesser amounts of alkalic olivine basalt and ankaramite. The thickness of these flows ranges from 750m near the summit to 15m at the coast.

West Maui appears to be extinct having passed through the four stages of development as defined by Stearns (1940, 1946). East Maui is currently in a period of volcanic quiescence and deep erosion, which may represent a dormant stage in its development.

Geology of Hawaii Island. The island of Hawaii consists of five volcanic mountains, named from oldest to youngest, 1) Kohala, 2) Mauna Kea, 3) Hualalai, 4) Mauna Loa, and 5) Kilauea (Fig. 17). The time of activity of these different volcanoes is correlated by the presence or absence of the Pahala ash, which is the only rock formation that is found on more than one of the volcanic mountains. The oldest radioactive dates from the rocks of Hawaii Island have been determined to be less than 1 million years and it is believed that none of the exposed rocks are older than Pleistocene (Macdonald et al., 1983). The rocks of Hawaii Island have been described and divided into series by Stearns and Macdonald (1946). These series

Figure 17: Location map of the island of Hawaii, Hawaii showing the 5 volcanoes that make up the island (after Macdonald et al., 1983).

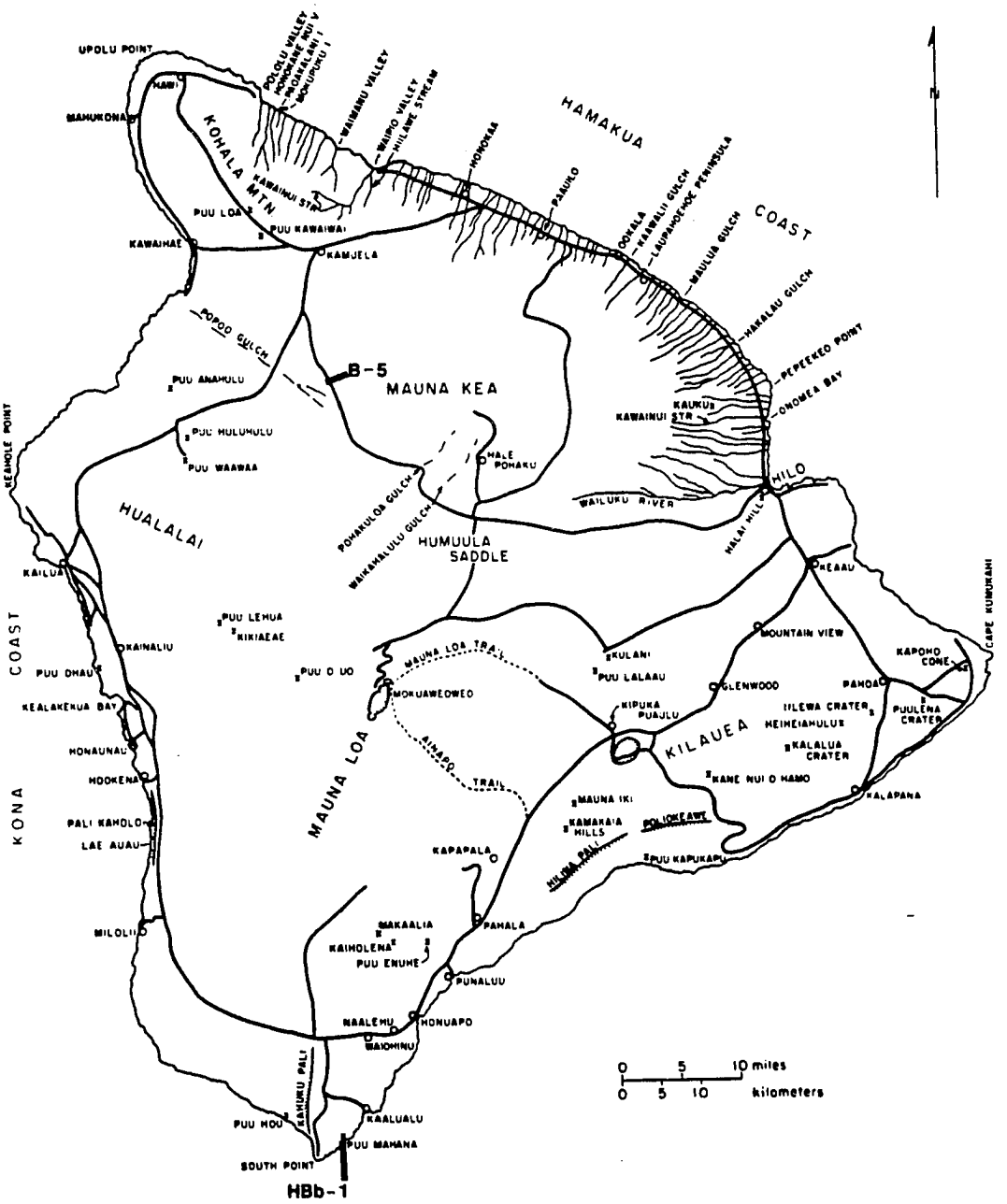

are summarized by Macdonald et al. (1983) and are briefly discussed here.

Kohala Mountain consists of an oval shield volcano built around two rift zones that trend northwestward and southeastward from the summit region. The rocks have been divided into two series 1) the Pololu Volcanic Series, which consists of tholeiitic basalt, tholeiitic olivine basalt, and oceanite with minor alkalic olivine basalts appearing at the top, and 2) the younger Hawi Volcanic Series, which lies unconformably on the Pololu Series and consists mostly of mugearite with a few domes and flows of trachyte and hawaiite.

Mauna Kea rocks have also been divided into two series 1) the Hamakua Volcanic Series, in which the lower member consists of tholeiitic basalts, olivine basalts, and oceanites of the early shield-building stage and grades into the upper member of alkalic olivine basalts, hawaiites, and ankaramites, and 2) the Laupahoehoe Volcanic Series, which consists predominantly of hawaiite with minor alkaline olivine basalt and ankaramite, and is separated from the Hamakua Series by a layer of Pahala ash.

Nearly all the lavas of Hualalai Mountain consist of alkalic olivine basalt (Hualalai Series) although a few of these flows grade into hawaiite. No tholeiitic lavas have been found, but it has been assumed that a tholeiitic

shield exists beneath the alkaline olivine basalts. A single trachyte pumice cone and flow (Waawaa volcanics) appears on the north slope of Hualalai.

The present mass of Mauna Loa Volcano is made up of at least two huge shield volcanoes built around two separate eruptive centers. The older shield (Ninole Shield) consists of tholeiitic basalts, olivine basalts, and oceanites (Ninole Volcanic Series) and has been buried beneath the present day volcanics (Ka'u Volcanic Series) which consist of the same rock types. A succession of large and small tholeiitic lava flows, covered by Pahala ash (Kahuku Volcanic Series), are present along the southern slope of Mauna Loa.

Kilauea Volcano consists of rocks which have been divided into two series 1) the older Hilina Volcanic Series which is made up of tholeiitic basalt, olivine basalt, and oceanite, is capped by the Pahala ash, and is coeval with the Kahuku Series of Mauna Loa, and 2) the Puna Volcanic Series which consists of the same rock types as the Hilina Series, overlies the Pahala ash, and is correlative with the Ka'u Series of Mauna Loa.

A diagram showing the principal rock units of Hawaii Island is shown in Figure 18.

Figure 18: Diagram showing the principal rock units on the island of Hawaii (after Macdonald et al., 1983).

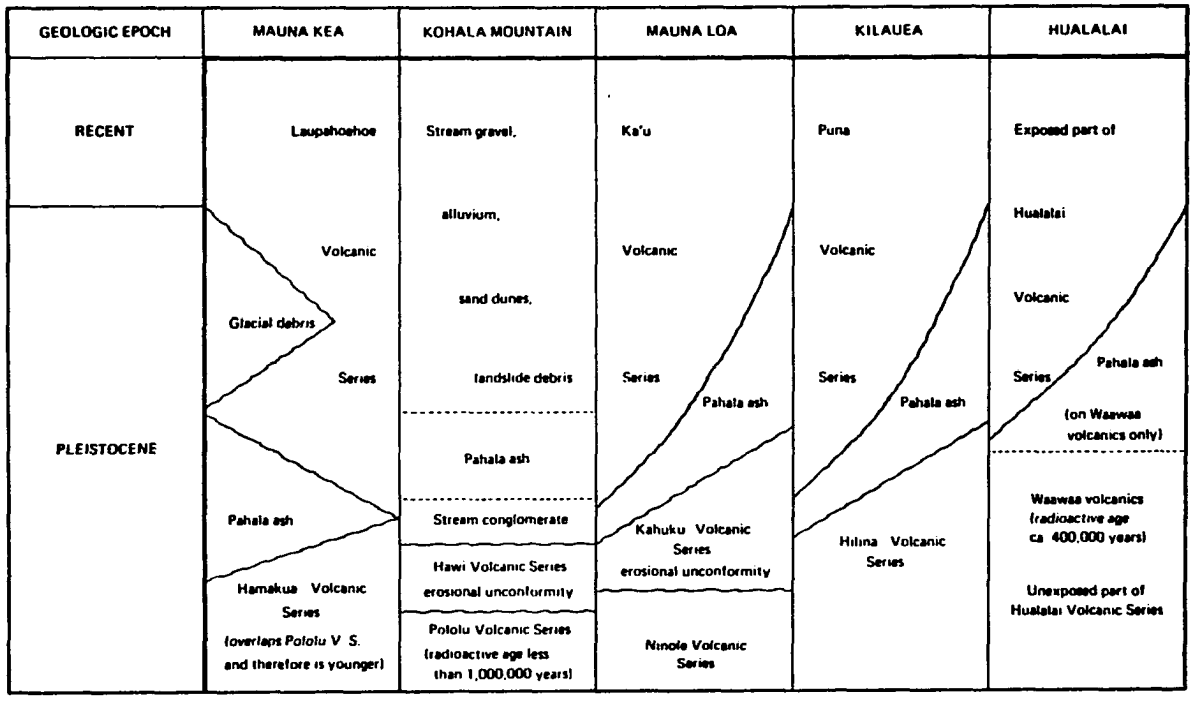

Ultramafic Samples

Geology of Loma de Hierro, Venezuela

Loma de Hierro is a serpentinized peridotite that outcrops between Tacata and Tiera in the states of Aragua and Miranda in north-central Venezuela (Fig. 19). The geology of Loma de Hierro has been studied by Smith (1953), Shagam (1960), MacLachlan et al. (1960), and summarized by Bellizzia (1967). In general, Loma de Hierro is a sheet-like body, approximately 700m thick, cut by gabbroic dikes. The sheet is composed of massive, serpentinized harzburgite consisting predominantly of "mesh-structure" chrysotile serpentine with serpophite. Prominent bastite pseudomorphs after enstatite are abundant, as are olivine and pyroxene relics. Accessory chromite and secondary magnetite occur throughout.

The Loma de Hierro sheet appears to be related to a series of subparallel lineaments associated with the Santa Rosa and Agua Fria fault zones. The sheet is overlain by the Tiera volcanics (a series of basalt flows and associated volcanic conglomerates and tuff beds) and intrudes the phyllites of the upper part of the Paracotos Formation. Shagam (1960) suggests a middle to early Late Cretaceous age for the intrusion. Chemical analysis data of the Loma de Hierro peridotite is not available.

Figure 19: Generalized geologic map of Loma de Hierro, Venezuela (After Bellizia et al., 1976).

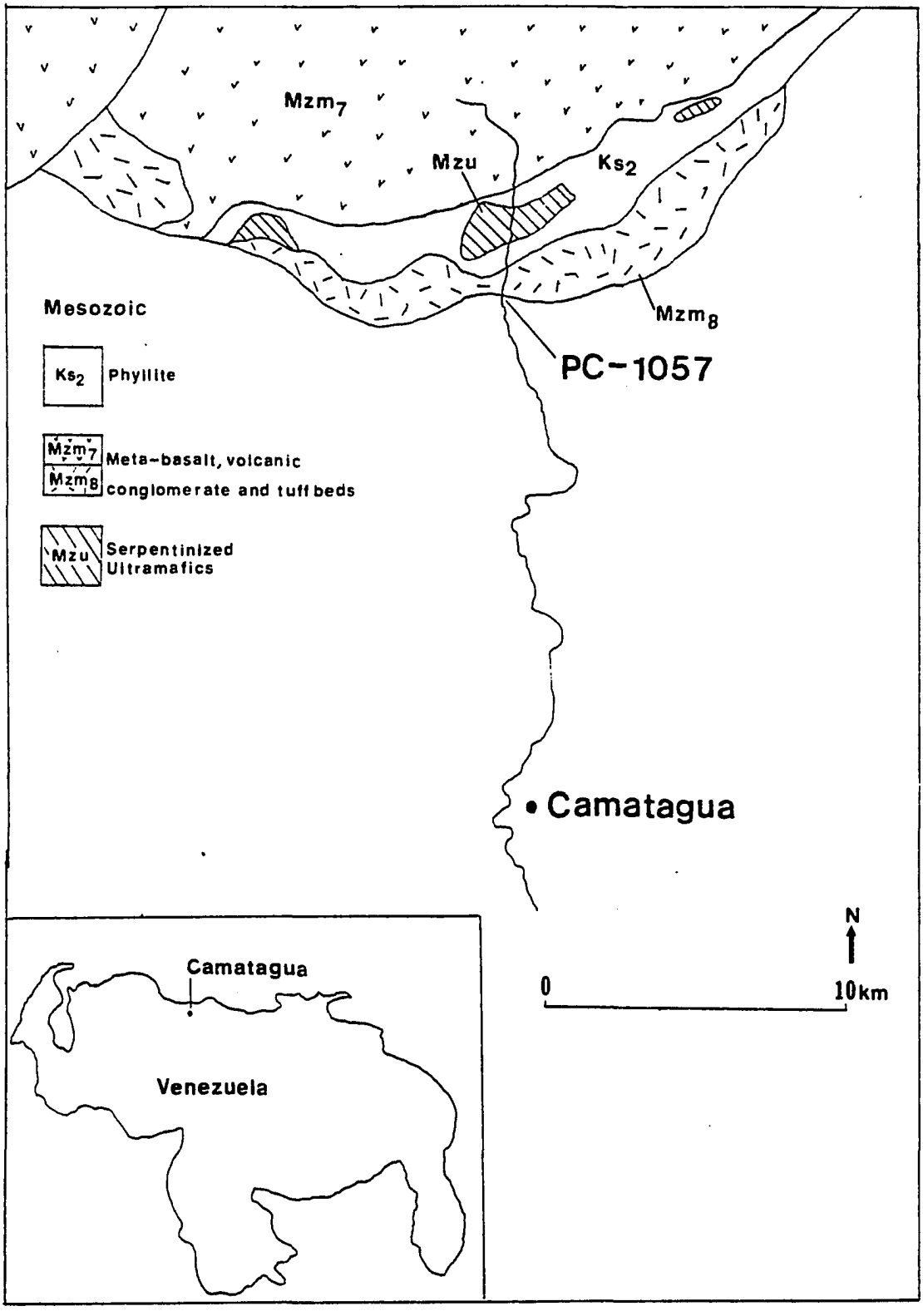

Geology of the Lewis Hills Ophiolite, Newfoundland

The Lewis Hills Ophiolite (Middle Ordovician age) is part of the Bay of Islands Igneous Complex located on the western edge of the island of Newfoundland (Fig. 20). Three other ophiolite suites make up this complex with the type section (as described by Smith, 1958) represented by the North Arm Mountain suite. This suite consists of a thick (4-6Km) ultramafic basal zone characterized by peridotite in excess of dunite at the base that grades upward into dunite in excess of peridotite at the top. The ultramafic zone overlies Ordovician sedimentary and volcanic rocks that have been metamorphosed to amphibolite and calcic hornfels near the contact. The ultramafic zone is in turn overlain by banded and massive gabbro: the contact of the mafic and ultramafic zones represented by a zone of interbanded gabbroic and ultramafic rocks. The massive gabbro at the top of this mafic zone is then overlain by a sequence of massive meta-volcanic rocks, sedimentary rocks, and pillow basalts. This sequence of rocks is found in all but the Lewis Hills suite.

The Lewis Hills suite is characterized by an erratic distribution of banded gabbro zones throughout the exposed ultramafic rocks, and also by an excess of dunite over peridotite. It has been proposed (Smith, 1958) that this is probably because of the nearly horizontal attitude of

Figure 20: Generalized geologic map of Lewis Hills ophiolite suite, western Newfoundland (after Smith, 1958).

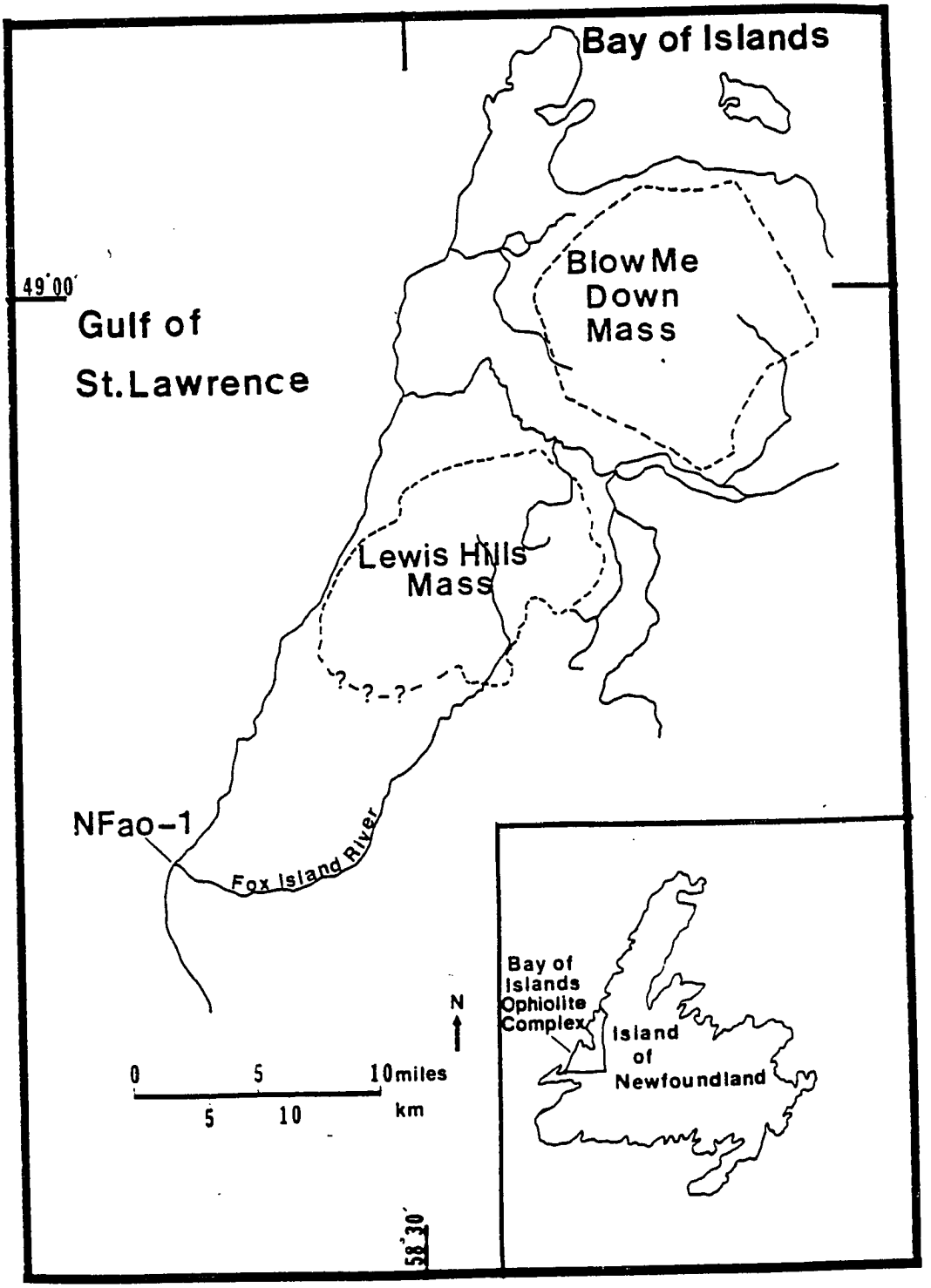

its main ultramafic-gabbro contact and the nonexposure of much of the ultramafic peridotite zone. The thick gabbroic zone is exposed and similar to the North Arm Mountain suite, but the volcanic roof rocks are only found on the western edge of the structure.

The primary minerals of the ultramafic rocks are olivine and orthopyroxene. Magnetite occurs as a secondary mineral formed by serpentinization. The gabbro consists predominantly of plagioclase (bytownite) and augite, and in some phases olivine. Primary magnetite is a common accessory mineral. For a more detailed discription of the structure and rock types of the Lewis Hills Ophiolite see Karson (1979).

Sedimentary Samples

Geology of the Gunflint Iron-Formation, Minnesota

The Gunflint Iron-Formation extends from Thunder Bay, Ontario on Lake Superior to Gunflint Lake, Minnesota for a total distance of 177Km (Fig. 21). It forms the base of the Kaministikwan Group, a thick sedimentary unit of Precambrian age that rests on an early Precambrian basement complex: the entire complex dipping 7 degrees to the southeast. The Gunflint Formation consists largely of iron- and silica-bearing sedimentary rocks and has an average thickness of 122m (Goodwin, 1956).

Goodwin (1956) divided the Gunflint Formation into

Figure 21: Index map showing location of the Gunflint Banded-Iron Formation and general geologic map of the Gunflint Range in the Thunder Bay District, Ontario and adjoining Cook County, Minnesota (after Goodwin, 1956; and Morey, 1972).

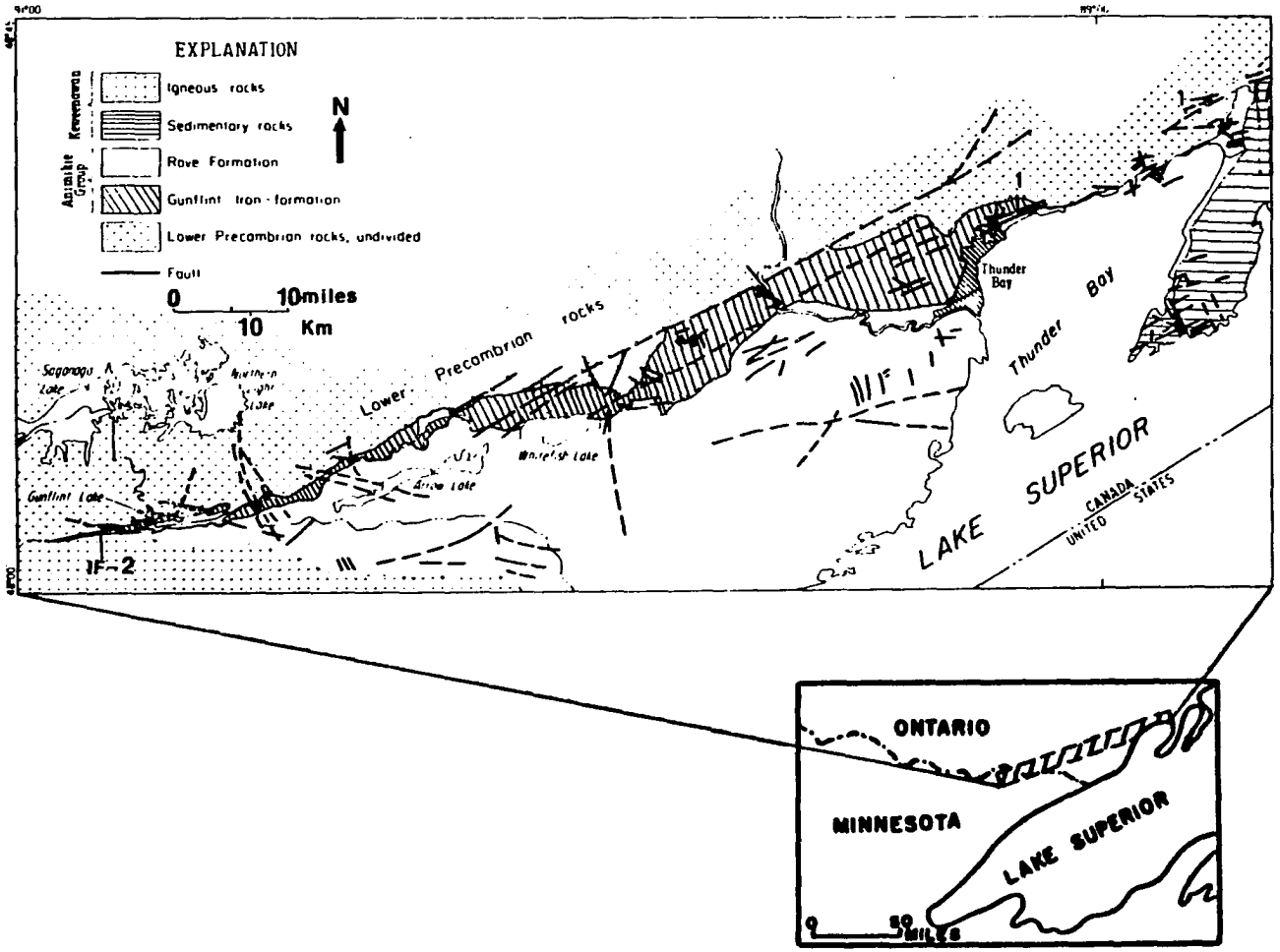

four members consisting of nine facies. The base of the formation is made up of the Basal Conglomerate Member, which is exposed along the northern fringe of the formation and ranges from 0.3m to 1.5m in thickness. The basal conglomerate is overlain by the Lower Gunflint Member that consists of, in ascending order, the Lower algal chert facies, the Lower tuffaceous shale facies, and the Lower west taconite facies. The taconite facies grades into the Lower banded chert-carbonate facies to the northeast, and this in turn is succeeded by the Lower east taconite facies. Total thickness of the Lower Gunflint Member ranges from 64m to 73m.

Following the Lower Gunflint Member a second cycle of deposition occurred which Goodwin (1956) named the Upper Gunflint Member. It consists of, in ascending order, the Upper algal chert facies, the Upper tuffaceous shale facies, the Upper taconite facies, and the Upper banded chert-carbonate facies. The Upper Gunflint Member ranges from 79m to 85m thick and is overlain by the Upper Limestone Member that marks the top of the Gunflint Formation. It ranges from 1.5m to 7m thick and consists of limestone and dolomite interbedded with chert and shale.

Magnetite is present in significant amounts in the following facies 1) Lower algal chert facies, 2) Upper algal chert facies, 3) Lower west taconite facies, and 4)

Upper taconite facies. In general, magnetite occupies broad stratigraphic horizons within these facies.

Whole Rock Chemical Analysis of Selected Provenance Areas

The current research is based on the difference in whole rock chemistry between the above sampled parent rock types, and the effects of these compositional differences on the chemical composition of magnetite and ilmenite derived from them. A number of studies have shown a direct relationship between the whole rock chemistry and the composition of the Fe-Ti oxides (see Fleisher, 1965; Molyneux, 1972; Neumann, 1974; Borisenko and Polkanov, 1975; Osborn and Boctor, 1981). A comparison of the whole rock chemistry of the above samples is given in Table 4.

Table 4: Whole rock chemical analyses of the various rock samples used in the current study (x = not analyzed, label numbers at top of columns refer to rock type and references indicated below).

Wt.%				Felsic				
Oxide	1	2	3	4	5	6	7	8
SiO_2	77.03	68.71	65.15	68.92	70.63	76.26	71.78	72.59
Al_2O_3	12.08	14.62	18.00	15.50	12.93	11.53	13.34	11.79
Fe_2O_3	0.56	2.58	1.03	1.08	2.49	2.22	3.00	2.51
FeO	0.48	x	1.39	1.65	2.12	0.31	1.07	2.30
MgO	0.09	0.70	1.53	0.76	1.07	0.03	0.50	0.19
CaO	0.89	2.14	4.66	1.04	0.92	0.00	1.00	1.06
Na_2O	3.75	3.15	5.82	4.72	4.14	0.13	3.69	2.76
K_2O	4.54	7.17	1.07	5.15	3.56	8.52	4.70	5.02
TiO_2	0.10	0.45	0.28	0.47	0.24	0.13	0.34	0.31
MnO	0.00	0.03	0.04	0.03	0.07	0.03	0.14	0.13
H_2O^-	0.05	x	0.05	0.00	0.34	0.03	0.08	0.09
H_2O^+	0.22	x	0.46	0.36	0.81	0.46	0.41	0.69
P_2O_5	0.01	0.25	0.14	0.03	0.08	0.01	0.09	0.04
CO_2	0.07	x	0.02	0.03	0.19	x	x	x
S	0.02	x	x	0.02	0.03	x	x	x
ZrO_2	0.02	x	x	x	0.22	x	x	x
BaO	0.01	x	0.03	0.06	0.07	x	x	x
F	0.28	x	x	x	x	0.02	0.05	0.10
Cr_2O_3	x	x	x	x	x	x	x	x
NiO	0.00	x	x	x	x	x	0.08	x
SrO	x	x	0.13	x	0.02	x	x	x
Rb_2O	x	x	0.00	x	x	x	x	x
Tot.	100.20	99.80	99.80	99.82	99.93	99.68	100.27	99.55

1 = Graniteville Granite (Kisvarsanyi, 1972).
2 = Favela Granite (Leonardos, Jr., 1973).
3 = Saganaga Tonalite (Goldich et al., 1972).
4 = Surgarloaf Peak Quartz Monzonite (Dunham, 1935).
5 = Granophrye Dike, Duluth Gabbro (Taylor, 1964).
6 = Royal Gorge Rhyolite (Kisvarsanyi, 1972).
7 = Stouts Creek Rhyolite (Kisvarsanyi, 1972).
8 = Rooiberg Felsite (Tankard et al., 1982).

Table 4 - continued.

Wt.%	Intermediate			Mafic				
Oxide	9	10	11	12	13	14	15	16
SiO_2	60.32	62.40	48.88	49.39	54.70	55.50	48.47	47.78
Al_2O_3	18.19	16.20	15.11	29.08	25.02	23.31	29.99	19.17
Fe_2O_3	4.52	2.18	3.41	0.34	0.89	0.96	1.47	0.65
FeO	x	2.64	13.50	2.89	1.80	3.03	0.63	10.63
MgO	2.93	3.88	2.27	2.26	1.23	0.71	2.09	8.94
CaO	5.57	5.17	7.28	13.06	9.52	7.94	13.66	8.42
Na_2O	3.42	4.33	3.37	2.89	4.71	4.81	1.83	2.92
K_2O	1.82	2.00	1.27	0.10	0.99	1.93	0.24	0.37
TiO_2	0.52	0.68	2.08	Tr	0.76	0.78	0.10	0.88
MnO	0.11	0.08	x	0.04	x	0.02	x	0.14
H_2O^-	x	x	1.76	0.09	0.07	0.08	0.63	0.07
H_2O^+	x	x	x	0.34	0.28	0.42	x	0.45
P_2O_5	x	x	x	0.09	0.03	0.30	x	0.15
CO_2	x	x	x	Tr	0.14	0.14	x	0.02
S	x	x	x	0.00	0.00	0.02	x	0.03
ZrO_2	x	x	x	x	x	x	x	x
BaO	x	x	x	x	x	x	x	x
F	x	x	x	x	x	x	x	x
Cr_2O_3	x	x	x	x	x	x	x	x
NiO	x	x	x	x	x	x	x	x
SrO	x	x	x	x	x	x	x	x
Rb_2O	x	x	x	x	x	x	x	x
Tot.	97.40	99.56	98.93	100.57	100.14	99.94	99.11	100.62

9 = Kuanyinshan Volcanoe Andesite (Hwang and Lo, 1986).
10 = Nevado de Toluca Andesite (Kilinc, oral communication).
11 = Diorite, Bushveld Complex (Liebenberg, 1960).
12 = Duluth Gabbro Anorthosite (Taylor, 1964).
13 = Marcy Anorthosite (Buddington, 1953).
14 = Whiteface Anorthosite (Buddington, 1953).
15 = Bushveld Complex Anorthosite (Liebenberg, 1960)
16 = Layered Series Rocks, Duluth Gabbro (Taylor, 1964).

Table 4 - continued.

Wt.%	Mafic - continued							
Oxide	17	18	19	20	21	22	23	24
SiO_2	51.00	53.2	48.29	50.11	46.93	47.77	49.05	49.40
Al_2O_3	18.94	15.71	15.62	17.11	13.37	15.33	14.49	13.90
Fe_2O_3	1.70	1.88	7.52	1.75	1.53	1.63	1.97	3.00
FeO	5.14	6.48	4.46	10.91	7.48	9.32	10.48	8.50
MgO	7.49	11.2	5.55	3.15	16.87	9.74	7.52	8.40
CaO	11.89	8.4	9.44	7.08	11.37	12.13	11.79	10.30
Na_2O	2.17	1.95	2.97	4.89	1.29	1.92	2.16	2.10
K_2O	0.27	0.44	0.84	1.33	0.03	0.12	0.17	0.40
TiO_2	0.31	0.25	1.75	2.46	0.51	1.48	1.72	2.50
MnO	x	x	0.16	0.34	0.15	0.19	0.21	0.20
H_2O^-	0.93	0.68	1.35	0.01	0.09	0.02	0.03	x
H_2O^+	x	x	2.19	0.05	0.28	0.16	0.19	x
P_2O_5	x	x	0.29	0.68	0.04	0.12	0.15	0.30
CO_2	x	x	0.10	x	x	x	x	x
S	x	x	x	x	x	x	x	x
ZrO_2	x	x	x	x	x	x	x	x
BaO	x	x	x	x	x	x	x	x
F	x	x	x	x	x	x	x	x
Cr_2O_3	x	x	x	x	0.18	0.05	0.02	x
NiO	x	x	x	x	0.20	0.03	0.02	x
SrO	x	x	x	x	x	x	x	x
Rb_2O	x	x	x	x	x	x	x	x
Tot.	99.84	100.19	100.53	99.87	100.17	100.01	100.07	99.00

17 = Bushveld Complex Gabbro (Liebenberg, 1960).
18 = Bushveld Complex Norite (Liebenberg, 1960).
19 = North Shore Volcanic Group Basalt (Green, 1972).
20 = Haimey, Iceland Basalt (Thorarinsson et al., 1973).
21 = Reykjanes Peninsula Picrite Basalt (Jakobsson et al., 1978).
22 = Reykjanes Peninsula Olivine Tholeiite (Jakobsson et al., 1978).
23 = Reykjanes Peninsula Tholeiite (Jakobsson et al., 1978).
24 = Tholeiitic Basalt, Hawaii (Macdonald et al., 1983).

Table 4 - continued.

Wt.%	Mafic - continued					
Oxide	25	26	27	28	29	30
SiO_2	46.40	44.10	46.50	48.60	51.90	61.70
Al_2O_3	8.50	11.20	14.60	16.50	16.60	18.00
Fe_2O_3	2.50	2.80	3.30	4.20	4.20	3.30
FeO	9.80	9.90	9.10	7.40	6.20	1.50
MgO	20.80	15.10	8.20	4.70	3.60	0.40
CaO	7.40	10.70	10.30	7.80	6.30	1.20
Na_2O	1.60	1.70	2.90	4.40	5.20	7.40
K_2O	0.30	0.50	0.80	1.60	2.00	4.20
TiO_2	2.00	2.70	3.00	3.20	2.60	0.50
MnO	0.20	0.20	0.10	0.20	0.20	0.20
H_2O^-	x	x	x	x	x	x
H_2O^+	x	x	x	x	x	x
P_2O_5	0.20	0.30	0.40	0.70	0.90	0.20
CO_2	x	x	x	x	x	x
S	x	x	x	x	x	x
ZrO_2	x	x	x	x	x	x
BaO	x	x	x	x	x	x
F	x	x	x	x	x	x
Cr_2O_3	x	x	x	x	x	x
NiO	x	x	x	x	x	x
SrO	x	x	x	x	x	x
Rb_2O	x	x	x	x	x	x
Tot.	99.70	99.20	99.20	99.30	99.70	98.60

25 = Oceanite, Hawaii (Macdonald et al., 1983).
26 = Ankaramite, Hawaii (Macdonald et al., 1983).
27 = Alkalic Basalt, Hawaii (Macdonald et al., 1983).
28 = Hawaiite, Hawaii (Macdonald et al., 1983).
29 = Mugearite, Hawaii (Macdonald et al., 1983).
30 = Trachyte, Hawaii (Macdonald et al., 1983).

Table 4 - continued.

Wt.%	Ultramafic				Sedimentary	
Oxide	31	32	33	34	35	36
SiO_2	42.90	40.75	52.36	39.26	33.91	56.70
Al_2O_3	2.30	1.05	4.09	1.82	0.60	3.16
Fe_2O_3	2.68	3.32	1.95	4.27	4.79	5.90
FeO	6.41	13.05	8.46	3.02	3.23	11.40
MgO	39.08	38.45	27.65	38.53	41.61	2.35
CaO	1.50	1.25	2.66	1.25	0.05	4.80
Na_2O	0.23	0.05	0.26	0.23	0.13	0.26
K_2O	0.08	0.01	0.07	x	x	0.78
TiO_2	0.10	0.11	0.20	0.04	tr	x
MnO	x	x	x	0.11	0.11	x
H_2O^-	2.94	1.54	1.02	0.58	0.53	2.60
H_2O^+	x	x	x	10.05	14.08	0.25
P_2O_5	x	x	x	x	x	9.10
CO_2	x	x	x	0.47	0.16	1.63
S	x	x	x	x	x	x
ZrO_2	x	x	x	x	x	x
BaO	x	x	x	x	x	x
F	x	x	x	x	x	x
Cr_2O_3	x	x	x	0.39	0.16	x
NiO	x	x	x	x	x	x
SrO	x	x	x	x	x	x
Rb_2O	x	x	x	x	x	x
Tot.	98.22	99.58	98.72	100.02	99.80	98.93

31 = Harzburgite, Bushveld Complex (Liebenberg, 1960).
32 = Dunite, Bushveld Complex (Liebenberg, 1960).
33 = Pyroxenite, Bushveld Complex (Liebenberg, 1960).
34 = Peridotite, Lewis Hills Ophiolite (Smith, 1958).
35 = Dunite, Lewis Hills Ophiolite (Smith, 1958).
36 = Gunflint Iron-Formation (Gross and McLeod, 1980).

CHAPTER VI

PETROGRAPHY OF MAGNETITE AND ILMENITE IN PROVENANCE AREAS

Textural Varieties of Magnetite and Ilmenite

The Fe-Ti oxides (magnetite and ilmenite) belong to the system FeO - TiO_2 - Fe_2O_3 (Fig. 22). Within this system Magnetite (Fe_3O_4) forms a complete solid solution with ulvospinel (Fe_2TiO_4) at temperatures greater than 600°C, forming the titanomagnetite series, and ilmenite ($FeTiO_3$) forms a complete solid solution with hematite (Fe_2O_3) at temperatures greater than 800°C. It is through the process of exsolution of the end-member phases, and the secondary process of oxidation in the Fe-Ti oxides that a variety of distinctive textures develop. A review of all of these textural variations is beyond the scope of this paper and the reader is referred to Edwards (1965), Haggerty (1976a, 1976b), and Ramdohr (1980) for a detailed discussion.

The following sections will discuss the most common textural varieties found in the detrital Fe-Ti oxide grains of the current study. An attempt will be made to relate these textures to changes in parent rock type and to determine their usefulness in provenance research.

Textural Variations of Magnetite

Four textural categories have been identified in the detrital magnetite of the current study. These include

Figure 22: Ternary plot in the system $FeO-TiO_2-Fe_2O_3$ showing the solid solution series between magnetite (Fe_3O_4) and ulvospinel (Fe_2TiO_4) at temperatures greater than 600°C, and ilmenite ($FeTiO_3$) and hematite (Fe_2O_3) at temperatures greater than 800°C. The third series is between pseudobrookite (Fe_2TiO_5) and ilmeno-rutile ($FeTi_2O_5$).

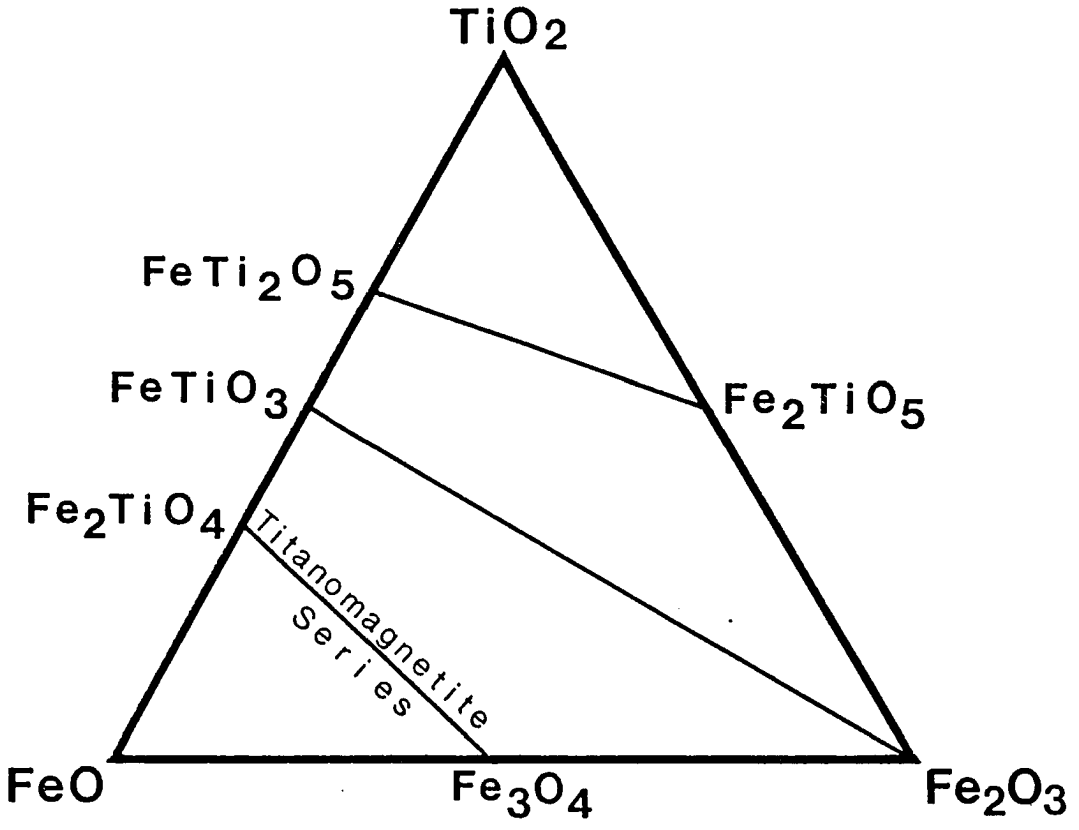

1) optically homogeneous grains, 2) grains that contain exsolution lamellae textures, 3) grains that contain high-temperature oxidation textures, and 4) grains that contain low-temperature oxidation textures.

Homogeneous grains. Homogeneous grains can be defined as those grains in which exsolution or high-temperature oxidation textures are absent. They may contain sulfide or silicate inclusions, as well as low-temperature oxidation textures. An example is shown in Figure 23a.

Exsolution textures in magnetite. The exsolution textures found in the detrital magnetite of the current study include 1) the exsolution of ulvospinel (Fe_2TiO_4), and 2) the exsolution of pleonaste spinel (composition along the $MgAl_2O_4$ - $FeAl_2O_4$ join). Both types of exsolution are strongly affected by temperature and oxygen fugacity. Ulvospinel exsolution occurs at temperatures greater than 600°C and low oxygen fugacity and the exsolved phase forms parallel to the (100) spinel planes. Textures have been described as woven, cloth, parquet, or lit-par-lit (Haggerty, 1976a) and an example is seen in Figure 23b. Associated with the exsolution of ulvospinel is the exsolution of pleonaste spinel. Pleonaste characteristically forms earlier than ulvospinel indicating a higher temperature solvus intersection than that of

Figure 23 (a-e): Photomicrographs of detrital magnetite textures a) homogeneous grain, b) magnetite with ulvospinel exsolution (ul), c) magnetite with pleonaste exsolution (pl), d) magnetite with the later stage of pleonaste exsolution (pl) associated with high-temperature oxidation (trellis-type magnetite-ilmenite intergrowths, il), e) trellis-type magnetite-ilmenite intergrowths (il). Bar scale equals 200um.

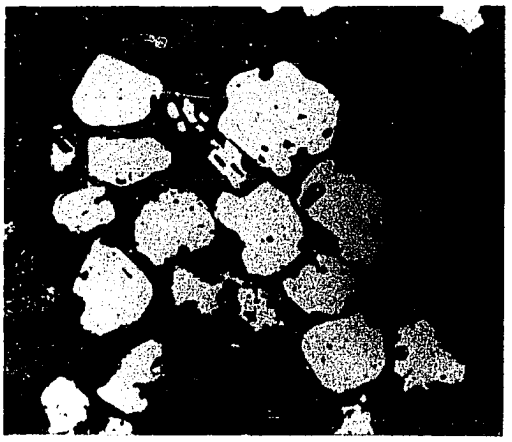

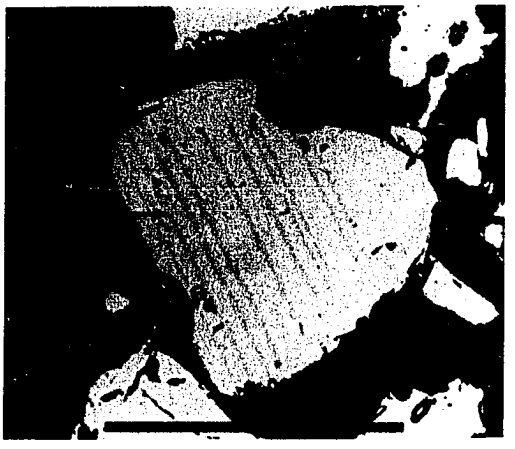

Fe_3O_4- Fe_2TiO_4. Pleonaste exsolution occurs as dark blebs that run parallel to the (100) spinel planes (Fig. 23c). In addition to this early exsolution of pleonaste spinel a less common later generation of pleonaste exsolution may occur in association with high-temperature oxidation and the formation of oxidation "exsolution" ilmenite (Fig. 23d). This relationship will be discussed further in the next section.

High-temperature oxidation textures. Two distinct textural assemblages present in the detrital magnetite grains develop during high-temperature oxidation 1) oxidation "exsolution" textures, and 2) pseudomorphic oxidation textures. Both assemblages develop at temperatures above 600°C but at radically different oxygen fugacities.

Oxidation "exsolution" textures form through the oxidation of ulvospinel in the magnetite - ulvospinel solid solution. For example, Verhoogen (1962) found experimentally that at a temperature of 800°C and an oxygen fugacity of $10^{-19.4}$ atm the oxidation of ulvospinel would result in the oxidation "exsolution" of ilmenite in the magnetite host by the following reaction

$$6Fe_2TiO_4 + O_2 = 6FeTiO_3 + 2Fe_3O_4$$
(ulvospinel) (ilmenite) (magnetite).

Buddington and Lindsley (1964) divided these ilmenite-magnetite intergrowths into three textural forms, all of

which are seen in the current study 1) trellis types (Fig. 23e), in which ilmenite oxidation "exsolution" lamellae form parallel to the (111) spinel planes. These lamellae may occur as fine spindles (<1-10um) of ilmenite along one set of the (111) planes to crowded lamellae along all sets of the spinel planes. Ilmenite lamellae that are parallel to any one set of octahedral planes are in optical continuity, show identical degrees of anisotropy, and similar pleochroism. The terminations of the lamellae are tapered at the intersection of two or more lamellae, which is typical and indicative of diffusion. Tapering may also occur in ilmenite lamellae that extend to the limits of magnetite grain boundaries: this feature being difficult to assess in detrital magnetite because of abrasion and rounding during transport. The width of ilmenite lamellae in any one grain tends to be fairly uniform, but a network of larger laths (10-20um) may be infilled by several generations of finer lamellae (1-10um). Sometimes associated with the formation of trellis lamellae is the exsolution of pleonaste spinel (Fig. 23d). This second generation of exsolution is thought to be a process related to oxidation and, according to Haggerty (1976b), it may be viewed as "an imposed exsolution induced by saturation of the host specifically in Al_2O_3 but also in MgO," 2) sandwich types (Fig. 24a), in which thick (25-50um) laths

Figure 24 (a-e): Photomicrographs of detrital magnetite textures a) sandwich-type magnetite-ilmenite intergrowths (il=ilmenite, mt=magnetite), b) composite-type magnetite-ilmenite intergrowths, c) magnetite with heating martite (rt=rutile, hm=hematite), d) magnetite with pseudobrookite alteration (ps), e) magnetite with low-temperature oxidation. Bar graph equals 200um.

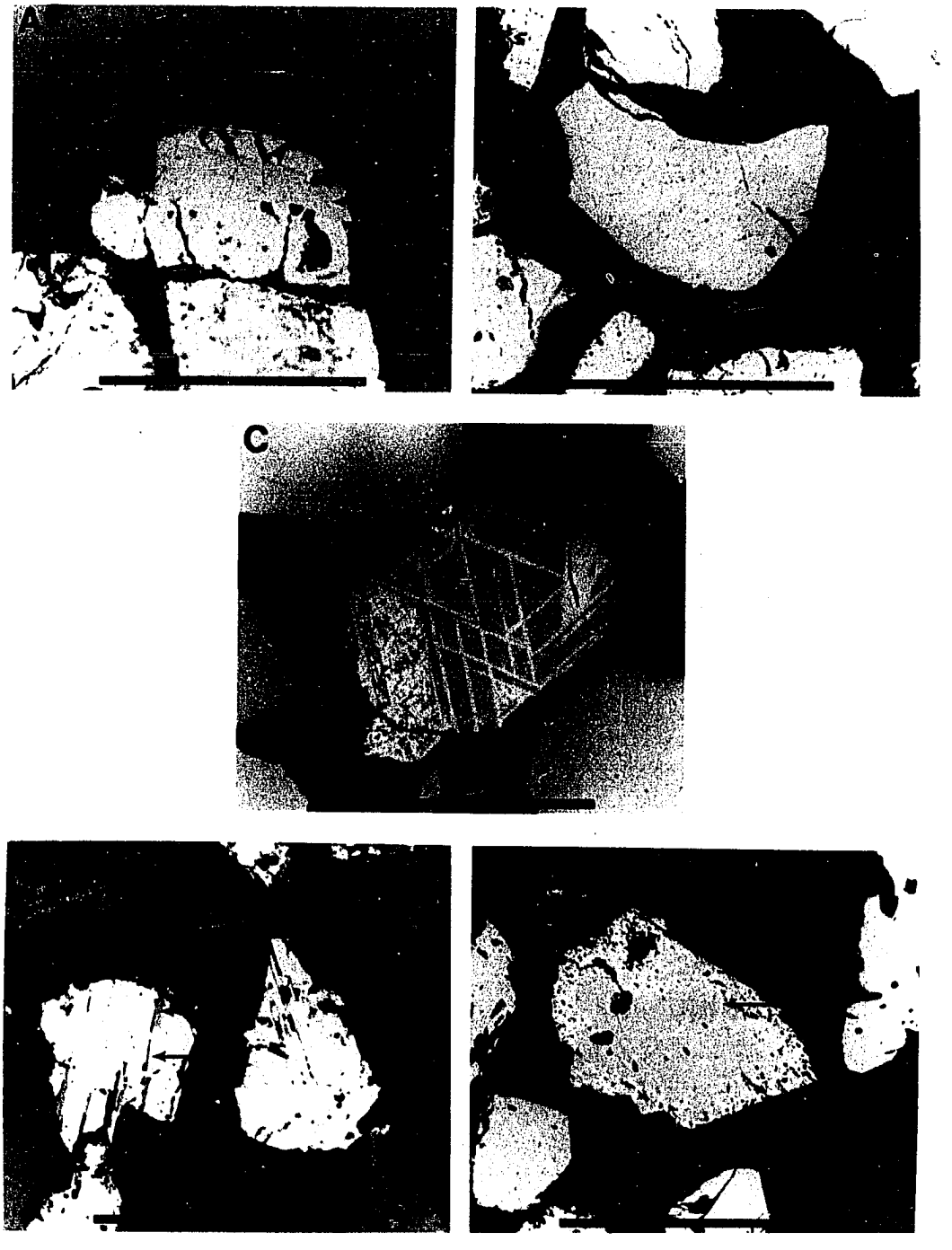

of ilmenite occur along one set of the spinel planes. The laths usually occur in small numbers, with a single lath being most common. They have sharply defined contacts with the magnetite host, and Haggerty (1976b) found that tapered terminations are rare, a feature difficult to assess in detrital grains, and 3) composite types (Fig. 24b), in which euhedral to anhedral inclusions of ilmenite are present in magnetite grains. These inclusions show sharp contacts with the magnetite hosts and are rarely oriented along either the (100) or (111) planes.

Although Buddington and Lindsley (1964) argued that this systematic series of fabrics was the result of increasing degrees of oxidation, Haggerty (1976b) found that while it has generally been accepted that trellis type magnetite-ilmenite intergrowths are clearly the result of oxidation "exsolution" the occurrence of sandwich- and composite-types has not been clearly defined. Electron microprobe scans across sandwich ilmenite-magnetite contacts to determine major element diffusion gradients have been inconclusive, and while accepting that composite intergrowths may develop by slow diffusion in deep seated intrusives (Wright, 1961; Buddington and Lindsley, 1964), Haggerty (1976b) has concluded that composite-type magnetite ilmenite intergrowths in volcanic rocks "are probably not the result of advanced oxidation and

diffusion, but rather the result of primary inclusions." Because of the difficulty in properly identifying sandwich-type laths from composite-types in detrital magnetite, the result of abrasion during transport, these two textural types will be counted together and listed as composite-type magnetite-ilmenite intergrowths.

Pseudomorphic oxidation develops paragenetically later than oxidation "exsolution" at a higher oxygen fugacity, and results in the formation of rutile (TiO_2), hematite (or titanohematite), and pseudobrookite (Fe_2TiO_5). For example, Verhoogen (1962) found experimentally that at a temperature of 800°C and oxygen fugacity of $10^{-8.1}$ atm the increased oxidation of the magnetite-ilmenite association would result in the following reaction

$$\underset{\text{(ilmenite)}}{4FeTiO_3} + O_2 = \underset{\text{(rutile)}}{4TiO_2} + \underset{\text{(hematite)}}{2Fe_2O_3}.$$

Because ilmenite produced by oxidation "exsolution" is structurally controlled within the magnetite host, the phases that develop from this ilmenite through pseudomorphic oxidation also appear to be structurally controlled, although this control is largely compositional (Haggerty, 1976b). In other words, rutile develops preferentially along planes of pre-exsolved ilmenite and hematite develops preferentially in regions of pre-existing magnetite (Fig. 24c). This texture has been termed heating martite by Ramdohr (1980).

As a consequence of continued intense oxidation, pseudobrookite (Fe_2TiO_5) forms from rutile and hematite. Pseudobrookite forms almost exclusively along the (111) relic planes (Fig. 24d), because of the initially higher Ti content and the correspondingly higher rutile:hematite ratio that results from the intense oxidation of pre-existing "exsolved" ilmenite lamellae (Haggerty, 1976b).

Low-temperature oxidation textures. Low-temperature oxidation, or martitization, results in the alteration of magnetite to hematite at temperatures < 600°C. In highly arid regions it may be brought about by incipient weathering of the parent rock (Ramdohr, 1980), and after transport, deposition and burial it may be brought about by diagenesis (Reynolds, 1982). The hematite occurs as lamellae that migrate and invade from the margins of grains, as well as from cracks, holes, silicate inclusions, and ilmenite lamellae, and may completely replace the magnetite grain (Fig 24e).

Textural Variations of Ilmenite

Besides magnetite, detrital ilmenite was also separated from the sands of the current study. Three grain types emerged as being most common: 1) homogeneous grains (Fig. 25a), 2) grains with hematite-ilmenite exsolution textures (Figs. 25b-d), and 3) twinned grains (Fig. 25e). Point count analysis of these grains types (Table 5)

Figure 25 (a-e): Photomicrographs of detrital ilmenite textures a) homogeneous ilmenite grain, b-d) a network of hematite and ilmenite (hm=hematite, il=ilmenite) intergrowths showing the various thicknesses of hematite exsolution, e) twinned ilmenite. Bar graph equals 200um.

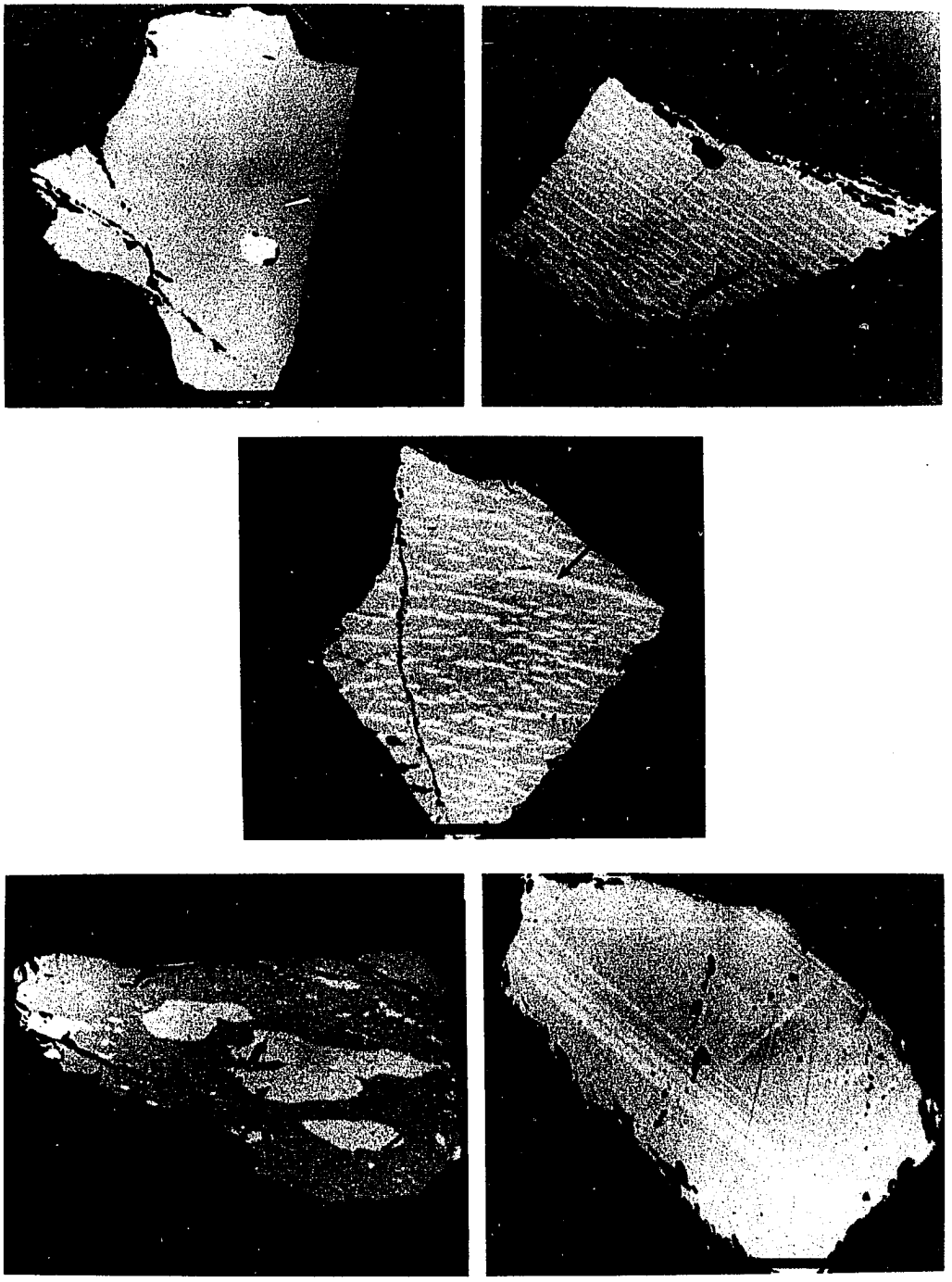

Table 5: Point count data of detrital ilmenite textures from the various parent rocks of the current study.

Rock Types	Sample Number	Homogeneous	Hematite Exsolution	Twinned Grains	Total
Felsic Plutonic	Cb-1	13	37	0	50
	As-1	61	39	0	100
	St-2	83	16	1	100
Felsic Volcanic	Vsc-1	35	5	10	50
	Rgr-1	44	0	6	50
	Dfv-2	49	0	1	50
Intermed. Volcanic	Tm-2	48	5	1	54
	Av-1	31	0	19	50
Mafic Plutonic	Dg-2	100	0	0	100
	Dg-3	91	4	5	100
	Sr-2	97	0	3	100
	Vu-2	82	2	16	100
Mafic Volcanic	Kb-2	20	29	1	50
	M-7*	1	9	0	10
	IL76-1*	1	12	0	13
	IL85-1*	3	10	0	13
Meta. Intrusive	pCwa-1	46	2	2	50
	pCma-1	5	95	0	100
	PC-1057	20	25	5	50

indicated no significant trends relating these grain types to parent rock types. Basu and Molinaroli (in press), in a study of the Fe-Ti oxides in sands derived from dissected arc and recycled orogen provenances, have suggested the measurement of minimum lamellae widths in magnetite and ilmenite as a means of distinguishing between these source areas. Although different widths of hematite lamellae in ilmenite were observed in the current study (Figs. 25b-d) there was not enough evidence to compare this study with that of Basu and Molinaroli.

Relationship between Textures of Magnetite in Modern Sands and Provenance

The parent rocks sampled in the current study can be divided into seven genetic types. These include 1) felsic plutonic, which are represented by the Graniteville Granite, the Favela Granite, the Surgarloaf Peak Quartz Monzonite, and the Saganaga Tonalite, 2) felsic volcanic, which are represented by the Stouts Creek Rhyolite, the Royal Gorge Rhyolite, and the Rooiberg Felsites, 3) intermediate volcanic, which are represented by the Kuanyinshan Andesite, the Toluca Mountain Andesite, and the andesites of Ovalau, Fiji, 4) mafic plutonic, which are represented by the Duluth Gabbro and the Bushveld Complex, 5) mafic volcanic, which are represented by the Keweenawan Basalts, the basalts of Maui and Hawaii Islands, and the basalts of Iceland, 6) metamorphosed igneous complexes,

which are represented by the meta-anorthosites of New york, a serpentinized ultramafic complex in Venezuela, and a serpentinized ophiolite suite in Newfoundland, and 7) a metamorphosed sedimentary complex, which is represented by the Gunflint Banded-Iron Formation (the location of the parent rocks, samples, and sample numbers are listed in Appendix A).

Based on the textural types discussed in the previous section the following relationships were seen in the detrital magnetite derived from the above genetic parent rock types. Average point count data for the seven genetic rock types sampled are given in table 6. Whole point count data for each sample are given in table 7.

Felsic Plutonic Parent Rocks

The detrital magnetite grains derived from the felsic plutonic parent rocks are dominated by a high percentage of homogeneous grains (≈90%, Table 6). Silicate and sulfide inclusions are common in these grains. The other 10% of the grains contain a fine network of trellis-type magnetite-ilmenite intergrowths. Low-temperature oxidation (martite or martitization) is seen in 43% of the grains, this number being variable between samples. Exsolution textures and pseudomorphic oxidation textures are absent.

Felsic Volcanic Parent Rocks

Petrographic analysis of detrital magnetite derived

Table 6: Average distribution of textural types associated with detrital magnetite grains derived from the various parent rocks of the current study (in percent).

	PARENT ROCK TYPES						
Textural Types	Felsic Plutonic	Felsic Volcanic	Intermed. Volcanic	Mafic Plutonic	Mafic Volcanic	Meta. Intrusive	Sedimentary
Homogeneous	90	19	69	15	46	36	100
Mag-Ilm Intergrowths							
Trellis-type	10	30	4	40	36	7	0
Composite-type	0	46	7	4	13	1	0
Total Mag-Ilm Intergrowths	10	76	11	44	49	8	0
Pleonaste	0	5	7	23	2	51	0
Ulvospinel	0	0	Tr	18	2	5	0
Heating Martite	0	0	13	0	1	0	0
Total	100	100	100	100	100	100	100
Additional Alterations							
Pseudobrookite	0	4	0	0	Tr	1	0
Martite	43	24	12	44	9	15	90

Table 7: Distribution of textural types associated with detrital magnetite for each sample derived from the various parent rocks of the current study.

Rock Types	Sample Number	Homogeneous	Magnetite-Ilmenite Intergrowths		Exsolution Textures		Heating	Additional Alteration		
			Trellis	Composite	Pleonaste	Ulvospinel	Martite	Total	Pseudobrookite	Martite
	Brg-1	98	2	0	0	0	0	100	0	60
Felsic	Cb-1	95	5	0	0	0	0	100	0	10
Plutonic	As-1	97	3	0	0	0	0	100	0	75
	St-2	70	30	0	0	0	0	100	0	28
	Vsc-1	31	20	47	2	0	0	100	19	43
Felsic	Rgr-1	43	16	31	6	0	0	96	0	13
Volcanic	Jsr-1	6	39	49	6	0	0	100	0	16
	Btr-1	9	38	45	8	0	0	100	0	10
	Dfv-1	6	37	56	1	0	0	100	0	35
	Tm-1	64	10	4	16	0	6	100	0	8
Intermed	Tm-2	75	6	19	7	1	4	112	0	9
Volcanic	Ta-1	93	1	2	4	0	36	136	0	9
	Av-1	87	1	5	6	1	15	115	0	31
	Dg-2	25	42	7	12	14	0	100	0	31
	Dg-3	39	29	0	8	24	0	100	0	20
Mafic	Dg-4	24	44	10	15	7	0	100	0	23
Plutonic	Sr-1	5	51	2	20	22	0	102	0	50
	Sr-2	8	53	4	19	16	0	100	0	71
	Vu-1	4	20	3	44	29	0	100	0	70
	Vu-2	1	41	5	41	12	0	100	0	67
	Kb-2	31	36	21	5	7	0	100	0	26
	M-7	51	40	7	2	0	3	103	1	3
Mafic	HBb-1	44	28	22	3	3	0	100	0	3
Volcanic	B-5*	18	4	2	0	0	0	24	0	3
	IL76-1*	26	5	1	1	0	0	33	0	3
	IL85-1	42	51	7	0	0	3	103	0	2
Meta.	pCva-1	52	7	2	44	2	0	107	0	20
Mafic/	pCma-3	23	9	1	67	0	0	100	0	3
Ultra-	PC-1057	34	4	0	71	8	0	117	2	32
mafic	MPao-1	40	10	1	32	10	0	93	1	7
Sed.	IF-2	100	0	0	0	0	0	100	0	90

from the felsic volcanic parent rocks found a predominance of trellis- and composite-type magnetite-ilmenite intergrowths (Table 6). Approximately 76% of the grains contained either or both of these textural types with the composite-type making up approximately 46% of the magnetite-ilmenite intergrowth textures. Homogeneous grains make up only 19% of the magnetite grains, while pleonaste, occurring with high-temperature oxidation "exsolution" of ilmenite trellis lamellae, is present in 5% of the detrital magnetite grains. Ulvospinel and heating martite are absent, while pseudobrookite appears only in sands derived from the Stouts Creek Rhyolite. Martitization occurred in approximately 24% of the magnetite grains.

Intermediate Volcanic Parent Rocks

Detrital magnetite derived from the andesitic parent rocks are dominated by homogeneous grains (≈69%, Table 6). Trellis- and composite-type intergrowths are relatively rare (≈10%) with composite-types making up 6% of the magnetite-ilmenite intergrowth textures. Some pleonaste-bearing grains are seen in each sand sample and make up 7% of the detrital magnetite grains. Ulvospinel is rare to absent (<0.5%). Heating martite is consistently seen in magnetite from each of the sand samples, and occurs in approximately 13% of the magnetite grains. Martitization

occurs in 12% of the grains. Pseudobrookite was not observed.

Mafic Plutonic Parent Rocks

Detrital magnetite derived from the mafic plutonic parent rocks are dominated by the presence of exsolution textures (≈40%) and magnetite-ilmenite intergrowths (≈44%). The percentage of magnetite-ilmenite intergrowths is in reality higher than the number reported here. This is because they commonly occur in association with exsolution textures, the exsolution textures receiving the nod in the point count analysis as defined in the procedures section. Trellis-type textures commonly occur as combinations of coarse ilmenite lamellae along some of the (111) planes with second, and even third sets of fine lamellae filling the interstitial areas. Pleonaste occurs as both large, dark blebs parallel to the (100) planes (typically pre-dating the ulvospinel), and associated with the high-temperature oxidation "exsolution" of ilmenite. Ulvospinel appears as a cloth-like texture as described earlier. Homogeneous grains make up 15% of the grains observed, but this number may be high because of submicroscopic textures not seen with the equipment available. Heating martite and pseudobrookite are absent. Martitization is present in 44% of the observed grains.

Mafic Volcanic Parent Rocks

Detrital magnetite derived from basaltic parent rocks typically showed a nearly 1:1 relationship between homogeneous grains (46%) and magnetite-ilmenite intergrowths (48%), with trellis-type intergrowths (35%) dominating over composite types (13%). Pleonaste (2%) and ulvospinel (2%) exsolution textures are rare, as is heating martite (1%) and pseudobrookite (<0.5%). Martitization was found in only 9% of the grains.

Metamorphosed Igneous Complexes

These samples collected in the current study were derived from metamorphosed mafic/ultramafic parent rock types. As would be expected from the previous discussion of mafic plutonic parent rocks, these samples are also dominated by exsolution textures (Tables 6 & 7). The difference is seen in the higher percentage of magnetite grains with pleonaste exsolution compared to magnetite grains with ulvospinel (Table 7). Also, while magnetite-ilmenite intergrowths are present as both trellis- and composite-types they are subordinate to the exsolution textures (Table 7). Homogeneous grains are common accessories, averaging 35%. Martitization varies considerably between samples.

Metamorphosed Sedimentary Parent Rocks

The detrital magnetite grains derived from the

metamorphosed sedimentary parent rocks, represented by the Gunflint Banded-Iron Formation, consist totally of homogeneous grains. Martitization is high, occurring in approximately 90% of the grains. All other textural types were absent.

Discussion

From the above descriptions and the average point count data in Table 6, it is clear that textural differences do occur in detrital magnetite derived from a variety of different parent rock types. What is not so clear is how to demonstrate these differences in a clear and concise way. It is first necessary to determine which textural types or combinations of textural types would best discriminate the various parent rocks, i.e. which textures would best reflect the chemical and physical differences between the sampled parent rock types. Since low-temperature oxidation has been found to be the result of weathering and diagenesis it can be assumed that magnetite grains derived from various parent rocks in the same area will alter at the same rate: this rate being dependent on climate, relief, vegetation, etc.. This assumption may not be completely true, based on the findings of Basu and Molinaroli (in press) who have suggested that magnetite with low TiO_2 and high Fe_2O_3 content may be more susceptible to low-temperature oxidation then magnetite

with high TiO_2 and low Fe_2O_3 content. Although this finding may be important in the final sand-sandstone composition, the usefulness of low-temperature oxidation textures in predicting provenance is questionable. In addition, although magnetite grains might undergo a high degree of alteration brought about by low-temperature oxidation, past studies have shown that the magnetite grains will retain their distinctive textures until the final stages of alteration and replacement (Basu and Molinaroli, in press).

Pseudomorphic oxidation textures also present problems in provenance interpretation. Previous studies (Stumpfl, 1958; Boctor, 1966; Riezebos, 1979; Ramdohr, 1980) have suggested that the conditions necessary for the formation of pseudobrookite and heating martite are restricted to volcanic parent rocks, therefore presenting a means of distinguishing volcanic sources from plutonic sources. However, the current study has found pseudobrookite textures in magnetite to be relatively rare in all the volcanic sands sampled except for sands derived from the Stouts Creek Rhyolite (Table 7). Heating martite is seen in sands derived from two of the five basaltic sands and is present in each of the four andesitic sands (Table 7 & Fig. 26), but it too is relatively rare. Therefore, although the presence of pseudomorphic oxidation

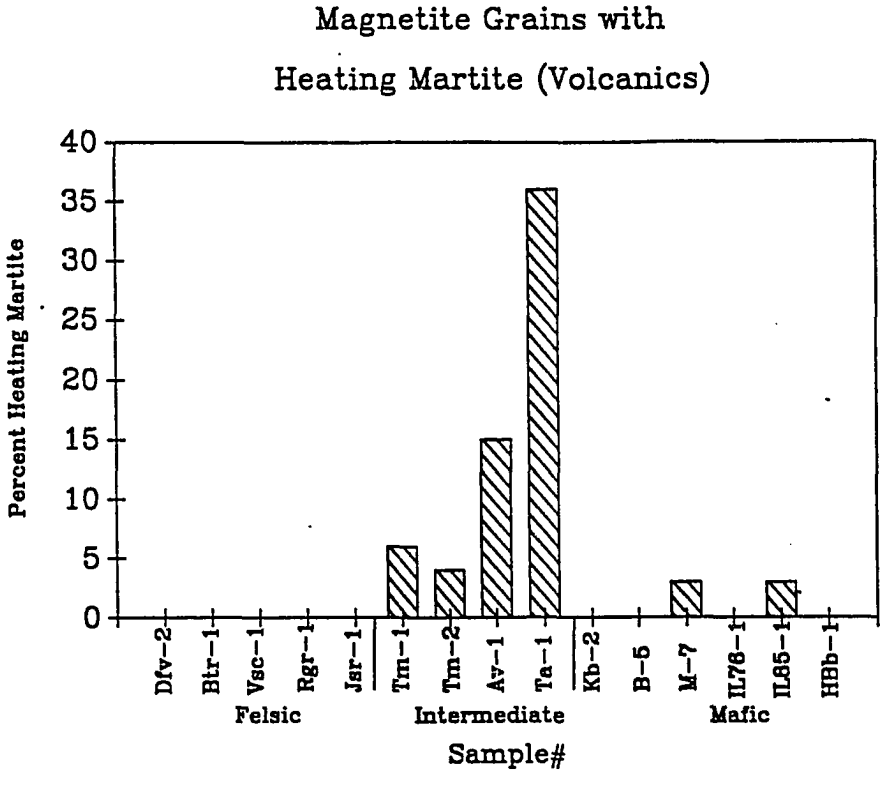

Figure 26: A bar graph showing the distribution of heating martite with detrital magnetite between the sands derived from the felsic, intermediate, and mafic volcanic parent rocks.

textures in detrital magnetite grains does provide evidence for a volcanic source, their absence in sands does not necessarily preclude the presence of a volcanic source.

From this discussion it appears that the textural types that may give the most information about the parent rocks are 1) the homogeneous magnetite grains, 2) the high-temperature oxidation "exsolution" textures, and 3) the exsolution textures. These textural features are present in all the samples of the current study and the averages of the point count analysis of the 7 genetic rock types studied (Table 6) indicates textural differences based on these textural types. Referring to Figure 27, a ternary plot has been developed using the above textural groups as corners. From this plot it is apparent that these textural groupings do separate sands derived from different parent rock types. Sands derived from felsic plutonic parent rocks (labeled with an open square) are separated from the sands derived from felsic volcanic parent rocks (filled square) on the basis of the high percentage of magnetite-ilmenite intergrowths found in the felsic volcanic sands. The felsic parent rocks (both plutonic and volcanic) are separated from the sands derived from the mafic intrusives (open triangle) and metamorphosed ultramafic/mafic intrusives (filled circle and inverted filled triangle) by the high percentage of exsolution

Figure 27: Triangular diagram representing textural variations in detrital magnetite in relationship to parent rock type. Corners are represented by homogeneous grains, grains with trellis- and composite-type magnetite-ilmenite intergrowths, and ulvospinel or pleonaste exsolution textures. Filled circles = meta-anorthosites, Filled inverted triangles = serpentinized ultramafics, Open inverted triangles = mafic volcanics (basalt), Filled squares = felsic volcanics, Open squares = felsic plutonics, Open circles = intermediate volcanics (andesite), Open triangles = mafic plutonics, Filled triangle = sedimentary banded-iron formation.

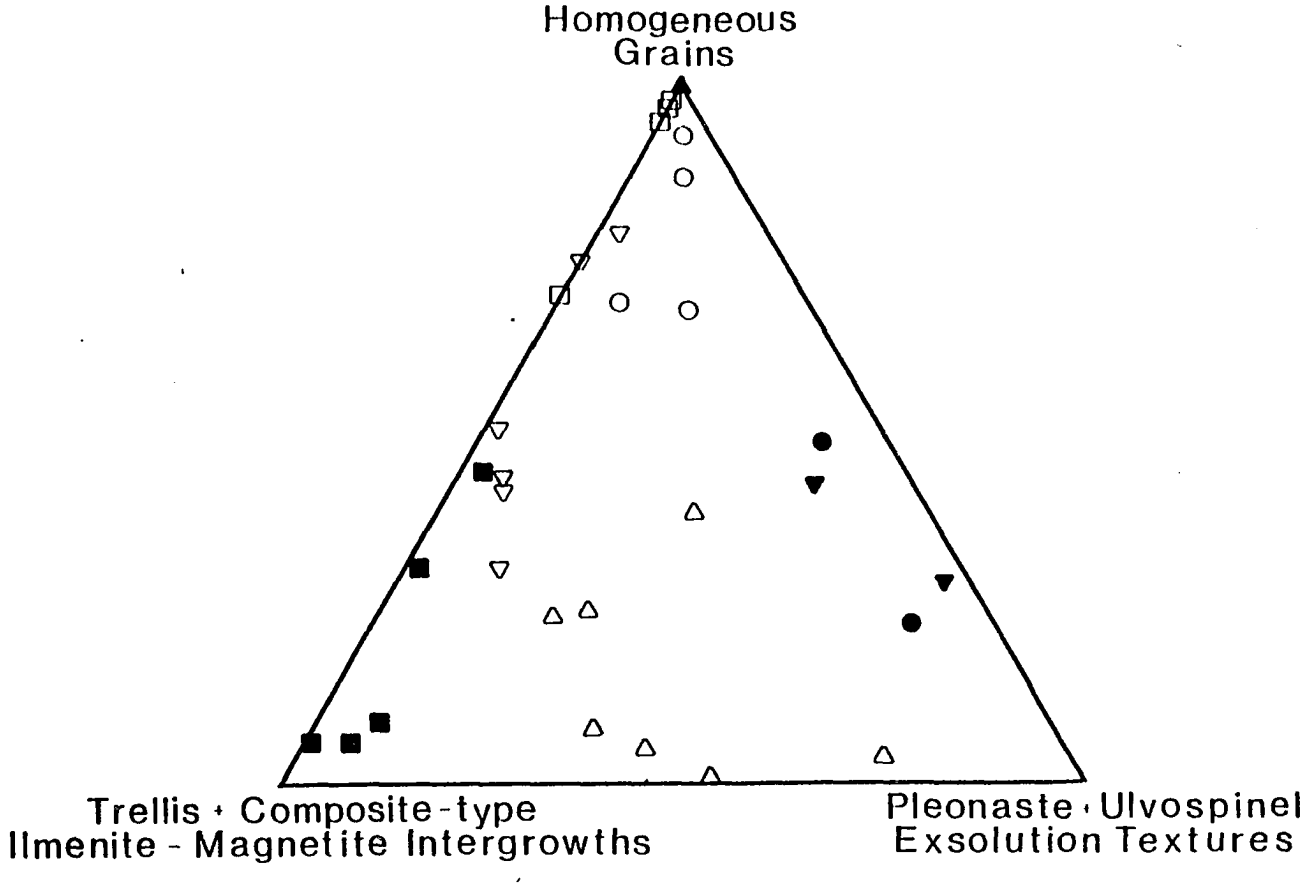

textures seen in the sands derived from the mafic parent rocks. The overlap between the sands derived from felsic volcanic parent rocks and the mafic volcanic parent rocks (inverted opened triangle) can be separated by looking at the composite-type:trellis-type magnetite-ilmenite intergrowth ratio (Fig. 28): the sands derived from the felsic volcanic parent rocks having a higher ratio than those of the sands derived from the mafic volcanic sands. The sands derived from the intermediate volcanic parent rocks (open circle) represent the largest problem because of the high percentage of homogeneous magnetite grains that dominate these sands. These sands are separated from the felsic plutonic sands only because a small percentage of parent rocks contain magnetite with pleonaste exsolution and heating martite.

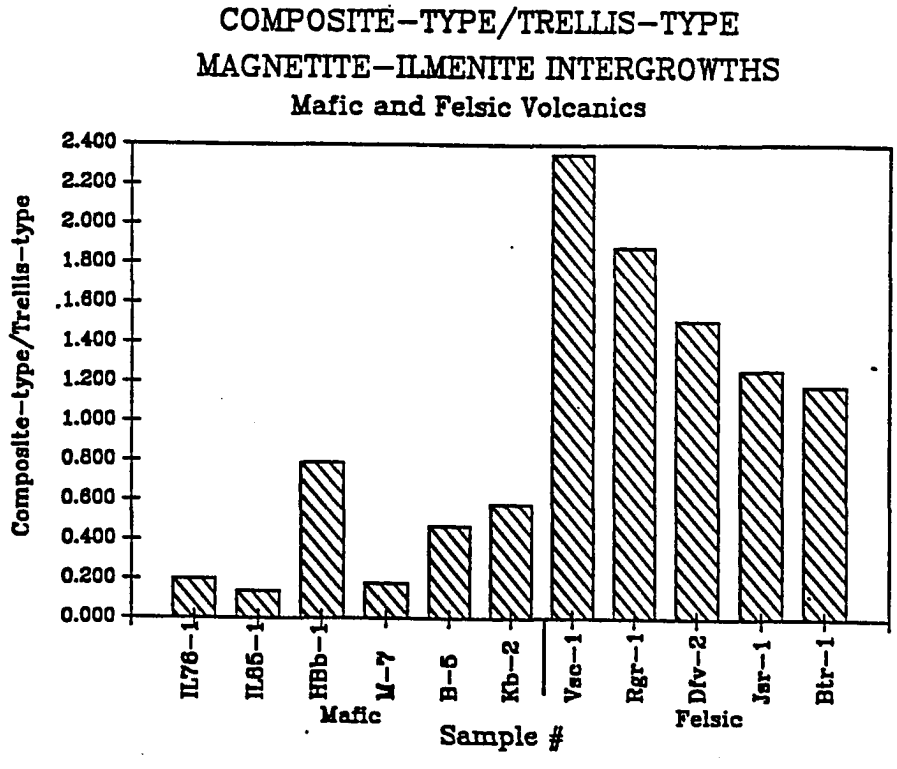

Figure 28: Bar graph representing the composite-type:trellis-type ratio found in detrital magnetite derived from mafic volcanic and felsic volcanic parent rocks.

CHAPTER VII

CHEMISTRY OF MAGNETITE AND ILMENITE IN PROVENANCE AREAS

Chemical Variations in Magnetite and Ilmenite

As discussed in the previous section magnetite and ilmenite are each part of a solid-solution series within the system $FeO-TiO_2-Fe_2O_3$ (Fig. 22). Magnetite is represented by the general formula Fe_3O_4, although it is more realistically expressed as $Fe^{3+}(Fe^{2+},Fe^{3+})_2O_4$, in which Mn^{2+} and Mg^{2+} can substitute for Fe^{2+} and Ti^{4+}, V^{3+}, Al^{3+}, and Cr^{3+} can substitute for Fe^{3+}. Ilmenite, which is represented by the general formula $FeTiO_3$, is also more realistically expressed as $(Fe,Mn,Mg)TiO_3$ where V^{3+}, Al^{3+}, and Cr^{3+} can also occur as substitutions (Hurlbut and Klein, 1977). These substitutions form the basis for the chemical variations present in the Fe-Ti oxides.

It is reasonable to suppose that variations in the whole rock chemical environment in which the Fe-Ti oxides are exposed should control the chemical composition of the magnetite and ilmenite grains formed there. This hypothesis has been supported in past studies such as Buddington and Lindsley (1964). The problem in strictly following the literature in observing these variations is that a variety of techniques have been employed to determine the chemical composition of the Fe-Ti oxides. If only data from electron probe microanalysis are considered,

which reduces the effects of inclusions and alteration on the composition of the grains common to other analytical techniques, Fe-Ti oxide composition can be related to specific parent rock types. This is supported by studies involving the electron microprobe analysis of magnetite and ilmenite found in mafic plutonic and volcanic rocks (Prèvot and Mergoil, 1973; Mathison, 1975; Johnson and Melson, 1979; Butcher and Merkle, 1987), in intermediate volcanic rocks (Luhr and Carmicheal, 1980), and in felsic plutonic rocks (Whalen and Chappel, 1988). Average electron microprobe chemical analysis of the Fe-Ti oxides from these studies is given in Table 8 for comparison. A problem to note from these analyses is that not all studies have analyzed for the same elements. This is particularly important in that vanadium is often ignored in electron microprobe analysis of the Fe-Ti oxides. This may be because of the attention that has been drawn to the near coincidence of the TiK_β x-ray emission line (λ= 2.514) with the VK_α line (λ= 2.505). For example, Wright and Lovering (1965) and Carmicheal (1967) stated that, owing to interference of TiK_β, estimation of vanadium content in Fe-Ti oxides would be difficult, if not impossible. However, Snetsinger et al. (1968), who studied the effects of this overlap, concluded that even in extreme cases of high titanium, interference with vanadium was minimal and,

Table 8: Average electron microprobe data for Fe-Ti oxides found in various igneous rock types as reported in the literature.

Wt.%	Magnetite						Ilmenite		
Oxide	1	2	3	4	5	6	2	5	6
TiO_2	11.88	5.25	21.87	27.90	9.21	NA	47.80	39.22	50.51
FeO	40.50	34.68	68.32*	33.90	36.76	NA	39.70	30.55	43.23*
Fe_2O_3	40.78	55.94	NA	31.10	48.82	NA	9.39	27.99	NA
MgO	1.27	0.97	0.76	2.20	2.04	NA	1.16	2.48	0.07
MnO	0.22	0.33	0.67	0.90	0.40	NA	1.06	0.30	5.55
Al_2O_3	3.26	2.62	1.34	2.30	2.47	NA	0.42	0.00	NA
Cr_2O_3	0.17	0.84	NA	0.60	0.13	NA	0.05	0.05	NA
V_2O_3	1.85	NA	NA	NA	0.54	NA	NA	0.20	NA
SiO_2	NA	NA	NA	NA	0.10	NA	NA	NA	NA
Total	99.93	100.62	92.96	98.90	100.47		99.60	100.78	99.36

1 = Bushveld Complex, Upper Zone (After Butcher and Merkle, 1987).
2 = Somerset Dam Layered Basic Intrusion (After Mathison, 1975).
3 = Oceanic Basalt (After Johnson and Melson, 1979).
4 = Alkali Basalt (After Prêvot and Mergoil, 1973).
5 = Colima Volcanic Complex Andesite (After Luhr and Carmicheal, 1980).
6 = I- and S-type Granites, Lachlan Fold Belt, SE Australia (Analyzed magnetite grains were reported as being almost pure Fe_3O_4 and representative analyses was not included; After Whalen and Chappel, 1988).

* indicates that iron was reported as total FeO only.

therefore, a good estimation of vanadium content in the Fe-Ti oxides could be obtained through the use of the electron microprobe. This is an important fact to consider because, as will be seen in a later section, vanadium is an important discriminator of magnetite derived from different parent rock types.

Chemical Variations in Magnetite

The chemical compositions of the detrital magnetite grains of the current study are given in Appendix B. Table 9 shows the general composition of these detrital magnetite grains in relationship to the parent rock from which they were derived. In general, the minor elements Ti, Mg, Mn, Al, V, and Cr appear to show the greatest variability. This is particularly true when relating magnetite derived from felsic sources with those derived from intermediate and mafic sources: the magnetite from the felsic sources being almost pure Fe_3O_4 with only small amounts of Ti, Mg, Mn, Al, V, and Cr, whereas the magnetite derived from the intermediate and mafic parent rocks contain appreciable amounts of these elements. The only exception to this finding was in magnetite derived from basaltic terrains in which approximately one-third of the grains were found to be Ti-free. A literature search undertaken in hopes to explain this finding was not successful. Non-igneous parent rocks (meta-anorthosites, serpentinized ultramafics,

Table 9: General examples of electron microprobe chemical analysis of detrital magnetite grains derived from the various parent rocks of the current study.

Wt% Oxide	1	2	3	4	5	6	7	8
FeO	31.02	30.86	35.08	36.60	39.83	31.41	31.03	30.28
Fe_2O_3	68.16	67.83	51.81	49.35	32.33	64.84	68.30	67.23
TiO_2	0.13	0.16	7.15	7.44	16.45	1.02	0.06	0.07
MgO	0.00	0.09	1.45	0.32	4.43	0.30	0.03	0.17
MnO	0.01	0.31	0.34	0.33	0.53	0.13	0.01	0.21
Al_2O_3	0.18	0.75	2.60	2.64	5.86	0.98	0.30	0.52
V_2O_3	0.01	0.15	0.54	1.62	0.35	0.57	0.49	0.09
Cr_2O^3	0.01	0.00	0.16	0.05	0.01	0.82	0.11	0.09
SiO_2	0.18	0.24	0.06	0.07	0.05	0.12	0.02	1.46
Total	99.69	100.39	99.25	98.41	99.84	100.19	100.35	100.12

1 = Graniteville Granite.
2 = Royal Gorge Rhyolite.
3 = Nevado de Toluca Andesite.
4 = Duluth Gabbro.
5 = Hawaii Island Basalt.
6 = Serpentinized Ultramafic (Loma de Hierro).
7 = Marcy-type Meta-anorthosite.
8 = Gunflint Banded-Iron Formation.

and sedimentary banded-iron formation) show compositions close to those of the magnetite grains derived from the felsic plutonic/volcanic parent rocks.

Chemical Variations in Ilmenite

The composition of ilmenite is quite variable within and between the parent rock groups of the current study (Table 10; Appendix C). This variability is greatest in the elements Ti, Mn, and Mg. In contrast to magnetite, few trends can be observed between the ilmenite composition and the parent rocks from which they were derived. There is some distinction in Mn and Mg between the ilmenite grains from the felsic sources and the ilmenite grains from the mafic sources, but this is not consistent.

Discriminant Analysis

Introduction

In order to determine which elements in detrital magnetite and ilmenite may best discriminate between the parent rock types studied, data from these samples were treated by step-wise discriminant analysis using the Statistical Package for the Social Sciences (see Nie et al., 1975). Discriminant analysis, as defined by Klecka (1987) "is a statistical technique which allows the researcher to study the differences between two or more groups of objects with respect to several variables simultaneously." The basic assumptions that are made in

Table 10: General examples of electron microprobe chemical analysis of detrital ilmenite grains derived from the various parent rocks of the current study.

Wt% Oxide	1	2	3	4	5	6	7
FeO	38.09	42.72	35.68	41.97	41.92	42.09	39.63
Fe_2O_3	10.18	5.36	16.40	5.69	7.19	5.89	11.82
TiO_2	46.67	49.11	44.10	49.39	48.54	48.65	45.95
MgO	0.03	0.54	2.23	1.30	1.21	0.18	1.03
MnO	4.06	0.94	0.45	0.50	0.00	1.71	0.33
Al_2O_3	0.43	0.67	0.63	0.50	0.59	0.37	0.64
V_2O_3	0.75	0.77	0.80	0.76	0.84	0.99	0.82
Cr_2O_3	0.00	0.00	0.06	0.03	0.02	0.16	0.07
SiO_2	0.07	0.00	0.03	0.09	0.04	0.07	0.01
Total	100.28	100.11	100.38	100.23	100.35	100.11	100.30

1 = Surgarloaf Peak Quartz Monzonite.
2 = Royal Gorge Rhyolite.
3 = Nevado de Toluca Andesite.
4 = Duluth Gabbro.
5 = Keweenawan Basalt.
6 = Serpentinized Ultramafic (Loma de Hierro).
7 = Marcy-type Meta-anorthosite.

discriminant analysis are 1) the data cases should be members of two or more mutually exclusive groups, 2) the groups must be defined so that each case belongs to one, and only one, group, 3) no variable may be a linear combination of other discriminating variables, 4) two variables that are perfectly correlated cannot be used at the same time, 5) the population covariance matrices are equal for each group, and 6) each group is drawn from a population that has a multivariate normal distribution. These assumptions constitute the mathematical model on which the most common approaches to discriminant analysis rest (Klecka, 1987).

In the current study the groups are defined by the specific rock types sampled and the variables are represented by the elemental composition of the detrital magnetite and ilmenite grains. Linear combinations of the elements, called canonical discriminant functions, are computed that maximize the separation between the parent rock types sampled. The greater the power of the discriminant functions to separate groups, the greater the ability to classify unknown samples correctly. The maximum number of canonical discriminant functions that can be derived is equal to the number of groups minus one or the number of discriminating variables, whichever is fewer. Because the functions are derived in order of their power

to discriminate between groups, only the number of functions that account for the greatest variance within the variables need be computed.

The discriminant functions can be thought of as a set of coordinate axes in geometric space with each data case representing a point in this space. If the groups differ in their behavior with respect to these variables they will form a cluster of points concentrated in some portion of the geometric space. While the groups may overlap, their respective territories are not identical. To summarize the position of a group, the group centroid is computed. The group centroid is defined as an imaginary point that has coordinates at the group's mean on each of the variables. Because each centroid represents the typical position for its group, the centroids can be studied to obtain an understanding of how the groups differ.

One of the objectives of this study was to identify the most effective group of elements contained in magnetite and ilmenite for discriminating between parent rock types. To do this, a stepwise procedure was used. This procedure begins by selecting the individual variable that provides the greatest univariant discrimination. The procedure then pairs the first variable with each of the remaining variables and the second variable that contributes to the best pair is chosen. This process of selecting variables

based on the one that adds the most discrimination continues until all possible variables have been selected, or the remaining variables do not contribute to the discrimination (see Appendix D for the discriminant analysis program).

This process of discriminant analysis has been used successfully in various fields of geology. These include the interpretation of provenance signatures of mudstone based on major element data (Roser and Korsch, 1988), the correlation of Middle Ordovician K-bentonite beds (Huff, 1983), the identification of Holocene tephras based on magnetite composition (Beauduin and King, 1986), and the separation of drainage basins based on ilmenite composition (Darby and Tsang, 1987). For further information on the mathematical basis for discriminant analysis and the development of computer programs see Davis (1973) and Klecka (1975).

Results of Discriminant Analysis

Magnetite. Because interest was in determining the compositional variations that exist in detrital magnetite derived from felsic, intermediate, and mafic igneous rocks, stepwise discriminant analysis was used to determine the discriminating power of the analyzed elements. The summary in Table 11 lists the results of the stepwise discriminant analysis using the Wilkes' lambda method. Wilkes' lambda

Table 11: Summary table for 6 elements ranked according to their power to discriminate between the various igneous rock types sampled (Magnetite).

Step	Action Entered	Removed	Vars In	Wilkes' Lambda
1	Ti		1	0.25052
2	Mg		2	0.09315
3	V		3	0.06925
4	Al		4	0.05347
5	Mn		5	0.04968
6	Cr		6	0.04709

is defined as a multivariate measure of group differences over several variables (the discriminating variables) and is an inverse measure of the discriminating power in the original set of variables that has not yet been removed by the discriminating functions. The most successful element in discriminating between the igneous rock groups (felsic plutonic/volcanic, intermediate volcanic, and mafic plutonic) is Ti, followed in order by Mg, V, Al, Mn, and Cr. A further aid in judging the importance of a discriminant function is its associated canonical correlation. This correlation is a measure of association between the single discriminant function and the set of variables (elements) that define the group membership and indicates how closely the function and the group variable are related. Table 12 lists the eigenvalues, their associated canonical correlations, and the cumulative percent of the discrimination accounted for by each successive function calculation. Two discriminant functions were derived from the three igneous rock groups following the basic rule of discriminant analysis that states that the number of functions is equal to the number of groups minus one or the number of variables, whichever is smaller. The discriminant functions are represented by the general equation

$$F_{km} = u_o + u_1X_{1km} + u_2X_{2km} + \ldots + u_iX_{ikm}$$

Table 12: Canonical discriminant functions for detrital magnetite from the defined groups (6 elements).

			Canonical Discriminant Functions						
Function	Eigenvalue	Percent of Variance	Cumulative Percent	Canonical Correlation	:	After Function	Wilks' Lambda	Chi-Squared	D.F. Significance
					:	0	0.0470868	728.80	12 0.0000
1	5.30148	69.10	69.10	0.9172280	:	1	0.2967167	289.77	5 0.0000
2	2.37022	30.90	100.00	0.8386199	:				

where F_{km} is the discriminant score on the canonical discriminant function for case m in group k, u_i's are the unstandardized discriminant function coefficients with u_o equaling a constant, and X_{ikm}'s are the raw values on the discriminating variable X_i for case m in group k. Calculation of the two functions in Table 12 accounts for 100% of the discriminating power of the variables. The right side of Table 12 shows the changes in Wilkes' lambda and their associated chi-square tests of statistical significance as the information in successive discriminant functions is removed. Before removal of any functions lambda was 0.0470868. This low value indicates that enormous discriminating power exists in the variables being used, since the smaller the value of lambda the greater the discriminating power. After some power has been removed by placing it in the first discriminating function there is a slight increase in lambda, but the chi-squared value indicates that a significant amount of discriminating information still exists. Verification of the high degree of strength in the discriminant model is provided by the classification of the three igneous rock groups. When each is compared individually with the discriminant model the correct identification of each rock group can be predicted 97.13% of the time (Table 13). Therefore, within the limits of the rock types studied each of the detrital

Table 13: Results of the discriminant analysis classification. Group 1 = Felsic plutonic/volcanic parent rocks, Group 2 = Intermediate volcanic(andesitic) parent rocks, Group 3 = Mafic plutonic parent rocks (Magnetite).

	No. of	Predicted Group Membership		
Actual Group	Cases	1	2	3
Group 1	105	103 (98.1%)	2 (1.9%)	0
Group 2	61	0	61 (100%)	0
Group 3	78	5 (6.4%)	0	73 (93.6%)

Percent of grouped cases correctly classified = 97.13%

magnetite grains carries a unique and identifiable chemical fingerprint.

The two functions developed during this analysis are used to construct a territorial map that displays the boundaries of the regions defined by each of the three groups. Within these boundaries are plotted the discriminant score of the group centroids for each group and the score for each individual magnetite grain (Fig. 29). To determine if any given unknown sample is chemically similar to one of the three igneous rock groups, the analyzed value for a particular element or group of elements in that sample is multiplied by the corresponding discriminant coefficients (Table 14) and plotted on the territorial map.

The rock types that were included in this statistical plot were chosen on the premise that they would supply detrital magnetite to the site of deposition. The felsic plutonic/volcanic field, in which 98.1% of the magnetite grains were correctly classified, was represented by detrital magnetite derived from the Graniteville Granite, the Favela Granite, the Sugarloaf Peak Quartz Monzonite, the Saganaga Tonalite, the Royal Gorge Rhyolite, and the Stouts Creek Rhyolite (microprobe data is given in Appendix B, tables 27-32). The Rooiberg Felsite (Appendix B, Table 33) was not included in this initial classification because

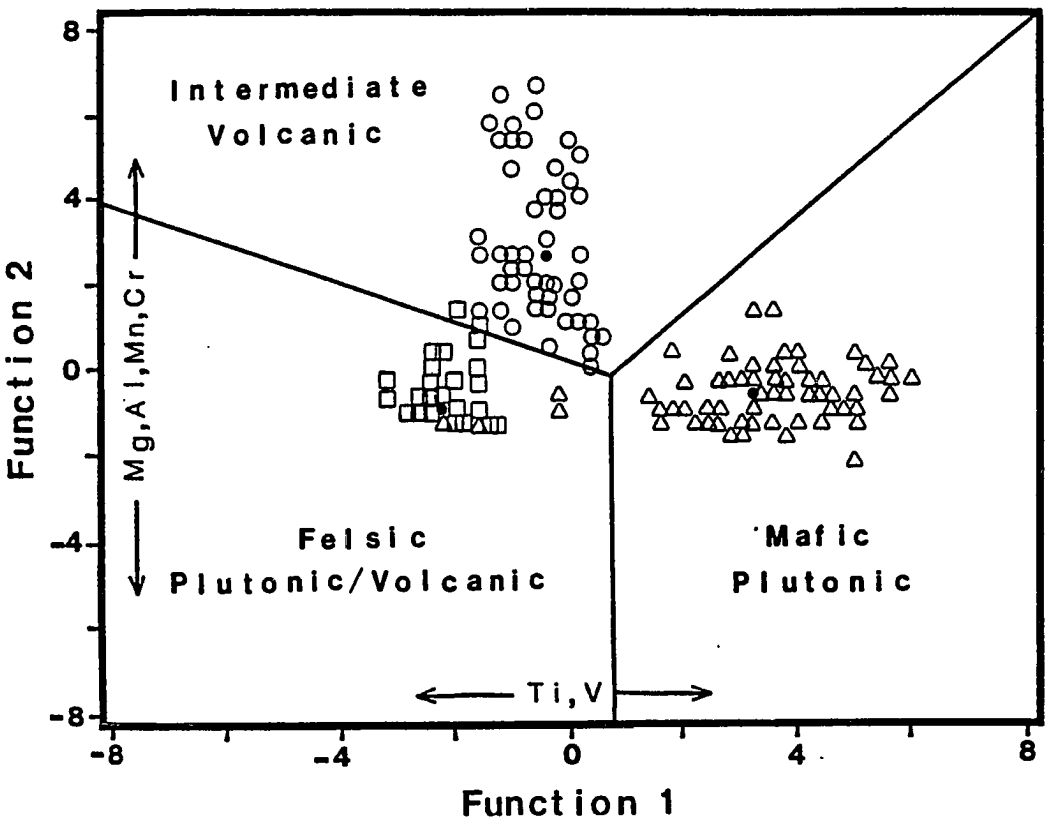

Figure 29: Territorial map constructed from the first (Function 1) and second (Function 2) discriminant functions calculated for the six elements analyzed for in detrital magnetite. Open squares = felsic plutonic/volcanic parent rocks, Open circles = intermediate volcanic parent rocks, and Open triangles = mafic plutonic parent rocks, small filled circles = group centroids of defined fields.

Table 14: List of unstandardized canonical discriminant function coefficients as determined through the discriminant analysis of magnetite.

	Function 1	Function 2
Ti	0.2384642	0.8535054E - 01
V	1.410390	-0.2953255
Al	0.5414264	-0.3958246
Cr	-1.842684	1.008869
Mg	-0.9313623	1.859722
Mn	-2.315731	1.445311
(Constant)	-2.315731	-1.274669

of the extreme compositional differences found to exist between the detrital magnetite derived from it and the other felsic parent rocks. Plotting the discriminant scores of the detrital magnetite from the Rooiberg Felsite onto the territorial map indicates that the grains plot between the intermediate volcanic and mafic plutonic fields (Fig. 30). Because of the small size of the sand sample available from this area the exact cause of the difference between these grains and those derived from the other felsic volcanics could not be determined. Two hypotheses are suggested 1) the high percentage of magnetite-ilmenite intergrowths, shown in the petrographic section, may indicate that the analyzed homogeneous grains actually contained submicroscopic ilmenite inclusions causing interference in the compositional analysis, and 2) there exists a genetic relationship between the Bushveld Complex and the Rooiberg Felsite that may have influenced the magnetite composition.

The intermediate volcanic field, in which 100% of the magnetite grains were correctly classified, was represented by detrital magnetite derived from andesitic parent rocks at Nevado de Toluca, Mexico, northern Taiwan, and Ovalau, Fiji (microprobe data are listed in Appendix B, tables 34-37). No intermediate intrusive rocks were sampled.

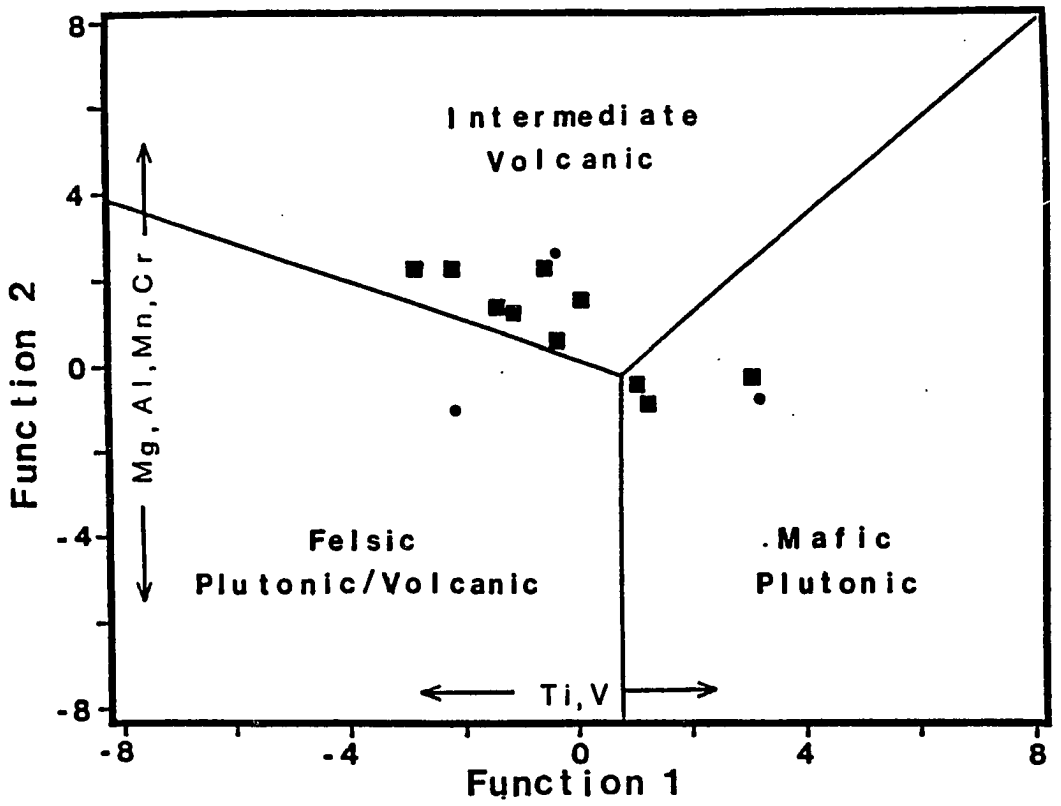

Figure 30: A plot of the discriminant scores calculated from the analysis of detrital magnetite derived from the Rooiberg Felsite onto the standard plot in Figure 29. Filled squares = Rooiberg Felsite, small filled circles = group centroids of defined fields.

The mafic plutonic field, in which 93.6% of the magnetite grains were correctly classified (this percent of correctly classified grains was the lowest of the three igneous rock groups and may be explained by the presence of granophyre dikes, discussed in the "Geology of the Duluth Gabbro," that could supply detrital magnetite of almost pure Fe_3O_4 to the sand), was represented by detrital magnetite derived from the Duluth Gabbro and the Bushveld Complex (microprobe data are listed in Appendix B, tables 38-43). Mafic volcanics (basalt) were excluded from this field because of the wide compositional variations found in the detrital magnetite of basaltic sands (Appendix B; tables 44-49). This large variation was unexpected, particularly the high percentage of Ti-free magnetite found in these sands. Although there are reports that Ti-free magnetite may form through the oxidation of olivine and sulfides (Haggerty, 1976a; Johnson and Melson, 1979) the possibility of this process forming sand-sized detrital magnetite is questionable and not substantiated anywhere in the literature. Another possible explanation for the existance of Ti-free magnetite is the presence of a high-temperature miscibility gap in which slight changes in temperature could result in the formation of both high- and low-Ti magnetite (Sack, 1982). A plot of the discriminant scores of the detrital magnetite derived from the basaltic

sands onto the earlier discussed territorial map shows an almost even distribution between all three defined fields (Fig. 31; Table 15). The overlap into the intermediate field was not as unexpected and may be explained in two ways 1) the variability of the whole rock chemistry of basalt, particularly in the areas sampled as seen in Table 4, could influence magnetite composition, and 2) the increase in the weight percentage of Mn and Cr in many of the basaltic detrital magnetite grains was great enough to push them up into the intermediate volcanic fields.

In addition to the igneous rocks discussed above three other rock types, which could supply magnetite to a depositional environment, were analyzed and plotted with discriminant analysis for comparison. These included sand samples derived from the Marcy- and Whiteface-type meta-anorthosites, serpentinized ultramafics from Venezuela and Newfoundland, and the metamorphosed Gunflint Banded-Iron Formation of Minnesota (microprobe data are listed in Appendix A, tables 50-54). The discriminant scores of these samples plotted dominantly into the felsic field except for three grains from the Venezuela sample that plotted in the andesitic field (Fig. 32). This was expected of the Gunflint banded-iron formation, which is thought to be the result of direct precipitation of Ti-free Fe_3O_4. It was unexpected of the detrital magnetite grains

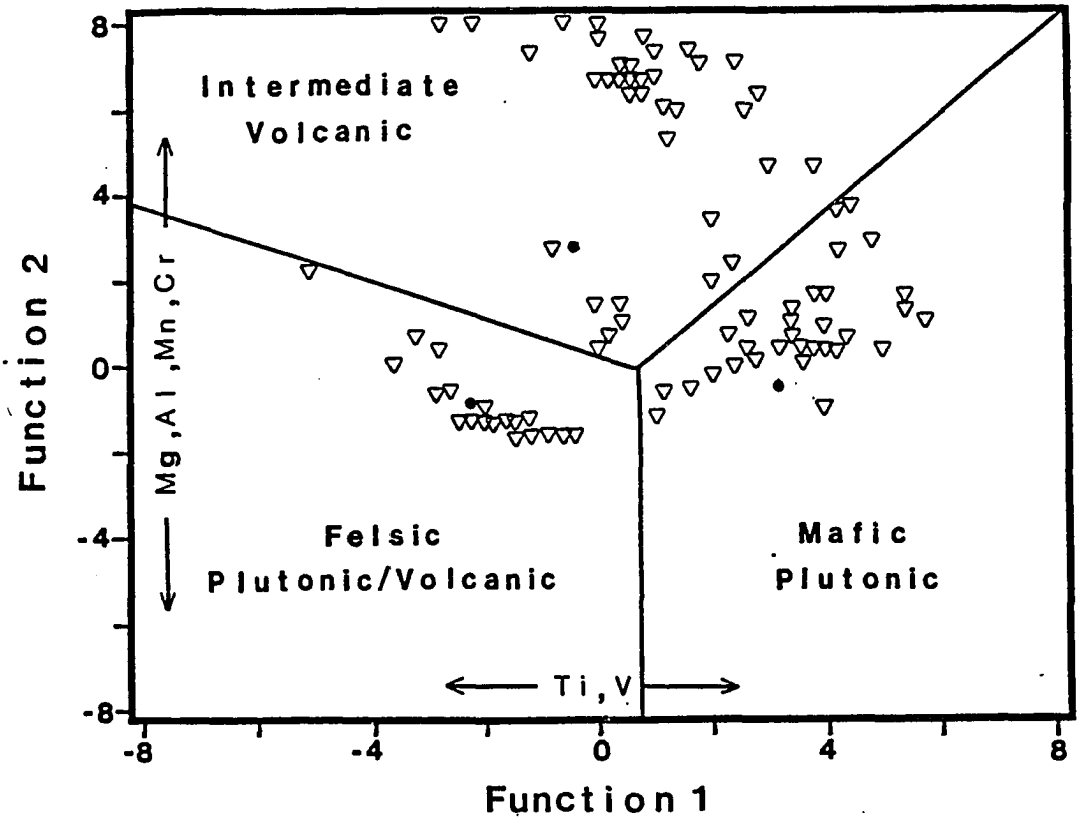

Figure 31: A plot of the discriminant scores of the detrital magnetite grains derived from various basaltic parent rocks. Open inverted triangles = magnetite of basaltic source, small filled circles = group centroids of the defined fields.

Table 15: Results of discriminant analysis classification of detrital magnetite derived from mafic volcanic parent rocks.

Rock Type	No. of Cases	Predicted Group Membership		
		Felsic	Intermediate	Mafic
Mafic Volcanic	111	35 (31.5%)	44 (39.6%)	32 (28.8%)

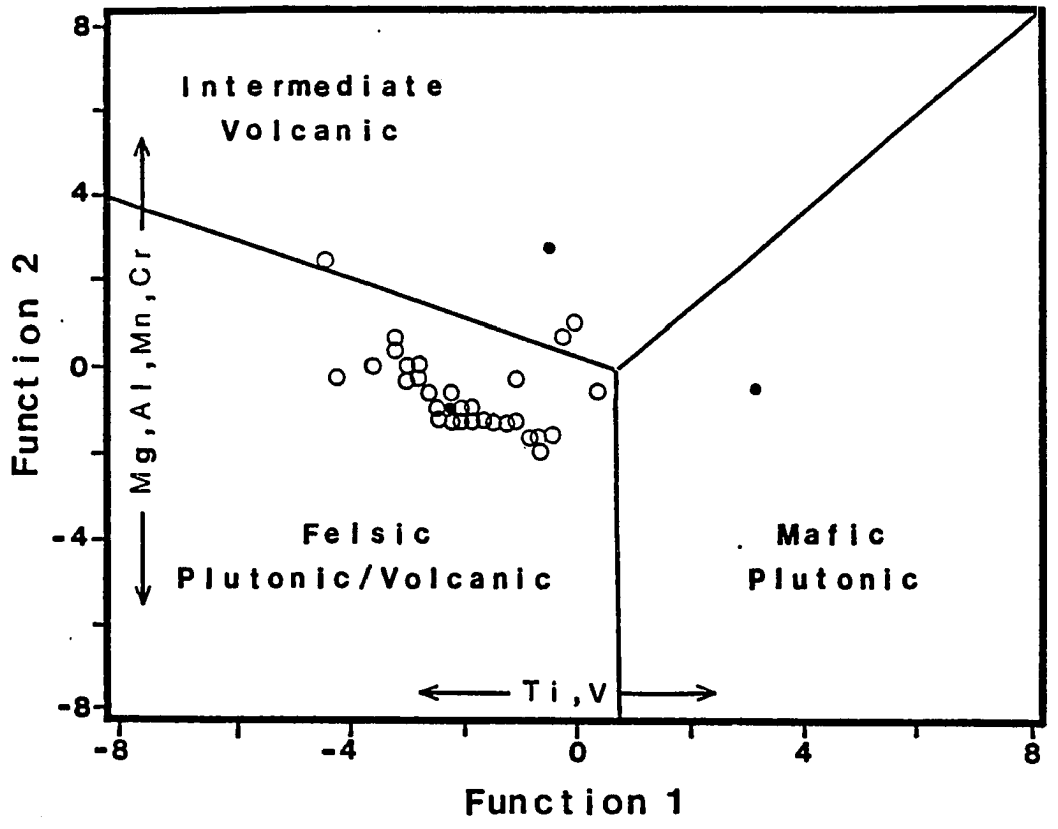

Figure 32: Plot of the discriminant scores of the detrital magnetite grains derived from meta-anorthosites, serpentinized ultramafics, and banded-iron formation. Open circles = all grain types from above sources, small filled circles = group centroids of the defined fields.

from the meta-anorthosites and the serpentinized ultramafics in which compositions similar to the mafic plutonic parent rocks, discussed earlier, were thought to occur. Secondary magnetite is one of the principal products of serpentinization of ultramafics (Hall and Fischer, 1977; Johnson, 1979). This magnetite is Ti-free and homogeneous. It is logical that the homogeneous magnetite grains derived from these serpentinized ultramafics would be dominated by the secondary magnetite formed during serpentinization. This would result in the findings in Figure 32 and the overlap with the felsic plutonic/volcanic field. The possibility that similar reasoning can be used to explain the Ti-free magnetite derived from the meta-anorthosites can not be substantiated at this time.

Ilmenite. The discriminant analysis technique for ilmenite was the same as that used for magnetite. The variables tested for in the stepwise analysis included Ti, V, Al, Cr, Mg, and Mn. The igneous parent rocks from which detrital ilmenite was derived included felsic plutonic/ volcanic sources (represented by the Favela granite, the Surgarloaf Peak quartz monzonite, the Saganaga tonalite, the Royal Gorge rhyolite, the Stouts Creek rhyolite, and the Rooiberg felsite), intermediate volcanics (represented by andesites from Nevado de Toluca, Mexico and Ovalau,

Fiji), and mafic plutonic/volcanic sources (represented by the Duluth Gabbro, the Bushveld Complex, and the Keweenawan basalt). Microprobe data from these ilmenite grains are listed in Appendix C, tables 55-67.

The results of the discriminant analysis are as follows. The summary in Table 16 indicates that Mn was the most powerful discriminator followed by Ti, V, Mg, and Cr. Aluminum could not reduce the variance remaining within the three igneous rock groups when in combination with the other five elements and was not included in the remaining analysis. Table 17 lists the eigenvalues, their associated canonical correlations, and the cumulative percent of the discrimination accounted for by each successive function calculation. As before, two discriminant functions were derived for the three igneous rock groups with the unstandardized discriminant function coefficients shown in Table 18. Table 17 indicates that before the removal of any functions, lambda was 0.5525750. This value is relatively high, particularly when compared to the low value obtained in the analysis of magnetite, and indicates a lesser ability of the analyzed elements in ilmenite to discriminate between the igneous rock groups. After some of this power has been removed by placing the variables in the first discriminant function there is a significant increase in Wilkes' lambda and the chi-squared value

Table 16: Summary table for 5 elements ranked according to their power to discriminate between the igneous rock groups (Ilmenite).

Step	Action Entered	Removed	Vars In	Wilkes' Lambda
1	Mn		1	0.75836
2	Ti		2	0.67703
3	V		3	0.60762
4	Mg		4	0.57376
5	Cr		5	0.55258

Table 17: Canonical discriminant functions for detrital ilmenite from the defined groups (5 elements).

Canonical Discriminant Functions

Function	Eigenvalue	Percent of Variance	Cumulative Percent	Canonical Correlation	After Function	Wilks' Lambda	Chi-Squared	D.F.	Significance
					0	0.5525750	97.872	10	0.0000
1	0.65360	87.38	87.38	0.6206959	1	0.9137377	14.885	4	0.0049
2	0.09441	12.62	100.00	0.2937045					

Table 18: List of unstandardized canonical discriminant coefficients as determined through the discriminant analysis of Ilmenite.

	Function 1	Function 2
Ti	0.3089405	0.2552722
V	2.245382	3.570910
Cr	4.240627	2.202616
Mg	0.4669297	-0.5317609
Mn	-0.2489496	0.3101706
(constant)	-16.96572	-15.42945

indicates that little discriminating power is left. This lack of discrimination is obvious in Figure 33 and Table 19. They show that when each group is compared individually with the discriminant model the correct identification of all ilmenite grains can be predicted only 57.06% of the time. Because of this lack of discrimination the ilmenite derived from the metamorphosed igneous rocks were not included in the discriminant analysis (data presented in Appendix C).

Discussion

From the previous section it was found that the use of discriminant analysis to assign the compositional variations present in detrital ilmenite to specific parent rocks resulted in only 57.06% of the ilmenite grains correctly classified. This low percentage is surprising considering the findings of Darby and Tsang (1987). In their study they were able to separate drainage basins based on compositional variations in detrital ilmenite and concluded that these variations were directly related to changes in parent rock types surrounding these drainage basins. The differences between the Darby and Tsang study and the current study are 1) Darby and Tsang used atomic absorption techniques rather than the electron microprobe for chemical analysis, and 2) they analyzed for three elements (Cu, Zn, Ni), in addition to the elements covered

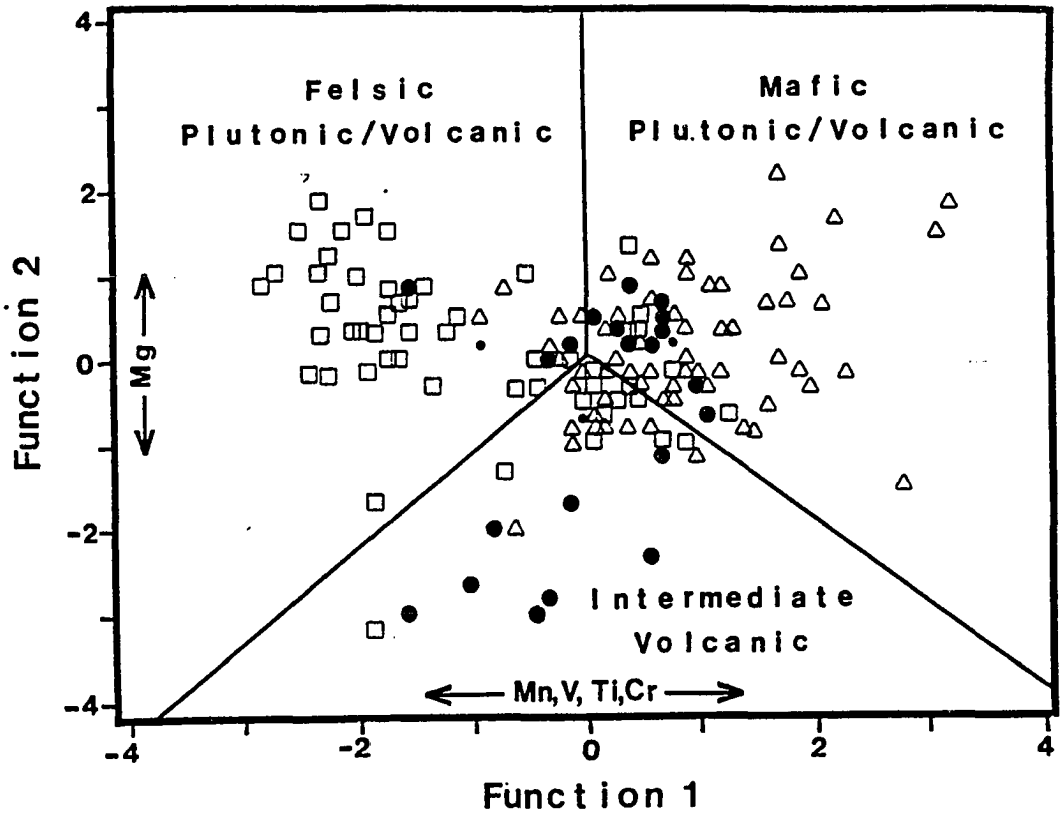

Figure 33: Territorial map constructed from the first (function 1) and second (function 2) discriminant functions calculated for the 5 elements analyzed in detrital ilmenite from the various parent rocks. Open squares = felsic plutonic/volcanic parent rocks, Filled circles = intermediate volcanic parent rocks, Open triangles = mafic plutonic/volcanic parent rocks, small filled circles = group centroids of the defined fields.

Table 19: Results of the discriminant analysis classification for ilmenite. Group 1 = Felsic plutonic/volcanic parent rocks, Group 2 = Intermediate volcanic parent rocks, Group 3 = Mafic plutonic/volcanic parent rocks.

	No. of	Predicted Group Membership		
Actual Group	Cases	1	2	3
Group 1	70	39	20	11
		(55.7%)	(28.6%)	(15.7%)
Group 2	26	3	11	12
		(11.5%)	(29.7%)	(46.2%)
Group 3	74	5	22	47
		(6.8%)	(29.7%)	(63.5%)

Percent of "grouped" cases correctly classified: 57.06%

in the current study, that occur in such small proportions that they are not detectable by the electron microprobe. These three additional elements became important in their discriminant analysis classification and may have led to the separation they found. Therefore, while admitting that the chemical analysis of detrital ilmenite may yield more information than the current study implies, the additional time required in the separation of detrital ilmenite, through magnetic separation or heavy liquids, and preparation of the grains for atomic absorption analysis may make the usefulness of detrital ilmenite in provenance studies rather limited.

In contrast to ilmenite, the use of discriminant analysis to assign compositional variations in detrital magnetite derived from three igneous rock groups (felsic plutonic/volcanic, intermediate volcanic, and mafic plutonic) was quite successful with 97.13% of the magnetite grains correctly classified. This analysis (stepwise discriminant analysis) was important in distinguishing which elements had the greatest power to discriminate between the various parent rocks. With this knowledge it is possible to derive simpler unweighted plots to use in assigning provenances. Based on the discriminant analysis, the two best variables are weight percent Mg/(Mg+Al) versus Ti+V. The results of such a plot, using the same data that

was used in the discriminant analysis technique, was successful in correctly classifying the detrital magnetite grains 95.9% of the time (Fig. 34; Table 20). This compares quite favorably with the 97.13% of correctly classified grains attained through discriminant analysis. Thus a simpler, easier to visualize technique proved to be nearly as good as discriminant analysis without the large commitment of mainframe computer time needed by that technique. In addition to simplifying the classification technique for future research, the results attained when the simple graphical technique is applied to the detrital magnetite derived from the mafic volcanic source rocks is quite promising (Fig. 35; Table 21). Approximately 62% of the detrital magnetite derived from the basaltic parent rocks fall into the mafic field, whereas only 7% plot into the intermediate volcanic field. This compares to 28.8% and 39.6%, respectively, determined by discriminant analysis. The percentage of grains that plot in the felsic field remains about the same (31% compared to 31.5%). The question may be raised as to why Mn and Cr have been ignored in these plots? Referring to Table 11, which lists the order of discriminating power of the elements, it is found that Mn and Cr add little to the discriminant functions. This is seen in the small changes in Wilkes' lambda at the addition of these elements. Therefore, it

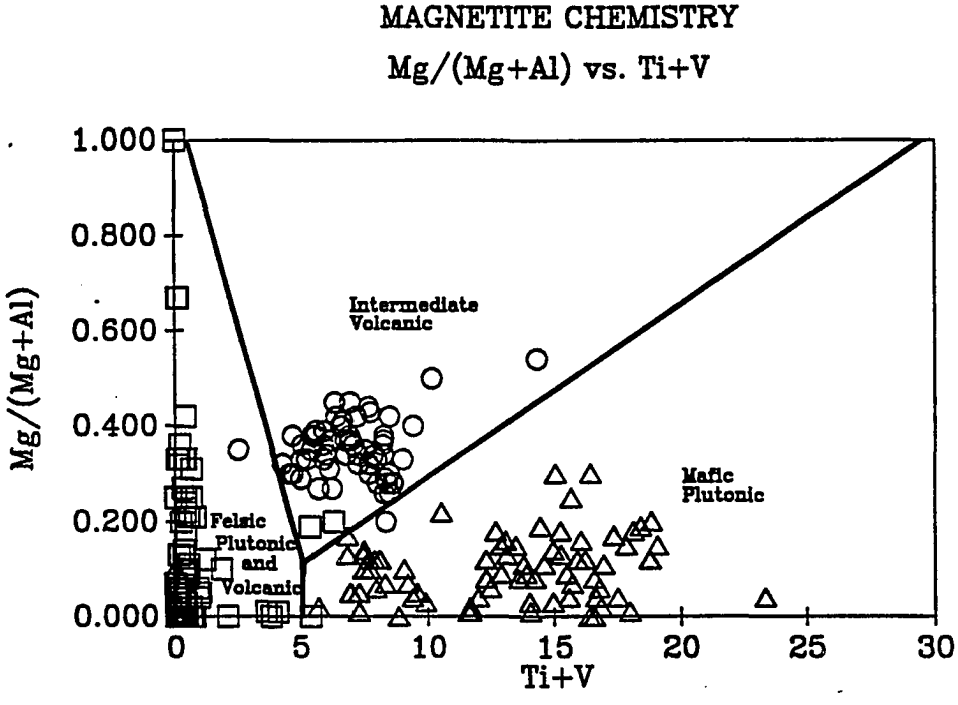

Figure 34: Plot of the weight percent Mg/(Mg+Al) vs. Ti+V based on the electron microprobe chemical analysis of detrital magnetite derived from various parent rocks. Open squares = felsic plutonic/volcanic parent rocks, Open circles = intermediate volcanic parent rocks, Open triangles = mafic plutonic parent rocks.

Table 20: Percent of correctly classified detrital magnetite using the alternative technique of comparing the weight percent of Mg/(Mg+Al) vs. Ti+V. Group 1 = Felsic plutonic/volcanic parent rocks, Group 2 = Intermediate parent rocks, Group 3 = Mafic plutonic parent rocks.

	No. of	Predicted Group Membership		
Actual Group	Cases	1	2	3
Group 1	105	102 (97.1%)	2 (1.9%)	1 (1.0%)
Group 2	61	1 (1.6%)	59 (96.7%)	1 (1.6%)
Group 3	78	5 (6.4%)	0	73 (93.6%)

Percent of "Grouped" cases correctly classified = 95.9%

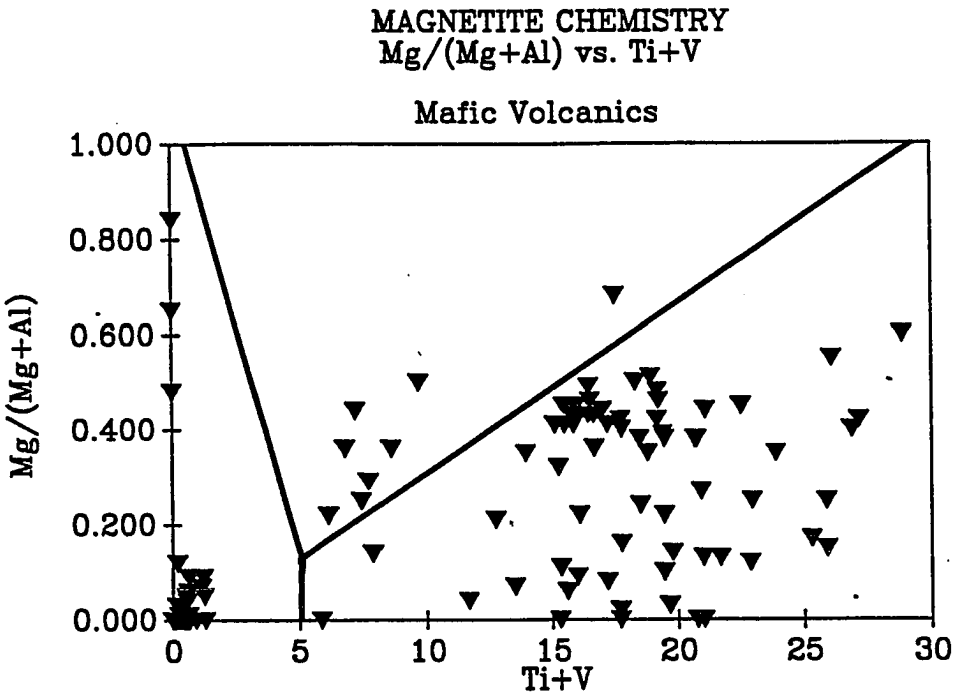

Figure 35: A plot of the weight percent Mg/(Mg+Al) vs. Ti+V for detrital magnetite derived from mafic volcanic parent rocks.

Table 21: Percentage of detrital magnetite derived from mafic volcanic parent rocks correctly classified using the alternate technique of classification (Mg/(Mg+Al) vs. Ti+V).

Rock Type	No. of Cases	Predicted Group Membership Felsic	Intermediate	Mafic
Mafic Volcanic	111	34 (31%)	8 (7%)	69 (62%)

was decided that these two elements added little to the separation of groups and that Ti, V, Mg, and Al could lead to a good classification system that Figure 34 verifies. For the sake of comparison the compositional data for the detrital magnetite derived from the Rooiberg felsite, the meta-anorthosites, the serpentinized ultramafics, and the banded-iron formation were plotted using this technique and are shown in Figures 36-39.

These plots, derived through the compositional analysis of detrital magnetite, indicate the importance of this Fe-Ti oxide in future provenance research. It is apparent that each individual magnetite grain carries with it a chemical fingerprint that tells a story about the parent rock from which it was derived. Although further research is needed to determine the source of the Ti-free magnetite found in the basaltic sands, and a better understanding is needed of the magnetite derived from metamorphosed parent rocks, this method of analysis appears to be quite promising. Because homogeneous grains were the only grains analyzed in the current study care must be taken in the petrographic identification of these grains. This limitation in the electron microprobe analysis does present some problems as was seen in the case of the meta-anorthosites and the serpentinized ultramafics where the presence of secondary magnetite dominated the homogeneous

Figure 36: A plot of the weight percent Mg/(Mg+Al) vs. Ti+V for detrital magnetite derived from the Rooiberg Felsite (Filled square).

Figure 37: A plot of the weight percent Mg/(Mg+Al) vs. Ti+V for detrital magnetite derived from the Marcy-type and Whiteface-type meta-anorthosites. Open circle = Marcy-type, open triangle = Whiteface-type.

MAGNETITE CHEMISTRY
Mg/(Mg+Al) vs. Ti+V

Rooiberg Felsite

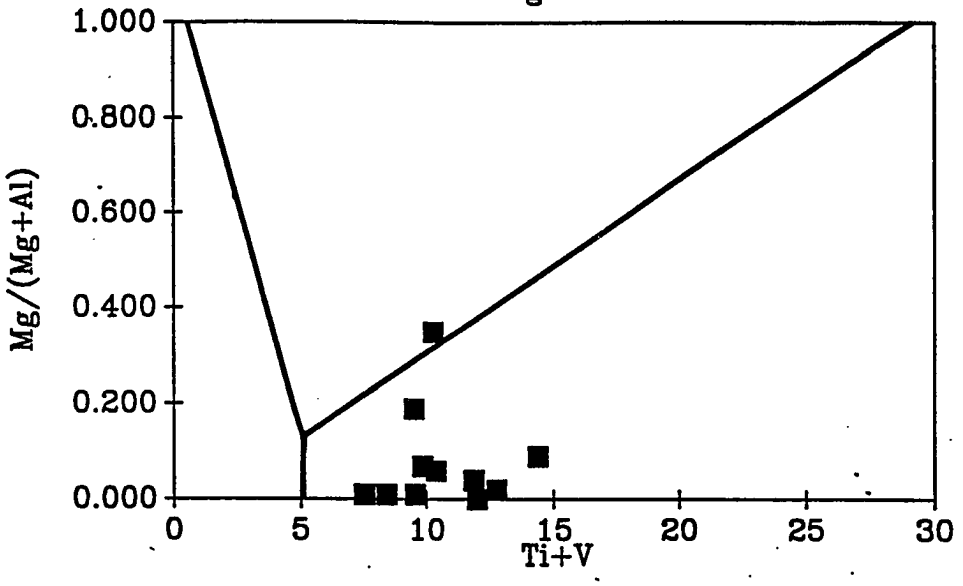

MAGNETITE CHEMISTRY
Mg/(Mg+Al) vs. Ti+V

Meta–Anorthosites

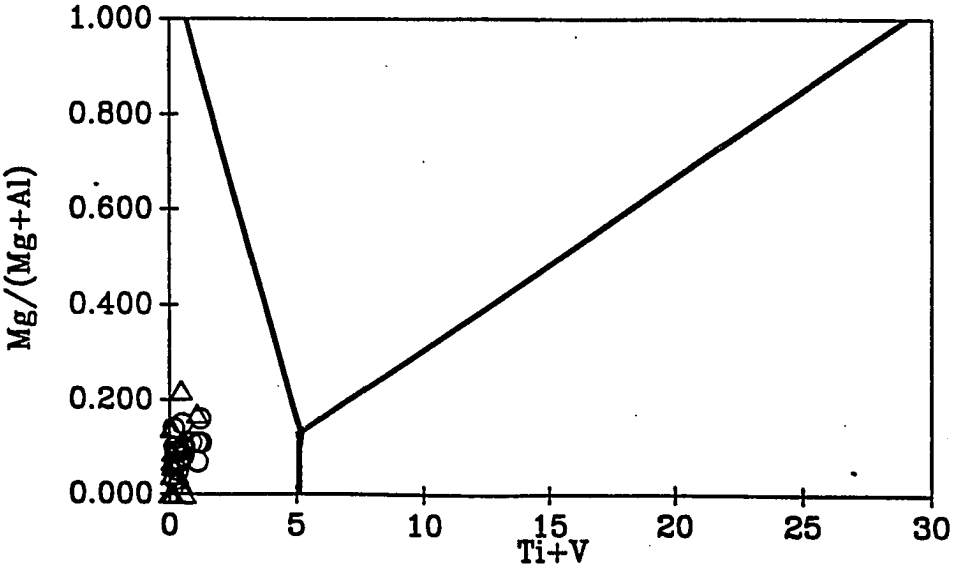

Figure 38: A plot of the weight percent Mg/(Mg+Al) vs. Ti+V for magnetite derived from the serpentinized ultramafic parent rocks. Open circle = Loma de Hierro, open triangle = Lewis Hills ophiolite.

Figure 39: A plot of the weight percent Mg/(Mg+Al) vs. Ti+V for detrital magnetite derived from the Gunflint Banded-Iron Formation (open circle).

MAGNETITE CHEMISTRY
Mg/(Mg+Al) vs. Ti+V

Serpentinized Ultramafics

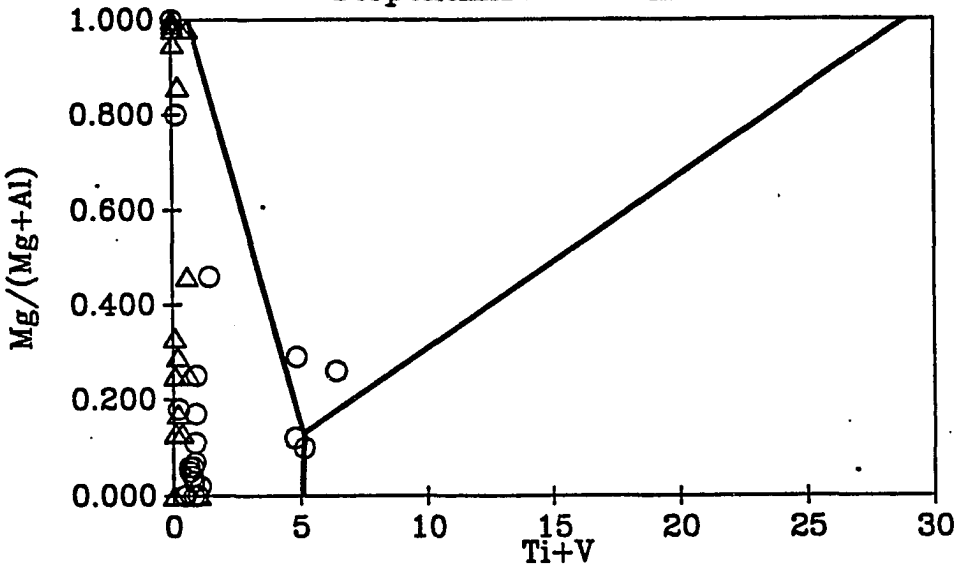

MAGNETITE CHEMISTRY
Mg/(Mg+Al) vs. Ti+V
Metamorphosed
Banded–Iron Formation

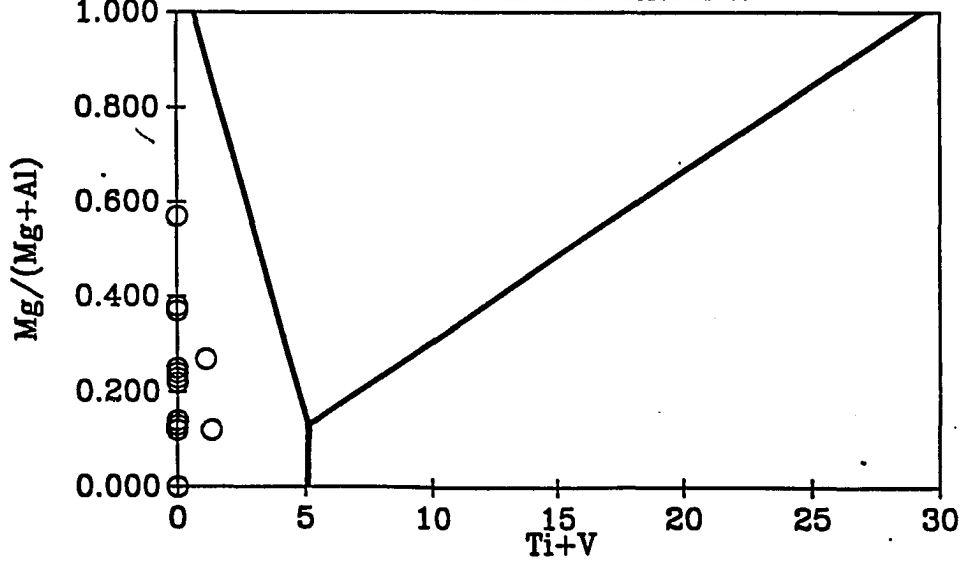

grains available. To counter this limitation further research is necessary to determine compositional trends that may be found through the use of heterogeneous grains.

CHAPTER VIII

PETROGRAPHIC AND CHEMICAL ANALYSES OF DETRITAL MAGNETITE, ROSARITO BEACH, MEXICO

Introduction

Based on the petrographic and chemical properties of detrital magnetite grains derived from the various parent rocks of the current study, it is possible to examine a sand of unknown source. The sample to be considered is a beach sand collected off the Baja California coast near Rosarito, Mexico (Fig. 40). Following the procedures described earlier in the text, the detrital magnetite grains were separated and mounted for petrographic and chemical analyses (sample number, location, and percent magnetite in the sand is given in Appendix A).

The geology of the sample area was not known at the time of analyses in order to not bias the conclusions presented below. A point count of the light sand fraction was also completed after analysis in order to compare and support (or contradict) the conclusions drawn from the detrital magnetite study (Appendix E).

The following sections will discuss the geology of northwestern Baja California, the results of the petrographic and chemical analyses, and how these results relate to the provenance history of the sand.

Figure 40: General geology and distribution of igneous rocks in the northwest corner of Baja California. Igneous rocks: Tmb = Miocene basalt and basaltic andesite; gd = granodiorite; gr = granite; gb = gabbro; Pbv = Mesozoic undifferentiated volcanics (predominantly pyroclastic dacite and andesite with subordinate basalt and rhyolite); Sedimentary rocks: Tpm = Pliocene marine; Tmf = Miocene fluvial; Tem = Eocene marine; Kuc = Cretaceous Redondo Formation; Krm = Cretaceous Rosario Group (marine) (after Gastil et al., 1975).

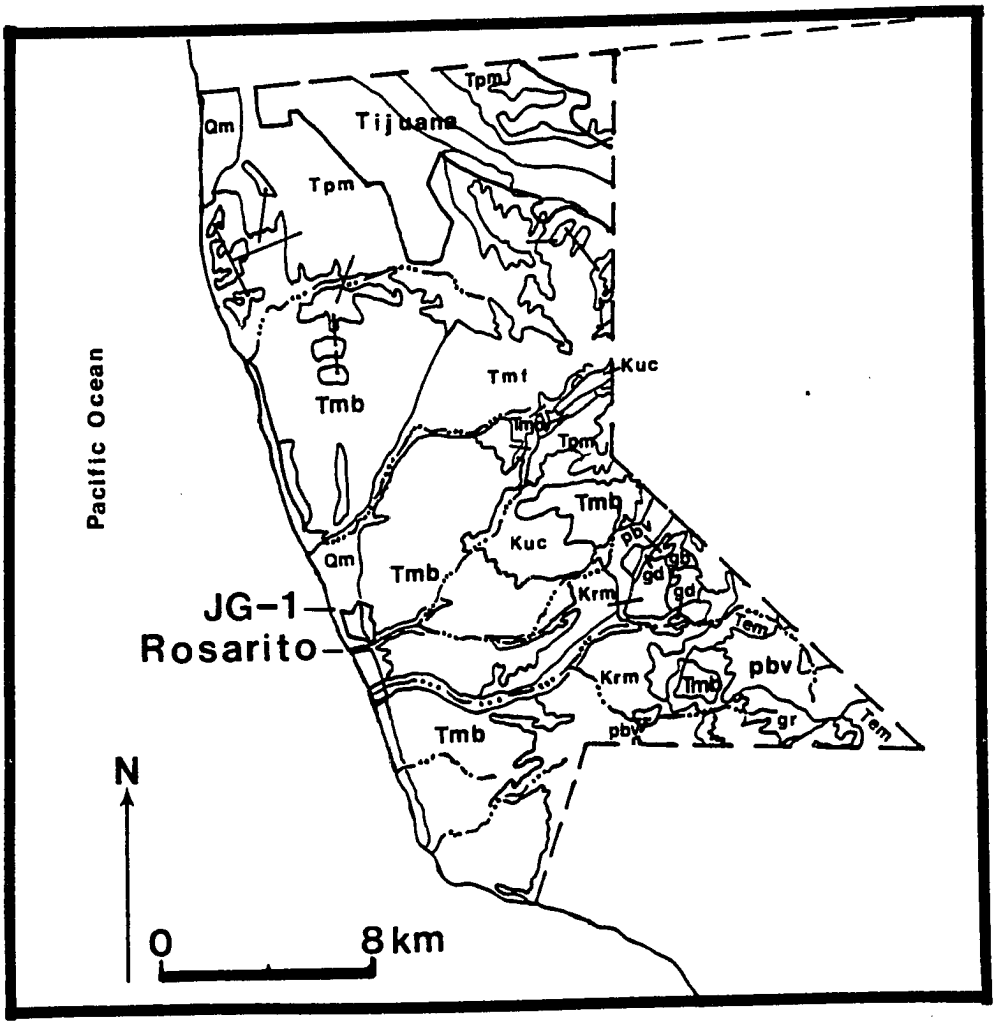

General Geology of Northwestern Baja California

One of the best reviews of the geology of the state of Baja California is presented by Gastil et al. (1975). In this review they describe three terrains of igneous rocks as prebatholithic, batholithic, and postbatholithic.

Prebatholithic rocks (labeled Pbv, Fig. 40) consist of the Mesozoic Volcanic Belt of Gastil et al. (1975) and are found exposed throughout the length of the state of Baja California. These rocks consist predominantly of pyroclastic dacite and andesite with subordinate amounts of basalt and rhyolite. These rocks cover approximately 4% of the drainage area supplying sediment to Rosarito Beach.

Batholithic rocks, in most cases, are thought to have been intruded contemporaneously with the prebatholithic volcanics, although evidence suggests that some plutonism occurred well after deposition of the youngest recognized prebatholithic strata (Gastil et al., 1975). These rocks consist predominantly of tonalite (t), granodiorite (gd), and adamellite (ad), with smaller plutons of granite (gr) and gabbro (gb). In the area supplying sediment to Rosarito Beach only granite and granodiorite (covering 1% of the drainage area) are found. A small pluton of gabbro is also present but it covers less than 0.5% of the drainage area.

Postbatholithic rocks, which commonly occur near the

sample area, are referred to as the Pacific Coast Volcanic Province by Gastil et al. (1975). These rocks consist predominantly of Miocene and younger basalt units that occur at many points on the continental borderland and adjacent Pacific coast (labeled Tmb, Fig. 40). The best documented of these is the Rosarito Beach Formation between Tijuana and the Rosarito Beach area. Minch (1967) defined the Rosarito Beach Formation as a sequence of five members with a total exposed thickness of approximately 400m. This sequence consists of interbedded basalt flows, pyroclastic rocks, and marine clastic sedimentary rocks. The Mira al Mar Member is the lowest member of this formation and is a sedimentary breccia. As described by Minch (1967) it consists of "abundant clasts of glaucophane schist, sericite schist, serpentine, saussuritized gabbro, bedded chert, quarrtzites, and minor amounts of acidic volcanic and plutonic rocks." The four upper members of the Rosarito Formation (Costa Azul, Amado Nervo, Los Glorias, Los Buenos Members) are predominantly basalt with interbedded tuffaceous sandstone and shale. The modes (Table 22) of basalt from these members indicate an olivine basalt composition. These basaltic rocks cover approximately 39% of the drainage area.

In addition to the igneous rock sequences described above, much of the drainage area is covered ($\approx$ 56% of the

Table 22: Modes (in percent) of basalt from the Rosarito Beach Formation. Numbers at the top of the columns represent the members of the formation and are named below (after Minch, 1967).

	1	2	3	4	5
Plagioclase	60.8	50.3	42.5	57.0	54.2
Augite	20.8	20.4	27.5	16.5	24.4
Olivine	5.8	7.8	11.5	9.5	6.4
Magnetite	5.4	8.1	7.0	9.5	4.2
Glass and Alteration	7.2	11.0	11.5	7.5	10.8

1 = Costa Azul Member (middle basalt)
2 = Costa Azul Member (upper unit)
3 = Amado Nervo Member (eastern block)
4 = Las Glorias Member
5 = Los Buenos Member

drainage area) by marine and fluvial sedimentary rocks ranging in age from Cretaceous to Pliocene. The Cretaceous rocks, as described by Flynn (1970), are divided into the Redonda Formation (Kuc, Fig. 40) and the marine facies of the Rosario Formation (Krm, Fig. 40). According to Flynn (1970) the Redonda Formation (≈ 120m thick) consists of a sequence of massive, unfossiliferous conglomerate and breccia with interbedded sandstone lenses. In the type locality he describes the clasts as " subrounded to well-rounded cobbles of arkose, green and red porphyry, varicolored quartzite, volcanic breccia, felsite, and scattered clasts of granitic material in a matrix of brown to tan, fine- to medium-grained, poorly sorted, argillaceous sandstone."

The Rosario Formation, according to Flynn (1970), can be divided into a lower sandstone member and an upper mudstone member. The lower sandstone member (≈ 75m thick) consists of " brown to white, medium- to coarse-grained, massive to thinly bedded arkosic sandstones, with interbeds of gray to green mudstone 0.5 to 1m thick." The upper member (≈ 45m thick) is composed of "gray to green mudstone with abundant microfossil fauna and sandstone interbeds."

Marine deposits of Eocene age (Tem, Fig. 40) are divided by Flynn (1970) into the Delicias Formation and the Buenos Aires Formation. The Delicias Formation, which lies

disconformably on the Rosario Formation consists of a lower mudstone member and an upper sandstone member. The lower mudstone member is composed of "3m of white, lateritic, coarse grained sandstone, overlain by approximately 40m of green mudstones, siltstones, and fine-grained sandstones." The upper member is composed of "a sequence of brown to tan, fine- to medium-grained, yellow weathering sandstones and interbedded green mudstone and siltstone...."

The Buenos Aires Formation can be divided into 1) a lower conglomeratic member (≈ 70m thick) composed of "cobbles and boulders of quartzite, porphyry, breccias, and dacites, and granitic rocks in a matrix of brown to tan, fine- to medium-grained sandstones and muddy sandstones," and 2) an upper sandstone member (≈ 60 - 80m thick) of "white to tan, fine- to medium-grained sandstones."

The sedimentary rocks of Miocene and Pliocene in age (Tpm and Tmf, Fig. 40) are part of the Rosarito Formation discribed above.

Petrography

Table 23 is a summary table of the point count analysis of the detrital magnetite grains from the Rosarito Beach sand. According to the petrographic classification of detrital magnetite grains described earlier in the text it was found that the Rosarito Beach sand is dominated by homogeneous magnetite grains (54%). Magnetite-ilmenite

Table 23: Point count data for detrital magnetite derived from the Rosarito Beach sand (sample # JG-1).

Grain Types		Number of Grains	Percent
Homogeneous		63	54
Magnetite + Ilmenite Intergrowths			
	Trellis-Type	31	27
	Composite-Type	6	5
Total Magnetite-Ilmenite Intergrowths		37	32
Pleonaste Exsolution		9	8
Ulvospinel Exsolution		0	0
Heating Martite		7	6
Total		116	100
Additional Alteration:			
Pseudobrookite		16	14
Martite		42	36

and pleonaste (associated in all but three grains with trellis-type magnetite-ilmenite intergrowths) occurring in only 8% of the grains. Heating martite was seen in 6% of the grains.

Of the additional alteration types pseudobrookite occurred in 14% and martite in 36% of the counted grains.

Chemistry

Electron probe microanalysis was performed on 27 unaltered homogeneous grains from the Rosarito Beach sand sample. The results of this analysis (Table 24) indicates the compositional variability present within these detrital grains.

Discussion

From the discussion on the geology of northwestern Baja California it is apparent that the Rosarito Beach sand has been derived from a variety of parent rocks. If these sources can be identified through the petrographic and chemical analyses of detrital magnetite grains then an extension in provenance studies will be attained.

The first step is to compare the petrographic results from the Rosarito Beach sand with the results from the known sources. It is apparent that the detrital magnetite textures are most similar to the textures of the mafic volcanic (basaltic) parent rocks (Table 25). A composite-type/trellis-type ratio of 0.19 also lies within the range

Table 24: Electron microprobe data of detrital magnetite grains derived from the Rosarito beach area, Baja California, Mexico.

Wt%
Oxide

Sample#	Ti	V	Al	Cr	Mg	Si	Mn	Fe^{2+}	Fe^{3+}	Total
Jg-1-1	17.39	0.22	0.35	0.00	0.00	0.52	0.22	33.45	46.35	98.50
-2	0.01	0.13	0.11	0.00	0.00	0.07	0.05	30.74	68.24	99.35
-3	0.05	0.62	0.14	0.00	0.00	0.09	0.04	30.63	67.76	99.33
-4	6.95	0.95	1.82	0.00	0.92	0.08	0.40	35.94	53.81	100.87
-5	0.46	0.61	0.20	0.00	0.00	0.12	0.08	31.47	67.98	100.92
-6	0.13	0.10	0.12	0.00	0.00	0.02	0.75	30.55	68.90	100.57
-7	0.02	0.46	0.27	0.00	0.00	0.00	0.15	30.57	67.80	99.27
-8	0.00	0.38	0.07	0.00	0.00	0.00	0.07	31.25	69.50	101.27
-9	0.02	0.15	0.17	0.00	0.00	0.05	0.12	31.22	69.32	101.05
-10	0.00	0.53	0.19	0.00	0.03	0.00	0.04	30.67	68.09	99.55
-11	0.04	0.07	0.26	0.00	0.71	0.00	0.02	30.24	69.51	100.85
-12	0.00	0.63	0.74	0.00	0.00	0.03	0.00	30.89	67.49	99.78
-13	0.00	0.90	0.41	0.00	0.05	0.00	0.06	30.74	68.03	100.19
-14	0.00	0.50	0.07	0.00	0.00	0.01	0.02	30.40	67.52	98.52
-15	0.03	0.22	0.14	0.00	0.00	0.00	0.10	31.07	68.95	100.51
-16	0.29	0.34	0.41	0.00	0.00	0.12	0.08	31.42	68.21	100.87
-17	1.22	0.44	0.09	0.00	0.00	0.09	0.05	31.97	66.16	100.02
-18	9.15	0.66	0.92	0.00	0.00	0.18	0.78	38.63	49.61	99.93
-19	0.12	1.49	0.22	0.00	0.00	0.08	0.04	30.34	66.70	98.99
-20	17.10	1.15	2.08	0.00	0.00	0.21	0.06	31.33	46.25	98.18
-21	8.67	0.80	1.68	0.00	0.06	0.11	0.67	38.47	49.97	100.43
-22	6.40	0.94	2.27	0.00	1.78	0.07	0.41	33.41	53.10	98.37
-23	2.71	1.06	0.25	0.00	0.01	0.13	0.07	33.43	63.27	100.80
-24	4.12	0.68	0.99	0.00	0.00	0.08	0.43	34.08	58.70	99.08
-25	16.46	0.68	0.06	0.00	0.00	0.09	1.20	44.74	36.25	99.48
-26	3.78	1.36	1.09	0.00	0.26	0.00	0.19	33.71	59.57	100.16
-27	9.37	1.12	0.93	0.00	0.02	0.11	0.60	38.18	47.39	97.72
Avg	3.87	0.64	0.59	0.00	0.14	0.08	0.25	32.95	61.28	
Std	5.57	0.38	0.65	0.00	0.39	0.10	0.30	3.41	9.49	

Table 25: Comparison of the point-count data (in percent) of detrital magnetite derived from known basaltic parent rocks with the detrital magnetite derived from the Rosarito Beach area.

Grain Types		Mafic Volcanic	Rosarito Beach Sand
Homogeneous		46	54
Magnetite-Ilmenite Intergrowths			
	Trellis-Type	36	27
	Composite-Type	13	5
Total Magnetite-Ilmenite Intergrowths		49	32
Pleonaste		2	8
Ulvospinel		2	0
Heating Martite		1	6
Total		100	100
Additional Alteration			
	Pseudobrookite	Tr	14
	Martite	9	36
Composite-type/Trellis-type Ratio		0.36 (Range = 0.14-0.79)	0.19

for mafic volcanics and is consistent with this type of source (Table 25) (the presence of pseudobrookite alteration supports a volcanic source, although the type of volcanics cannot be determined with this texture). The high percentage of homogeneous grains and grains with heating martite indicates that additional sources may be delivering magnetite to the sand. Although the percentage of pleonaste exsolution is also slightly higher and more consistent with an andesitic source, the overlap between the percentage of grains with pleonaste exsolution from known basaltic and andesitic sources precludes the use of this texture to describe a source in this case. However, because 6 of the 9 grains with pleonaste exsolution are associated with trellis-type magnetite-ilmenite intergrowths, and are the result of high-temperature oxidation, these grains can be safely placed with the grains of basaltic source. The absence of ulvospinel exsolution in the detrital magnetite grains precludes a mafic intrusive source. Further answers from the petrographic data alone are highly subjective at best, although evidence supports the possibility of a felsic or andesitic source.

The second step is to analyze chemically, with an electron microprobe, a number of unaltered homogeneous grains to test for chemical variability (Table 24). The

elements of greatest importance, as determined by discriminant analysis, are Mg^{2+}, Al^{3+}, V^{3+}, and Ti^{4+}. A plot of the weight percent Mg/(Mg+Al) versus Ti+V of the data from table 24 results in the scatter of points within the three fields (mafic plutonic/volcanic, intermediate volcanic, and felsic plutonic/volcanic) defined earlier in the study (Fig. 41). Table 26 is a summary table of the number and percentage of detrital magnetite grains that fell into each of these fields. It is apparent that both mafic and intermediate igneous parent rocks have supplied sediment to Rosarito Beach. The high percentage of grains that plotted in the felsic field was unexpected and is not consistent with either a mafic volcanic or andesitic source. It suggests that a felsic (possibly metamorphic) parent rock has also influenced sediment deposition in the Rosarito Beach area.

It is possible, from our knowledge of the physical and chemical properties of detrital magnetite derived from various known parent rocks, to combine the chemical data gathered from the homogeneous grains with the petrographical data gathered from the heterogeneous grains. This combining of data should allow one to make a rough approximation of the influence each of the parent rocks have had on the composition of the Rosarito Beach sand.

Referring to Appendix F, a step-by-step procedure is

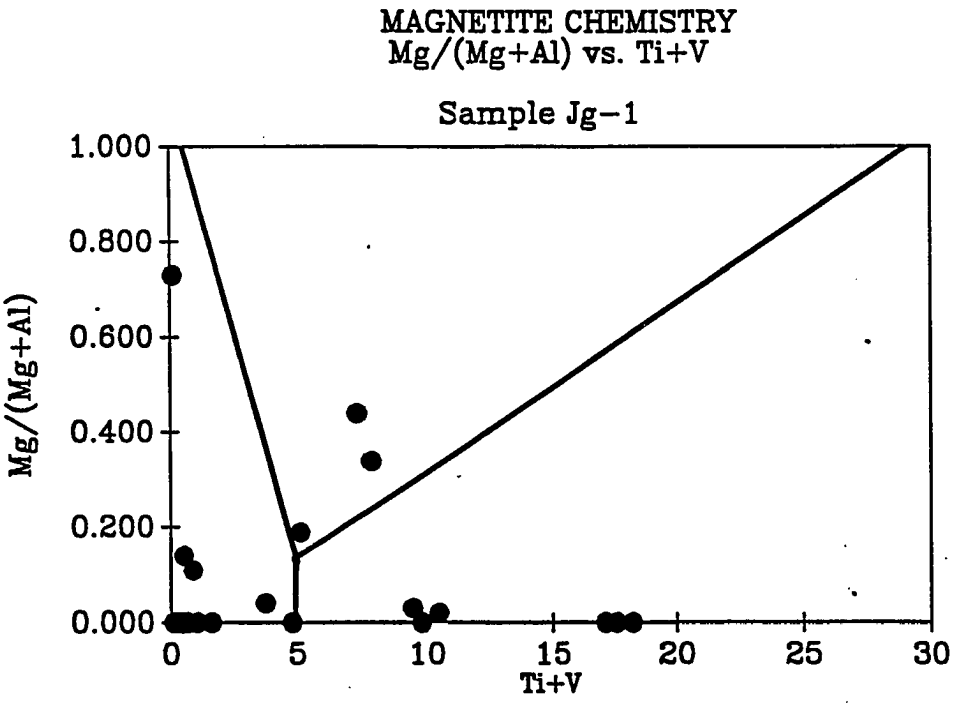

Figure 41: Plot of the weight percent Mg/(Mg+Al) vs. Ti+V based on the electron microprobe chemical analysis of detrital magnetite derived from the Rosarito Beach Sand, Baja California, Mexico.

Table 26: Percentage of detrital magnetite grains, based on electron microprobe data, that fall into the 3 defined fields as discussed earlier in the text.

Sample #	No. of Cases	Group Membership		
		Felsic	Intermediate	Mafic
JG-1	27	18 (67%)	3 (11%)	6 (22%)

presented for the calculation of the number of detrital magnetite grains that can be inferred to have been produced by mafic volcanic (basalt), intermediate volcanic (andesite), and felsic parent rocks. It is concluded, of the 116 grains analyzed (63 homogeneous and 53 heterogeneous), that 67($\pm$5) grains are of basaltic source, 35($\pm$5) grains are of felsic source (most likely felsic plutonic because of the high percentage of homogeneous grains and the low percentage of composite-type magnetite-ilmenite intergrowths characteristic of felsic volcanic sources), and 14 are of intermediate (andesite) volcanic source. The point-count analysis of the light sand fraction (54% plagioclase, 19% quartz, 15% volcanic rock fragments, 8% K-feldspar, and 4% quartzofeldspathic rock fragments; Appendix E) supports the presence of mafic and andesitic volcanic sources, as well as a felsic plutonic source. Both correspond with the general geology of northwest Baja California (it must be remembered that much of the area is covered by marine and fluvial clastic deposits and some of the magnetite grains may have been recycled).

CHAPTER IX

SUMMARY AND CONCLUSIONS

The petrographic and compositional characteristics of detrital magnetite and ilmenite have been studied to determine if these properties can lead to a better understanding of the provenance history of sands, especially mature, quartz-rich sands. Recent work concerning tectonics and sandstone mineralogy, which concentrate on thin-section petrology of the light mineral fraction of sands, have led to a greater understanding of the relationship between sandstone composition and provenance, but have failed to consider the importance of heavy minerals. Hydraulic sorting and intrastratal solution can severely restrict the usefulness of heavy minerals, but these problems can be minimized by examining the relative abundance of the physical or chemical varieties of a single mineral or mineral group (termed a varietal study). Magnetite and ilmenite are ideal minerals for a varietal study because: a) both occur in a wide variety of igneous rocks, both intrusive and extrusive, as well as pegmatites, other vein rocks, and metamorphic rocks, b) both show petrographic and chemical variations based on source rock paragenesis, c) both are relatively stable, d) both are relatively abundant in sands and sandstones, and e) both are easily separated using magnetic techniques.

In the current study thirty-one modern sand samples were collected from eight different parent rock types (felsic plutonic, felsic volcanic, intermediate volcanic, mafic plutonic, mafic volcanic, serpentinized ultramafic complexes, meta-anorthosite, and sedimentary banded-iron formation), and the Fe-Ti oxides (magnetite and ilmenite) were separated magnetically from the 150um to 250um size fraction to determine the utility of the detrital Fe-Ti oxides as provenance indicators. A number of conclusions emerged from this study:

1. Detrital magnetite is a useful provenance indicator. In contrast, detrital ilmenite grains derived from the same sources as the magnetite show no petrographic or chemical trends with variation in parent rock type.

2. Petrographically detrital magnetite can be classified into 3 groups 1) homogeneous grains, 2) grains with trellis- or composite-type magnetite-ilmenite intergrowths, and 3) grains with pleonaste or ulvospinel exsolution.

3. A ternary plot, with the above three groups as corners, indicates the following relationships:

   a) Detrital magnetite grains derived from felsic plutonic and intermediate volcanic parent rocks are dominated by homogeneous grains.

b) Detrital magnetite grains derived from felsic volcanic parent rocks are dominated by composite-type magnetite-ilmenite intergrowths (a composite-type/trellis-type ratio > 1).

c) Detrital magnetite grains derived from mafic/ultramafic plutonic sources (including serpentinized ultramafics and meta-anorthosites) are dominated by pleonaste or ulvospinel exsolution textures.

d) Detrital magnetite grains from the mafic volcanic sources have an even split between homogeneous grains and grains with magnetite-ilmenite intergrowths (a composite-type/trellis-type ratio <1).

e) Detrital magnetite derived from the sedimentary banded-iron formation consists of 100% homogeneous grains.

4. Electron probe microanalysis of the homogeneous magnetite grains derived from the various sources indicates a relationship between the parent rock type and magnetite composition.

5. Discriminant analysis of the electron microprobe data, to determine which elements can best discriminate between the felsic plutonic/volcanic, intermediate volcanic, and mafic plutonic parent rock types, has found

that Ti is most important followed by Mg, V, Al, Mn, and Cr.

6. A statistical plot of the microprobe data from the three igneous rock groups above (excluding basaltic, serpentinized ultramafic, meta-anorthosite, and banded-iron formation parent rocks), based on discriminant analysis, has found that 97% of the time the detrital magnetite grains can correctly classified with the parent rock from which they were derived.

7. In an attempt to simplify this classification the most important discriminating elements (Ti, Mg, V, Al) were chosen to derive a plot following the relationships as determined by discriminant analysis. It was found that by plotting the weight percent Mg/(Mg+Al) vs. Ti+V the detrital magnetite grains can be correctly classified 96% of the time.

8. In both classification schemes above the magnetite grains derived from the serpentinized ultramafics, the meta-anorthosites, and the Rooiberg felsite plotted outside of their predicted fields. It was found that the homogeneous magnetite grains derived from the serpentinized ultramafics were dominated by Ti-free magnetite formed during the serpentinization event. Ti-free grains associated with the meta-anorthosites and the high-Ti grains associated with the Rooiberg felsite could

not be explained. Detrital magnetite derived from the banded-iron formation, which are low-Ti grains, plot in the felsic field.

9. Detrital magnetite grains derived from mafic volcanics (basaltic parent rocks) are best classified by plotting the weight percent Mg/(Mg+Al) vs. Ti+V. In this classification scheme 62% of the grains fall in the mafic field and 30% fall in the felsic field indicating that two chemically different magnetite phases are derived from the basaltic parent rocks.

10. Based on the procedures developed in the current study the detrital magnetite grains of a beach sand of unknown source, collected near Rosarito, Mexico, were analyzed. It was determined that 58($\pm$5)% of the detrital magnetite grains studied were of basaltic source, 30($\pm$5)% were of felsic plutonic source, and 12% were of andesitic source. The current drainage area supplying sediment to this beach consists of 39% olivine basalt, 4% andesitic to dacitic volcanics, and 1% felsic plutonic. Fifty-six percent of the area is covered by Cretaceous to Pliocene marine and fluvial sediments providing a source of recycled detrital magnetite grains. Point count analyses of the light sand fraction (54% plagioclase, 19% quartz, 15% volcanic rock fragments, 8% K-feldspar, and 4% quartzofeldspathic rock fragments) is in agreement with the

findings of the detrital magnetite grains indicating that this is a plausible means of provenance determination.

11. It is recommended that electron microprobe chemical analysis should be used only after careful and objective petrographic observation indicates that additional information is required to determine the source of the sand being studied. This allows for the determination of the relative percentage of the magnetite textural varieties, the degree of alteration of the grains, and the choosing of relatively unaltered homogeneous grains for electron probe microanalysis.

12. The petrographic and chemical properties of detrital magnetite should be used in conjunction with other methods of provenance determination for additional evidence. This is especially true for quartz-rich, mature sands. Used together, this procedure offers an extension in provenance research that past studies have lacked.

LIST OF REFERENCES

Adams, S. S., et al., 1974, Alteration of detrital magnetite-ilmenite in continental sandstones of the Morrison Formation, New Mexico: in Formation of Uranium Ore Deposits, Vienna International Atomic Energy Agency, pp. 219-253.

Ade-Hall, J. M., et al., 1976, Rock magnetism of basalts, Leg 34: Initial Repts. of the Deep Sea Drilling Proj., v. 34, pp. 459-468.

Akimoto, T., et al., 1984, Electronprobe microanalysis study on processes of low-temperature oxidation of titanomagnetite: Earth and Planetary Science Letters, v. 71, pp. 263-278.

Akimoto, S., 1954, Thermomagnetic study of ferromagnetic minerals contained in igneous rocks: Jour. Geophys. Geoelectr., v. 6, pp. 1-14.

Alvarado, B., 1970, Iron ore deposits of South America: in Survey of World Ore Resources, United Nations, New York, pp. 302-380.

Anand, R. R. and Gilkes, R. J., 1984, Weathering of ilmenite in a lateritic pallid zone: Clays and Clay Minerals, v. 32, pp. 363-374.

Anderson, A. T., 1968, Oxidation of the LaBlache Lake titaniferous magnetite deposit, Quebec: Jour. Geology, v. 76, pp. 528-547.

Anderson Jr., J. E., et al., 1969, Some age relations and structural features of the Precambrian volcanic terrain, St. Francois Mountains, southwestern Missouri: Geol. Soc. Amer. Bull., v. 80, pp. 1815-1818.

Anderson, R. E., 1962, Igneous petrology of the Taum Sauk area, Missouri: Unpublished Ph.D. dissertation, Washington Univ., St. Louis, 100 pp.

Austin, S. R., 1960, Ilmenite, magnetite, and feldspar alteration under reducing conditions: Econ. Geology, v. 55, pp. 1758-1759.

Badham, J. P. N. and Morton, R. D., 1976, Magnetite-apatite intrusions and calc-alkaline magnetism, Camsell River, N. W. T.: Can. Jour. Earth Sci., v. 13, pp. 348-354.

Bailey, S. W., et al., 1956, The alteration of ilmenite in beach sands: Econ. Geology, v. 51, pp. 263-279.

Baker, E. B., 1988, Quantitative photospectrometric cathodoluminescence of quartz: Geol. Soc. Amer. Abstracts with Programs, v. 20, p.

Baker, G., 1962, Detrital heavy minerals in natural accumulates: Australian Inst. Mining Metall. Mono., v. 1, 146 pp.

Balk, R., 1930, Structural survey of the Adirondack anorthosite: Jour. Geology, v. 38, pp. 289-302.

Balsley, J. R. and Buddington, A. F., 1958, Iron-titanium oxide minerals, rocks, and aeromagnetic anomalies of the Adirondack area, New York: Econ. Geology, v. 53, pp. 777-805.

Basu, A., 1976, Petrology of Halocene fluvial sand derived from plutonic source rocks: Implications to paleoclimatic interpretations: Jour. Sed. Petr., v. 46, pp. 694-709.

Basu, A. and Hood, L., 1985, Provenance significance of detrital opaque oxide minerals in Lake Erie sands near Sandusky, Ohio: Amer. Assoc. Petr. Geol. Notes and Abstracts, v.17, p. 279.

Basu, A. and Molinaroli, E. (in press), Provenance characteristics of detrital opaque Fe-Ti oxide minerals: Jour. Sed. Petr.

Basu, A. and Molinaroli, L., 1986, Provenance of detrital opaque particles: S. E. P. M. Annual Mid-Year Meeting, v. 3, p. 6.

Basu, A., et al., 1975, Re-evaluation of the use of undulatory extinction and polycrystallinity in detrital quartz for provenance interpretations: Jour. Sed. Petr., v. 45, pp. 873-883.

Bateman, A. M., 1951, The formation of late magnetic oxide ores: Econ. Geology, v. 46, pp. 404-426.

Beaudoin, A. B. and King, R. H., 1986, Using discriminant function analysis to identify Holocene tephras based on magnetite composition: a case study from the Sunwapta Pass area, Jaspar National Park: Can. Jour. Earth Sci., v. 23, pp. 804-812.

Bellizzia, A. G., 1967, Rocas ultrabasicas en el sistema Montañoso del Caribe y Yacimientos Minerales Asociados: Ministerio de Minas e Hidrocarburos, v. 8, pp. 159-197.

Bellizia, A. G., et al, 1976, Mapa geologico estructural de Venezuela: Ministerio de Minas e Hidrocarburos, Venezuela.

Bence, A. E. and Albee, A. L., 1968, Empirical correction factors for the electron microanalysis of silicates and oxides: Jour. Geology, v. 76, pp. 382-403.

Benthian, R., et al., 1986, Origin of magnetization in the Phosphoric Formation (Sheep Mountain, Wyoming): A possible relationship with hydrocarbons: Eos Trans., Amer. Geophys. Union, v. 67, p. 265.

Berkman, D. A., 1975, Magnetite beach sand deposits of southeast Papua: Economic Geology of Australia and Papua, New Guinea, Monograph Series 5 (Metals), pp. 1088-1090.

Berner, R. A., 1964, Stability fields of iron minerals in anaerobic marine sediments: Jour. Geology, v. 72, pp. 826-834.

Berry, A. W., Jr. and Bickford, M. E., 1972, Precambrian volcanics associated with the Taum Sauk Caldera, St. Francois Mountains, Missouri, U.S.A.: Bull. Volcanologique, v. 36, pp. 303-318.

Bickford, M. E. and Mose, D. G., 1975, Geochronology of Precambrian rocks in the St. Francois Mountains, southeast Missouri: Geol. Soc. Am. Spec. Pap. 165, 48 pp.

Blakemore, R. P., 1975, Magnetotactic bacteria: Science, v. 190, pp. 377-379.

Blakemore, R. P., 1981, Magnetite formation by bacteria: Eos Trans., Amer. Geophys. Union, v. 62, pp. 849-850.

Blakemore, R. P., et al., 1985, Microaerobic conditions are required for magnetite formation within Aquaspirillum Magnetotacticum: Geomicrobiology Jour., v. 4, pp. 53-71.

Blatt, H., 1967, Provenance determinations and recycling of sediments: Jour. Sed. Petr., v. 37, pp. 1031- 1044.

Bloomfield, K. and Valastro, Jr., S., 1974, Late Pleistocene eruptive history of Nevado de Toluca volcano, Central Mexico: Geol. Soc. Amer. Bull., v. 85, pp. 901-906.

Boctor, N. Z., 1966, Mineralogical study of the opaque minerals in the Black Sands, Rosetta-Damietta, Egypt: unpubl. M.S. thesis, Cairo University, 80 pp.

Borisenko, L. F. and Polkanov, Yu. A., 1975, Vanadium in ilmenite of diverse origin: Doklady Akademii Nauk SSSR, v. 221, pp. 239-242.

Boswell, P. G. H., 1923, Some aspects of the petrology of sedimentary rocks: Proc. Liverpool Geol. Soc., v. 13, pp. 231-303.

Boswell, P. G. H., 1933, Mineralogy of sedimentary rocks: Murby, London, 363 pp.

Bramlette, M. N., 1941, The stability of minerals in sandstone: Jour. Sed. Petr., v. 11, pp. 32-36.

Briggs, L. I., 1965, Heavy mineral correlations and provenances: Jour. Sed. Petr., v. 35, pp. 939-955.

Briggs, L. J., McCullock, D. S., and Moses, F., 1962, The hydraulic shape of sand particles: Jour. Sed. Petr., v. 32, pp. 645-656.

Broderick, T. M., 1917, The relation of titaniferous magnetites of northeast Minnesota to the Duluth Gabbro: Econ. Geology, v. 12, pp. 663-696.

Brown, P. J., et al., 1980, Origin of patterns of quartz sand types on the southeastern United States shelf sedimentation-Fourier grain shape analysis: Jour. Sed. Petr., v. 50, pp. 1095-1100.

Buddington, A. F., 1953, Geology of the Saranac Quadrangle, New York: New York State Museum Bull., v. 346, 85 pp.

Buddington, A. F. and Lindsley, D. H., 1964, Iron-Titanium oxide minerals and synthetic equivalents: Jour. Petr., v. 5, pp. 310-357.

Buddington, A. F., et al, 1955, Thermometric and petrogenic significance of titaniferous magnetite: Amer. Jour. Sci., v. 253, pp. 497-532.

Butcher, A. R. and Merkle, R. K. W., 1987, Postcumulus modification of magnetite grains in the upper zone of the Bushveld Complex, South Africa: Lithos, v. 20, pp. 247-260.

Callender, D. L. and Folk, R. L., 1958, Idiomorphic zircon key to volcanism in the Lower Tertiary sands of central Texas: Amer. Jour. Sci., v. 256, pp. 257-269.

Cameron, K. C. and Blatt, H., 1971, Durabilities of sand size schist and "volcanic" rock fragments during fluvial transport, Elk Creek, Black Hills, South Dakota: Jour. Sed. Petr., v. 41, pp. 565-576.

Carmichael, I. S. E., 1967, The iron-titanium oxides of salic volcanic rocks and their associated ferromagnesium silicates: Contr. Min. and Petr., v. 14, pp. 36-64.

Cawood, P. A., 1983, Model composition and detrital climopyroxene geochemistry of lithic sandstones from the New England Fold Belt (east Australia): a paleozoic forearc terrane: Geol. Soc. Amer. Bull., v. 94, pp. 1199-1214.

Chevallier, R. J., et al, 1955, Titanomagnetites et ilmenites ferromagnetiques: Bull. Soc. Fr. Min. Cristallogr., v. 78, pp. 307-346.

Connally, G. G., 1964, Garnet ratios and provenance in the glacial drift of western New York: Science, v. 144, pp. 1452-1453.

Cornwall, H. R., 1951, Ilmenite, magnetite, and copper in lavas of the Keweenawan series: Econ. Geology, v. 46, pp. 51-67.

Craddock, C., 1972, Late Precambrian: Regional geological setting: in Sims, P. K., and Morey, G. B., eds., Geology of Minnesota: a centennial volume, Minnesota Geol. Surv., St. Paul, pp. 281-291.

Creer, K. M. and Ibbetson, J. D., 1970, Electron microprobe analyses and magnetic properties of nonstoichiometric titanomagnetites in basaltic rocks: Geophys. Jour. Roy. Astron. Soc., v. 21, pp. 485-511.

Creer, K. M. and Stephenson, A., 1972, Some consequences of aluminum and magnesium impurities in naturally occurring titanomagnetite: Jour. Geophys. Res., v. 77, pp. 3698-3710.

Crosby, P., 1969, Petrogenic and statistical implications of modal studies in Adirondack anorthosite: in Isachsen, Y. W., ed., Origin of Anorthosite and Related Rocks, New York State Museum and Science Service, Memoir 18, pp. 281-287.

Dake, C. L., 1921, The problem of the St. Peter Sandstone: Univ. Missouri School of Mines and Metall. Bull. Tech., Ser. 6, 158 pp.

Darby, D., 1984, Trace elements in ilmenite: A way to discriminate provenance or age in coastal sands: Geol. Soc. Amer. Bull., v. 95, pp. 1208-1218.

Darby, D. and Tsang, Y. W., 1987, Variation in ilmenite element composition within and among drainage basins: Implications for provenance: Jour. Sed. Petr., v. 57, pp. 831-838.

DaSilva, Maria Augusta, M., 1979, Provenance of heavy minerals in beach sands, southeastern Brazil: From Rio Grande to Chui (Rio Grande Do Sul State): Sed. Geology, v. 24, pp. 133-148.

Davis, J. C., 1973, Statistics and data analysis in geology: John Wiley and Sons, Inc., New York, 550 pp.

Derby, C. A., 1891, On the separation and study of the heavy accessories of rocks: Proc. Rochester Acad. Sci., v. 1, pp. 198-206.

Dewey, J. F. and Bird, F. M., 1970, Mountain belts and the new global tectonics: Jour. Geophys. Res., v. 75, pp. 2625-2647.

Dickinson, W. R., 1970, Interpreting detrital modes of graywacke and arkose: Jour. Sed. Petr., v. 40, pp. 695-707.

Dickinson, W. R., 1985, Interpreting provenance relations from detrital modes of sandstones: in Zuffa, G. G., ed., Provenance of Aremites: D. Reidel Pub Co., Boston, pp. 332-361.

Dickinson, W. R. and Suezek, C., 1979, Plate tectonics and sandstone composition: Amer. Assoc. Petr. Geol. Bull., v. 63, pp. 2164-2182.

Dickinson, W. R., et al., 1983, Provenance of North American Phanerozoic sandstones in relation to tectonic setting: Geol. Soc. Amer. Bull., v. 94, pp. 222-235.

Dietz, V., 1973, Experiments on the influence of transport on shape and roundness of heavy minerals: Contr. to Sed., No. 1, Struttgert: Schweizerbart'sche Verlag, pp. 99-102.

Dimanche, F. and Bartholome, P., 1976, The alteration of ilmenite in sediments: Minerals Sci. Engng., v. 8, pp. 187-201.

Donovan, T. J., et al., 1979, Aeromagnetic detection of diagenetic magnetite over oil fields: Amer. Assoc. Petr. Geol., v. 63, pp. 245-248.

Dreimanis, A., et al., 1957, Heavy mineral studies in tills of Ontario and adjacent areas: Jour. Sed. Petr., v. 27, pp. 148-161.

Dunham, K. G., 1935, The geology of the Organ Mountains: New Mexico State Bureau of Mines and Mineral Resources Bulletin, v. 11, 272 pp.

Edwards, A. B., 1965, Textures of the ore minerals and their significance: The Australasian Institute of Mines and Metallurgy.

Ehrlich, R. and Weinberg, B., 1970, An exact method for characterization of grain shape: Jour. Sed. Petr., v. 40, pp. 205-212.

Elmore, R. D., et al., 1986, Authigenic magnetite and hydrocarbon migration: Testing the hypothesis in the Lower Ordivician Arbuckle Group, southern Oklahoma: Eos Trans., Amer. Geophys. Union, v. 67, p. 265.

Emslie, R. F., 1975, Major rock units of the Morin Complex, southwestern Quebec: Can. Geol. Survey Paper, 74-48, 37 pp.

Feo-Codecido, G., 1956, Heavy mineral techniques and their application to Venezuelan stratigraphy: Amer. Assoc. Petr. Geol. Bull., v. 40, pp. 984-1000.

Fischer, R., 1950, Entmischungen in Schmelzen aus Schwermetalloxyden Silikaten und Phospaten: Neues Jahrb. Mineral. Abh., v. 81, pp. 315-364.

Fitch, F. J. and Miller, J. A., 1971, Atmospheric argon correction in the K-Ar dating of young volcanic rocks: Geol. Soc. London Jour., v. 127, pp. 277-280.

Fitch, F. J., 1972, Selection of suitable material for dating and the assessment of geological error in potassium-argon age determination: in Bishop, W. W. and Miller, J. A., eds., Calibration of hominoid evolution, Scottish Academic Press, Edinburgh, pp. 77-91.

Fleischer, M., 1965, Composition of magnetite as related to type of occurrence: U. S. Geol. Survey Prof. Paper 525-D, pp. D82-D84.

Flynn, C. J., 1970, Post-batholithic geology of the La Gloria - Presa Rodriquez area, Baja California, Mexico: Geol. Soc. Amer. Bull., v. 81, pp. 1789-1806.

Force, E. R., 1976, Metamorphic source rocks of titanium placer deposits in a geochemical cycle: U. S. Geol. Survey Prof. Paper B, 16 pp.

Frankel, R. B., et al., 1981, Magnetotactic bacteria at the Geomagnetic Equator: Science, v. 212, pp. 1269-1270.

Freeman, R., 1986, Magnetic mineralogy of pelagic limestones: Geophys. Jour. Roy. Astro. Soc., v. 85, pp. 433-452.

Friedman, S. A., 1954, Low temperature authigenic magnetite: Econ. Geology, v. 49, pp. 101-102.

Frietsch, R., 1978, On the magmatic origin of iron ores of the kiruna type: Econ. Geology, v. 73, pp. 478-485.

Galehouse, J. S., 1967, Provenance and paleocurrents of the Paso Robles Formation, California: Geol. Soc. Amer. Bull., v. 78, pp. 951-978.

Gallagher, K. K., et al., 1968, Mechanism of oxidation of magnetite to -Fe_2O_3: Nature, v. 217, pp. 1118-1121.

Gaspar, J. C. and Wyllie, P. J., 1983, Ilmenite (high Mg,Mn, Nb) in carbonatites from the Jacupiranga Complex, Brazil: Amer. Min., v. 68, pp. 960-971.

Gastil, R. G., et al., 1975, Reconnaissance geology of the state of Baja California: Geol. Soc. Amer. Memoir 140, 170 pp.

Geijer, P., 1967, Internal features of the apatite-bearing magnetite ores: Sveriges Geol. Undersokning, ser. C, v. 624, 32 pp.

Gillison, J. L., 1956, Genesis of titaniferous magnetites and associated rocks of the Lake Sanford district, New York: Amer. Inst. Mining Engng. Trans., v. 205, pp. 296-301.

Goldich, S. S., 1938, A study in rock weathering: Jour. Geology, v. 46, pp. 17-58.

Goldich, S. S., et al., 1972, Early Precambrian rocks in the Saganaga Lake-Northern Light Lake area, Minnesota-Ontario, Part I, Petrology and structure: in Doe, B. R. and Smith, D. K., eds., Studies in Precambrian Geology and Mineralogy (Gruner volume), Geol. Soc. Amer., Memoir 135.

Goodwin, A. M., 1956, Facies relations in the Gunflint Iron Formation: Econ. Geology, v. 51, pp. 565-595.

Gorai, M., 1951, Petrological studies on plagioclase twins: Amer. Min., v. 51, pp. 884-901.

Green, J. C., 1972, North Shore Volcanic Group: in Sims, P. K. and Morey, G. B., eds., Geology of Minnesota: a centennial volume, Minnesota Geol. Surv., pp. 294-332.

Grommè, C. S., et al., 1969, Magnetic properties and oxidation of iron-titanium oxide minerals in Alae and Makaopuhi Lava Lakes, Hawaii: Jour. Geophys. Res., v. 74, pp. 5277-5293.

Gross, G. A., 1970a, Nature and occurrence of iron ore deposits: in Survey of World Ore Resources, United Nations, New York, pp. 13-31.

Gross, G. A., 1970b, Iron ore deposits of Canada and the West Indies: in Survey of World Ore Resources, United Nations, New York, pp. 237-269.

Gross, G. A. and McLeod, C. R., 1980, A preliminary assessment of the chemical composition of iron formations in Canada: Can. Min., v. 18, pp. 223-229.

Guilbert, J. M. and Park, Jr., C. F., 1986, Ore deposits: W. H. Freeman and Co., New York, 985 pp.

Haggerty, S. E., 1976a, Opaque mineral oxides in terrestrial igneous rocks: in Rumble III, D., ed., Reviews in Mineralogy, Oxide minerals, v.3, pp. Hg101-Hg300.

Haggerty, S. E., 1976b, Oxidation of opaque oxides in basalts: in Rumble III, D., ed., Reviews in Mineralogy, Oxide minerals, v. 3, pp. Hg1-Hg100.

Hall, J. M. and Fischer, J. F., 1977, Opaque mineralogy of basement rocks, Leg 37: Initial Repts. of the Deep Sea Drilling Proj., v. 37, pp. 857-873.

Hanson, G. N., 1972, Saganaga Batholith: in Sims, P. K. and Morey, G. B., eds., Geology of Minnesota: A centennial volume, Minnesota Geol. Survey, St. Paul, pp. 102-107.

Herz, N., et al., 1970, Rutile and ilmenite places deposits Roseland District, Nelson and Anherst Counties, Virginia: Contr. to Econ. Geology, U. S. Geol. Survey Bull., v. 1312-F, 19 pp.

Hess, H. H., 1962, History of ocean basins: in Engel, A. E. J., et al., eds., Petrologic Studies: a volume in honor of A. F. Buddington, Geol. Soc. Amer., pp. 599-620.

Hubert, J. F., 1971, Procedures in sedimentary petrology: in Carver, R. E. ed., Wiley-Interscience, New York, pp. 453-478.

Hudson, C. B. and Ehrlich, R., 1980, Determination of relative provenance contributions in samples of quartz sand using Q-mode factor analysis of Fourier grain shape data: Jour. Sed. Petr., v. 50, pp. 1101-1110.

Huff, W. D., 1983, Correlation of Middle Ordivician K-bentonites based on chemical fingerprinting: Jour. Geology, v. 91, pp. 657-669.

Huguenin, R. L., 1973, Photostimulated oxidation of magnetite 2. Mechanism: Jour. Geophys. Res., v. 78, pp. 8495-8506.

Hurlbut, Jr., C. S. and Klein, C., 1977, Manual of Mineralogy: John Wiley and Sons, New York, 532 pp.

Hutton, C. O., 1950, Studies of heavy detrital minerals: Geol. Soc. Amer. Bull., v. 61, pp. 635-716.

Hwang, W. T. and Lo, H., 1986, Volcanological aspects and the petrogenesis of the Kuanyinshan volcanic rocks, Northern Taiwan: Acta Geologica Taiwanica, v. 24, pp. 123-148.

Ibbotson, P., 1961, The geology of Ovalau, Moturiki, and Naingani: Geol. Survey Department, Suva, Fiji, Bull. 9, 7 pp.

Ingersoll, R. V., et al., 1984, The effect of grain size on detrital modes: A test of the Gazzi-Dickinson pointing-counting method: Jour. Sed. Petr., v. 54, pp. 103-116.

Isachsen, Y. W. and Moxham, R. L., 1969, Chemical variation in plagioclase megacrysts from two vertical sections in the main Adirondack metaanorthosite massif: in Isachsen, Y. W., ed., Origin of Anorthosite and Related Rocks, New York State Museum and Sci. Service, Memoir 18, pp. 255-265.

Jakobsson, S. P., et al., 1978, Petrology of the Western Reykjanes Peninsula, Iceland: Jour. of Petr., v. 19, pp. 669-705.

Johnson, H. P., 1979, Opaque mineralogy of the igneous rock samples from DSDP Hole 395A: Initial Repts. of the Deep Sea Drilling Proj., v. 45, pp. 407-420.

Johnson, H. P. and Melson, W. G., 1979, Electron microprobe analyses of some titanomagnetite grains from Hole 395A: Initial Repts. Deep Sea Drilling Proj., v. 45, pp. 575-579.

Karson, J. A., 1979, Geological map and descriptive notes of Lewis Hills Massif, Western Newfoundland: Geol. Soc. Canada, open file 628, 20 pp.

Kirschvink, J. L. and Chang, S. R., 1984, Ultrafine-grained magnetite in deep-sea sediments: Possible bacterial magnetofossils: Geology, v. 12, pp. 559-562.

Kisvarsanyi, E. B., 1972, Petrochemistry of a Precambrian igneous province, St. Francois Mountains, Missouri: Missouri Geol. Survey and Water Resources, Rept. of Invest., v. 51, 96 pp.

Klecka, W. R., 1975, Discriminant analysis: in Nie, N. H., et al., eds., Statistical Package for the Social Sciences, McGraw-Hill Book Company, New York, 675 pp.

Klecka, W. R., 1987, Discriminant analysis: Sage Pub., Beverly Hills, 71 pp.

Klemic, H., 1970, Iron ore deposits of the United States of America, Puerto Rico, Mexico, and Central America: in Survey of World Ore Resources, United Nations, New York, pp. 411-477.

Kolker, A., 1982, Mineralogy and geochemistry of Fe-Ti oxide and apatite (Nelsonite) deposits and evaluation of the liquid immiscibility hypothesis: Econ. Geology, v. 77, pp. 1146-1158.

Korneliussen, A., et al., 1985, Titanium ores: an introduction to a review of titaniferous magnetite, ilmenite, and rutile deposits in Norway: Nor. Geol. Unders. Bull., v. 402, pp. 7-23.

Krumbein, W. C. and Pettijohn, F. J., 1938, Manual of sedimentary petrography: Appleton-Century, New York, 549 pp.

Krynine, P. D., 1935, Arkose deposits in the humid tropics: A study in sedimentation in southern Mexico: Amer. Jour. Sci., Ser. 5, v. 29, pp. 353-363.

Krynine, P. D., 1940, Petrology and genesis of the Third Bradford Sand: Pennsylvania State College Min. Ind. Expt. Sta. Bull., v. 77, 134 pp.

Krynine, P. D., 1943, Diastrophism and the evolution of sedimentary rocks: Pennsylvania Min. Ind. Tech. Paper, v. 84-A, 21 pp.

Krynine, P. D., 1946, The tourmaline group in sediments: Jour. Geology, v. 54, pp. 65-87.

Kyte, F. T. and Smit, J., 1986, Regional variations in spinel compositions: An important key to the Cretaceous/Tertiary event: Geology, v. 14, pp. 485-487.

Leake, B. E., 1978, Nomenclature of amphiboles: Amer. Min., v. 63, pp. 1023-1052.

Leonardos, Jr., O. H., 1973, The origin and alteration of granite rocks in Brazil: A study of metamorphism, anatexis, weathering and soil fertility within granitic terrain in eastern Brazil: Univ. Manchester, unpubl. Ph.D. thesis, 183 pp.

Liebenberg, C. J., 1960, The trace elements of the rocks of the Bushveld Igneous Complex: Univ. Pretoria Publ. New Series, no. 12, 69 pp.

Lindsley, D. H., 1976, Experimental studies of oxide minerals: in Rumble III, D., ed., Min. Soc. of Amer. Short Course Notes, v. 3, Oxide Minerals, L61-L88.

Lindsley, D. H., 1981, Some experiments pertaining to the magnetite-ulvospinel miscibility gap: Amer. Min., v. 66, pp. 759-762.

Lissiman, J. C. and Oxenford, R. J., 1975, Eneabba rutile-zircon-ilmenite sand deposit, W. A.: Econ. Geology of Australia and Papua, New Guinea, Monograph Ser. 5 (Metals), pp. 1062-1070.

Lister, G. F., 1966, The composition and origin of selected iron-titanium deposits: Econ. Geology, v. 61, pp. 275-310.

Loring, A. K. and Loring, R. B., 1980, K/Ar ages of middle Tertiary igneous rocks from southern New Mexico: New Mexico Bureau of Mines and Mineral Resources, Isochron/West, no. 28, pp. 17-19.

Lovering, J. F. and Widdowson, J. R., 1968, The petrological environment of magnesium ilmenites: Earth and Planetary Science Letters, v. 4, pp. 310-314.

Lowenstam, H. A., 1981, Magnetite biomineralization by organisms: Eos, Trans. Amer. Geophys. Union, v. 62, p. 849.

Lowright, R., Williams, E. G., and Dachille, F., 1972, An analysis of factors controlling deviations in hydraulic equivalence in some modern sands: Jour. Sed. Petr., v. 42, pp. 635-645.

Luepke, G., 1980, Opaque minerals as aids in distinguishing between source and sorting effects on beach-sand mineralogy in southwestern Oregon: Jour. Sed. Petr., v. 50, pp. 489-496.

Luepke, G. (ed.), 1984, Stability of Heavy Minerals in sediments: Van Nostrand Reinhold Company Inc., New York, 306 pp.

Luhr, J. F. and Carmichael, I. S. E., 1980, The Colima Volcanic Complex, Mexico I. Post-caldera andesites from Volcan Colima: Contr. to Min. and Petr., v. 71, pp. 343-372.

Lumpkin, G. R. and Zaikawski, A., 1980, A method for performing magnetic mineral separations in a liquid medium: Amer. Min., v. 65, pp. 390-392.

Macdonald, G. A., 1968, Composition and origin of Hawaiian lavas: Mem. Geol. Soc. Amer., v. 116, pp. 477-522.

Macdonald, G. A. and Katsura, T., 1964, Chemical composition of Hawaiian lavas: Jour. Petr., v. 5, pp. 82-133.

Macdonald, G. A., et al., 1983, Volcanoes in the Sea: The geology of Hawaii: University of Hawaii Press, Honolulu, 517 pp.

Mack, G. H., 1984, Exceptions to the relationship between plate tectonics and sandstone composition: Jour. Sed. Petr., v. 54, pp. 212-220.

Mackie, W., 1899, The sands and sandstones of eastern Moray: Edinburgh Geol. Soc. Trans., v. 7, pp. 48-172.

Mackie, W., 1923, The source of the purple zircons in the sedimentary rocks of Scotland: Edinburgh Geol. Soc. Trans., v. 11, pp. 200-213.

MacLachlan, J. C., et. al., 1960, Geology of the La Victoria area, Aragua, Venezuela: Geol. Soc. Amer. Bull., v. 71, pp. 241-248.

Mange-Rajetzky, M. A., 1981, Detrital blue sodic amphibole in recent sediments, southern coast, Turkey: Geol. Soc. London, v. 138, pp. 87-92.

Mann, S., et al., 1984, Structure, morphology, and crystal growth of bacterial magnetite: Nature, v. 310, pp. 405-507.

Marelle, A., 1970, Iron ore deposits of Europe: in Survey of World Ore Resources, United Nations, New York, pp. 270-301.

Marelle, A. and Abdulla, M. A., 1970, Iron ore deposits of Africa: in Survey of World Iron Ore Resources, United Nations, New York, pp. 62-101.

Martens, J. H. C., 1928, Beach deposits of ilmenite, zircon, and rutile in Florida: Florida Geol. Survey Annual Repts., v. 19, pp. 124-154.

Mathison, C. I., 1975, Magnetites and ilmenites in the Somerset Dam layered basic intrusion, southeastern Queensland: Lithos, v. 8, pp. 93-111.

Matter, A. and Ramseyer, K., 1985, Cathodoluminesence microscopy as a tool for provenance studies of sandstones: in Zuffa, G. G., ed., Provenance of Arenites, pp. 191-212.

Maynard, J. B., 1983, Geochemistry of sedimentary ore deposits: Springer-Verlag, New York, 305 pp.

Maynard, J. B., 1984, Composition of plagioclase feldspar in modern deep-sea sands: Relationship to tectonic setting: Sedimentology, v. 31, pp. 493-501.

McBride, E. F., 1985, Diagenetic processes that affect provenance determinations in sandstone: in Zuffa, G. G., ed., Provenance of Arenites, D. Reidel Pub. Co., Boston, pp. 95-113.

McCabe, C., 1986, Do hydrocarbons cause secondary magnetizations?: Eos, Trans. Amer. Geophys. Union, v. 67, p. 265.

McCabe, C., et al., 1983, Diagenetic magnetite carries ancient yet secondary remanence in some Paleozoic sedimentary carbonates: Geology, v. 11, pp. 221-223.

McDonald, B. C., 1968, Composition of some garnets used in provenance studies of tills: Jour. Sed. Petr., v. 38, pp. 956-957.

Milner, H. B., 1926, Supplemental to introduction to sedimentary petrography: Murby, London, 157 pp.

Milner, H. B., 1962, Sedimentary petrology: Macmillan, New York, v. 2, 715 pp.

Minch, J. A., 1967, Stratigraphy and structure of the Tijuana-Rosarito Beach area, Northwestern Baja California, Mexico: Geol. Soc. Amer. Bull., v. 78, pp. 1155-1178.

Mitchell, R. H., et al., 1973, Part II: Trace elements in magnesium ilmenites from Lesotho Kimberlites: Lesotho National Devel. Corp., Masera, Cape and Transvaal Printers LTD, Capetown, pp. 230-235.

Molyneux, T. C., 1972, X-ray data and chemical analyses of some titanomagnetite and ilmenite samples from the Bushveld Complex, South Africa: Min. Mag., v. 38, pp. 863-871.

Mooser, F., 1969, The Mexican volcanic belt, structure, and development: Formation of fractures by differential crustal heating: Pan-American Symposium on the Upper Mantle, Mexico, 1968, Group II, Upper Mantle Petrology and Tectonics, v. 2, pp. 15-22.

Morad, S. and Aldahan, A. A., 1986, Alteration of detrital Fe-Ti oxides in sedimentary rocks: Geol. Soc. Amer. Bull., v. 97, pp. 567-578.

Morey, G. B., 1972, Gunflint Range: in Sims, P. K. and Morey, G. B., eds., Geology of Minnesota: a centennial volume, Minnesota Geol. Surv., St. Paul, pp. 218-225.

Morton, A. C., 1984, Heavy minerals from Paleogene sediments, Deep Sea Drilling Projects Log 81: their bearing on stratigraphy, sediment provenance, and the evolution of the north Atlantic: Initial Repts. of the Deep Sea Drilling Proj., v. 81, pp. 653-661.

Morton, A. C., 1985a, Heavy minerals in provenance studies: in Zuffa, G. G., ed., Provenance of Arenites, pp. 249-277.

Morton, A. C., 1985b, A new approach to provenance studies: electron microprobe analysis of detrital garnets from Middle Jurassic sandstones of the northern North Sea: Sedimentology, v. 32, pp. 553-566.

Neel, L., 1955, Some theoretical aspects of rock magnetism: Advan. Phys., v. 4, pp. 191-243.

Neuman, E. R., 1974, The distribution of Mn^{2+} and Fe^{2+} between ilmenites and magnetites in igneous rocks: Amer. Jour. Sci., v. 274, pp. 1074-1088.

Nickel, E., 1973, Experimental dissolution of light and heavy minerals in comparison with weathering and intrastratal solution: Contr. to Sed. (Struttgart), v. 1, pp. 1-68.

Nie, N. H., et al., 1975, Statistical Package for the Social Sciences (2nd edition): New York, Mcgraw-Hill, 675 pp.

Nisbet, E. G. and Pearce, J. B., 1977, Clinopyroxene composition in mafic lavas from different tectonic settings: Contr. Min. Petr., v. 63, pp. 149-160.

Nishitani, T., 1981, Magnetic properties of titano-magnetites containing Spinel ($MgAl_2O_4$): Jour. Geomag. Geoelectr., v. 33, pp. 171-179.

Nixon, P. H. and Kreston, P., 1973, Part III: Chromium and nickel in Kimberlites: Lesotho National Devel. Corp., Masera, Cape and Transvaal Printers LTD, Capetown, pp. 235-237.

Osborn, E. F. and Boctor, N. Z., 1981, Some additional observations on magnetite in calc-alkaline volcanic rocks: Carnegie Inst., Geophys. Laboratory, pp. 324-327.

Osborne, F. F., 1928, Certain titaniferous magnetite deposits and their origin: Econ. Geology, v. 23, pp. 724-761, 895-922.

Owen, M. R. and Carozzi, A. V., 1986, Southern provenance of upper Jackford Sandstones, southern Ouachita Mountains: Cathodoluminescence petrology: Geol. Soc. Amer. Bull., v. 97, pp. 110-115.

Ozima, M. and Larson, E. E., 1970, Low- and high-temperature oxidation of titanomagnetite in relation to irreversible changes in the magnetic properties of submarine basalts: Jour. Geophys. Res., v. 75, No. 5, pp. 1003-1017.

Park, Jr., C. F. and MacDiarmid, 1975, Ore deposits: W. H. Freeman and Co., San Francisco, 530 pp.

Pettijohn, F. J., 1941, Persistance of heavy minerals and geologic age: Jour. Geology, v. 79, pp. 610-625.

Pettijohn, F. J. and Ridge, J. D., 1933, A mineral variation series of beach sands from Cedar Point, Ohio: Jour. Sed. Petr., v. 3, pp. 92-94.

Pettijohn, F. J., et al., 1987, Sand and Sandstone: Springer-Verlag, New York, 553 pp.

Philpotts, A. R., 1967, Origin of certain iron-titanium oxide and apatite rocks: Econ. Geology, v. 62, pp. 303-315.

Phinney, W. C., 1969, The Duluth Complex in the Gabbro Lake quadrangle, Minnesota: Minn. Geol. Survey Rept. Inv. 9, 20 pp.

Phinney, W. C., 1972, Duluth Complex, history and nomenclature: in Sims, P. K. and Morey, G. B., eds., Geology of Minnesota: A Centennial Volume, pp. 333-334.

Pires, F. R. M., et al., 1982, Multistage generation of granite in Rio de Janeiro, Brazil: An. Acad. brasil. Ciênc., v. 54, pp. 563-574.

Pittman, E. D., 1963, Plagioclase feldspar as an indicator of provenance: Jour. Sed. Petr., v. 33, pp. 380-386.

Poldervaart, A., 1956, Zircon in rocks, 2 Igneous rocks: Amer. Jour. Sci., v. 254, pp. 521-554.

Prèvot, M. and Mergoil, J., 1973, Crystallization trend of titanomagnetite in an alkali basalt from Saint-Clèment (Massif Central, France): Min. Mag., v. 39, pp. 474-481.

Price, G. D., 1981, Subsolidus phase relations in the titanomagnetite solid solution series: Amer. Min., v. 66, pp. 751-758.

Puffer, J. H., 1972, Iron-bearing minerals as indicators of intensive variables pertaining to granitic rocks from the Pegmatite Points area, Colorado: Amer. Jour. Sci., v. 272, pp. 273-289.

Ramdohr, P., 1980, The ore minerals and their intergrowths: Pergamon Press, New York, pp. 911-940.

Rao, N. K. and Rao, G. V. U., 1965, Intergrowths in ilmenite of the beach sands of Kerala: Min. Mag., v. 35, pp. 118-130.

Reynolds, R. L., 1982, Post-depositional alteration of titanomagnetite in a Miocene sandstone, south Texas (U.S.A.): Earth and Planetary Science Letters, v. 61, pp. 381-391.

Riezebos, P. A., 1979, Compositional downstream variation of opaque and translucent heavy residues in some modern Rio Magdalene sands (Columbia): Sed. Geol., v. 24, pp. 197-225.

Rimsaite, J., 1967, Optical heterogeneity of feldspars observed in diverse Canadian rocks: Scheiz. Min. Pet. Mitt., v. 47, pp. 61-76.

Rittenhouse, G., 1943, Transportation and deposition of heavy minerals: Geol. Soc. Amer. Bull., v. 54, pp. 1725-1780.

Rosenblum, S., 1958, Magnetic susceptibilities of minerals in the Frantz magnetic separator: Amer. Min., v. 43, pp. 170-173.

Roser, B. P. and Karsch, R. J., 1988, Provenance signatures of sandstone-mudstone suites determined using discriminant function analysis of major-element data: Chemical Geology, v. 67, pp. 119-139.

Ross, C. S., 1941, Titanium deposits of Nelson and Amherst Counties, Virginia: U. S. G. S. Prof. Paper 198, 58 pp.

Rubey, W. W., 1933, Settling velocity of gravel, sand, and silt particles: Amer. Jour. Sci., 5th Ser., v. 25, pp. 325-338.

Russell, R. D., 1936, The size distribution of minerals in Mississippi River sands: Jour. Sed. Petr., v. 6, pp. 125-142.

Russell, R. D., 1937, Mineral composition of Mississippi River sands: Geol. Soc. Amer. Bull., v. 48, pp. 1307-1348.

Sack, R. O., 1982, Spinels as petrogenetic indicators: activity-composition relations a low pressures: Contrib. Mineral. Petrol., v. 79, pp. 169-186.

Sandberg, A. E., 1938, Section across Keweenawan lavas at Duluth, Minnesota: Geol. Soc. Amer. Bull., v. 49, pp. 795-830.

Sanderson, D. D., 1974, Spatial distribution and origin of magnetite in an intrusive igneous mass: Geol. Soc. Amer., v. 85, pp. 1183-1188.

Savage, K., 1986, Petrographic studies of quartz-rich South American modern sands: Unpublished M.S. thesis, University of Cincinnati, Cincinnati, 152 pp.

Seager, W. R., 1981, Geology of Organ Mountains and southern San Andres Mountains, New Mexico: New Mexico Bureau of Mines and Mineral Resources, Memoir 36, 97 pp.

Shagam, R., 1960, Geology of central Aragua, Venezuela: Geol. Soc. Amer. Bull., v. 71, pp. 249-302.

Sides, J. R., 1976, Stratigraphy of volcanic rocks in the Lake Killarney quadrangle, Iron and Madison Counties: in Kisvarsanyi, E. B., ed., Studies in Precambrian Geology of Missouri, Rep. of Invest. Mo. Geol. Surv., v. 61, pp. 105-113.

Sides, J. R., et al., 1981, Calderas in the Precambrian terrane of the St. Francois Mountains, southeastern Missouri: Jour. Geophys. Res., v. 86, pp. 10349-10364.

Siever, R. and Woodford, N., 1979, Dissolution kinetics and the weathering of mafic minerals: Geochimica et Cosmochimica Acta, v. 43, pp. 717-724.

Silver, L. T., 1969, A geochronologic investigation of the Anorthosite Complex, Adirondack Mountains, New York: in Isachsen, Y. W., ed., Origin of Anorthosite and Related Rocks, New York State Museum and Science Service, Memoir 18, pp. 233-251.

Simmons, G., 1954, Gravity survey and geological interpretation, northern New York: Geol. Soc. Amer. Bull., v. 75, pp. 81-98.

Slingerland, R. L., 1977, The effects of entrainment on the hydraulic equivalence relationships of light and heavy minerals in sands: Jour. Sed. Petr., v. 47, pp. 753-770.

Smith, C. H., 1958, Bay of Islands Igneous Complex, western Newfoundland: Can. Geol. Survey Memoir, v. 290, 132 pp.

Smith, R. J., 1953, Geology of the Los Teques-Cua region, Venezuela: Geol. Soc. Amer. Bull., v. 64, pp. 41-64.

Snetsinger, K. G., et al., 1968, Electron microprobe analysis of vanadium in the presence of titanium: Amer. Min., v. 53, pp. 1770-1773.

Sorby, H. C., 1880, On the structure and origin of non-calcareous stratified rocks: Geol. Soc. London Proc., v. 76, pp. 46-92.

Speidel, D. H., 1970, Effect of magnesium on the iron-titanium oxides: Amer. Jour. Sci., v. 268, pp. 341-353.

Spencer, K. J. and Lindsley, D. H., 1981, A solution model for coexisting iron-titanium oxides: Amer. Min., v. 66, pp. 1189-1201.

Spiroff, K., 1938, Magnetite crystals from meteoric solutions: Econ. Geology, v. 33, pp. 818-828.

Stacey, F. D. and Banerjee, S. K., 1974, The physical principles of rock magnetism: New York, Elsevier Sci. Pub. Co., 195 pp.

Stattegger, K., 1987, Heavy minerals and provenance of sands: Modeling of lithological end members from river sands of Northern Austria and from sandstones of the Austroalpine Gosan Formation (Late Cretaceous): Jour. Sed. Petr., v. 57, pp. 301-310.

Stearns, H. T., 1940, Four-phase volcanism in Hawaii (Abst.): Geol. Soc. Amer. Bull., v. 51, pp. 1947-8.

Stearns, H. T., 1946, Geology of the Hawaiian Islands: Hawaii Div. Hydrography Bull., v. 8, 196 pp.

Stearns, H. T. and Macdonald, G. A., 1946, Geology and groundwater resources of the island of Hawaii: Hawaii Div. Hydrography Bull., v. 9, 363 pp.

Stephenson, R. C., 1948, Titaniferous magnetite deposits of the Lake Sanford Area, New York: Amer. Inst. Min. Eng. Trans., v. 178, pp. 397-421.

Stephenson, A., 1969, The temperature dependent cation distribution in titanomagnetites: Geophys. Jour. Roy. Astron. Soc., v. 18, pp. 199-210.

Stormer, Jr., J. C., 1983, The effects of recalculation on estimates of temperature and oxygen fugacity from analyses of multicomponent iron-titanium oxides: Amer. Min., v. 68, pp. 586-594.

Stow, M. H., 1938, Dating Cretaceous-Eocene tectonic movements in Big Horn Basin by heavy minerals: Geol. Soc. Amer. Bull., v. 49, pp. 731-762.

Stow, M. H., 1939, Reflection of provenance in heavy minerals of James River, Virginia: Jour. Sed. Petr., v. 9, pp. 86-91.

Strangway, D. W., et al., 1968, A possible cause of high magnetic stability in volcanic rocks: Jour. Geophys. Res., v. 73, pp. 3787-3795.

Stumpfl, V. E., 1958, Erzmikroskopische untersuchungen an schwermineralien in sanden: Geol. Jb., Bd. 73, pp. 685-724.

Suttner, L. J. and Basu, A., 1977, Structural state of detrital alkali feldspars: Sedimentology, v. 24, pp. 63-73.

Suttner, L. J., et al., 1981, Climate and origin of quartz arenites: Jour. Sed. Petr., v. 51, pp. 1235-1246.

Tankard, A. J., et al., 1982, Crustal Evolution of Southern Africa: Springer-Verlag, New York, 523 pp.

Taylor, R. B., 1964, Geology of the Duluth Gabbro Complex near Duluth, Minnesota: Minn. Geol. Surv. Bull., v. 44, 63 pp.

Temple, A. K., 1966, Alteration of ilmenite: Econ. Geology, v. 61, pp. 695-714.

Theil, G. A., 1940, The relative resistance to abrasion of mineral grains of sand: Jour. Sed. Petr., v. 10, pp. 103-124.

Thomas, R. B., et al., 1988, Geochemistry of heavy minerals in provenance studies: V. M. Goldschmidt Conference, Programs and Abstracts, The Geochemical Society, p. 78.

Thorarinsson, S., et al., 1973, The eruption on Heimaey, Iceland: Nature, v. 241, pp. 372-375.

Thoulet, J., 1913, Notes sur lithologie sous-marine: Ann. Inst. Oceanogr., v. 5, pp. 1-14.

Tolman, C. F. and Robertson, F., 1969, Exposed Precambrian rocks in S. E. Missouri: Missouri Geol. Surv. and Water Resources Rept. of Invest., v. 44, 68 pp.

Travena, A. S. and Nash, W. P., An electron microscope study of detrital feldspar: Jour. Sed. Petr., v. 51, pp. 137-149.

Tucker, P. and O'Reilly, W., 1980, The laboratory simulation of deuteric oxidation of titanomagnetites: effect on magnetic properties and stability of thermoremanence: Physics of the Earth and Planetary Interiors, v. 23, pp. 112-133.

Turner, P., 1979, The paleomagnetic evolution of continental red beds: Geological Mag., v. 116, pp. 289-301.

Twist, D. and French, B. M., 1983, Voluminous acid volcanism in the Bushveld Complex: A review of the Rooiberg Felsite: Bulletin Volcanologique, v. 46, pp. 225-242.

Vali, H., et al., 1987, Magnetotactic bacteria and their magnetofossils in sediments: Earth and Planetary Science Letters, v. 86, pp. 389-400.

Van Andel, T. H. and Poole, D. M., 1960, Sources of recent sediments in the northern Gulf of Mexico: Jour. Sed. Petr., v. 30, pp. 91-122.

Van Houten, F. B., 1968, Iron oxides in red beds: Geol. Soc. Amer. Bull., v. 79, pp. 399-416.

Verhoogen, J., 1956, Ionic ordering and self-reversal of magnetization in impure titanomagnetites: Jour. Geophys. Res., v. 61, pp. 201-209.

Verhoogen, J., 1962, Oxidation of iron-titanium oxides in igneous rocks: Jour. Geol., v. 70, pp. 168-181.

Vine, F. S. and Matthews, D. H., 1963, Magnetic anomalies over oceanic ridges: Nature, v. 199, pp. 947-949.

Vintanage, P. W., 1957, Studies of zircon types in Ceylon Pre-Cambrian complex: Jour. Geol., v. 65, pp. 117-138.

Walker, T. R., 1967, Formation of red beds in modern and ancient deserts: Geol. Soc. Amer. Bull., v. 78, pp. 353-368.

Walker, T. R., et al., 1981, Nature and origin of hematite in the Moenkopi Formation (Triassic), Colorado Plateau: A contribution to the origin of magnetism in red beds: Jour. Geophys. Res., v. 86, pp. 317-333.

Welch, B. K., et al., 1975, Mineral sand deposits of the Capal Area W. A.: Econ. Geol. of Australia and Papua, New Guinea, Monograph Series 5 (Metals), pp. 1070-1088.

Whalen, J. B. and Chappell, B. W., 1988, Opaque mineralogy and mafic mineral chemistry of I- and S-type granites of the Lachlan fold belt, southeast Australia: Amer. Min., v. 73, pp. 281-296.

Wilson, S. T., 1965, A new class of faults and their bearing on continental drift: Nature, v. 207, pp. 343-347.

Wright, J. F. and Lovering, J. F., 1965, Electron-probe micro-analysis of the iron-titanium oxides in some New Zealand ironsands: Min. Mag., v. 35, pp. 604-621.

Wright, J. B., 1961, Solid-solution relationships in some titaniferous iron oxide ores of basic igneous rocks: Min. Mag., v. 32, pp. 778-789.

Yen, T. P., 1958, Cenozoic volcanic activity in Taiwan: Taiwan Min. Indus., v. 10, pp. 1-39.

Young, S. W., 1976, Petrographic textures of detrital polygonal quartz as an aid to interpreting crystalline source rocks: Jour. Sed. Petr., v. 46, pp. 595-603.

Yurkova, R. H., 1970, Comparison of post-sedimentary alteration of oil-gas and water-bearing rocks: Sedimentology, v. 15, pp. 53-68.

Zuffa, G. G., 1980, Hybrid arenites: Their composition and classification: Jour. Sed. Petr., v. 50, pp. 21-29.

Zuffa, G. G., 1985, Optical analysis of arenites: Influence of methodology on compositional results: in Zuffa, G. G., ed., Provenance of Arenites, D. Reidel Pub. Co., Boston, pp. 165-189.

APPENDIX A

Sample numbers, Rock types, Locations, and Percent magnetite and ilmenite in sand samples

Sample Number	Rock Type	Location	% Fe_3O_4	% $FeTiO_3$
Erg-1	Graniteville Granite	Elephant Rock State Park on Rt. 21, Missouri; stream sand.	1.13	N/A
Cb-1	Favela Granite	Near Costa Brava Club, Rio de Janiero, Brazil; soil sample.	Tr	0.14
As-1	Surgarloaf Peak Quartz Monzonite	Aquirre Springs Recreational Area, east side Organ Mtns. off I-70, 56Km NE of Las Cruces, N.M.; stream sand.	11.40	2.70
St-2	Saganaga Tonalite	Seagull Lake off Gunflint Trail, 48Km N.W. of Grand Marais, Minnesota; beach sand.	0.67	1.56
Vsc-1	Stouts Creek Rhyolite	Near Knobkick Lookout Tower, off Rt. H, Missouri; stream sand.	0.12	Tr
Rgr-1	Royal Gorge Rhyolite	Royal Gorge Scenic View, Rt. 21, Missouri; stream sand.	0.34	1.72
Jsr-1	Undifferentiated Felsic Volcanics	Johnson Shut-ins State Park off Rt. N, Missouri; Black River stream sand.	1.53	N/A
Btr-1	Undifferentiated Felsic Volcanics	Johnson Shut-ins State Park off Rt. N, Missouri; tributary to Black River 3Km south of camp grounds, stream sand.	0.20	N/A
Dfv-2	Rooiberg Felsite	Near Wapadskloof, Republic of South Africa; stream sand.	0.64	2.25
Tm-1	Nevado de Toluca Andesite	15Km west of Toluca on 134/13, Estado de Mexico, Mexico, north side of volcano; stream sand.	1.13	N/A

Sample Number	Rock Type	Location	% Fe_3O_4	% $FeTiO_3$
Tm-2	Nevado de Toluca Andesite	10Km west of Toluca on 134/13, Estado de Mexico, Mexico, north side of volcano; stream sand.	2.12	1.08
Ta-1	Kuanyinshan Andesite	Northern coast of Taiwan, 30Km north of Taipei; beach sand.	69.90	Tr
Av-1	Andesite	Ovalau Island, Fiji, south side of island; beach sand.	35.43	14.96
Dg-2	Duluth Gabbro	Keene Creek along Skyline Parkway west of Hwy 61, Duluth, MN; stream sand.	3.34	8.69
Dg-3	Duluth Gabbro	1 mile west of sample Dg-2 along Skyline Parkway, Duluth, MN; soil/stream sand.	2.80	5.98
Dg-4	Duluth Gabbro	Small stream draining "Sea Cliff" (bluff of gabbro) along Skyline Parkway, Duluth, MN; stream sand.	1.94	10.27
Sr-1	Bushveld Complex	Steelpoort River draining a large number of magnetite layers in Upper Zone, Eastern lobe, Transvaal, Republic of South Africa; stream sand.	12.59	N/A
Sr-2	Bushveld Complex	Tributary to Steepoort River draining area with 1 or 2 magnetite layers, Upper Zone, Eastern Lobe, Transvaal, Republic of South Africa; stream sand.	49.41	28.08

Sample Number	Rock Type	Location	% Fe_3O_4	% $FeTiO_3$
Vu-1	Bushveld Complex	Upper Zone, Eastern Lobe, Transvaal, Republic of South Africa; stream sand.	11.16	19.20
Vu-2	Bushveld Complex	Upper Zone, Eastern Lobe, runoff of magnetite layers along mining road, Transvaal, Republic of South Africa.	22.23	2.34
Kb-2	Keweenawan Basalt	Near Crystal Creek and junction with Hwy 1 off Hwy 61, northeast MN; stream sand.	0.44	0.15
M-7	Basalt	Maui, Hawaii; north side of island off Hwy 36 near Pa'ia, Maui; beach sand.	27.07	Tr
HBb-1	Basalt	Hawaii Island, Hawaii; 3Km NE of South Point at Mahana Bay; beach sand.	2.44	Tr
B-5	Basalt	Hawaii Island, Hawaii; Loess deposit 3Km SE of Waiki'i off Saddle Road; wind blown material.	2.50	Tr
IL76-1	Basalt	Haimeay Island, Iceland; East coast of island along the new coast line formed by the 1973 eruption; beach sand.	11.11	Tr
IL85-1	Basalt	Tip of Reykjanes Peninsula, Iceland; beach sand.	6.25	Tr
pCwa-1	Whiteface-Type Meta-Anorthosite	Whiteface Mtn., New York; sand/soil sample near peak.	0.20	9.99

Sample Number	Rock Type	Location	% Fe_3O_4	% $FeTiO_3$
pCma-3	Marcy-Type Meta-Anorthosite	Indian Falls 5Km from summit of Mt. Marcy, New York; stream sand.	2.30	10.06
PC-1057	Ultramafic Complex (serpentinized harzburgite)	Rio Guarico, a tributary to Rio Apure, near Comataqua Dam, Comataqua, Estado de Araqua, Venezuela (Lat. 9 50'N, Long. 66 55'W); stream sand.	0.72	0.99
NFao-1	Lewis Hills Ophiolite Suite	Bay of Islands Ophiolite Complex, western Newfoundland along Port au Port Bay, Beach sand at the mouth of Fox Island River.	37.65	Tr

APPENDIX B

ELECTRON MICROPROBE DATA

MAGNETITE

Table 27: Electron microprobe data, Surgarloaf Peak Quartz Monzonite.

Wt.% Oxide Sample#	Ti	V	Al	Cr	Mg	Si	Mn	Fe^{2+}	Fe^{3+}	Total
As-1-1	0.08	0.26	0.06	0.00	0.01	0.03	0.08	30.94	68.54	100.04
-2	0.15	0.30	0.09	0.05	0.01	0.01	0.07	31.26	68.86	100.78
-3	0.12	0.27	0.07	0.05	0.02	0.03	0.07	31.06	68.66	100.34
-4	0.06	0.26	0.08	0.05	0.03	0.02	0.09	30.86	68.49	99.93
-5	0.19	0.28	0.12	0.06	0.01	0.02	0.08	31.14	68.47	100.37
-6	0.17	0.28	0.06	0.06	0.02	0.02	0.09	31.06	68.48	100.25
-7	0.20	0.32	0.10	0.06	0.01	0.02	0.04	31.20	68.44	100.39
-8	0.27	0.27	0.33	0.05	0.04	0.02	0.15	31.35	68.54	101.01
-9	0.17	0.29	0.06	0.05	0.00	0.02	0.09	31.07	68.46	100.20
-10	0.12	0.25	0.06	0.03	0.00	0.03	0.08	30.98	68.44	100.01
-11	0.16	0.22	0.07	0.04	0.00	0.03	0.08	31.05	68.43	100.09
-12	0.17	0.25	0.07	0.04	0.02	0.01	0.10	31.25	68.92	100.83
-13	0.10	0.27	0.06	0.06	0.01	0.01	0.04	31.38	69.33	101.27
-14	0.15	0.26	0.11	0.06	0.08	0.25	0.06	31.07	68.69	100.73
-15	0.15	0.26	0.09	0.05	0.01	0.02	0.08	31.01	68.36	100.01
-16	0.17	0.29	0.12	0.04	0.01	0.02	0.11	31.19	68.71	100.64
-17	0.15	0.28	0.07	0.04	0.02	0.01	0.08	31.18	68.80	100.62
-18	0.07	0.23	0.06	0.04	0.00	0.03	0.08	31.11	68.95	100.57
-19	0.15	0.28	0.10	0.05	0.02	0.02	0.05	31.26	68.89	100.82
-20	0.09	0.25	0.06	0.06	0.01	0.03	0.06	31.17	68.90	100.63
Avg	0.14	0.27	0.09	0.05	0.02	0.03	0.08	31.13	68.67	
Std	0.05	0.02	0.06	0.01	0.02	0.05	0.02	0.13	0.24	

Table 28: Electron microprobe data, Saganaga Tonalite.

Wt.% Oxide Sample#	Ti	V	Al	Cr	Mg	Si	Mn	Fe^{2+}	Fe^{3+}	Total
St-2-1	0.52	0.14	0.03	0.02	0.01	0.01	0.46	30.87	67.53	99.59
-2	0.02	0.25	0.02	0.44	0.00	0.01	0.03	30.49	67.16	98.44
-3	0.01	0.23	0.03	0.21	0.00	0.02	0.03	30.60	67.81	98.94
-4	0.03	0.30	0.09	0.05	0.01	0.01	0.02	30.60	67.77	98.88
-5	0.01	0.12	0.01	0.03	0.00	0.01	0.49	30.16	68.04	98.38
-6	0.05	0.15	0.05	0.09	0.00	0.03	0.04	30.65	67.85	98.90
-7	0.00	0.10	0.01	0.36	0.02	0.00	0.05	30.51	67.60	98.65
-8	0.01	0.09	0.02	0.55	0.01	0.01	0.02	30.75	67.80	99.27
-9	0.01	0.18	0.17	0.04	0.01	0.01	0.04	30.76	68.15	99.36
-10	0.01	0.15	0.01	0.06	0.02	0.02	0.03	30.67	68.22	99.19
-12	0.02	0.29	0.11	0.03	0.00	0.01	0.12	30.21	67.14	97.93
-13	0.04	0.14	0.57	0.35	0.00	0.12	0.10	31.23	68.23	100.78
-14	0.02	0.09	0.54	0.19	0.00	0.11	0.14	31.23	68.61	100.93
-15	0.01	0.24	0.54	0.42	0.00	0.20	0.11	31.26	68.42	101.20
-16	0.00	0.10	0.53	0.42	0.01	0.18	0.11	31.05	68.04	100.44
-17	0.00	0.00	0.47	0.00	0.01	0.25	0.05	30.88	68.06	99.72
-18	0.00	0.21	0.51	0.27	0.00	0.18	0.18	30.93	67.85	100.13
-19	0.00	0.11	0.59	0.12	0.04	0.20	0.11	31.10	68.50	100.77
-20	0.00	0.21	0.54	0.33	0.00	0.13	0.09	31.04	68.02	100.36
Avg	0.04	0.16	0.25	0.21	0.01	0.08	0.12	30.79	67.94	
Std	0.11	0.08	0.24	0.17	0.01	0.08	0.13	0.32	0.39	

Table 29: Electron microprobe data, Pavela Granite.

Wt% Oxide Sample#	Ti	V	Al	Cr	Mg	Si	Mn	Fe^{2+}	Fe^{3+}	Total
Cb-1-1	0.16	0.63	0.73	1.12	0.19	0.01	0.03	30.94	66.63	100.44
-2	0.03	0.14	0.07	0.03	0.01	0.03	0.03	31.17	69.12	100.61
-3	0.56	0.05	0.43	0.03	0.01	0.01	0.04	31.61	67.60	100.35
-4	0.03	0.32	0.16	0.04	0.02	0.02	0.17	30.98	68.90	100.64
-5	0.29	0.14	0.33	0.01	0.01	0.02	0.08	31.49	68.34	100.61
-6	0.00	0.02	0.00	0.00	0.10	0.09	0.01	31.30	69.98	101.50
-7	0.05	0.61	0.31	0.14	0.14	0.01	0.00	31.00	68.66	100.91
-8	0.04	0.51	0.31	0.07	0.08	0.01	0.00	30.94	68.38	100.36
-9	0.03	0.36	0.06	0.05	0.00	0.00	0.03	31.13	69.04	100.71
-10	0.03	0.31	0.17	0.13	0.01	0.01	0.05	31.14	68.88	100.74
-11	0.02	0.39	0.05	0.06	0.00	0.02	0.03	31.05	68.88	100.49
-12	0.16	0.73	0.15	0.10	0.01	0.01	0.00	31.13	68.27	100.54
-13	0.05	0.40	0.02	0.04	0.01	0.02	0.06	31.17	69.19	100.99
-14	0.03	0.04	0.06	0.00	0.00	0.01	0.03	31.11	69.02	100.28
-15	0.03	0.68	0.10	0.07	0.00	0.03	0.01	31.06	68.71	100.69
-16	0.05	0.61	0.34	0.15	0.15	0.01	0.01	30.85	68.33	100.49
-17	0.01	0.41	0.05	0.04	0.00	0.01	0.06	31.22	69.36	101.17
Avg	0.09	0.37	0.20	0.12	0.04	0.02	0.04	31.13	68.66	
Std	0.14	0.23	0.18	0.25	0.06	0.02	0.04	0.19	0.72	

Table 30: Electron microprobe data, Graniteville Granite.

Wt% Oxide Sample#	Ti	V	Al	Cr	Mg	Si	Mn	Fe^{2+}	Fe^{3+}	Total
Erg-1	0.23	0.01	0.17	0.01	0.00	0.02	0.00	31.09	67.88	99.40
-2	0.03	0.01	0.02	0.00	0.00	0.02	0.00	30.90	68.54	99.52
-3	0.03	0.01	0.03	0.01	0.00	0.05	0.00	31.29	69.40	100.82
-4	0.04	0.01	0.03	0.00	0.01	0.05	0.00	30.85	68.37	99.36
-5	0.42	0.01	0.12	0.01	0.00	0.64	0.02	31.32	67.78	100.31
-6	0.13	0.01	0.07	0.01	0.00	0.07	0.00	30.94	68.15	99.38
-7	0.19	0.01	0.68	0.02	0.00	0.52	0.02	30.77	66.61	98.81
-8	0.06	0.01	0.60	0.00	0.01	0.43	0.02	30.64	66.99	98.74
-9	0.17	0.00	0.33	0.01	0.01	0.15	0.01	30.87	67.47	99.00
-10	0.06	0.02	0.03	0.01	0.00	0.02	0.00	30.83	68.23	99.21
-11	0.13	0.02	0.23	0.00	0.00	0.02	0.01	31.26	68.64	100.31
-12	0.06	0.01	0.06	0.01	0.00	0.12	0.01	31.00	68.61	99.87
-13	0.35	0.01	0.22	0.01	0.01	0.12	0.00	31.32	67.88	99.92
-14	0.11	0.00	0.08	0.00	0.00	0.02	0.01	31.13	68.66	100.00
-15	0.20	0.00	0.18	0.00	0.00	0.02	0.01	31.51	69.02	100.95
-16	0.08	0.01	0.08	0.01	0.00	0.67	0.00	30.99	68.43	100.28
-17	0.10	0.01	0.07	0.00	0.00	0.01	0.00	31.10	68.65	99.94
-18	0.14	0.01	0.36	0.00	0.00	0.03	0.02	31.13	68.12	99.81
-19	0.06	0.01	0.19	0.00	0.00	0.17	0.02	30.74	67.84	99.03
-20	0.04	0.00	0.10	0.00	0.00	0.40	0.01	30.70	67.96	99.22
Avg	0.13	0.01	0.18	0.01	0.00	0.18	0.01	31.02	68.16	
Std	0.10	0.01	0.18	0.01	0.00	0.22	0.01	0.23	0.64	

Table 31: Electron microprobe data, Royal Gorge Rhyolite.

Wt% Oxide Sample#	Ti	V	Al	Cr	Mg	Si	Mn	Fe2+	Fe3+	Total
Rgr-1	0.00	0.00	0.79	0.00	0.03	0.29	0.13	31.08	68.25	100.57
-2	0.02	0.11	0.70	0.00	0.03	0.32	0.11	30.81	67.68	99.78
-3	0.02	0.01	0.69	0.00	0.04	0.15	0.15	31.14	68.56	100.76
-4	0.71	0.29	0.76	0.00	0.04	0.17	1.29	30.47	66.77	100.40
-5	0.09	0.07	0.76	0.00	0.11	0.34	0.10	31.11	68.27	100.85
-6	0.32	0.62	0.73	0.00	0.03	0.17	0.28	31.13	67.52	100.80
-7	0.00	0.00	0.75	0.00	0.01	0.09	0.09	31.11	68.22	100.18
-8	0.25	0.18	0.78	0.00	0.25	0.35	0.56	30.57	67.97	100.91
-9	0.03	0.13	0.63	0.00	0.03	0.19	0.16	30.89	68.03	100.09
-10	0.00	0.06	0.73	0.00	0.03	0.10	0.20	30.98	68.28	100.38
-11	0.00	0.20	0.88	0.00	0.50	0.35	0.52	29.85	68.12	100.42
-12	0.00	0.00	0.66	0.00	0.05	0.05	0.43	30.43	67.77	99.39
-13	0.03	0.02	1.04	0.00	0.04	0.63	0.18	30.88	67.45	100.27
-14	0.80	0.38	0.66	0.00	0.09	0.11	0.11	31.63	66.69	100.47
Avg	0.16	0.15	0.75	0.00	0.09	0.24	0.31	30.86	67.83	
Std	0.26	0.17	0.10	0.00	0.13	0.15	0.31	0.41	0.54	

Table 32: Electron microprobe data, Stouts Creek Rhyolite.

Wt% Oxide Sample#	Ti	V	Al	Cr	Mg	Si	Mn	Fe^{2+}	Fe^{3+}	Total
Vsc-1	0.71	0.05	0.17	0.02	0.00	0.76	0.03	31.20	66.34	99.28
-2	1.69	0.15	0.09	0.16	0.01	0.60	0.25	31.98	64.63	99.54
-3	3.39	0.21	1.02	0.07	0.01	0.08	0.82	33.65	61.45	100.70
-4	0.57	0.09	0.02	0.02	0.00	0.09	0.09	31.73	68.40	101.01
-5	3.91	0.17	0.67	0.32	0.01	0.08	0.86	33.77	60.14	100.00
-6	0.14	0.10	0.04	0.12	0.01	0.07	0.01	31.16	68.60	100.23
-7	1.91	0.16	0.19	0.08	0.00	0.08	0.48	32.42	65.15	100.46
-8	0.31	0.09	0.02	0.01	0.01	0.06	0.42	32.34	66.64	101.12
-9	0.58	0.06	0.05	0.02	0.00	0.07	0.19	31.45	67.95	100.36
-10	5.20	0.17	0.38	0.06	0.00	0.07	1.05	34.78	58.22	99.93
-11	0.10	0.09	0.02	0.02	0.01	0.08	0.03	31.27	69.17	100.78
-12	3.60	0.20	0.79	0.05	0.00	0.08	0.81	33.42	60.42	99.37
-13	6.15	0.16	0.25	0.02	0.01	0.08	1.26	35.37	56.50	99.81
-14	5.17	0.20	0.60	0.11	0.14	0.30	1.39	34.11	57.77	99.77
-15	0.26	0.09	0.07	0.03	0.00	0.08	0.05	31.20	68.30	100.08
Avg	2.25	0.13	0.29	0.07	0.01	0.17	0.52	32.66	63.98	
Std	2.06	0.05	0.31	0.08	0.03	0.21	0.46	1.37	4.31	

Table 33: Electron microprobe data, Roolberg Felsite.

Wt% Oxide Sample#	Ti	V	Al	Cr	Mg	Si	Mn	Fe^{2+}	Fe^{3+}	Total
Dfv-2	7.51	0.04	0.85	0.01	0.01	0.08	1.54	36.29	52.84	99.14
-2	8.36	0.06	0.74	0.01	0.01	0.09	1.57	36.86	50.94	98.63
-3	9.71	0.67	1.10	0.08	0.07	0.08	0.42	39.19	47.72	99.04
-4	13.38	1.01	2.35	0.10	0.23	0.20	0.29	42.21	38.11	97.88
-5	9.49	0.07	0.84	0.00	0.01	0.09	0.93	38.64	48.75	98.82
-6	12.55	0.20	0.96	0.06	0.02	0.07	1.64	40.66	42.41	98.57
-7	8.70	0.82	2.26	1.97	0.54	0.05	0.81	37.05	45.93	98.16
-8	11.82	0.17	0.92	0.02	0.00	0.12	2.00	39.52	43.65	98.21
-9	9.51	0.77	1.50	1.58	0.80	0.04	0.40	37.71	45.83	98.13
-10	11.74	0.12	1.09	0.00	0.04	0.08	0.44	41.06	43.75	98.32
-11	9.04	0.83	1.03	0.08	0.08	0.06	0.14	38.62	48.64	98.52
Avg	10.16	0.43	1.24	0.35	0.16	0.09	0.92	38.89	46.23	
Std	1.81	0.37	0.54	0.67	0.25	0.04	0.62	1.79	3.97	

Table 34: Electron microprobe data, Pleistocene andesites, Taiwan.

Wt% Oxide Sample#	Ti	V	Al	Cr	Mg	Si	Mn	Fe^{2+}	Fe^{3+}	Total
Ta-1-1	4.58	0.49	2.72	0.06	1.55	0.05	0.74	32.53	57.46	100.18
-2	7.73	0.74	1.71	0.08	1.31	0.06	0.55	35.60	51.92	99.71
-3	6.45	0.63	2.77	0.08	1.56	0.05	0.64	34.33	53.72	100.22
-4	6.35	0.92	4.57	0.17	2.13	0.07	0.43	33.85	51.93	100.43
-5	5.30	0.63	3.25	0.09	1.57	0.07	0.50	33.44	55.30	100.15
-6	7.06	0.59	2.40	0.05	1.86	0.05	0.65	34.52	53.52	100.68
-7	5.14	0.59	3.18	0.83	1.19	0.04	0.47	33.88	55.46	100.03
-8	6.47	0.71	1.85	0.08	1.33	0.07	0.56	34.46	54.25	99.79
-9	1.93	0.60	4.72	0.07	2.59	0.05	0.73	28.95	61.09	100.74
-10	5.96	0.60	1.84	0.05	1.24	0.04	0.43	34.31	55.39	99.86
-11	9.39	0.79	2.01	0.09	2.00	0.04	0.48	36.26	48.84	99.86
-12	6.23	0.72	2.13	0.09	1.71	0.02	0.52	33.93	55.01	100.36
-13	6.21	0.76	2.19	0.11	1.27	0.05	0.50	34.35	54.13	99.55
-14	6.16	0.70	2.22	0.09	1.28	0.06	0.47	34.30	54.20	99.49
-15	7.45	0.81	2.29	0.10	1.36	0.07	0.46	35.65	52.20	100.38
-16	6.88	0.64	3.09	0.07	1.63	0.06	0.58	34.62	52.31	99.87
-17	6.02	0.59	3.01	0.07	1.98	0.06	0.59	33.43	54.63	100.37
-18	5.80	0.59	2.18	0.07	1.56	0.05	0.55	33.81	55.91	100.52
-19	5.83	0.52	2.56	0.09	2.12	0.05	0.64	32.69	55.12	99.62
-20	3.96	0.72	3.77	0.09	2.34	0.06	0.60	30.47	56.54	98.55
Avg	6.05	0.67	2.72	0.12	1.68	0.05	0.55	33.77	54.45	
Std	1.47	0.10	0.83	0.16	0.39	0.01	0.09	1.63	2.43	

Table 35: Electron microprobe data, Ovalau, Fiji andesite.

Wt.% Oxide Sample#	Ti	V	Al	Cr	Mg	Si	Mn	Fe^{2+}	Fe^{3+}	Total
Av-1-1	3.71	0.58	8.45	0.06	4.06	0.09	0.29	28.80	52.63	98.67
-2	4.14	0.58	8.97	0.54	3.89	0.10	0.37	29.85	51.42	99.85
-3	5.49	0.66	9.72	0.39	4.44	0.09	0.39	30.42	48.51	100.12
-4	6.22	0.68	7.56	0.26	4.58	0.07	0.40	30.60	50.09	100.46
-5	6.57	0.68	9.78	0.25	5.06	0.12	0.37	30.51	46.88	100.20
-6	7.57	0.66	5.93	0.29	3.37	0.09	0.50	33.06	48.30	99.58
-7	4.66	0.60	11.68	0.49	5.74	0.09	0.32	28.35	49.04	100.96
-8	4.44	0.61	10.65	0.09	5.24	0.07	0.25	28.81	50.80	100.95
-9	5.37	0.57	6.92	0.14	4.42	0.10	0.40	29.76	52.09	99.77
-10	4.02	0.57	6.97	0.20	3.02	0.09	0.40	30.64	53.75	99.67
-11	5.31	0.60	9.72	0.41	5.53	0.08	0.35	28.83	49.92	100.76
-12	6.16	0.63	8.27	0.17	4.32	0.10	0.42	30.84	48.88	99.79
-13	5.41	0.60	9.41	0.53	4.91	0.09	0.35	29.71	49.35	100.36
-14	7.59	0.69	6.93	0.15	3.64	0.09	0.49	32.83	47.15	99.55
-15	6.05	0.61	6.63	0.16	4.56	0.09	0.39	29.88	50.62	99.49
-16	7.83	0.66	6.08	0.18	4.32	0.11	0.45	31.83	47.90	99.35
-17	4.38	0.64	11.34	0.07	4.65	0.08	0.26	29.38	48.99	99.80
-18	5.62	0.56	6.78	0.14	4.05	0.09	0.43	30.46	51.50	99.62
-19	7.58	0.68	5.74	0.12	3.49	0.08	0.36	32.34	47.12	97.52
-20	7.01	0.68	5.84	0.14	2.71	0.08	0.50	33.65	49.34	99.96
Avg	5.76	0.63	8.17	0.24	4.30	0.09	0.38	30.53	49.71	
Std	1.27	0.04	1.85	0.15	0.78	0.01	0.07	1.48	1.85	

Table 36: Electron microprobe data, Nevado de Toluca andesite.

Wt% Oxide Sample#	Ti	V	Al	Cr	Mg	Si	Mn	Fe^{2+}	Fe^{3+}	Total
Tm-1-1	7.58	0.76	3.04	0.12	1.22	0.07	0.34	36.04	50.51	99.68
-2	7.58	0.43	3.51	0.16	1.74	0.20	0.50	35.58	51.15	100.85
-3	7.34	0.69	2.99	0.19	1.18	0.20	0.37	35.79	50.83	99.58
-4	8.00	0.63	2.84	0.23	1.11	0.10	0.28	36.73	49.99	99.91
-5	7.30	0.72	2.97	0.17	1.16	0.16	0.39	35.50	50.37	98.74
-6	7.93	0.74	3.20	0.21	1.25	0.30	0.36	36.27	49.45	99.71
-7	7.43	0.44	3.36	0.16	1.76	0.23	0.38	35.26	51.26	100.28
-8	7.70	0.72	3.11	0.16	1.22	0.33	0.40	36.33	50.67	100.64
Avg	7.61	0.64	3.13	0.18	1.33	0.20	0.38	35.94	50.53	
Std	0.24	0.12	0.21	0.03	0.25	0.08	0.06	0.46	0.56	

Table 37: Electron microprobe data, Nevado de Toluca andesite, Mexico.

Wt% Oxide Sample#	Ti	V	Al	Cr	Mg	Si	Mn	Fe^{2+}	Fe^{3+}	Total
Tm-2-1	5.09	0.37	2.19	0.09	1.35	0.05	0.43	33.27	56.42	99.25
-2	5.25	0.37	1.53	0.10	0.99	0.05	0.31	33.16	56.68	99.25
-3	7.71	0.78	2.37	0.22	1.03	0.03	0.34	35.93	49.94	98.33
-4	6.12	0.14	2.82	0.02	1.03	0.07	0.26	35.26	54.15	99.88
-5	6.31	0.67	3.17	0.31	2.14	0.07	0.36	33.42	53.05	99.50
-6	7.57	0.79	2.06	0.30	0.53	0.05	0.37	36.89	51.15	99.72
-7	7.57	0.72	2.10	0.16	0.73	0.07	0.35	36.39	50.84	98.93
-8	8.44	0.59	2.55	0.10	1.27	0.06	0.30	36.65	49.34	99.30
-9	7.08	0.62	2.55	0.21	1.11	0.06	0.31	35.57	51.66	99.16
-10	5.28	0.31	4.25	0.09	2.57	0.07	0.36	32.26	54.86	100.03
-11	5.05	0.37	2.35	0.10	1.24	0.05	0.37	33.79	56.90	100.21
-12	7.78	0.73	2.32	0.27	0.80	0.06	0.30	35.99	48.81	97.06
-13	13.73	0.62	3.50	0.11	4.04	0.07	0.39	37.48	39.70	99.63
Avg	7.15	0.54	2.60	0.16	1.45	0.06	0.34	35.08	51.81	
Std	2.21	0.20	0.68	0.09	0.92	0.01	0.04	1.63	4.42	

Table 38: Electron microprobe data, Bushveld Complex.

Wt% Oxide Sample#	Ti	V	Al	Cr	Mg	Si	Mn	Fe^{2+}	Fe^{3+}	Total
Vu-1-1	8.21	1.36	1.32	0.06	0.07	0.04	0.19	37.89	49.98	99.13
-2	10.98	1.49	3.21	0.05	0.21	0.03	0.29	40.37	42.24	98.87
-3	9.21	1.33	1.85	0.04	0.51	0.03	0.23	38.16	47.59	98.95
-4	13.48	0.56	7.11	0.01	0.19	0.10	0.39	42.65	31.35	95.82
-5	7.12	0.16	1.09	0.00	0.01	0.04	0.36	36.92	52.72	98.41
-6	16.54	0.95	4.14	0.03	0.17	0.11	0.48	45.33	29.86	97.60
-7	13.61	1.65	3.10	0.05	0.47	0.04	0.30	41.95	36.49	97.65
-8	10.25	1.45	2.45	0.03	0.03	0.03	0.28	39.55	43.79	97.85
-9	13.69	0.93	3.03	0.03	0.36	0.03	0.34	42.27	36.79	97.47
-10	10.18	1.40	1.96	0.08	0.02	0.03	0.36	39.27	44.30	97.59
-11	17.12	1.00	3.01	0.02	0.67	0.05	0.34	46.22	32.97	101.40
-12	13.71	1.96	2.80	0.06	0.93	0.03	0.30	41.54	37.46	98.79
-13	17.23	1.59	1.28	0.04	0.32	0.51	0.32	44.99	31.06	97.34
-14	6.16	1.79	1.08	0.05	0.07	0.11	0.25	35.65	53.68	98.84
-15	10.89	1.43	3.54	0.02	0.50	0.03	0.27	39.88	42.14	98.71
-16	11.55	1.54	2.06	0.11	0.40	0.03	0.25	40.52	42.70	99.14
-17	13.50	1.75	2.93	0.05	0.63	0.04	0.30	41.83	37.58	98.61
-18	14.69	1.74	3.08	0.06	1.34	0.05	0.35	41.88	35.59	98.76
-19	11.96	1.72	3.50	0.04	0.19	0.04	0.29	40.92	39.02	97.67
Avg	12.11	1.36	2.76	0.04	0.37	0.07	0.31	40.94	40.39	
Std	3.10	0.44	1.35	0.02	0.34	0.11	0.06	2.70	6.94	

Table 39: Electron microprobe data, Bushveld Complex.

Wt% Oxide Sample#	Ti	V	Al	Cr	Mg	Si	Mn	Fe^{2+}	Fe^{3+}	Total
Vu-2-1	15.25	2.10	3.87	0.13	0.78	0.10	0.33	43.31	32.95	98.82
-2	7.59	1.80	2.68	0.13	0.10	0.16	0.10	37.45	49.18	99.19
-3	11.90	2.34	3.53	0.11	0.31	0.16	0.19	41.36	40.38	100.28
-4	13.23	2.82	3.46	0.20	0.68	0.46	0.31	41.26	36.59	99.01
-5	16.82	1.95	3.88	0.11	0.55	0.18	0.29	45.07	29.58	98.43
-6	14.27	1.95	3.96	0.11	0.55	0.27	0.26	43.23	35.49	100.09
-7	13.00	2.07	2.80	0.40	1.21	0.52	0.29	40.40	38.47	99.16
-8	16.08	2.32	3.11	0.17	0.73	0.16	0.45	43.31	30.85	97.18
-9	9.86	1.82	3.05	0.06	0.06	0.29	0.30	39.60	44.68	99.78
-10	16.97	2.09	3.93	0.09	0.70	0.20	0.37	45.27	30.16	99.78
Avg	13.50	2.13	3.43	0.15	0.57	0.25	0.29	42.03	36.83	
Std	2.91	0.29	0.46	0.09	0.33	0.13	0.09	2.35	6.16	

Table 40: Electron microprobe data, Bushveld Complex.

Wt% Oxide Sample#	Ti	V	Al	Cr	Mg	Si	Mn	Fe^{2+}	Fe^{3+}	Total
Sr-1-1	7.32	1.53	1.22	0.10	0.00	0.32	0.23	36.95	51.38	99.05
-2	23.08	0.26	4.13	0.00	0.16	0.38	0.71	51.74	18.51	98.97
-3	5.55	0.13	1.64	0.02	0.03	0.13	0.20	36.31	56.50	100.51
-4	5.96	0.87	4.07	0.05	0.81	0.32	0.23	35.66	52.74	100.71
-5	16.70	1.13	4.09	0.23	0.71	0.07	0.39	44.89	30.06	98.27
-6	14.50	1.08	4.60	0.03	0.18	0.00	0.46	43.87	34.07	98.79
-7	11.20	1.50	4.48	0.09	0.99	0.01	0.31	39.79	41.18	99.55
-8	11.25	1.07	3.71	0.07	0.34	0.00	0.38	40.52	41.42	98.76
-9	15.46	1.31	4.74	0.04	0.32	0.02	0.38	44.45	31.65	98.37
-10	13.11	0.98	4.12	0.02	0.05	0.04	0.45	43.01	37.93	99.71
-11	17.09	0.88	2.23	0.00	0.02	0.02	0.48	46.62	32.98	100.32
-12	15.63	1.20	2.14	0.16	0.05	0.16	0.33	44.87	34.67	99.21
-13	14.36	1.34	3.57	0.06	0.27	0.60	0.53	43.56	36.02	100.31
-14	11.79	0.21	4.29	0.00	0.18	0.00	0.36	41.77	40.52	99.12
Avg	13.07	0.96	3.50	0.06	0.29	0.15	0.39	42.43	38.55	
Std	4.58	0.44	1.13	0.06	0.31	0.18	0.13	4.21	9.64	

Table 41: Electron microprobe data, Duluth Gabbro.

Wt% Oxide Sample#	Ti	V	Al	Cr	Mg	Si	Mn	Fe^{2+}	Fe^{3+}	Total
Dg-2-1	16.20	2.55	3.17	0.06	0.42	0.07	0.40	44.44	31.56	98.87
-2	7.57	1.50	3.39	0.07	0.37	0.46	0.42	37.30	49.60	100.76
-3	12.48	1.01	3.67	0.05	0.64	0.08	0.38	41.29	39.48	99.08
-4	13.39	1.57	2.64	0.04	0.09	0.10	0.56	42.03	37.33	97.75
-5	0.00	0.24	0.80	0.02	0.00	0.04	0.11	31.23	68.40	100.84
-6	11.90	3.05	3.65	0.16	0.58	0.01	0.38	40.13	38.90	98.76
-7	15.13	1.50	2.93	0.06	0.13	0.27	0.50	43.88	34.05	98.45
-8	14.58	0.91	4.72	0.02	0.47	0.06	0.44	43.76	34.43	99.39
-9	15.39	1.17	1.77	0.07	0.00	0.13	0.66	44.45	35.91	99.55
-10	15.75	1.20	3.20	0.06	0.41	0.05	0.50	44.60	33.85	99.62
Avg	12.24	1.47	2.99	0.06	0.31	0.13	0.44	41.31	40.35	
Std	4.74	0.77	1.03	0.04	0.22	0.13	0.14	4.03	10.48	

Table 42: Electron microprobe data, Duluth Gabbro.

Wt% Oxide Sample#	Ti	V	Al	Cr	Mg	Si	Mn	Fe^{2+}	Fe^{3+}	Total
Dg-3-1	7.30	1.35	3.19	0.03	0.45	0.04	0.28	36.42	49.17	98.22
-2	6.45	1.62	3.07	0.05	0.43	0.23	0.35	35.16	50.01	97.37
-3	6.56	1.15	3.52	0.04	0.39	0.03	0.27	36.11	50.63	98.69
-4	7.23	1.24	3.34	0.04	0.38	0.04	0.26	36.40	48.82	97.75
-5	5.95	1.48	2.21	0.05	0.32	0.05	0.34	35.32	53.25	98.96
-6	5.99	2.32	2.42	0.06	0.19	0.04	0.43	35.55	51.84	98.84
-7	6.83	1.07	2.97	0.04	0.39	0.03	0.23	35.74	49.49	96.76
-8	6.28	1.20	3.45	0.03	0.55	0.04	0.24	34.98	49.94	96.71
-9	10.91	2.22	4.16	0.05	0.62	0.03	0.26	39.27	40.15	97.68
-10	6.72	1.40	2.64	0.04	0.35	0.03	0.28	35.71	50.38	97.55
-11	5.79	1.05	3.38	0.04	0.50	0.04	0.20	35.54	52.96	99.49
-12	5.45	1.83	3.16	0.06	0.15	0.06	0.36	35.40	53.30	99.77
-13	0.02	0.01	0.02	0.00	0.00	0.83	0.01	31.01	68.85	100.74
-14	12.31	0.61	1.60	0.01	0.15	0.07	0.26	41.76	42.28	99.04
-15	6.32	2.89	0.96	0.07	0.07	0.04	0.53	35.25	52.99	99.11
-16	6.55	3.36	0.78	0.10	0.02	0.04	0.73	35.41	52.89	99.89
-17	12.50	1.13	1.31	0.02	0.11	0.36	0.25	41.61	41.46	98.73
Avg	7.01	1.53	2.48	0.04	0.30	0.12	0.31	36.27	50.49	
Std	2.77	0.79	1.12	0.02	0.19	0.20	0.15	2.47	6.11	

Table 43: Electron microprobe data, Duluth Gabbro.

Wt% Oxide Sample#	Ti	V	Al	Cr	Mg	Si	Mn	Fe^{2+}	Fe^{3+}	Total
Dg-4-1	15.54	0.36	0.72	0.00	0.10	0.10	0.35	44.88	37.70	99.75
-2	11.81	1.09	3.07	0.07	0.55	0.05	0.34	41.29	42.64	100.91
-3	12.80	1.11	3.05	0.09	0.31	0.30	0.29	42.26	39.77	99.98
-4	14.74	1.82	2.51	0.08	0.21	0.23	0.42	43.81	36.21	100.03
-5	14.63	1.75	1.20	0.06	0.00	0.29	0.36	43.87	37.90	100.06
-6	0.00	0.00	0.61	0.02	0.07	0.13	0.07	31.20	68.80	100.90
-7	12.96	1.51	1.59	0.11	0.38	0.27	0.47	41.85	41.18	100.32
-8	12.44	1.37	3.57	0.28	0.43	0.04	0.45	41.82	40.05	100.45
Avg	11.87	1.13	2.04	0.09	0.26	0.18	0.34	41.37	43.03	
Std	4.64	0.61	1.08	0.08	0.18	0.10	0.12	4.02	9.93	

Table 44: Electron microprobe data, Keweenawan basalt.

Wt% Oxide Sample#	Ti	V	Al	Cr	Mg	Si	Mn	Fe^{2+}	Fe^{3+}	Total
Kb-2-1	9.19	0.52	4.03	16.46	4.09	0.02	0.43	33.43	31.10	99.26
-2	16.79	0.98	1.75	0.10	0.34	0.06	0.39	45.80	34.05	100.27
-3	0.14	1.00	0.53	0.13	0.04	0.03	0.02	30.78	67.12	99.79
-4	12.65	0.86	1.15	0.09	0.08	0.06	0.33	42.07	42.08	99.37
-5	11.60	1.16	3.46	0.29	0.94	0.04	0.34	39.93	41.17	99.09
-6	18.62	1.17	1.78	0.41	0.28	0.08	0.40	46.64	28.00	97.38
-7	15.10	0.92	1.38	0.10	0.13	0.17	0.44	44.24	37.22	99.69
-8	0.01	0.11	0.09	0.03	0.00	0.02	0.02	31.20	69.22	100.69
-9	0.07	0.08	0.02	0.00	0.00	0.47	0.01	31.00	68.87	100.38
-10	15.10	1.00	2.62	0.10	0.72	3.05	0.70	41.66	32.47	97.42
-11	17.89	1.57	1.42	0.17	0.16	0.06	0.33	46.66	31.20	99.46
-12	11.04	0.63	1.65	0.06	0.07	0.06	0.27	41.06	45.40	100.25
-13	18.69	0.98	1.70	0.15	0.05	0.07	0.48	47.32	28.96	98.40
-14	0.00	0.01	0.00	0.00	0.00	0.11	0.01	31.12	69.19	100.43
-15	14.45	0.91	2.09	0.13	0.27	0.05	0.35	43.62	37.65	99.51
-16	16.86	0.86	1.48	0.40	0.03	0.38	5.85	39.42	30.79	96.07
-17	0.07	0.26	0.17	0.10	0.00	0.01	0.05	31.35	69.17	101.18
-18	6.85	1.07	1.82	0.13	0.30	0.09	0.20	36.53	52.46	99.45
-19	15.01	0.61	1.13	0.04	0.07	0.09	0.32	44.04	37.10	98.41
-20	16.62	0.59	1.19	0.06	0.11	0.07	0.32	45.59	34.10	98.65
Avg	10.84	0.76	1.47	0.95	0.38	0.25	0.56	39.67	44.37	
Std	6.88	0.40	1.04	3.56	0.88	0.65	1.23	5.97	15.15	

Table 45: Electron micrprobe data, Haimaey Island basalt.

Wt% Oxide Sample#	Ti	V	Al	Cr	Mg	Si	Mn	Fe^{2+}	Fe^{3+}	Total
IL76-1	0.00	0.00	0.66	4.86	0.61	0.16	0.16	30.20	63.77	100.42
-2	18.35	1.04	6.75	0.11	4.26	0.25	0.54	41.45	26.28	98.93
-3	18.50	0.96	7.39	0.04	4.54	0.20	0.51	41.88	26.65	100.67
-4	0.00	0.27	0.76	0.06	0.01	0.10	1.30	29.90	68.17	100.57
-5	5.83	1.00	2.50	0.04	1.41	0.18	0.59	33.99	55.21	100.75
-6	0.21	0.00	0.67	0.02	0.09	2.49	0.23	29.96	65.57	99.24
-7	20.05	1.04	5.79	0.02	4.54	0.22	0.52	42.77	25.00	99.95
-8	6.84	0.91	2.57	0.10	1.07	0.12	0.58	35.26	52.46	99.91
-9	0.05	0.59	0.94	0.21	0.09	0.09	0.06	30.96	67.43	100.42
-10	0.00	0.00	0.62	0.03	1.14	1.55	0.09	28.82	67.78	100.03
-11	0.00	0.16	0.83	0.08	0.00	0.15	0.12	30.89	67.55	99.78
-12	17.46	1.02	7.09	1.28	4.29	0.27	0.45	41.10	27.13	100.09
-13	7.57	1.05	2.34	0.06	1.30	0.26	0.52	35.80	51.91	100.81
-14	0.02	0.56	0.79	0.86	0.03	0.08	0.09	30.66	66.26	99.35
-15	0.00	0.55	0.64	0.08	0.00	0.25	0.07	30.69	67.30	99.58
-16	0.00	0.27	0.76	0.00	0.00	0.22	0.12	30.61	67.11	99.09
-17	0.00	0.00	0.79	0.02	0.00	0.13	0.18	30.75	67.51	99.38
-18	20.22	0.52	6.41	0.00	3.95	0.26	0.53	44.22	24.26	100.37
-19	0.00	0.52	0.80	0.05	0.00	0.16	0.11	30.58	66.91	99.13
-20	0.00	0.63	0.68	0.06	0.01	0.11	0.09	30.67	67.29	99.54
Avg	5.76	0.55	2.49	0.40	1.37	0.36	0.34	34.06	54.58	
Std	7.97	0.39	2.51	1.07	1.77	0.58	0.30	5.07	17.28	

Table 46: Electron microprobe data, Reykjanes Peninsula, Iceland, basalt.

Wt% Oxide Sample#	Ti	V	Al	Cr	Mg	Si	Mn	Fe^{2+}	Fe^{3+}	Total
IL85-1	17.49	1.02	2.48	0.00	0.79	0.24	0.48	45.58	31.73	99.81
-2	14.24	1.02	2.44	0.05	1.17	0.80	0.75	38.11	41.65	100.23
-3	0.00	0.54	0.78	0.13	0.04	0.05	0.10	30.52	66.86	99.02
-4	21.78	1.07	2.35	0.02	0.20	0.25	0.48	50.62	23.62	100.39
-5	0.00	0.52	0.98	0.03	0.00	0.12	0.14	30.52	66.59	98.90
-6	0.00	1.28	0.66	4.35	0.00	0.31	0.16	30.66	62.92	100.34
-7	24.62	1.30	2.45	0.08	0.43	0.23	0.48	52.70	17.58	99.87
-8	24.57	1.34	2.31	0.04	0.77	0.25	0.54	52.15	18.31	100.28
-9	0.04	0.57	0.75	0.04	0.00	0.17	0.04	30.62	66.79	99.02
-10	24.09	1.23	2.24	0.07	0.47	0.27	0.53	52.27	19.35	100.52
-11	18.01	0.80	2.17	0.10	1.16	0.23	0.60	45.61	31.82	100.50
-12	19.99	0.93	2.44	0.02	0.88	0.22	0.47	47.88	27.22	100.05
-13	0.00	0.93	0.86	0.05	0.00	0.21	0.07	30.47	66.48	99.07
-14	0.02	1.20	0.96	0.11	0.09	0.10	0.12	30.43	66.57	99.60
-15	0.02	0.17	0.94	0.04	0.03	0.14	0.13	30.39	66.37	98.23
-16	18.61	0.86	2.63	0.04	0.76	0.18	0.71	46.58	29.59	99.96
-17	21.79	1.13	2.13	0.36	0.72	0.23	0.38	49.98	23.97	100.69
-18	0.00	0.42	0.85	0.04	0.00	0.20	0.17	30.53	66.87	99.08
-19	22.77	1.11	2.38	0.04	1.27	0.14	0.59	50.01	22.73	101.04
-20	20.21	0.80	2.42	0.00	0.37	0.34	0.68	48.42	26.05	99.29
Avg	12.41	0.91	1.76	0.28	0.46	0.23	0.38	41.20	42.15	
Std	10.40	0.32	0.76	0.44	0.15	0.15	0.23	9.23	20.29	

Table 47: Electron microprobe data, Maui basalt.

Wt% Oxide Sample#	Ti	V	Al	Cr	Mg	Si	Mn	Fe^{2+}	Fe^{3+}	Total
M-7-1	0.00	0.50	0.59	0.02	0.00	0.00	0.09	30.78	67.68	99.66
-2	6.55	0.69	2.71	0.04	2.10	0.05	0.59	33.72	54.13	100.58
-3	0.60	0.65	0.59	1.41	0.03	0.05	0.01	31.05	64.35	98.74
-4	28.04	0.83	0.70	0.01	1.07	0.05	0.22	54.19	11.98	97.09
-5	0.02	0.61	0.64	0.32	0.04	0.34	0.02	30.70	67.02	99.71
-6	24.68	1.43	1.49	0.05	1.79	0.14	1.00	49.22	17.70	97.50
-7	15.25	0.22	5.32	0.00	4.33	0.25	0.59	38.56	34.90	99.42
-8	25.99	1.18	2.10	0.20	1.53	0.11	0.55	51.74	14.91	98.31
-9	16.19	0.27	4.24	0.58	4.13	0.52	0.55	39.18	32.73	98.39
-10	0.02	0.00	0.30	0.70	1.54	1.42	0.16	27.98	67.38	99.50
-11	18.49	0.69	4.70	0.05	4.34	0.13	0.63	41.53	29.60	100.16
-12	15.66	0.30	5.11	0.00	4.25	0.06	0.52	39.37	34.91	100.18
-13	26.02	0.88	2.46	0.06	1.65	0.42	0.61	51.59	14.66	98.35
-14	19.93	0.75	5.22	0.00	3.17	0.17	0.50	44.51	24.77	99.02
-15	13.34	0.61	10.15	2.40	5.54	0.07	0.40	36.01	31.06	99.58
-16	15.99	0.71	9.14	0.18	5.23	0.07	0.52	38.61	29.15	99.60
-17	14.48	0.64	8.20	0.09	5.61	0.05	0.32	36.25	32.76	98.40
-18	15.42	0.56	8.43	0.64	6.32	0.03	0.32	36.19	31.32	99.23
-19	18.61	0.57	6.93	0.00	5.02	0.06	0.45	40.85	26.47	98.96
Avg	14.49	0.64	4.16	0.36	3.04	0.21	0.42	39.58	36.18	
Std	8.91	0.32	3.14	0.60	2.03	0.32	0.24	7.48	18.16	

Table 48: Electron microprobe data, Hawaii Island basalt.

Wt% Oxide Sample#	Ti	V	Al	Cr	Mg	Si	Mn	Fe^{2+}	Fe^{3+}	Total
B-5-1	15.69	0.32	5.92	0.02	4.38	0.07	0.50	39.28	33.94	100.12
-2	15.67	0.37	6.30	0.00	4.68	0.01	0.45	38.93	33.46	99.87
-3	18.84	0.39	5.25	0.00	4.48	0.12	0.56	41.92	28.66	100.22
-4	16.65	0.35	5.98	0.02	4.61	0.09	0.56	39.53	31.38	99.17
-5	15.49	0.38	6.15	0.00	4.31	0.04	0.55	39.19	34.02	100.13
-6	17.38	0.38	6.02	0.03	3.98	0.08	0.55	41.36	30.18	99.96
-7	17.90	0.42	4.00	0.00	4.02	0.00	1.03	40.83	31.54	99.74
-8	16.20	0.47	5.98	0.00	4.48	0.02	0.47	39.84	33.14	100.58
-9	16.18	0.32	6.08	0.02	5.25	0.05	0.45	38.58	33.06	99.99
-10	15.47	0.30	5.95	0.03	4.41	0.04	0.48	38.93	33.78	99.39
-11	15.71	0.25	6.09	0.00	4.43	0.02	0.50	39.37	33.86	100.23
-12	15.23	0.27	6.34	0.05	4.36	0.16	0.40	39.09	33.94	99.84
-13	16.84	0.37	5.89	0.00	4.12	0.00	0.50	40.56	30.98	99.26
-14	17.30	0.41	6.15	0.00	4.45	0.03	0.56	40.81	30.82	100.53
-15	16.14	0.32	5.84	0.00	4.46	0.09	0.42	39.26	32.26	98.79
Avg	16.45	0.35	3.11	0.01	4.43	0.05	0.53	39.83	32.33	
Std	1.00	0.06	0.55	0.02	0.29	0.04	0.14	0.98	1.61	

Table 49: Electron microprobe data, Hawaii Island basalt.

Wt% Oxide Sample#	Ti	V	Al	Cr	Mg	Si	Mn	Fe^{2+}	Fe^{3+}	Total
HBb-1	20.31	1.39	1.38	0.19	0.21	0.13	0.35	48.90	26.75	99.61
-2	13.17	2.16	0.47	0.01	0.00	4.04	0.07	41.43	38.84	100.19
-3	16.43	1.29	1.47	0.14	0.00	0.14	0.40	45.12	33.05	98.04
-4	6.61	0.86	2.70	0.20	0.90	0.09	0.68	35.51	53.17	100.72
-5	0.00	0.66	0.12	0.70	0.00	0.05	0.05	30.71	67.45	99.74
-6	0.00	0.59	0.19	0.34	0.00	0.11	0.09	31.04	68.55	100.91
-7	0.00	0.46	0.21	0.06	0.00	0.15	0.18	30.87	68.63	100.56
-8	0.00	0.64	0.16	0.27	0.00	0.05	0.15	30.96	68.63	100.86
-9	5.44	0.75	2.48	0.04	0.71	0.11	0.75	34.18	54.80	99.26
-10	20.17	0.59	1.43	0.01	0.00	0.32	0.50	49.10	27.39	99.51
-11	16.38	1.13	2.17	0.12	4.68	0.13	0.32	38.79	36.48	100.20
-12	16.23	2.69	1.39	1.32	1.46	0.14	0.45	42.42	32.65	98.75
-13	0.04	0.88	0.51	0.21	0.00	0.07	0.09	30.84	67.58	100.22
-14	5.26	0.64	3.57	0.18	0.00	0.00	0.54	35.85	54.10	100.14
-15	19.96	1.08	1.25	0.08	0.00	0.10	0.49	40.03	28.26	100.25
-16	0.00	0.00	0.69	0.13	0.00	0.79	0.16	30.92	67.88	100.57
-17	21.07	1.42	2.99	1.32	2.47	0.09	0.38	46.77	24.30	100.81
Avg	9.47	1.01	1.05	0.31	0.61	0.38	0.33	37.85	48.15	
Std	8.44	0.63	1.05	0.40	1.21	0.93	0.21	6.57	17.22	

Table 50: Electron microprobe data, Marcy-type meta-anorthosite.

Wt% Oxide Sample#	Ti	V	Al	Cr	Mg	Si	Mn	Fe2+	Fe3+	Total
pCma-3	0.05	0.57	0.37	0.14	0.04	0.01	0.00	31.02	68.15	100.35
-2	0.07	0.35	0.27	0.15	0.02	0.03	0.00	31.19	68.56	100.64
-3	0.04	0.15	0.29	0.06	0.02	0.05	0.00	31.31	69.02	100.93
-4	0.06	1.16	0.32	0.05	0.06	0.03	0.00	30.81	67.93	100.41
-5	0.07	1.17	0.33	0.25	0.04	0.01	0.00	30.77	68.03	100.67
-6	0.10	0.11	0.28	0.01	0.01	0.02	0.00	31.04	68.20	99.76
-7	0.05	0.32	0.32	0.15	0.03	0.01	0.01	31.16	68.53	100.59
-8	0.04	0.14	0.18	0.01	0.03	0.03	0.00	31.02	68.62	100.07
-9	0.08	0.11	0.46	0.01	0.05	0.03	0.02	30.88	67.84	99.48
-10	0.09	0.13	0.41	0.02	0.04	0.01	0.03	31.18	68.53	100.44
-11	0.13	0.41	0.36	0.07	0.03	0.01	0.00	31.17	68.26	100.43
-12	0.01	0.51	0.43	0.30	0.05	0.01	0.01	31.07	67.90	100.31
-13	0.07	0.44	0.29	0.16	0.05	0.02	0.00	30.92	68.05	100.00
-14	0.06	1.05	0.25	0.03	0.02	0.03	0.01	30.98	68.33	100.76
-15	0.01	0.32	0.19	0.02	0.01	0.01	0.01	31.10	68.83	100.49
-16	0.05	0.15	0.19	0.03	0.03	0.02	0.01	31.01	68.54	100.03
-17	0.08	1.02	0.25	0.02	0.03	0.02	0.01	30.93	68.19	100.54
-18	0.06	0.80	0.25	0.44	0.03	0.02	0.00	30.95	67.90	100.45
Avg	0.06	0.49	0.30	0.11	0.03	0.02	0.01	31.03	68.30	
Std	0.03	0.37	0.08	0.12	0.01	0.01	0.01	0.14	0.33	

Table 51: Electron microprobe data, Whiteface-type meta-anorthosite.

Wt% Oxide Sample#	Ti	V	Al	Cr	Mg	Si	Mn	Fe^{2+}	Fe^{3+}	Total
pCwa-1	0.06	0.01	0.11	0.00	0.00	0.02	0.04	31.33	69.34	100.89
-2	0.05	0.08	0.43	0.03	0.04	0.01	0.08	31.17	68.70	100.60
-3	0.01	0.13	0.09	0.03	0.00	0.02	0.00	31.17	69.11	100.55
-4	0.03	0.06	0.27	0.01	0.01	0.01	0.08	31.15	68.94	100.56
-5	0.03	0.07	0.14	0.02	0.01	0.02	0.05	31.08	68.90	100.34
-6	0.01	0.08	0.12	0.01	0.02	0.01	0.05	31.01	68.92	100.23
-7	0.37	0.09	0.28	0.00	0.08	0.02	0.06	31.58	68.71	101.19
-8	0.02	0.05	0.04	0.00	0.00	0.01	0.02	31.30	69.48	100.88
-9	0.06	0.08	0.33	0.02	0.02	0.03	0.11	31.27	69.08	100.99
-10	0.00	0.01	0.01	0.01	0.00	0.01	0.02	31.40	69.84	101.31
-11	0.07	0.01	0.10	0.01	0.00	0.01	0.05	31.25	69.16	100.66
-12	0.25	0.08	0.67	0.02	0.03	0.01	0.10	31.30	67.84	100.28
-13	0.46	0.10	0.56	0.01	0.06	0.04	0.20	31.17	67.26	99.86
-14	0.01	0.00	0.09	0.01	0.00	0.01	0.02	31.26	69.36	100.75
-15	0.02	0.00	0.04	0.01	0.00	0.00	0.03	31.13	69.16	100.39
-16	1.07	0.02	0.30	0.01	0.06	0.05	0.06	32.15	67.10	100.80
-17	0.05	0.06	0.14	0.01	0.00	0.02	0.03	30.98	68.51	99.80
-18	0.02	0.08	0.18	0.03	0.00	0.01	0.01	30.97	68.51	99.81
-19	0.36	0.12	0.60	0.01	0.01	0.10	0.01	31.51	67.72	100.42
-20	0.01	0.60	0.06	0.01	0.00	0.03	0.00	31.42	69.71	101.28
Avg	0.15	0.09	0.23	0.01	0.02	0.02	0.05	31.28	68.77	
Std	0.25	0.12	0.19	0.01	0.02	0.02	0.05	0.26	0.74	

Table 52: Electron microprobe data, Loma de Hierro Ultramafic Complex.

Wt% Oxide Sample#	Ti	V	Al	Cr	Mg	Si	Mn	Fe^{2+}	Fe^{3+}	Total
PC1057	0.06	0.78	0.14	0.42	0.01	0.01	0.02	30.94	67.96	100.35
-2	0.16	0.58	0.82	0.61	0.03	0.01	0.04	31.13	66.85	100.22
-3	0.25	0.54	0.32	0.06	0.01	0.02	0.05	31.18	67.88	100.30
-4	4.09	0.77	3.84	0.26	1.55	0.06	0.22	32.57	56.40	99.75
-5	0.03	0.83	0.15	0.18	0.03	0.02	0.05	30.87	68.32	100.45
-6	0.07	0.57	0.18	0.06	0.01	0.03	0.05	31.26	69.02	101.24
-7	5.70	0.71	4.26	0.32	1.50	0.01	0.32	33.75	51.91	98.50
-8	0.18	0.87	1.69	0.21	0.04	0.03	0.02	31.26	66.09	100.38
-9	0.03	0.74	0.17	0.11	0.01	0.03	0.03	31.07	68.66	100.86
-10	0.05	0.74	0.19	0.20	0.00	0.03	0.05	30.89	68.06	100.19
-11	0.18	0.00	0.01	0.03	0.04	0.56	0.03	31.18	68.76	100.78
-12	0.20	0.01	0.18	0.00	0.04	0.01	0.10	30.98	68.15	99.68
-13	4.34	0.81	4.39	0.46	0.51	0.01	0.50	34.19	54.45	99.66
-14	0.06	0.88	0.22	0.18	0.00	0.01	0.02	30.88	67.96	100.22
-15	0.08	0.55	0.17	0.06	0.01	0.03	0.04	30.96	68.30	100.20
-16	0.15	0.76	0.03	0.10	0.01	0.01	0.03	31.13	68.53	100.74
-17	1.33	0.11	2.20	12.76	1.85	0.01	0.76	29.14	51.65	99.83
-18	4.19	0.59	1.33	0.44	0.18	0.51	0.39	34.10	58.10	99.84
-19	0.00	0.00	0.00	0.48	0.44	1.14	0.03	30.19	68.44	100.73
-20	0.12	0.33	0.14	0.06	0.00	0.02	0.03	30.90	68.01	99.60
-21	0.07	0.78	0.17	0.29	0.02	0.01	0.04	31.00	68.22	100.61
Avg	1.02	0.57	0.98	0.82	0.30	0.12	0.13	31.41	64.84	
Std	1.77	0.29	1.42	2.67	0.57	0.27	0.19	1.21	5.94	

Table 53: Electron microprobe data, Levis Hills Ophiolite Complex, serpentinized ultramafics.

Wt% Oxide Sample#	Ti	V	Al	Cr	Mg	Si	Mn	Fe^{2+}	Fe^{3+}	Total
MPao-1	0.04	0.02	0.01	0.03	0.19	0.04	0.49	30.20	68.79	99.82
-2	0.01	0.07	0.12	0.01	0.04	0.23	0.00	30.75	68.28	99.50
-3	0.00	0.20	0.05	0.05	0.02	0.02	0.04	30.97	68.85	100.21
-4	0.01	0.01	0.00	0.02	0.33	0.78	0.05	29.88	67.81	98.90
-5	0.01	1.01	0.03	0.12	0.00	0.01	0.04	30.89	68.55	100.67
-6	0.03	0.06	0.02	0.02	0.01	0.02	0.03	31.12	69.11	100.42
-7	0.32	0.25	1.90	16.22	1.62	0.01	0.28	29.19	50.62	100.41
-8	0.01	0.08	0.07	0.01	0.01	0.01	0.04	31.07	69.01	100.30
-9	0.11	0.08	0.05	0.10	0.01	0.02	0.02	31.22	69.54	100.42
-10	0.57	0.05	0.01	0.01	0.53	0.04	0.10	30.80	68.49	100.59
-11	0.01	0.01	0.01	0.00	0.00	0.05	0.02	30.80	68.46	99.37
-12	0.01	0.00	0.00	0.01	0.50	0.04	0.09	30.26	69.39	100.29
-13	0.01	0.33	0.07	0.05	0.01	0.01	0.05	31.19	69.26	100.98
-14	0.01	0.01	0.01	0.02	0.87	1.20	1.37	28.02	68.72	100.23
-15	0.24	0.01	0.09	0.01	0.55	2.28	0.20	29.72	67.59	100.68
-16	0.34	0.02	0.02	0.00	0.94	0.72	0.16	29.63	68.47	100.33
-17	0.07	0.00	0.01	0.02	0.57	0.22	0.38	29.79	69.03	100.08
-18	0.04	0.01	0.01	0.01	0.58	0.22	0.38	29.91	69.49	100.64
-19	0.43	0.18	0.03	0.21	0.01	0.01	0.02	31.38	67.86	100.12
Avg	0.12	0.13	0.13	0.89	0.36	0.31	0.20	30.36	67.75	
Std	0.17	0.23	0.42	3.61	0.43	0.56	0.31	0.84	4.07	

Table 54: Electron microprobe data, Gunflint Banded-Iron Formation.

Wt% Oxide Sample#	Ti	V	Al	Cr	Mg	Si	Mn	Fe^{2+}	Fe^{3+}	Total
IF-2-1	0.00	0.00	0.44	0.03	0.13	1.47	0.15	30.38	67.67	100.27
-2	0.00	0.00	0.43	0.02	0.25	2.29	0.19	30.08	67.17	100.43
-3	0.00	0.00	0.50	0.00	0.17	1.71	0.14	30.52	68.05	101.09
-4	0.00	0.00	0.48	0.01	0.07	1.40	0.13	30.22	66.98	99.29
-5	0.00	0.00	0.57	0.01	0.35	2.28	0.17	29.36	66.28	99.02
-6	0.00	0.00	0.48	0.00	0.00	0.61	0.10	30.69	67.70	99.58
-7	0.00	0.00	0.54	1.11	0.00	0.69	0.08	30.70	66.41	99.53
-8	0.00	1.34	0.53	0.00	0.07	1.12	0.12	30.19	66.82	100.19
-9	0.00	0.00	0.51	0.03	0.14	0.71	0.15	30.14	67.05	98.73
-10	0.00	0.00	0.50	0.00	0.65	2.52	0.18	29.55	67.88	101.28
-11	1.12	0.00	0.49	0.03	0.18	1.55	0.18	31.39	65.61	100.55
-12	0.00	0.00	0.51	0.06	0.08	1.12	0.09	30.65	67.78	100.29
-13	0.00	0.00	0.44	0.00	0.14	2.02	0.07	30.22	67.20	100.09
-14	0.00	0.00	0.82	0.01	0.24	2.05	0.20	29.88	66.52	99.72
-15	0.00	0.00	0.50	0.00	0.07	0.36	1.21	30.20	69.34	101.68
Avg	0.07	0.09	0.52	0.09	0.17	1.46	0.21	30.28	67.23	
Std	0.28	0.33	0.09	0.27	0.16	0.66	0.27	0.48	0.87	

APPENDIX C

ELECTRON MICROPROBE DATA

ILMENITE

Table 55: Electron microprobe data, Surgarloaf Peak Quartz Monzonite.

Wt% Oxide Sample#	Ti	V	Al	Cr	Mg	Si	Mn	Fe2+	Fe3+	Total
As-1-1	47.04	0.71	0.34	0.00	0.03	0.11	3.72	38.72	10.27	100.97
-2	47.55	0.76	0.73	0.00	0.02	0.05	4.41	38.77	9.29	101.58
-3	45.77	0.74	0.34	0.00	0.06	0.07	3.05	38.20	10.65	98.88
-4	46.21	0.84	0.37	0.00	0.01	0.10	3.57	38.18	9.86	99.14
-5	46.15	0.66	0.42	0.00	0.05	0.00	3.95	37.70	10.49	99.42
-6	48.34	0.66	0.37	0.00	0.00	0.06	3.64	40.04	7.50	100.61
-7	46.41	0.76	0.69	0.00	0.10	0.09	3.20	38.80	10.12	100.17
-8	47.00	0.70	0.40	0.00	0.03	0.00	4.11	38.33	10.34	100.91
-9	46.97	0.68	0.41	0.00	0.00	0.07	4.48	37.99	8.57	99.17
-10	45.82	0.94	0.39	0.00	0.07	0.10	3.54	37.77	11.77	100.40
-11	47.75	0.77	0.41	0.00	0.00	0.05	3.88	39.30	8.43	100.59
-12	47.47	0.74	0.40	0.00	0.00	0.16	5.60	37.30	9.14	100.81
-13	46.26	0.61	0.37	0.00	0.00	0.05	4.36	37.44	11.55	100.64
-14	47.28	0.84	0.39	0.00	0.02	0.05	3.83	38.87	10.49	101.77
-15	47.80	0.69	0.35	0.00	0.00	0.00	6.04	37.11	7.99	99.98
-16	45.82	0.82	0.68	0.00	0.05	0.10	3.20	38.35	11.61	100.63
-17	45.19	0.71	0.43	0.00	0.00	0.07	4.10	36.79	12.55	99.84
-18	46.87	0.82	0.35	0.00	0.07	0.00	4.11	38.11	10.38	100.71
-19	46.31	0.68	0.39	0.00	0.07	0.04	4.82	36.91	10.46	99.68
-20	46.12	0.79	0.38	0.00	0.00	0.20	5.04	36.63	11.24	100.40
-21	45.87	0.81	0.42	0.00	0.11	0.04	2.71	38.60	11.00	99.56
Avg	46.67	0.75	0.43	0.00	0.03	0.07	4.06	38.09	10.18	
Std	0.81	0.08	0.11	0.00	0.03	0.05	0.80	0.85	1.27	

Table 56: Electron microprobe data, Saganaga Tonalite.

Wt% Oxide Sample#	Ti	V	Al	Cr	Mg	Si	Mn	Fe^{2+}	Fe^{3+}	Total
St-2-1	49.89	0.84	0.47	0.00	0.99	0.04	0.00	43.43	4.62	100.28
-2	48.05	0.99	0.46	0.11	1.41	0.00	0.00	41.07	7.43	99.52
-3	49.42	0.79	0.48	0.00	1.77	0.06	0.00	41.62	5.91	100.05
-4	48.04	0.85	0.49	0.00	0.29	0.00	0.00	43.03	7.03	99.73
-5	47.48	0.93	0.56	0.00	0.17	0.00	0.00	42.79	8.06	99.99
-6	49.26	0.77	0.54	0.00	1.64	0.00	0.00	41.75	6.75	100.71
-7	49.75	0.77	0.47	0.05	1.00	0.05	0.00	43.31	4.78	100.18
-8	49.94	0.86	0.50	0.01	0.14	0.00	0.00	45.01	4.18	100.64
-9	49.07	0.90	0.63	0.02	2.06	0.00	0.00	40.91	6.85	100.44
-10	49.43	0.90	0.59	0.00	0.21	0.04	0.00	44.49	5.19	100.85
Avg	49.03	0.86	0.52	0.02	0.97	0.02	0.00	42.74	6.08	
Std	0.82	0.07	0.06	0.03	0.70	0.02	0.00	1.32	1.26	

Table 57: Electron microprobe data, Pavela Granite.

Wt% Oxide Sample#	Ti	V	Al	Cr	Mg	Si	Mn	Fe^{2+}	Fe^{3+}	Total
Cb-1-1	45.64	0.73	0.31	0.10	0.01	0.00	1.82	39.44	12.72	100.77
-2	49.75	0.64	0.26	0.02	0.00	0.00	6.39	38.46	4.34	99.86
-3	40.21	0.80	0.33	0.07	0.83	0.03	0.47	34.47	23.45	100.66
-4	51.85	0.61	0.31	0.00	0.03	0.00	3.59	43.15	0.69	100.23
-5	45.67	0.79	0.28	0.00	1.52	0.00	1.16	37.38	12.98	99.78
-6	43.35	0.63	0.28	0.11	0.16	0.00	0.77	38.16	17.42	100.88
-7	48.00	0.81	0.35	0.03	0.93	0.00	1.32	40.43	8.85	100.72
-8	47.06	0.69	0.30	0.13	0.31	0.00	1.82	40.19	10.55	101.05
-9	47.85	0.81	0.37	0.05	0.58	0.04	1.63	40.63	9.33	99.66
-10	47.92	0.73	0.30	0.01	0.11	0.00	3.05	40.02	8.89	101.03
Avg	46.73	0.72	0.31	0.05	0.45	0.01	2.20	39.23	10.92	
Std	3.10	0.07	0.03	0.05	0.48	0.01	1.66	2.19	6.05	

Table 58: Electron microprobe data, Stouts Creek Rhyolite.

Wt% Oxide Sample#	Ti	V	Al	Cr	Mg	Si	Mn	Fe^{2+}	Fe^{3+}	Total
Vsc-1	48.77	0.59	0.41	0.00	0.00	0.01	7.57	36.48	6.78	100.61
-2	47.92	0.61	0.42	0.00	0.45	0.00	7.10	35.98	8.43	100.32
-3	47.62	0.54	0.46	0.00	0.00	0.00	7.21	35.84	8.59	100.26
-4	41.50	0.68	0.61	0.02	2.00	0.09	0.61	33.57	21.50	100.58
-5	48.50	0.70	0.42	0.00	0.01	0.04	6.73	37.07	7.36	100.83
-6	49.20	0.65	0.41	0.03	0.52	0.05	7.89	35.63	5.73	100.11
-7	48.97	0.66	0.43	0.00	0.00	0.00	13.25	30.92	6.64	100.87
-8	47.43	0.54	0.45	0.07	0.01	0.04	7.44	35.45	8.83	100.26
-9	48.20	0.74	0.46	0.00	0.00	0.01	7.41	36.16	7.14	100.12
Avg	47.57	0.63	0.45	0.01	0.33	0.03	7.25	35.23	9.00	
Std	2.22	0.07	0.06	0.02	0.62	0.03	3.00	1.77	4.52	

Table 59: Electron microprobe data, Royal Gorge Rhyolite.

Wt% Oxide Sample#	Ti	V	Al	Cr	Mg	Si	Mn	Fe^{2+}	Fe^{3+}	Total
Rgr-1	49.37	0.62	1.04	0.00	0.02	0.00	0.99	44.09	3.20	99.30
-2	47.35	0.83	0.71	0.00	1.56	0.00	0.70	39.59	9.71	100.45
-3	49.13	0.68	0.56	0.00	0.22	0.00	0.94	43.23	5.12	99.88
-4	50.51	0.82	0.62	0.00	0.32	0.00	0.68	44.60	3.20	100.75
-5	50.77	0.69	0.64	0.00	1.12	0.00	0.56	43.54	3.07	100.39
-6	49.53	0.78	0.61	0.00	0.27	0.00	0.51	43.97	4.96	100.62
-7	49.19	0.79	0.66	0.00	0.55	0.00	0.70	43.01	5.68	100.58
-8	47.83	0.88	0.63	0.00	1.02	0.00	0.81	40.81	8.37	100.35
-9	49.33	0.87	0.63	0.00	0.34	0.04	0.53	43.66	3.89	99.29
-10	48.12	0.76	0.61	0.00	0.01	0.00	2.99	40.65	6.39	99.53
Avg	49.11	0.77	0.67	0.00	0.54	0.00	0.94	42.72	5.36	
Std	1.04	0.08	0.13	0.00	0.49	0.01	0.70	1.63	2.15	

Table 60: Electron microprobe data, Rooiberg Felsite.

Wt% Oxide Sample	Ti	V	Al	Cr	Mg	Si	Mn	Fe^{2+}	Fe^{3+}	Total
Dfv-2	49.84	0.66	0.25	0.00	0.08	0.30	1.27	43.56	4.15	100.11
-2	47.28	1.18	0.24	0.08	0.35	0.27	1.65	41.82	7.34	100.21
-3	49.00	0.77	0.28	0.04	1.20	0.34	0.60	41.53	7.03	100.79
-4	50.38	0.86	0.43	0.02	0.43	0.30	0.62	44.22	1.52	98.78
-5	50.06	0.69	0.29	0.00	0.08	0.33	0.80	44.27	3.44	99.95
-6	50.27	0.69	0.29	0.00	0.92	0.33	0.68	43.08	4.16	100.42
-7	47.57	0.83	0.64	0.04	0.83	0.35	0.64	41.12	8.41	100.43
-8	49.17	0.68	0.29	0.04	0.79	0.30	0.54	42.49	5.79	100.10
-9	50.26	0.66	0.27	0.00	0.80	0.31	0.56	43.39	4.05	100.30
-10	50.47	0.56	0.29	0.00	0.99	0.39	0.51	43.31	3.32	99.84
Avg	49.43	0.76	0.33	0.02	0.65	0.32	0.32	42.88	4.92	
Std	1.11	0.16	0.12	0.03	0.37	0.03	0.36	1.04	2.04	

Table 61: Electron microprobe data, Ovalau, Fiji andesite.

Wt% Oxide Sample#	Ti	V	Al	Cr	Mg	Si	Mn	Fe^{2+}	Fe^{3+}	Total
Av-1-1	49.77	0.70	0.39	0.00	0.05	0.27	1.03	43.90	3.38	99.49
-2	51.60	0.76	0.34	0.00	0.41	0.03	0.61	45.29	0.80	99.84
-3	50.16	0.82	0.41	0.00	0.36	0.00	0.82	43.92	3.48	99.97
-4	51.27	0.73	0.37	0.00	0.51	0.02	0.69	44.76	2.21	100.56
-5	49.74	0.84	0.40	0.00	0.29	0.06	0.63	43.85	3.50	99.31
-6	50.79	0.77	0.36	0.00	0.58	0.07	0.52	44.36	1.72	99.17
-7	51.15	0.77	0.29	0.00	0.53	0.00	0.53	44.72	0.60	98.56
-8	49.92	0.72	0.35	0.00	0.01	0.03	0.78	44.33	4.08	100.22
-9	50.24	0.78	0.39	0.00	1.98	0.13	0.61	41.30	4.54	99.97
-10	49.68	0.91	0.36	0.03	0.11	0.11	0.84	43.89	3.96	99.89
-11	50.10	0.79	0.32	0.00	0.00	0.11	0.51	44.76	2.45	99.04
-12	48.51	0.72	0.37	0.00	0.00	0.00	4.43	39.39	6.22	99.64
-13	51.05	0.83	0.39	0.00	0.29	0.05	0.62	45.04	1.29	99.56
-14	50.82	0.76	0.32	0.00	1.38	0.04	0.52	42.94	0.33	97.11
-15	51.36	0.69	0.41	0.00	0.00	0.02	1.31	45.15	0.07	99.01
-16	50.76	0.66	0.35	0.00	0.43	0.06	0.69	44.43	2.75	100.13
Avg	50.43	0.77	0.36	0.00	0.43	0.06	0.95	43.88	2.59	
Std	0.79	0.06	0.03	0.01	0.52	0.07	0.92	1.49	1.67	

Table 62: Electron microprobe data, Nevado de Toluca andesite.

Wt% Oxide Sample#	Ti	V	Al	Cr	Mg	Si	Mn	Fe^{2+}	Fe^{3+}	Total
Tm-2-1	44.64	0.80	0.58	0.02	1.75	0.01	0.46	36.97	15.15	100.38
-2	43.89	0.84	0.60	0.04	1.84	0.06	0.45	36.17	16.26	100.15
-3	43.07	0.77	0.59	0.00	2.14	0.07	0.39	34.93	18.52	100.75
-4	46.09	0.75	0.66	0.08	3.14	0.06	0.48	35.86	13.25	100.37
-5	44.83	0.84	0.58	0.09	1.96	0.00	0.50	36.76	14.92	100.48
-6	41.84	1.21	0.49	0.23	2.44	0.01	0.32	33.40	19.88	99.82
-7	44.44	0.71	0.66	0.03	2.94	0.00	0.45	34.74	16.80	100.77
-8	46.03	0.64	0.48	0.00	1.43	0.00	0.66	38.51	12.39	100.14
-9	42.12	0.71	1.00	0.02	1.89	0.00	0.49	34.72	19.96	100.91
-10	44.05	0.68	0.64	0.05	2.80	0.04	0.34	34.75	16.87	100.22
Avg	44.10	0.80	0.63	0.06	2.23	0.03	0.45	35.68	16.40	
Std	1.37	0.15	0.14	0.06	0.54	0.03	0.09	1.40	2.44	

Table 63: Electron microprobe data, Bushveld Complex.

Wt% Oxide Sample#	Ti	V	Al	Cr	Mg	Si	Mn	Fe^{2+}	Fe^{3+}	Total
Sr-2-1	51.35	0.50	0.26	0.00	0.14	0.09	0.64	45.46	0.93	99.37
-2	50.46	0.83	0.31	0.05	0.71	0.09	0.72	43.62	2.78	99.57
-3	50.43	0.61	0.42	0.05	0.29	0.04	0.58	44.56	2.44	99.42
-4	51.31	0.58	0.29	0.00	0.13	0.04	0.95	45.15	1.02	99.47
-5	50.53	0.75	0.29	0.00	0.88	0.03	0.50	43.57	3.33	99.88
-6	51.29	0.80	0.27	0.00	1.46	0.06	0.55	43.15	2.25	99.83
-7	50.78	0.67	0.27	0.00	1.25	0.08	0.52	43.10	3.26	99.93
-8	51.02	0.71	0.51	0.00	0.36	0.14	0.63	44.96	1.58	99.91
-9	50.36	0.64	0.24	0.03	0.41	0.11	0.65	44.08	3.56	100.08
-10	51.22	0.77	0.32	0.00	0.78	0.09	0.54	44.35	1.64	99.71
Avg	50.88	0.69	0.32	0.01	0.64	0.08	0.63	44.20	2.28	
Std	0.39	0.10	0.08	0.02	0.43	0.03	0.13	0.79	0.91	

Table 64: Electron microprobe data, Bushveld Complex.

Wt% Oxide Sample#	Ti	V	Al	Cr	Mg	Si	Mn	Fe^{2+}	Fe^{3+}	Total
Vu-2-1	48.41	0.79	0.36	0.00	0.84	0.20	1.02	41.25	8.23	101.10
-2	48.29	0.85	0.40	0.00	0.08	0.28	0.84	42.71	6.69	100.14
-3	48.13	0.99	0.36	0.00	0.59	0.08	0.72	41.75	6.57	99.19
-4	50.46	0.90	0.37	0.00	2.29	0.11	0.41	41.14	4.16	99.84
-5	50.52	0.84	0.35	0.00	1.37	0.21	0.54	42.69	3.14	99.66
-6	49.28	0.86	0.41	0.00	0.01	0.18	0.80	43.77	2.86	99.17
-7	50.46	0.79	0.36	0.00	2.50	0.23	0.55	40.61	4.00	99.50
-8	48.07	0.89	0.32	0.00	0.01	0.16	2.55	40.85	7.66	100.51
-9	51.76	0.80	0.34	0.00	4.37	0.18	0.40	38.59	2.39	98.83
-10	50.43	0.83	0.40	0.00	2.46	0.15	0.47	40.77	3.28	98.79
-11	50.99	0.90	0.33	0.02	0.00	0.21	1.21	44.87	2.07	100.60
-12	49.56	1.05	0.39	0.00	1.51	0.15	0.53	41.61	5.13	99.93
-13	50.38	0.88	0.68	0.00	1.58	0.27	0.54	42.42	3.14	99.89
-14	46.53	0.80	0.42	0.79	0.20	0.12	3.88	38.22	9.51	100.47
-15	50.29	0.80	0.34	0.00	0.63	0.14	0.58	43.75	2.68	99.21
-16	49.86	0.95	0.34	0.00	0.63	0.25	1.14	42.80	3.95	99.24
-17	46.61	0.95	0.39	0.00	0.32	0.38	2.48	39.10	10.23	100.46
-18	49.33	0.81	0.42	0.00	1.06	0.19	0.56	42.20	6.25	100.82
-19	50.35	0.73	0.37	0.00	0.00	0.23	1.73	43.78	3.56	100.75
-20	48.02	0.88	0.42	0.00	0.83	0.23	0.84	41.15	6.53	98.90
Avg	49.39	0.86	0.39	0.04	1.06	0.20	1.09	41.70	5.10	
Std	1.40	0.08	0.07	0.17	1.11	0.07	0.89	1.72	2.39	

Table 65: Electron microprobe data, Duluth Gabbro.

Wt% Oxide Sample#	Ti	V	Al	Cr	Mg	Si	Mn	Fe^{2+}	Fe^{3+}	Total
Dg-2-1	50.21	0.94	0.34	0.07	0.27	0.15	0.70	44.23	4.05	100.96
-2	48.96	1.18	0.32	0.04	1.60	0.05	0.46	40.95	7.61	101.17
-3	49.51	1.05	0.29	0.05	0.93	0.06	0.63	42.45	4.31	99.28
-4	49.60	0.98	0.30	0.09	1.88	0.18	0.49	41.06	6.48	101.06
-5	49.83	0.96	0.37	0.02	0.66	0.20	0.53	43.36	5.27	101.20
-6	48.50	0.95	0.34	0.09	0.05	0.06	1.30	42.49	6.35	100.13
-7	49.23	1.10	0.36	0.04	0.44	0.12	0.59	43.16	4.58	99.62
-8	49.05	1.16	0.32	0.08	1.77	0.04	0.52	40.69	6.61	100.24
-9	51.41	1.12	0.26	0.11	0.89	0.09	0.52	44.35	1.42	100.17
-10	49.13	1.32	0.32	0.02	1.16	0.16	0.51	41.83	5.92	100.37
-11	49.23	1.12	0.27	0.17	1.20	0.04	0.44	41.95	5.23	99.74
-12	48.53	1.09	0.35	0.25	1.59	0.10	0.59	40.57	6.87	99.94
-13	49.36	1.07	0.28	0.05	0.68	0.06	0.41	42.98	3.80	98.69
-14	48.54	0.79	0.31	0.02	0.16	0.02	0.79	42.79	5.33	99.49
-15	50.28	0.80	0.64	0.02	0.07	0.16	0.80	44.74	2.78	100.29
-16	49.62	1.04	0.29	0.02	0.06	0.11	0.79	43.93	3.51	99.37
-17	49.88	1.20	0.28	0.29	1.72	0.00	0.42	41.70	4.07	99.56
-18	49.35	1.87	0.28	0.07	0.35	0.04	0.53	43.45	4.21	100.15
-19	49.27	0.80	0.32	0.05	0.49	0.08	0.65	43.02	4.84	99.52
-20	51.69	1.25	0.34	0.16	1.79	0.06	0.52	43.08	1.64	100.53
-21	48.59	0.98	0.32	0.09	1.07	0.05	1.18	40.86	7.66	100.80
-22	48.68	1.04	0.32	0.08	1.17	0.06	0.41	41.54	8.06	101.36
-23	47.98	0.90	0.32	0.04	1.16	0.09	0.54	40.77	8.91	100.71
-24	50.32	0.86	0.29	0.14	2.00	0.03	0.50	41.45	4.96	100.55
Avg	49.45	1.07	0.33	0.09	0.97	0.08	0.62	42.39	5.19	
Std	0.87	0.22	0.07	0.07	0.63	0.05	0.22	1.24	1.88	

Table 66: Electron microprobe data, Duluth Gabbro.

Wt% Oxide Sample#	Ti	V	Al	Cr	Mg	Si	Mn	Fe^{2+}	Fe^{3+}	Total
Dg-3-1	48.60	0.76	0.40	0.00	1.22	0.11	0.37	41.43	6.95	99.84
-2	48.51	0.94	0.43	0.07	1.69	0.07	0.34	40.60	7.57	100.22
-3	49.50	0.74	0.47	0.00	1.52	0.12	0.47	41.66	6.13	100.61
-4	49.29	0.85	0.49	0.04	1.28	0.04	0.41	41.99	5.83	100.22
-5	49.93	0.74	0.45	0.10	1.07	0.03	0.62	42.83	4.56	100.23
-6	49.79	0.81	0.47	0.00	1.55	0.10	0.59	41.74	5.38	100.43
-7	49.41	0.67	0.80	0.04	1.08	0.04	0.48	42.60	5.10	100.22
-8	49.16	0.79	0.50	0.03	0.91	0.15	0.75	42.19	5.49	99.97
-9	48.99	0.64	0.57	0.05	0.63	0.11	0.51	42.84	6.09	100.43
-10	50.74	0.65	0.45	0.00	2.08	0.08	0.43	41.80	3.84	100.07
Avg	49.39	0.76	0.50	0.03	1.30	0.09	0.50	41.97	5.69	
Std	0.63	0.09	0.11	0.03	0.40	0.04	0.12	0.65	1.03	

Table 67: Electron microprobe data, Keveenavan Basalt.

Wt% Oxide Sample#	Ti	V	Al	Cr	Mg	Si	Mn	Fe^{2+}	Fe^{3+}	Total
Kb-2-1	47.64	0.81	0.64	0.00	0.77	0.00	0.00	41.92	8.85	100.63
-2	50.04	1.11	0.63	0.00	2.87	0.14	0.00	40.32	3.17	98.28
-3	48.31	0.83	0.63	0.00	0.84	0.01	0.00	42.39	7.78	100.79
-4	50.20	0.92	0.45	0.08	2.25	0.12	0.00	41.48	4.87	100.37
-5	49.86	0.87	0.64	0.03	0.79	0.07	0.00	43.89	4.05	100.20
-6	47.64	0.78	0.64	0.04	0.88	0.02	0.00	41.74	9.02	100.76
-7	48.04	0.77	0.61	0.03	0.72	0.00	0.00	42.39	8.32	100.92
-8	47.67	0.76	0.50	0.01	0.89	0.00	0.00	41.64	8.07	99.54
-9	48.73	0.64	0.60	0.00	0.71	0.00	0.00	42.98	7.29	100.95
-10	47.23	0.92	0.55	0.01	1.33	0.00	0.00	40.49	10.43	100.96
Avg	48.54	0.84	0.59	0.02	1.21	0.04	0.00	41.92	7.19	
Std	1.06	0.12	0.06	0.02	0.71	0.05	0.00	1.02	2.25	

Table 68: Electron microprobe data, Marcy-type meta-anorthosite.

Wt% Oxide Sample#	Ti	V	Al	Cr	Mg	Si	Mn	Fe^{2+}	Fe^{3+}	Total
pCma-3	46.13	0.70	0.65	0.00	0.71	0.00	0.33	40.34	11.26	100.12
-2	46.37	0.95	0.66	0.00	1.01	0.00	0.29	40.07	10.79	100.14
-3	45.69	0.88	0.50	0.14	1.29	0.04	0.40	38.80	12.61	100.35
-4	47.00	0.78	0.68	0.06	0.00	0.01	0.50	42.26	9.55	100.84
-5	47.51	0.82	0.54	0.00	0.84	0.00	0.25	41.35	8.52	99.83
-6	45.01	0.81	0.63	0.00	0.98	0.06	0.27	38.90	13.11	99.77
-7	47.59	0.89	1.04	0.13	1.27	0.00	0.36	40.96	8.49	100.73
-8	45.55	0.73	0.54	0.06	0.60	0.00	0.38	39.91	12.44	100.21
-9	44.21	0.86	0.61	0.16	1.26	0.00	0.24	37.77	15.20	100.31
-10	44.39	0.79	0.59	0.16	2.32	0.00	0.30	35.97	16.23	100.75
Avg	45.95	0.82	0.64	0.07	1.03	0.01	0.33	39.63	11.82	
Std	1.14	0.07	0.14	0.07	0.57	0.02	0.08	1.75	2.49	

Table 69: Electron microprobe data, Whiteface-type meta-anorthosite.

Wt% Oxide Sample#	Ti	V	Al	Cr	Mg	Si	Mn	Fe^{2+}	Fe^{3+}	Total
pCwa-1	48.23	0.70	0.74	0.11	0.94	0.01	0.47	41.79	7.79	100.78
-2	46.45	0.68	0.36	0.00	0.48	0.04	0.42	40.74	10.99	100.16
-3	48.79	0.82	0.30	0.16	0.42	0.01	0.45	42.96	6.80	100.71
-4	49.26	0.82	0.34	0.08	0.11	0.00	0.50	43.87	5.79	100.77
-5	47.78	0.55	0.45	0.05	0.28	0.02	0.21	42.59	8.70	100.63
-6	49.08	0.69	0.38	0.10	0.28	0.00	0.53	43.41	6.21	100.68
-7	49.20	0.76	0.34	0.14	0.75	0.00	0.30	42.91	7.79	102.19
-8	48.64	0.90	0.34	0.13	0.78	0.00	0.61	42.03	7.56	100.99
-9	46.99	0.60	0.26	0.03	0.40	0.04	0.52	41.21	10.12	100.17
-10	49.24	0.86	0.29	0.14	0.73	0.04	0.38	42.86	6.33	100.87
Avg	48.37	0.74	0.38	0.09	0.52	0.02	0.44	42.44	7.81	
Std	0.95	0.11	0.13	0.05	0.25	0.02	0.11	0.93	1.62	

Table 70: Electron microprobe data, Loma de Hierro Ultramafic Complex.

Wt% Oxide Sample#	Ti	V	Al	Cr	Mg	Si	Mn	Fe^{2+}	Fe^{3+}	Total
PC1057	50.00	1.27	0.39	0.11	0.30	0.08	2.02	42.71	3.13	100.01
-2	48.61	1.32	0.40	0.05	0.36	0.07	1.14	42.22	5.97	100.14
-3	47.76	1.03	0.35	0.04	0.07	0.03	1.11	41.69	7.11	98.89
-4	49.51	0.99	0.39	0.00	0.05	0.11	1.32	43.37	3.71	99.45
-5	48.71	0.71	0.43	0.00	0.13	0.01	1.15	42.71	6.66	100.51
-6	49.36	0.89	0.45	0.00	0.07	0.04	1.61	42.95	4.72	100.09
-7	49.04	0.97	0.30	0.02	0.79	0.10	1.60	41.29	6.33	100.44
-8	48.53	0.95	0.44	0.02	0.05	0.14	0.96	42.90	7.84	98.83
-9	47.08	0.96	0.30	1.29	0.00	0.04	1.95	41.99	4.89	99.40
-10	47.88	0.76	0.28	0.04	0.00	0.07	4.20	39.02	8.56	100.81
Avg	48.65	0.99	0.37	0.16	0.18	0.07	1.71	42.09	5.89	
Std	0.84	0.18	0.06	0.38	0.23	0.04	0.90	1.19	1.67	

APPENDIX D

Job Control Language for Discriminant Analysis Program

```
//  JOB
// EXEC  SPSSX
//SYSIN  DD  *
DATA LIST  FILE=RAW
 /1  ID 1-6 (A) TI 9-13 V 16-20 AL 23-27 CR 30-34 MG 37-41
     MN 44-48 GRP 51
LIST
CONDESCRIPTIVE TI TO MN
DISCRIMINANT   GROUPS=GRP(1,3)/VARIABLES=TI TO MN/
  ANALYSIS=TI  TO  MN/ METHOD=WILKS/  FUNTIONS=2/
  PIN=.05
STATISTICS  1 2 5 6 7 10 11 12 13 15 16
SORT CASES BY GRP
SPLIT FILE BY GRP
CONDESCRIPTIVE   TI TO MN
/*
//RAW  DD  *
  (data lines)
/*
```

APPENDIX E

Point Count Analysis of the Light Sand Fraction for the Sands of the Current Study

Rock Type	Sample	Quartz	K-Feldspar	Plagioclase	VRF*	CRF*	MRF*	QRF*	Accessories					Total Counts
									Biotite	Amphibole	Pyroxene	Olivine	Opaques	
Felsic	Cb-1	36	59	56	2	0	0	0	45	1	1	0	1	200
Plutonic	As-1	34	16	102	0	0	0	1	13	20	0	0	4	200
	St-2	76	50	19	3	0	0	10	1	16	17	0	6	200
	Erg-1	42	94	54	0	0	0	4	0	0	0	0	6	200
Felsic	Vsc-1	28	24	2	146	0	0	0	0	0	0	0	0	200
Volcanic	Dfv-2	38	22	6	130	0	0	0	0	0	0	0	4	200
	Rgr-1	40	32	8	120	0	0	0	0	0	0	0	0	200
Intermed.	Ta-1	16	3	59	27	0	0	0	0	49	10	0	36	200
Volcanic	Tm-1	6	7	91	67	0	0	0	0	21	5	0	3	200
	Av-1	0	0	14	12	20	0	0	0	0	154	0	4	200
Mafic	Vu-2	22	0	145	2	0	0	0	3	0	7	0	21	200
Plutonic	Sr-1	2	0	165	5	0	0	0	1	1	16	0	10	200
	Dg-2	37	0	89	26	0	0	0	0	0	23	0	25	200
	Dg-3	21	0	149	6	0	0	0	12	6	5	0	1	200
Mafic	M-7	0	0	1	6	192	0	0	1	0	0	0	0	200
Volcanic	HBb-1	0	0	34	31	70	0	0	0	1	13	47	4	200
	B-5	0	0	28	170	0	0	0	0	0	2	0	0	200
	Kb-2	2	0	44	136	0	0	0	0	0	0	2	6	200
	IL85-1	0	0	20	65	12	0	0	0	15	74	0	14	200
	IL76-1	1	0	5	56	19	0	0	0	0	3	13	3	100
Meta-	PCma-1	0	0	162	0	0	0	0	2	2	28	0	6	200
Anorth.	PCva-1	3	1	128	3	0	0	0	0	32	25	0	8	200
Serpent.	PC-1057	40	0	48	52	0	29	0	0	18	11	0	2	200
Ultra.	NFao-1	1	0	9	18	2	0	0	0	2	8	0	160	200
Unknown	JG-1	35	14	99	28	0	0	7	2	11	4	0	0	200

*VRF = volcanic rock fragments
CRF = carbonate rock fragments
MRF = metamorphic rock fragments
QRF = quartzofeldspathic rock fragments

APPENDIX F

Calculation of the Proportion of Detrital Magnetite Grains Derived from the Various Sources of the Rosarito Beach Sand

Table 26 is a summary diagram of the percentage of Low-Ti detrital magnetite grains found to be associated with sands of basaltic source. It is proposed that, by calculating the mean and standard deviation of these percentages, an approximation of the proportion of detrital magnetite grains found in the Rosarito Beach sand can be related to the parent rocks from which they were derived. It is conceivable that by combining the electron microprobe chemical data gathered from the homogeneous grains with the petrographic data gathered from the heterogeneous grains that the number of individual magnetite grains derived from each parent rock can be approximated. This would determine the influence of each source has on the composition of the sand. The following steps will diagram this procedure.

A. Homogeneous grains and electron microprobe chemical analyses

1) Calculate the mean and standard deviation of the percentage of low-Ti magnetite associated with sands of basaltic source (Table 26).

2) Let x = the total number of detrital magnetite grains of basaltic source in the Rosarito Beach sand.

3) If x = the total number of basaltic magnetite grains then

$0.30x$ = the number of low-Ti grains
and
$0.70x$ = the number of high-Ti grains

Table 71: Percentage of low-Ti magnetite grains associated with sands of basaltic source.

Sample Number	Percent Low-Ti Grains
Kb-2	25
IL76-1	60
IL85-1	40
M-7	21
B-5	0
HBb-1	35
Mean =	30%
Standard Deviation =	18%

4) From the microprobe data and plot in figure 41 the following associations can be made.

a) High-Ti magnetite of basaltic source = 6 grains.
b) Projected low-Ti magnetite of basaltic source =x(0.30) grains.
c) Low-Ti magnetite of felsic source = 18-x(0.30) grains.
d) Magnetite of intermediate source = 3 grains.

5) Since we know that there are 6 high-Ti magnetite grains of basaltic source and that 0.70x equals the number of high-Ti grains we can calculate the total number of magnetite grains of basaltic source (x).

a) $0.70x = 6$
$x = 6/0.70 = 9$ grains of basaltic source.
b) at a standard deviation of 0.18
$x_{max} = 6/0.52 = 11$ grains of basaltic source
or
$x_{min} = 6/0.88 = 7$ grains of basaltic source.
c) The total number of detrital magnetite grains of basaltic source as determined by the electron microprobe thus equals $9(\pm 2)$.

6) In the case of the Rosarito Beach sand the 27 probed homogeneous detrital magnetite grains can be divided between parent rocks as follows.

a) High-Ti magnetite grains of basaltic source = 6 grains.
b) Low-Ti magnetite grains of presumed basaltic source = $3(\pm 2)$grains.
c) Total basaltic magnetite grains = $9(\pm 2)$ grains.
d) Low-Ti magnetite of felsic source = $15(\pm 2)$ grains.
e) Magnetite of intermediate source = 3 grains.

7) Calculating the percentage of these grain types in the original 27 probed grains lets us determine the distribution of all the homogeneous grains between the three specified parent rocks.

a) Total detrital magnetite of basaltic source = $21(\pm 5)$
b) Low-Ti magnetite of felsic source = $35(\pm 5)$
c) Magnetite of intermediate source = 7
d) Total homogeneous grains = 63

B. Distribution of heterogeneous grains.

1) There were a total of 53 heterogeneous detrital magnetite grains counted.

   a) Total grains with magnetite-ilmenite intergrowths = 37.
   b) Grains with pleonaste exsolution = 9
   c) Grains with ulvospinel exsolution = 0
   d) Grains with heating martite = 7

2) From the discussion in the text it is safe to assign all of the grains with magnetite-ilmenite intergowths and pleonaste exsolution to the basaltic source. The grains with heating martite can safely be assigned to the intermediate source.

C. Combining the results from the homogeneous grains with those of the heterogeneous grains indicates that the distribution of the detrital magnetite grains from Rosarito Beach between the various parent rocks is as follows.

1) Felsic Plutonic Source

   a) Homogeneous grains = 35($\pm$5)
   b) Heterogeneous grains = 0
   c) Total = 35($\pm$5) or 30($\pm$5)%

2) Intermediate (Andesite) Volcanic Source

   a) Homogeneous grains = 7
   b) Heterogeneous grains = 7
   c) Total = 14 or 12%

3) Mafic (Basalt) Volcanic Source

   a) Homogeneous grains = 21($\pm$5)
   b) Heterogeneous grains = 46
   c) Total = 67($\pm$5) or 58($\pm$5)%

Total number of grains analyzed = 116.